Advanced, Energy-Efficient Hybrid Membrane System for Industrial Water Reuse

Final Technical Report

Period of Performance:
September 1, 2012 to December 30, 2016

by

Lora Toy (ltoy@rti.org; (919) 316-3393)
Young Chul Choi (ycchoi@rti.org; (919) 316-3885)
Zachary Hendren (zhendren@rti.org; (919) 541-6605)
Gyu Dong Kim (gkim@rti.org; (919) 990-8448)

DOE Cooperative Agreement No. DE-EE0005758

Submitted by Prime Recipient:
RTI International[1]
3040 Cornwallis Road
P.O. 12194
Research Triangle Park, NC 27709-2194

Project Partners:
Duke University
Veolia Water Technologies

March 31, 2017

[1] RTI International is a registered trademark and a trade name of Research Triangle Institute.

Disclaimer

Proprietary Data Notice

This final technical report does not include any proprietary or protected data.

Acknowledgements

This report is based upon work supported by the Advanced Manufacturing Office (AMO) under the Office of Energy Efficiency & Renewable Energy (EERE) of the U.S. Department of Energy (DOE) under Cooperative Agreement No. DE-EE0005758. RTI gratefully acknowledges the assistance of DOE/EERE-AMO representatives for their project guidance and support. In addition, the majority of the cost share for this project was provided by project partner Veolia Water Technologies (Cary, NC) as in-kind labor for technical expertise and guidance. The remaining cost share was provided as in-kind RTI labor paid from RTI's State of North Carolina (non-Federal) funding. Recognition of contributing individuals from these organizations is provided below.

DOE/EERE-AMO: Robert Gemmer (technology manager), Gibson Asuquo (project officer), Chad Sapp (project monitor) and Bhima Sastri (predecessor technology manager).

Veolia Water Technologies: Hervé Buisson (project manager), Shan Yong (project engineer), Bernie Mack (process engineer), James Newton (pilot manager), Adrien Moreau (project engineer), Eric Barbier (R&D project manager), and Claire Machinal (R&D engineer).

Duke University: Mark Wiesner (professor), Judith Winglee (doctoral student), Alexis Wells Carpenter (postdoctoral researcher), and Nathan Bossa (postdoctoral researcher).

RTI International: Predecessor Principal Investigator: James Cunningham. Experimental, Engineering, and Technical Support: Steven Mazzarelli, Matthew Von Holle, Lamar Perry, Chinh Hoang, David Bollinger, and Martin Lee. Analytical Support: Kelly Amato, John Albritton, Michael Levine, Eric Poitras, and T. Doug Burnette. Process Modeling and Engineering Support: Nandita Akunuri and Atish Kataria. Pilot-Unit Commissioning Support: Douglas Lowe and John Berkley. Senior Advisors: Markus Lesemann (technology partnerships and commercialization planning) and Raghubir Gupta (technology development). Financial Support: Jacqueline Bateman and Aaron Wachholz. Project Management Coordination Support: Thomas Nelson, Jason Norman, and Jonathan Peters.

RTI also gratefully acknowledges Veolia's plant operations staff for collecting and shipping real industrial wastewater from a water treatment facility operated and managed by Veolia for one of their oil and gas production clients.

TABLE OF CONTENTS

FIGURES

TABLES

List of Acronyms

A	Characteristic water permeability [L/(m^2·h·bar)] of forward osmosis membrane
B	Characteristic salt permeability [L/(m^2·h)] of forward osmosis membrane
cm/s	Centimeters per second
COD	Chemical oxygen demand
CPVC	Chlorinated polyvinyl chloride
CTA	Cellulose triacetate
DCMD	Direct contact membrane distillation
FO	Forward osmosis
gpd	gallons per day (gal/day)
gpm	gallons per minute (gal/min)
J_W	Water flux [L/(m^2·h)] in forward osmosis or membrane distillation
J_S	Reverse draw-salt flux [mol/(m^2·h)] in forward osmosis
J_W/J_S	Water/salt selectivity (L/mol) of forward osmosis membrane
L/min	Liters per minute
LMH	Liters per square meter per hour [L/(m^2·h)]
MD	Membrane distillation
MF	Microfiltration
P&ID	Piping & instrumentation diagram
PFD	Process flow diagram
PP	Polypropylene
PTFE	Polytetrafluoroethylene
PVC	Polyvinyl chloride
PVDF	Polyvinylidene fluoride
R^2	Coefficient of determination
RO	Reverse osmosis
S	Characteristic membrane structural parameter (μm) of forward osmosis membrane
TDS	Total dissolved solids
TFC	Thin film composite
UF	Ultrafiltration
VMD	Vacuum membrane distillation
VOCs	Volatile organic compounds

Executive Summary

In the U.S. manufacturing sector, current industrial water use practices are energy-intensive and utilize and discharge high volumes of waters, rendering them not sustainable especially in light of the growing scarcity of suitable water supplies. To help address this problem, the goal of this project was to develop an advanced, cost-effective, hybrid membrane-based water treatment system that can improve the energy efficiency of industrial wastewater treatment while allowing at least 50% water reuse efficiency. This hybrid process would combine emerging Forward Osmosis (FO) and Membrane Distillation (MD) technology components into an integrated FO-MD system that can beneficially utilize low-grade waste heat (i.e., T < 450 °F) in industrial facilities to produce distilled-quality product water for reuse.

In this project, laboratory-, bench-, and pilot-scale experiments on the hybrid FO-MD system were conducted for industrial wastewater treatment. It was demonstrated at laboratory, bench, and pilot scales that FO-MD membrane technology can concentrate brine to very high total dissolved solids (TDS) levels (>200,000 ppm) that are at least 2.5 times higher than the TDS level to which RO can achieve. In laboratory testing, currently available FO and MD membranes were tested to select for high-performing membranes with high salt rejection and high water flux. Multiple FO membrane/draw-salt solution combinations that gave high water flux with higher than 98% salt rejection were also identified. Reverse draw-salt fluxes were observed to be much lower for divalent salts than for monovalent salts. MD membranes were identified that had 99.9+% salt rejection and water flux as high as 50-90 L/(m^2·h) for flat-sheet membranes and >20 L/(m^2·h) for hollow fibers. In bench-scale testing, a single unit of commercially available FO and MD membrane modules were evaluated for continuous, integrated operation. Using the laboratory- and bench-scale test data, numerical modeling was performed on the FO and MD processes to estimate engineering parameters for a larger-scale pilot unit.

Based on the experimental studies and modeling results, a pilot-scale, integrated FO-MD prototype unit was designed and built for trailer-mounted operation. This prototype system was fed real industrial wastewater, which could not be further treated by conventional technologies, from an oil production facility and was successfully operated for over 15 weeks without major stoppage. About 90% water recovery was possible, while concentrating the TDS from 12,000 ppm up to 190,500 ppm. The FO-MD prototype rejected most wastewater contaminants while producing water with <300 ppm TDS, even when the feed TDS was higher than 150,000 ppm. No chemical cleaning was necessary during the pilot testing period. Flushing the system with dechlorinated tap water was sufficient to reset the membranes for the next set of test conditions. Pilot performance and membrane autopsy showed that, even though the feed was concentrated more than 10 times, membrane fouling was unnoticeable and no defects were detected on the FO and MD membrane surfaces.

This project demonstrated the technical feasibility of the hybrid FO-MD process by taking water already treated to the limit with the highest level of current technologies and further concentrating it 10-fold by using mostly low-cost materials. Because no membranes suitable for full-scale plant applications are available at present, economical feasibility of the hybrid technology is still uncertain, but it is expected that broader industry participation can further reduce FO-MD process costs.

1. INTRODUCTION

In the U.S. manufacturing sector, industrial water effluents contain high levels of contaminants such as particles, organics, bacteria, and dissolved salts. Most contaminants can be effectively removed by various water treatment technologies currently available, such as ultrafiltration for particles and chemical precipitation or biological methods for organic materials. Dissolved salts, though, are the most difficult to treat and require the most energy-intensive treatment processes. Because many manufacturing processes require total dissolved solids (TDS) to be as low as or even lower than levels allowed by drinking water standards, developing efficient methods of treating TDS in waters is critical. Current state-of-the-art technology for TDS removal is reverse osmosis (RO). RO membranes have been developed and improved over the last 60 years, and their performance is near the theoretical limit. However, RO cannot handle very high TDS, which is a critical drawback. RO is effective for feed water containing roughly 50,000 ppm or lower TDS. For water with higher salinity, current RO technology cannot be used largely because RO is a pressure-driven process and the pressure requirement is generally proportional to the amount of TDS in the feed water. The piping and pressure vessels, as well as the RO membrane itself, are limited to 1,200 psi. Furthermore, the critical part of the RO membrane's energy savings, the Energy Recovery Device (ERD), would reach its maximum design point around the same pressure. Many industrial processes, such as manufacturing, hydraulic fracturing, and carbon management, have waters containing high levels of TDS. The only currently available solution for treating high-TDS waters is using thermal evaporator and crystallizer technologies. These processes have very limited adaptation in the industry because of their high energy consumption and high cost of construction, which often requires exotic material alloys. Additionally, other aspects of their operation and maintenance can cost significantly more than membrane-based processes. In thermal processes, the solubility of a divalent-ion salt such as $Mg(OH)_2$ may increase with high recovery rates. This phenomenon decreases the pH in the system when the temperature is high. This decreased pH creates a highly corrosive environment, and NaOH may need to be injected constantly. Overall, thermal processes have inherent disadvantages that are extremely difficult to rectify.

In this project, a novel forward osmosis-membrane distillation (FO-MD) process that uses mostly polymeric materials of construction was developed. Using plastic materials not only decreases the cost of construction but also offers the advantage of low-cost maintenance and replacement.

Technology Description

In this project, a hybrid FO-MD process technology that can treat industrial water with high levels of contaminants was developed and advanced from the laboratory scale to the bench scale to the pilot scale. FO is a process that uses the osmotic pressure of a draw solution across a semi-permeable membrane as the flux driving force compared to the hydraulic-pressure driving force in RO. FO has received worldwide attention because it is an emerging technology for water reuse and seawater desalination. Historically, FO has been used in food processing, protein concentration, and alcohol dehydration but has received little attention as a water treatment technology until recently. Only pure water in the feed stream migrates into the draw-solution side due to the osmotic-pressure gradient. The FO process has several important

advantages over the RO process. First, FO does not require a high-pressure system so that all pipes and containers can be made of polymeric materials, such as CPVC [chlorinated poly(vinyl chloride)]. This significantly reduces the cost of construction compared to RO, which requires a high-grade metal alloy for high-pressure and high-salinity process conditions. Second, FO is more compatible with much higher TDS than RO, and FO is primarily limited by the osmotic strength of the draw solution used. Figure 1-1 illustrates the basic mechanism for salt rejection and water transport in an FO system.

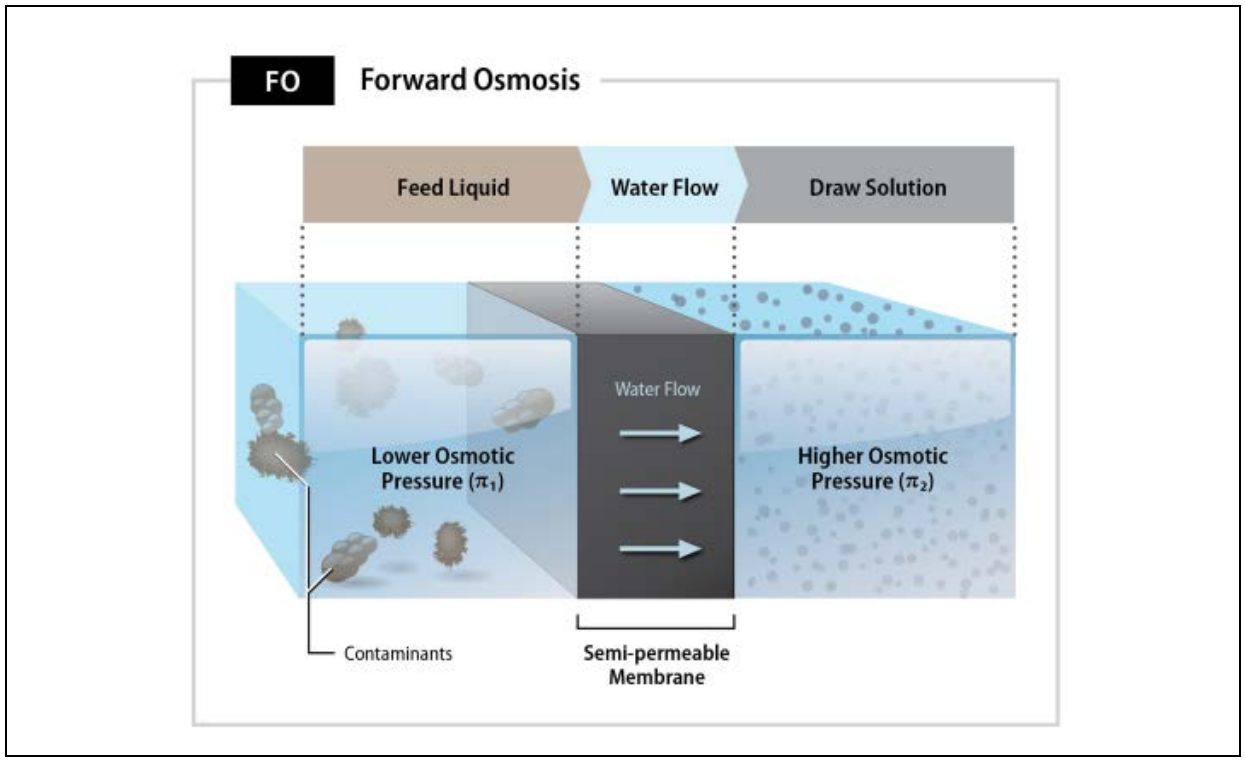

Figure 1-1. Forward osmosis process

Despite the potential benefits of the FO process, this technology has limited application due to the lack of cost-effective processes to regenerate the draw solution and produce clean finished water. Some of the earlier developments in FO technology used a draw solution of thermally unstable ammonium salts composed of ammonia and carbon dioxide [1]. RO was also used as a method for separating the clean water from the diluted FO draw solution. These methods did not produce satisfactory performance in terms of the final product water quality.

In this project, MD was used as the separation method for recovering the clean water from the draw solution as well as regenerating the draw solution for reuse by the FO process. MD is an exciting and novel water treatment technology that has garnered attention for potential application in the water and wastewater industries for water reuse and desalination [2]. MD is a thermally driven process that achieves separation via phase change through a vapor pressure gradient that is established across a membrane by the temperature differential between the feed water heated relative to the surrounding environment. The heated feed water evaporates (leaving behind non-volatile solutes), is transported across the MD

membrane, and collected on the permeate side by condensation on a cooler surface (receiving water or condenser plate). The membrane must possess several essential characteristics to establish and maintain the vapor–liquid equilibrium between the feed and condensing sides of the membrane: 1) be porous; 2) be hydrophobic so as not to be wetted by the liquids during operation; and 3) not allow condensation within the pores. Figure 1-2 is a conceptual illustration of this water transport through the cross-section of an MD membrane.

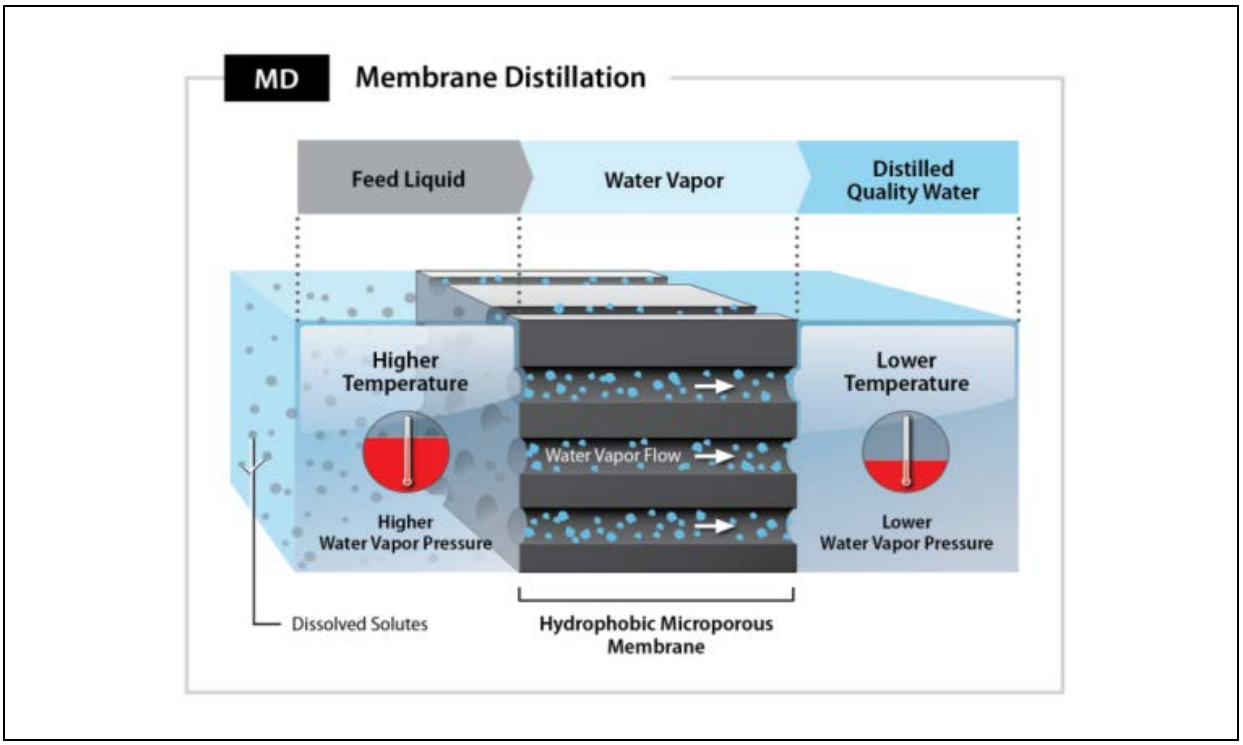

Figure 1-2. Membrane distillation process

MD offers several chief benefits. First, it has a drastically higher salt rejection rate compared to current RO technology. Relative to the nominal RO salt rejection rate of 99.8%, MD can achieve 99.99% or higher rejection because of the distillation-based mechanism. This advantage also allows MD to handle feed waters having much higher TDS levels; consequently, overall MD water recovery can be much higher than that in RO. Second, MD is a low-pressure membrane process, meaning that polymeric materials can be used so that construction cost is significantly reduced. The most common MD membrane materials are poly(vinylidene fluoride) (PVDF), poly(tetrafluoroethylene) (PTFE), and polypropylene (PP). All of these materials are mass produced and used for building membranes in various industries, which provides the economy of scale in terms of the core material. As in the FO process, the pipes can be made of mostly CPVC for MD as well.

The final major advantage of MD is the feasibility of using low-grade waste heat as the energy source to drive water purification. Most (~60%) unrecovered industrial waste heat is considered low grade (i.e., T < 450 °F) [3]. The modest temperatures to which water is heated enables separation (~140 °F), making

MD an ideal candidate for waste heat recovery with the added benefit of significantly improving water resource utilization.

The hybrid membrane-based system developed and tested in this project takes advantage of two promising technologies while addressing the technical hurdle of each by combining them. FO exploits the natural tendency of water to migrate across a semi-permeable membrane into a solution of higher osmotic pressure (i.e., draw solution). The diluted draw solution then flows into the MD unit where a temperature differential induces a water phase change across the hydrophobic membrane, resulting in distilled-quality product water. The draw solution is reconcentrated by the MD component and recycled back to the FO unit for reuse.

The coupling of these two technologies neatly addresses the current shortcomings of using either as a stand-alone treatment: In MD, volatile organic compounds (VOCs) and surfactants present in industrial waters limit its removal efficiency and process performance; MD is best used when the feed consists mainly of dissolved solids with little organic content. In FO, a draw solution that produces high osmotic pressure but is still easily separable is a major challenge that limits the applicability of this low-energy membrane process. Combining these two technologies such that the FO draw solution is a salt solution that is continually regenerated in the MD unit allows the FO membrane to not only serve as a barrier to feed-side organics/surfactants but also provide a very well-controlled feed to the MD unit. The combination also allows the use of a high osmotic-pressure FO draw solution for treating high-TDS feeds.

Potential Technology Applications and Impacts

The dual-barrier, hybrid FO-MD membrane-based process provides a water treatment solution where current state-of-the-art RO technology cannot be used. The hybrid FO-MD technology can be applied to various industries in the following ways:

- Reduction of liquid waste or discharge volume (e.g., before final brine disposal)
- Reuse of highly contaminated industrial wastewater
- Significant increase in overall water recovery as an add-on system that can either replace thermal evaporation systems or supplement the existing water treatment train
- Beneficial utilization of waste heat from various industrial sources

The key to the hybrid FO-MD technology's approach is the use of waste heat as the major energy source for water purification, which is why this approach is particularly suited for manufacturing settings. A recent study on the state of waste heat practices in U.S. industries found that one of the major barriers to waste heat recovery was the lack of a viable end use for the energy recovery [3]. However, because virtually all industrial facilities have water requirements; implementation of the hybrid FO-MD process to simultaneously improve water reuse while recovering energy is therefore a viable end use for the energy recovery that could be done across multiple industries with excess waste heat. This is an elegant solution to two problems: the simultaneous tapping of a currently underused energy source and improving industrial water reuse efficiency.

Commercialization Plan

The trailer-mounted FO-MD pilot system developed in this project can be deployed to actual industrial sites where its benefits can be demonstrated onsite. Because it is the first of its kind, and given the conservative, risk-adverse nature of the water industry, it is necessary to demonstrate the feasibility of the FO-MD process at more locations with different types of contaminated waters. Currently, various groups studying deep-well, high-TDS brines and oil production and hydraulic fracturing sites that could benefit from this technology are interested in the pilot prototype. Consulting engineers who can provide technical information about this process have also shown interest, and they look forward to the accumulation of more process-relevant data on the technology.

The current generations of FO and MD membranes and modules used in this project are good starting points for piloting and scaling up efforts on the path to full-scale plants. Their membrane chemistry and module design have been proven to be compatible with the extreme conditions necessary for industrial operation. However, the FO and MD membranes and modules still require significant improvements before a full-scale plant can be designed and built. Though there has been an unexpected downturn in FO and MD membrane producers over the last few years, the remaining manufacturers are still actively working to improve their membrane products. Only with better membranes and modules and more pilot data can a more efficient, overall FO-MD system be designed to maximize plant performance in terms of circulation flow and heat management.

2. BACKGROUND

Identification and Significance of Technology Need

Energy and water are mutually dependent resources that are critical for the development and economic stability of the United States. Specifically, energy production requires large volumes of water, and water treatment and distribution requires large amounts of energy. This relationship is often referred to as the water–energy nexus. For example, in 2009, USGS reported thermoelectric energy production requires 143,000 million gallons of water per day, accounting for 49% of all freshwater withdrawals [4]. In turn, an estimated 4% of the U.S. power production is used to pump and treat water, and 75% of the cost of municipal water processing and distribution is electricity. Additionally, water required for oil and natural gas extraction through hydraulic fracturing is increasing and critical to ensure the growth of domestic energy supplies.

It is important to understand the water–energy relationship and the use of each resource to help manage them as they inevitably become limited. Growing population and climate change will result in increased demand on these limited resources, which are not sustainable at present use levels. According to the 2011 National Energy Policy, population and economic growth will require an additional 393,000 MW of new electrical capacity. This anticipated demand will require an additional 1,300 to 1,900 new power plants and their associated water demands by 2020. In 2005, an estimated 31% of the total freshwater withdrawals were used for agricultural demands [4], and this will increase with population growth. These factors will force other sectors to adapt to a water-limited environment or discontinue operation. Specifically, the industrial and mining sectors used approximately 4% of the total freshwater withdrawals in 2005 [4] but will be forced in the foreseeable future to increase output with limited or reduced water resources. To ensure U.S. economic viability, it is therefore critical that the industrial sector addresses this issue by mindfully and effectively managing available resources and adopting new technologies enabling cost-effective, energy-efficient water reuse.

One of the first steps in water use management is understanding the uses and quality requirements as well as the resulting wastewater characteristics. In most industrial operations, the three primary uses of water are for cooling, boiler feed for steam production, and process requirements. As water proceeds through the industrial use cycle, the quality is altered by the addition of soluble and insoluble constituents as well as a temperature increase. The typical approach has been to use water once-through and treat it to discharge quality prior to returning it to a receiving water body. This approach is non-sustainable in the projected water-limited environment of the future. There exists a critical need for a reliable energy-efficient and cost-effective water reuse technology for the U.S. industrial sector.

The current approach to wastewater treatment in the industrial sector is typically to treat the water to the quality standards for direct discharge to a receiving water body. This is accomplished through a series of physical/chemical and biological wastewater treatment unit processes. The typical system includes primary treatment for the removal of free oils and solids and secondary biological treatment to remove biodegradable organics and nutrients. If water reuse is desired, the water must be further treated to meet

the requirements of the intended use (e.g., cooling tower makeup, boiler feed, process). The removal of dissolved constituents not accomplished by conventional treatment can be done by a variety of demineralization technologies that include: 1) distillation; 2) reverse osmosis (RO); 3) electrodialysis; 4) ion exchange; and 5) freezing processes. Of these technologies, RO has been the most widely used in the industrial sector for water reuse applications and is considered state-of-the-art.

RO is a membrane separation process that utilizes pressure to force water through a semi-permeable membrane and retains larger molecules and dissolved solutes/ions. Typical energy requirements for RO desalination depends directly on the feed water TDS. Seawater can range between 3–7 kWh/m^3 and brackish water may require 0.5–3 kWh/m^3. Extensive pre-treatment of industrial wastewaters is also required for RO to be successful. Residual dissolved organics and solids can degrade and foul the RO membrane, rendering them ineffective.

Once the feed water TDS increases to higher than 50,000 ppm, the RO process reaches the limit of technical and economic feasibility. There are many issues that need to be solved simultaneously, such as pipe and pressure-vessel materials compatible with both high-pressure and high-salinity process conditions in addition to the membranes. Furthermore, the high RO feed pressure required for higher-TDS water treatment would make it impossible for current Energy Recovery Devices to operate.

Energy derived as waste heat from industrial facilities and chemical fuels from emissions are an untapped resource that could be exploited. Through various studies, the U.S. DOE has identified 1,831 trillion BTUs of industrial waste heat and 1,400 trillion BTUs of energy from chemical fuel from air emissions [5, 6]. The hybrid membrane process taps into this underutilized resource by using industrial waste heat to drive a water treatment process.

Combining the need for water desalination technology that can process very high TDS and the availability of low-grade heat, the FO-MD process tested in this project is one of the promising technologies. It is designed to treat high-TDS water while using low pressure and temperature so that low-cost material can be used for the bulk of the construction. There are many areas in the industrial and manufacturing sectors where high-TDS brine is produced as a part of the overall process or from water treatment for discharge. Below is a summary of the 2015 Global Water Intelligence report that was focused on the demands of eight major water-using industries [7]:

Most of these industries historically have not employed water reuse facilities and they used to rely on outside contractors to “haul off” the brine once the wastewater reaches concentration that cannot be treated further by current technologies. Recent reports on industrial water have found that the water scarcity and sustainability cannot be ignored and embracing new water reuse technology can benefit the bottom line. It is expected that the industrial wastewater reuse will grow about 11.4% in the next five years and reach a total market value of $11,963bn by 2025.

In the petrochemical industry, water consumption in refineries is actually more than crude oil. The steam, cooling and process applications require highly desalinated water, but the raw water sources are becoming more challenging as the new resources may not always be found on land. This means that

seawater desalination is going to be an increasingly important technology for the refinery sector, and that greater emphasis will be put on reuse technologies. Despite the recent dip in oil prices, the market is set to double to $4.5 billion in 2020, depending on the recovery of oil prices. This will create opportunities for desalination technologies because of the need for enhanced oil recovery methods (EOR), and also to deal with challenging wastewater streams for zero liquid discharge.

Power generation is the largest industrial consumer of water, and the customers are putting a growing emphasis on the consistency, reliability and specification of their cooling water and ultrapure water systems. As more power is needed in the future, this sector is expected to use more desalination and water reuse technologies, including reverse osmosis, ion exchange (IX), low pressure membranes, electrodeionization (EDI) and evaporators.

In the **food and beverage industry**, most companies have already made commitments to reduce their water consumption per unit of product. Water reuse is an important part of the strategy for achieving this. In developed markets, emerging concerns about trace contaminants such as pharmaceutical by-products and personal care products making their way into the product have led to greater interest and use of desalination technologies on the process water side. Another important aspect about the food and beverage industry is that anaerobic digester technology combined with membranes is producing biogas which can help reducing the overall energy cost.

For the **pharmaceutical industry**, water reuse has not been on the agenda for process water. Drug companies remain a significant market for specialist desalination systems as they look to produce ultrapure and infection-free water for medicine manufacture. However, for the utilities and other les critical uses, there is interest in recycling water in the process. The highest quality water is for injections, which may be treated with activated carbon, ion exchange, electrodeionization, UV disinfection, ultrafiltration (UF), reverse osmosis and distillation before it is used in the product.

Microelectronics is an important market for water desalination systems and the challenges are getting greater as devices get smaller and the purity of the water required thus increases. In terms of water reuse, the industry has relatively conservative attitudes towards recycling water for ultrapure water applications, but wastewater is treated and reused for cooling and other less critical purposes. A chip maker in Texas for example, is keenly aware of the impacts of the droughts and started to make plans for providing water from diverse sources, such as its own well. Besides semiconductors, the increasing complexity of flat panel displays (FPD) and photovoltaics (PV) devices will create demand for even higher purity water. It is believed that short product cycles, together with the pressures on water resources in the key manufacturing markets will ensure strong demand for ultrapure water and water reuse technologies.

Historically the **pulp and paper industry** has had little need for desalination and reuse but they are moving towards recycling. As the production cost is rises along with higher water costs, there will be a greater interest in water efficiency, since pulp and paper industries consume a significant amount of water. In addition, the new generation of efficient boilers used in the industry require higher quality feedwater and this too will lead to greater demand for water desalination treatment technologies.

Water is becoming a significant issue for the **mining industry**; companies have to compete for water resources, but at the same time, they generate a high volume of wastewater. In addition to the water volume, many companies now invest to produce a high quality effluent, which can exceed the basic regulatory requirements. Membranes have begun to offer a solution for treating tailings water, while there is room for improvement in removing cyanides from waste- water following the processing of gold ore.

By tapping into currently underutilized industrial waste heat, the FO-MD hybrid membrane process developed in this project is viewed as a water treatment technology that can enable cost-effective water reuse, thereby ensuring U.S. economic viability. As population growth and associated factors stress water availability, the ability of U.S. manufacturers to move towards sustainable, efficient, and low-cost water management practices is crucial to ensuring their status as global competitors.

Project Goals and Objectives

The goal of the project was to develop and demonstrate an advanced water treatment and reuse system that synergistically combines the emerging membrane-based technologies of forward osmosis (FO) and membrane distillation (MD) to improve the energy efficiency associated with industrial wastewater treatment and reuse in the U.S. manufacturing sector by at least 50% relative to current technology. Additionally, FO-MD technology can potentially enable the U.S. manufacturing sector to become more water sustainable, reduce wastewater discharges towards zero liquid discharge (ZLD), reduce greenhouse gas emissions, and beneficially utilize waste heat.

The FO-MD hybrid membrane system takes advantage of two promising technologies while addressing the technical hurdle of each by combining them.

Specific project objectives were:

- FO process optimization for treating various industrial wastewaters
- Development of FO draw solution suitable for MD regeneration
- Development of bench-scale, integrated FO-MD system
- Process optimization of bench, integrated FO-MD system
- Development and validation of integrated FO-MD process model
- Construction and field demonstration of a prototype, integrated FO-MD system in an industrial water treatment facility

To achieve the overall project goal, the project team included an academic partner (Duke University) and an industrial partner (Veolia Water Technologies). The university partner has technical expertise in MD membrane development. The industrial partner is the leading global provider of water treatment technologies with extensive commercial wastewater treatment and engineering as well as operating experience. The prime recipient (RTI International) is a non-profit research institution specializing in translational technology development from bench-scale through commercialization with the mission of turning knowledge into practice.

The hybrid FO-MD membrane system takes advantage of two promising technologies while addressing the technical hurdle of each by combining them. FO exploits the natural tendency of water to migrate across a semi-permeable membrane into a solution of higher osmotic pressure (i.e., draw solution). The diluted draw solution then flows into the MD unit where a temperature differential induces a water phase-change across the hydrophobic membrane, resulting in distilled-quality product water. The draw solution is reconcentrated by the MD component and recycled back to the FO unit for reuse.

Project Approach

Given the challenges, needs, and barriers associated with industrial water reuse, the FO-MD technology was designed to be robust enough to handle a variety of potential waste streams from different processes, use minimal energy to achieve desired treatment levels, and require low maintenance to provide high operational availability. In addition, the process solution was made modular to be scalable to a wide range of treatment volumes. The approach herein met each of these criteria by using low-pressure membrane technology and available waste heat as the major energy source to produce high-quality water for reuse in industrial settings. Figure 2-1 presents a schematic of the project's process technology project, which is designed to take a minimally treated wastewater effluent stream, pass it through a hybrid FO-MD membrane system to produce distilled-quality water.

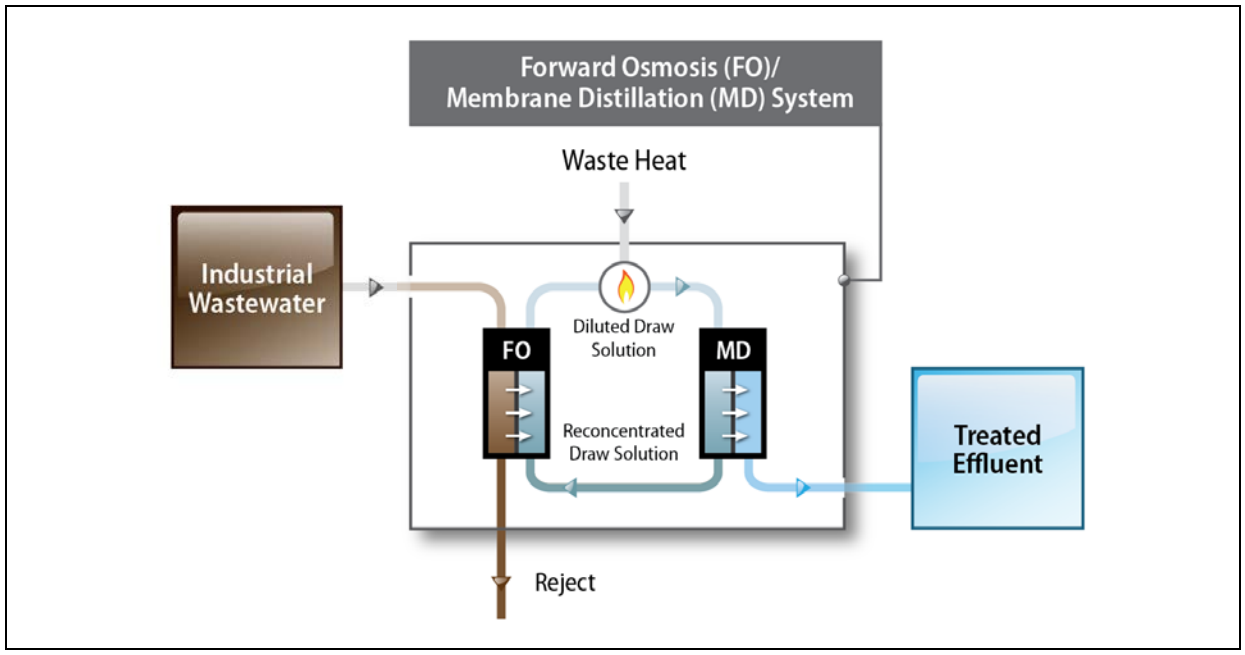

Figure 2-1. Overall process diagram for FO and MD hybrid membrane system

The project approach taken was as follows:

1. Identification of optimum FO and MD membranes (1 mL/min)

   Available FO and MD membranes were obtained from multiple manufacturers and tested at the laboratory scale for water flux, salt rejection, and fouling tendencies. For the most promising FO membrane candidates downselected from the laboratory results, several larger-scale, 4-in. FO

membrane elements were evaluated. For the MD, there was an even smaller number of manufacturers currently producing membranes of suitable scale for pilot testing. With guidance from the project's industrial partner, a feasible membrane manufacturer was identified for providing the MD membrane modules for further testing at larger scale.

2. Performance testing in bench-scale unit (50 gallons per day)

   The FO and MD membranes having the most promising water separation properties were tested at a larger scale using a 50-gal/day bench-scale test unit. A first-production, plate-and-frame FO membrane module with 0.21 m^2 of membrane area was used initially, but later a 4-in.-dia., spiral-wound FO element with approximately 3 m^2 (32 ft^2) of membrane surface area and at a more mature production stage was tested. For MD, a 2.5 in. × 8 in. hollow-fiber unit with PP membrane was tested at bench scale.

3. Modelling of FO-MD performance

   We developed in-house modeling capabilities to simulate and understand the mass balances and heat transfer in the FO and MD modules and the associated hybrid process. The project's university partner developed a model to track the permeation of volatile organic compounds (VOCs) of different partial pressure in the MD process. They used laboratory MD membrane data to identify the most likely organic species from the raw water that can end up in the final MD permeate.

4. FO-MD performance in pilot-scale prototype testing (500 gallons per day)

   All the base knowledge acquired in the early stages of this project culminated into a large-scale pilot for the project's final phase. This is one of the largest-scale FO-MD pilot in existence. Detailed performance was monitored using multiple sensors on the pilot skid. At this pilot scale using full-size membrane modules, a true understanding of the water quality that can be obtained from high-TDS wastewaters was finally possible.

Relevant Project Team Qualifications

The project work was executed by three organizations who have the capabilities as a team to cover the entire water technology development chain from research through commercialization:

- RTI International (prime recipient)
- Duke University (academic partner)
- Veolia Water Technologies (industrial partner)

Roles of Project Team Members

RTI International

The project lead was RTI, an independent, non-profit research institute specializing in translational clean energy and environmental R&D technology development from the bench scale through commercialization. RTI has a proven track record of working with the U.S. DOE and industrial partners to develop transformational concepts, validate technical feasibility, develop innovative process designs, and move technologies from concept to commercialization. RTI develops innovative technologies related

to the production and use of clean energy. Equipped with specialized and custom-designed reactors and testing equipment, RTI's Energy Technology Division (ETD) performs work for federal agencies (primarily DOE) and commercial clients. ETD's core strengths include materials development and testing, process engineering and evaluation (e.g., including techno-economic analyses of novel systems), and field testing of process units.

RTI's major technical roles were

- FO and MD membrane benchmarking and performance evaluation
- FO process development, evaluation, and optimization
- Bench-scale parametric studies and extended performance testing of the integrated, hybrid FO-MD process under industrially relevant conditions
- Process modeling, development, and integration
- Field testing of a larger prototype, integrated FO-MD test unit
- Techno-economic and environmental evaluations

Duke University

With active programs in membrane-based water treatment, drinking water technology, innovative wastewater solutions, and nanotechnology, Duke University provided expertise on the MD technology component in the hybrid FO-MD water treatment process and worked on advanced MD membrane development. Within the membrane science area, Duke has expertise in membrane fabrication, systems development/optimization, and cost modeling.

Duke's project roles were

- Hydrophobic, inorganic (ceramic) and omniphobic hierarchal MD membrane development, characterization, screening, and optimization
- Membrane fouling assessment (i.e., autopsy) of membranes used in the MD, FO, and anaerobic membrane bioreactor (AnMBR) operations
- MD process modeling and analysis support

Veolia Water Technologies

Veolia is a global provider of comprehensive water treatment technology and services. Veolia's capabilities and expertise range from economic studies, engineering, testing, and design to project management, construction, and project execution. Veolia is also active in water treatment R&D with a critical focus on integrating innovative, high-performance, cost-effective technical solutions into their current equipment and service offerings. Veolia's major project roles were

- Advanced MD membrane development support
- Provider of AnMBR technology initially considered as pretreatment to the hybrid FO-MD process

- FO and MD process development support by providing in-house and real-world expertise/knowledge in membrane-based water treatment processes
- Process engineering design and integration support
- Field-testing support for prototype, integrated FO-MD test unit, including assistance with prototype design and host-site selection/preparation
- Process techno-economic, environmental impact, and water market evaluation support

Veolia was also the project's primary cost-share partner, contributing all personnel labor costs, travel costs, fringe benefits, and indirect costs associated with their project activities as in-kind cost share.

3. EXPERIMENTAL METHODS

Laboratory-Scale Membrane Performance Testing and Characterization

Forward Osmosis

FO Water Test Bed

Laboratory performance screening and evaluation of FO membranes and different FO draw solutions were conducted on RTI's laboratory-scale FO water test-bed system (Figure 3-1). This system consisted of a rectangular, stainless-steel SEPA CF membrane test cell (Sterlitech Corporation, Kent, WA) that was designed for handling flat-sheet FO membrane coupons and had an effective membrane permeation area of 140 cm^2. The test cell had two 75-mil-high flow channels of the same dimensions, one on the feed side and the other on the permeate side. An aqueous feed was circulated through the flow channel on the feed side of the cell, and an osmotic draw solution was circulated through the permeate-side flow channel. Water from the feed was drawn through the membrane via the transmembrane osmotic pressure difference induced by the high-osmotic-pressure draw solution. Two low-pressure, liquid diaphragm pumps (Liquiport® NF series, KNF Neuberger, Inc., Trenton, NJ) were used to pump and circulate the feed and draw solutions through the respective sides of the membrane test cell. The FO feed and draw solutions were contained in 5-gallon polycarbonate reservoir vessels that sat on 20-kg-capacity balances (Model PGL-20001; Adam Equipment, Oxford, CT) with 0.1-g readability. The balances were used to monitor the mass changes in the feed and draw-solution reservoirs as a result of water permeation through the FO membrane. As water permeated the membrane from the feed into the draw solution, the weight of the draw solution increased, while weight of the feed reservoir decreased. Both feed and draw-solution balances were connected to an online data acquisition computer for recording weight changes in the reservoirs. Additionally, the feed-solution ionic conductivity during testing was monitored and measured with a conductivity meter (Model HQ40d; Hach Company, Loveland, CO), while the draw-solution ionic conductivity was measured only at the beginning and end of each experiment. Measured changes in conductivity were used to determine the reverse flow rate of draw-solute from the draw to the feed side.

To monitor stream flow rates and pressures into the membrane cell, in-line rotameters and pressure gauges, respectively, were installed downstream of the diaphragm pumps in the FO water test-bed apparatus. Two pressure gauges were also located in the effluent streams exiting the test cell. The pressure gauges were for monitoring purposes only because FO is a low-pressure process needing to operate only at pressures sufficient to overcome pressure drops in the system lines and the test cell. A metering valve was also installed in the effluent FO concentrate line to provide a degree of flow or backpressure control on this stream. Temperatures of the feed and draw solutions were monitored by the temperature sensor integrated into the probes used to measure conductivity of these solutions.

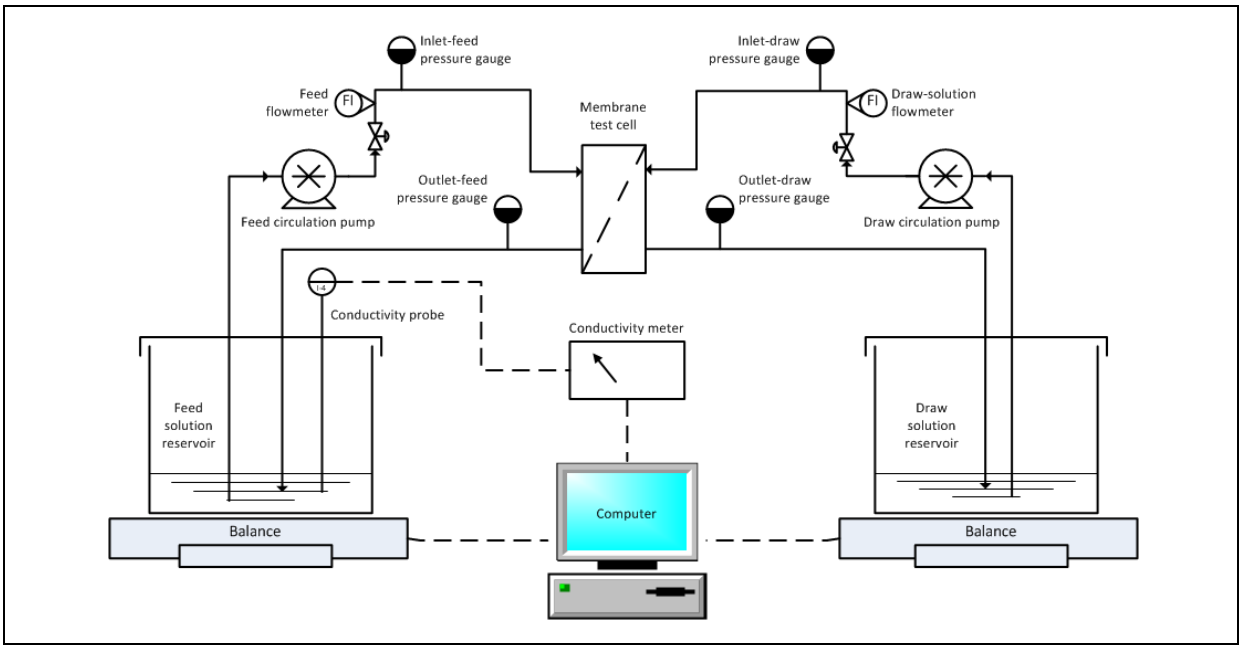

Figure 3-1. Schematic of RTI's bench-scale FO water test-bed apparatus

The bench-scale FO water test-bed system was also set up to enable membrane testing in "reverse-osmosis (RO)" mode, in which the aqueous feed flowing into the feed side of the test cell is pressurized. To allow for RO-mode testing, a high-pressure, three-piston pump head [Hydra-Cell® model #M03SASGSNSCA; Wanner Engineering, Inc., Minneapolis, MN) with maximum flow capacity of 6.8 L/min (1.8 gal/min) was incorporated into the bench water test-bed system. The high-pressure pump head was powered by a 1.5-HP motor that was operated using a Variable Frequency Drive (VFD) controller. At the high-pressure pump outlet, a pressure relief valve was installed and set to trigger and bypass the membrane test cell at 450 psig. A needle valve was installed to control the test-cell pressure after the high-pressure pump discharge. The liquid exiting these valves was plumbed to return directly to the feed reservoir. In RO mode, the high-pressure pump replaced the low-pressure, feed circulation pump used in FO mode, and the draw-side circulation pump and the feed- and draw-side balances were also not needed. Feed pressures used in the RO testing mode typically ranged from 15 psig to 70 psig and, in some tests, went as high as 150 psig. The RO-mode permeate flow rate was measured by timing the amount of aqueous permeate collected in a graduated cylinder. Additionally, as an option for testing smaller FO membrane coupons in RO mode, a smaller (4.7-cm-dia.), stainless-steel filter holder (Model XX4404700; EMD Millipore Corporation, Billerica, MA) was used in place of the larger SEPA CF test cell.

Membrane Installation into Test Cell. The semi-permeable membranes for FO usually comprise a dense, non-porous active (selective) layer on top of a non-selective porous support layer or mesh support layer. In FO testing, a membrane coupon was loaded into the SEPA CF test cell with its active separation layer contacting the feed flow and its support layer facing the draw-solution flow. A 25-mil shim was also used in the feed and draw sides of the test cell to reduce the flow channel height and, thus, increase the cross-flow velocity to as close to 24-25 cm/s for the experimental feed- and draw-side recirculation flow rate range of 1.7-1.8 L/min used. (A cross-flow velocity of 25 cm/s had been recommended as a testing

standard by Cath et al. [8].) A diamond mesh spacer (e.g., 17 mil) was also used in the feed and draw sides of the test cell to promote flow distribution in the flow channels. An interior leak-proof seal between the membrane and the test cell was provided by a double (inner and outer) Viton O-ring design on the feed side. The test cell loaded with the membrane was then inserted into a hydraulically pressurized cell holder that clamped the halves of the test cell together to maintain the leak-free cell seal during testing. In the RO testing mode, the membrane orientation used was the same as that used in the FO mode. Additionally, the bench water test-bed unit was also operated in "pressure-retarded osmosis (PRO)" mode in which the FO membrane was flipped over and installed into the test cell with its active separation layer directly facing the *draw*-solution side, instead of the feed side.

Before testing, FO membrane samples were generally soaked overnight or longer in deionized (DI) water to fully hydrate (saturate) them with water. This hydration step was particularly important for membranes that were received dry because these membranes were shipped in a glycerin preservative. Soaking these membranes in DI water extracted the glycerin and replaced it with water in the membrane structure. Moist (wet) FO membranes, though usually still well hydrated when received, were also rinsed and stored back wet in a small amount of DI water. Once wet, however, all FO membranes were kept and stored moist to prevent them from drying out and possibly changing (e.g., densifying) the starting membrane structure.

Performance Testing

The FO water separation properties of membranes were determined in the FO operating mode in the laboratory-scale water test-bed system. The FO membrane split the feed stream into (i) a brine (non-permeate) effluent depleted of water and more concentrated in salts (solutes) or TDS and (ii) a diluted draw effluent containing the permeated water.

Baseline FO membrane properties were first determined with DI water feed and different single-component draw solutions prepared from four types of inorganic salts (NaCl, KCl, $MgCl_2$, and $CaCl_2$) dissolved in water. The draw-salt concentrations used varied from 0.25-5 M for NaCl and from 0.25-4 M for KCl, $MgCl_2$, and $CaCl_2$. Depending on salt type, these draw-concentration ranges gave draw-solution osmotic pressures ranging from 6.7 atm up to 789 atm based on the electrolyte thermodynamics software from OLI Systems, Inc. (Cedar Knolls, NJ). Because osmotic pressure of the DI water feed is zero, the water permeation in FO mode was driven entirely by the osmotic-pressure gradient created by the draw solution. The temperatures of the feed and draw solutions were kept at room temperature (23 ± 1 °C) in these tests.

To evaluate the effect of feed salt concentration [i.e., feed total dissolved solids (TDS) content] on FO water flux, additional tests were performed on one promising membrane with synthetic, simple aqueous saline feeds and 1, 3, and, in one test series, 5 M NaCl draw solutions at room temperature. The feeds were aqueous NaCl, KCl, $MgCl_2$, and $CaCl_2$ solutions with salt content in the range of 500-12,000 mg/L, which encompasses the representative TDS content typically found in conventional industrial wastewater effluents. For example, the TDS content is in the region of 1,600 mg/L for refinery wastewater and 900-1,300 mg/L for pulp and paper. For comparison, the TDS level is 2,000-5,000 mg/L for brackish water and 32,000-35,000 mg/L for seawater.

Membranes exhibiting an attractive combination of baseline FO water separation properties were further evaluated at room temperature with an actual, aqueous effluent generated from our bench-scale anaerobic membrane bioreactor (AnMBR) as the FO feed. This aqueous AnMBR effluent contained small amounts of organic and suspended/dissolved solids contaminants. Representative contaminant concentrations in the AnMBR effluent were 120-140 mg/L COD (chemical oxygen demand, which is a measure of organic content in aqueous streams), 0-2 mg/L TSS (total suspended solids), and 2.8-3 mS/cm conductivity due to the presence of dissolved species. Testing of the FO membranes with the AnMBR effluent as feed was conducted with 3 M NaCl draw solution as extended runs having a duration of 3-4.5 days. The test runs were "semi-continuous"; that is, they were run continuously during the work day, stopped at the end of the work day, and restarted the next work day. Total cumulative time-on-stream achieved varied from 25 h to 36 h. To maintain a stable draw-side osmotic pressure, the draw-solution concentration was kept constant throughout the test by dosing with small quantities of a 5 M NaCl draw solution with a peristaltic pump set to a pre-determined pump flow rate. On the feed side, the FO feed reservoir was diluted every 1-2 h with DI water to keep the feed-side conductivity and, in turn, the original level of feed contaminants as constant as possible.

Industrial wastewaters were also used to further evaluate downselected FO membranes for separation performance and fouling susceptibility in test runs on the laboratory-scale FO water test-bed system (as well as the bench, integrated FO-MD system described later below). These tests with industrial wastewater samples as feed were performed at room temperature using draw solutions having suitable NaCl solute concentrations for handling the feed characteristics. Three real wastewater samples were sourced from two industrial facilities. One sample came from a location designated as Site 1. The other two samples were sourced from a location designated as Site 2. In general, the Site 1 wastewater sample had high alkalinity and moderately high TDS (~46,000 mg/L) that consisted primarily of high Na and Cl content and significant levels of Mg, Ca, carbonate, and sulfate. Because of these characteristics, the Site 1 wastewater was deemed to have very high scaling potential. On the other hand, the Site 2 wastewater samples had lower alkalinity and lower TDS (~2,500 mg/L) but contained potential foulants and/or contaminant challenges such as silica, hydrocarbon organics (e.g., aromatics, phenolics, ketones), and free oil and grease.

The FO water permeation flux J_w [L/(m^2·h)] through the membrane was calculated as

$$J_w = \frac{\Delta V_w}{A_m \Delta t} = \frac{(\Delta m_w/\rho)}{A_m \Delta t} \quad [1]$$

where ΔV_w is the volume change (L) in the feed- or draw-solution reservoir over a given time period Δt (h) and A_m is the effective membrane permeation area (m^2). As indicated in Eq. 1, ΔV_w is related to the mass change Δm_w in the feed- or draw-solution reservoir, as experimentally measured by the system balances, through the solution density ρ (kg/L). It is noted that the water flux computed from the feed-side data should be the same as the flux determined from the draw-side data due to mass conservation (i.e., the permeating water leaves the feed reservoir and goes into the draw-solution reservoir). Within the precision of the mass measurements, the calculated feed- and draw-based water flux

values were found to be in very good agreement. Thus, we took the average of the feed- and draw-based values to get the FO water fluxes reported in Section 4 below.

The reverse-salt flux J_s [mol/(m^2·h)] from the draw solution to the feed was computed from the increase in mass of salt $\Delta m_{s,F}$ (g) in the feed reservoir over the time period Δt as

$$J_s = \frac{(\Delta m_{s,F}/M_s)}{A_m \Delta t} = \frac{\Delta(C_{s,F} V_F)}{M_s A_m \Delta t} \quad [2]$$

where M_s is the molecular weight (g/mol) of the salt. As also shown in Eq. 2, $\Delta m_{s,F}$ is related to the change in feed-side salt concentration by $\Delta(C_{s,F} V_F)$ over the Δt time period, where $C_{s,F}$ is the feed-side salt concentration (g/L) and V_F is the volume (L) of the feed solution. The feed-side salt concentration $C_{s,F}$ values at the start and end of the Δt time period were obtained from the associated feed-side conductivity measurements by using a conductivity–concentration calibration curve for an aqueous solution of a single salt (e.g., NaCl). It should be noted that draw-side salt concentration changes were not used because the draw-side conductivity changes were typically much smaller relative to those on the feed side and, hence, less accurate for determining J_s. The higher salt content on the draw side, coupled with the small dilution effect of a small water permeate flux into the much larger draw-solution reservoir volume, usually masked the resolution of the draw conductivity changes.

The draw-salt rejection R_{FO} (%) of the FO membrane was determined as

$$R_{FO} = 100\left(1 - \frac{\left(\left(\Delta m_{s,F}/M_s\right)/\Delta V_w\right)}{C_{D,0}}\right) \quad [3]$$

where $\left[\left(\Delta m_{s,F}/M_s\right)/\Delta V_w\right]$ represents the moles of draw salt transferred to the feed divided by the volume of permeated water and $C_{D,0}$ is the starting draw-solution concentration (mol/L).

Determination of Intrinsic Membrane Characteristics

The intrinsic membrane characteristic parameters—A, B, and S—of the FO membranes samples are membrane mass-transport properties and were determined as part of their baseline performance evaluation. The parameters A and B represent the intrinsic, pure water permeability [L/(m^2·h·bar)] and the salt permeability [L/(m^2·h)], respectively, of the membrane's active separation layer. The parameter A can also be referred to as the membrane's "hydraulic water permeability" because it is obtained by testing the membrane in RO mode. The membrane characteristic S represents the structural parameter of the membrane support layer. It characterizes the average distance traveled by a draw-solute molecule in the support layer as it diffuses from the bulk draw solution to the membrane active layer. The parameter S (μm) is thus a high-level measure of the extent of internal concentration polarization in osmotically driven processes such as FO and is defined to be

$$S = \frac{t\tau}{\varepsilon} \quad [4]$$

where t, τ, and ε represent the thickness, tortuosity, and porosity, respectively, of the membrane porous support layer. These intrinsic membrane characteristics were needed to support the FO modeling work described later in this section.

To determine their A values, the FO membranes examined in this project were loaded into the test cell with its active separation layer facing the feed side and tested in RO mode with pressurized DI water feed over a range of feed pressures, while keeping the permeate side at atmospheric pressure. The difference between these two pressures is the transmembrane pressure driving force for water permeation. The transmembrane pressure range investigated in RO mode was typically 15-70 psi (1-4.83 bars); for some lower-permeability membranes, though, the transmembrane pressure was raised to as high as 150 psi (10.3 bars). The intrinsic water permeability A was computed as

$$A = \frac{J_w^{RO}}{\Delta P} \quad [5]$$

where J_w^{RO} is the membrane water flux measured in RO mode and ΔP is the applied transmembrane pressure.

To determine the B values of the FO membranes, tests were performed in the PRO operating mode in which the FO membrane was installed into the test cell with its active separation layer directly facing the draw-solution side, instead of the feed side. Following one common procedure described in the literature (e.g., [9]), the PRO-mode tests were conducted at room temperature (23 °C) with DI water feed and aqueous 0.5 M and 1 M NaCl draw solutions as the standard PRO testing conditions. To observe membrane PRO-mode behavior over a broader range of draw concentrations, PRO-mode tests were also done using higher NaCl draw concentrations up to 3 M for several membranes. The membrane orientation used in the PRO mode allowed for better determination of the intrinsic salt permeability of the membrane's active separation layer by placing this layer in closest direct contact with the source of the salt, thereby minimizing interference from the membrane support layer on the measurement of B. The PRO-mode water and reverse draw-salt fluxes and the draw-salt rejection were calculated from the same equations used for the FO mode (Eqs. 1, 2, and 3). From the PRO permeation data, the salt permeability B of the membrane active layer was calculated as [9]:

$$B = \frac{J_s^{PRO}}{C_D exp\left(-\frac{J_w^{PRO}}{k}\right)} \quad [6]$$

where J_s^{PRO} and J_w^{PRO} are the measured PRO-mode salt and water fluxes, respectively, C_D is the draw concentration at the membrane active layer, and k is the mass transfer coefficient for the rectangular channel in the test cell. For our test cell, k was estimated from the feed flow rate, flow channel geometry, and solute type [10] to be 56.5 L/(m^2·h) for the NaCl draw solutions used in the PRO tests.

From the measured water and salt permeabilities, A and B, respectively, and the FO-mode water flux J_w obtained using DI water feed and a 1 M NaCl draw solution, the membrane support structural parameter S was then estimated according to Eq. 7 [8, 9]:

$$S = \frac{D_s}{J_w} ln\left(\frac{B + A\pi_{D,b}}{B + J_w + A\pi_{F,b}}\right) \quad [7]$$

where $\pi_{D,b}$ and $\pi_{F,b}$ are the bulk osmotic pressures (bar) of the draw and feed solutions, respectively, and D_s is the draw-solute diffusivity (m^2/s) in 1 M solution. For test condition using 1 M NaCl draw solution and DI water feed, $\pi_{D,b}$ is 46.77 atm (based on OLI electrolyte solution software), $\pi_{F,b}$ is zero, and D_s is 1.49×10^{-9} m^2/s.

Membrane Distillation

Figure 3-2 details the experimental configuration, including all connection lines, balances, pumps, heat exchangers, and data acquisition probes. The hydraulic integrity of the system was tested at temperatures ranging between 10-70 °C to ensure a leak-free state of operation under a range of temperatures and flow rates and was verified fully operational.

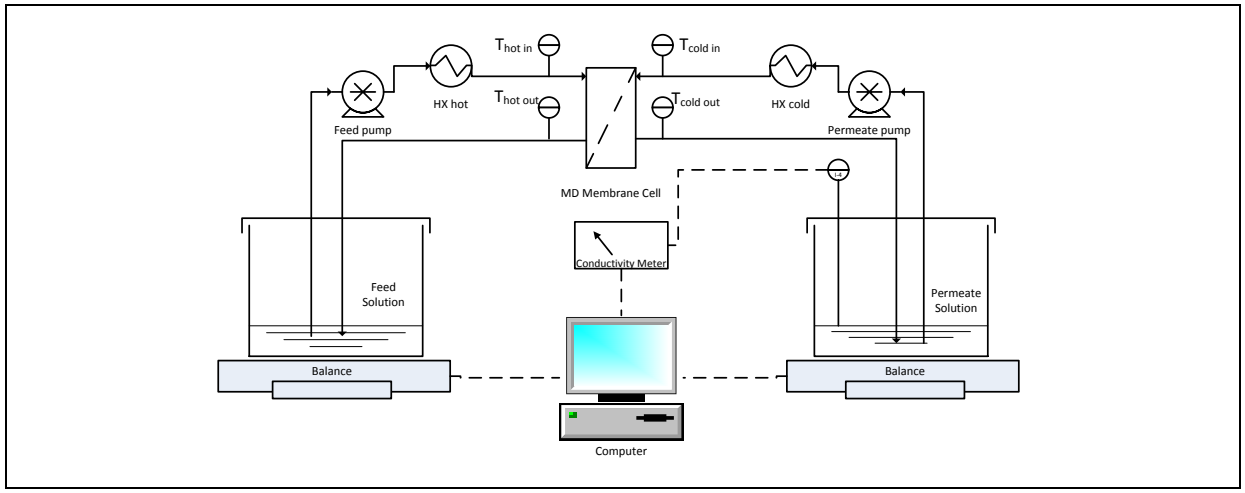

Figure 3-2. Schematic of RTI's MD test-bed water purification system. Temperature probes measure the water just entering and exiting the membrane module, and water flux is measured via weight change over time.

Hollow-Fiber MD Module Potting

To evaluate the performance of the hollow-fiber membranes in MD, the fibers were potted to make leakproof laboratory-scale modules. The potting used an epoxy or resin that bound to both the fibers as well as to the surrounding module housing, while leaving the original membrane structure intact. RTI examined a number of epoxy/resin combinations for the hollow fibers investigated and successfully developed repeatable potting methods for PP, PVDF, and PTFE hollow-fiber membranes. This expertise was used to fabricate modules to facilitate membrane-to-membrane comparison and allowed different membrane/module parameters, such as number of fibers, to be varied. A photograph of one RTI-potted hollow-fiber module is shown in Figure 3-3.

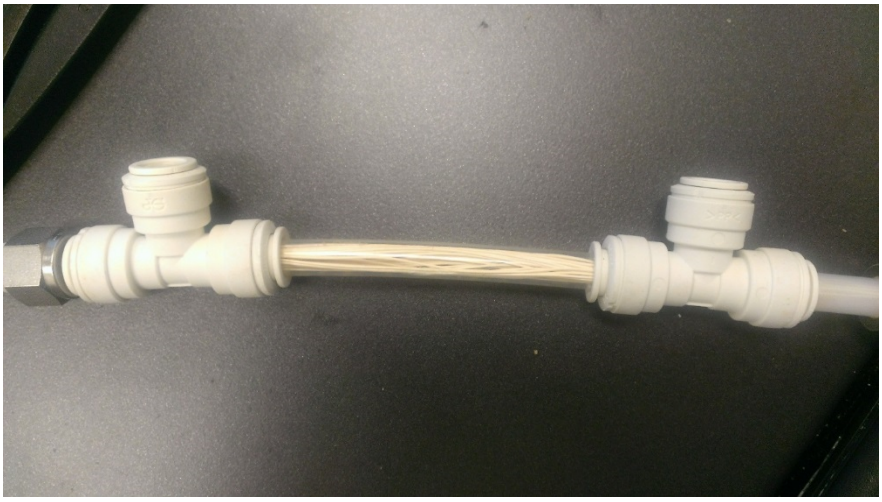

Figure 3-3. RTI-fabricated MD module containing polypropylene (PP) hollow-fiber membranes.

MD Membrane Baseline Performance Testing

Testing in the laboratory-scale MD water test-bed system was conducted on the various MD membranes to assess baseline water separation properties over a range of conditions. Flux and salt rejection tests for eight different polymeric membranes were completed. Polymeric materials evaluated included polytetrafluoroethylene (PTFE), polyvinylidene fluoride (PVDF), and polypropylene (PP)-based membrane materials with pore sizes ranging from 0.2 to 0.45 μm. Both flat-sheet and hollow-fiber module configurations were evaluated: six of the polymeric membranes were flat sheet samples, and two were hollow fibers. The active membrane surface area was 25 cm^2 for flat-sheet testing and 78 cm^2 for the hollow-fiber modules. The experimental tests measured the water flux at four feed NaCl salt concentrations (1, 2, 3, and 4 M) at inlet ΔT values of 20, 30, 40, 50 °C. All membranes exhibited a slight reduction in flux with increasing salt concentration; however, the reduction was markedly less that that typically seen in RO performance, and adequate values were recorded and sustained at TDS concentrations >250,000 mg/L, which is well above the RO threshold of 50,000 mg/L TDS. After a membrane coupon was loaded into the test cell with its active layer facing the feed side, the pumps were started and slowly increased until the flow velocity across the membrane reached 0.5 m/s.

MD Membrane Performance Testing

The MD membranes were also tested in a closed-loop, bench-scale DCMD setup to determine flux and rejection rates for the membranes at different feed solution concentrations. The feed solution was heated through a heat exchanger to the desired temperature, circulated through a flat-sheet membrane module, and fed back to the feed reservoir. The permeate stream was cooled with a heat exchanger to 20 °C, passed through the membrane module, and recovered in the permeate reservoir. The mass of the permeate reservoir was measured every 30 s for at least 30 min using a Vernier LabQuest2 data logger to calculate the flux for each testing condition. The feed concentration was assumed to be relatively constant, despite small mass losses due to distillation of the feed stream into the permeate stream, because the total volume of the feed reservoir was relatively large relative to the losses as permeate. The different thickness and strength of the Al-W200 and the Ti-T450 ceramic membranes required different membrane modules and

conditions to run flux tests. Because the Al-W200 membranes were thin and brittle, they were tested in the thinner membrane module (thickness: 1 mm, feed flow rate 4.7 L/min, permeate flowrate 4.3 L/min) with spacers to prevent breakage. The Ti-T450 membranes were tested in a thicker module (thickness: 7 mm, feed flowrate 6.9 L/min, permeate flowrate 4.8 L/min) without spacers.

Membrane Surface Modification

Imparting Hydrophobicity to Ceramic Membranes. One of the challenges for developing a membrane distillation system was determining the type of membrane to use. Ceramic membranes have several properties that make them appealing candidates as MD membranes, including thermal and chemical stability and high mechanical strength [11]. Although ceramic membranes have these useful properties, ceramic membranes are generally hydrophilic and must be modified to make them hydrophobic. Prior research has demonstrated that anhydrous deposition of perfluorinated silanes can produce a hydrophobic coating on the surface of ceramic materials [11, 12]. To further the work on ceramic membranes, additional ceramic membranes were coated with the perfluorinated silane coating. The goal of the coating process was to create a surface with a contact angle greater than 120°. Coated membranes that reached this threshold contact angle were then selected for additional testing and stress-tested under industrially relevant conditions and performance tested in a bench-scale DCMD system.

Two brands of anodized aluminum oxide membranes and one brand of zirconium dioxide and titanium dioxide membranes were treated with 1H,1H,2H,2H-perfluorodecyltriethoxysilane (PFS) from Sigma-Aldrich to increase the hydrophobicity of the membranes.

PFS coatings were applied by using liquid and vapor deposition methods. To coat the membranes using the liquid deposition method, the membranes were submerged in a 10mM PFS and chloroform solution for 24 h, rinsed and vacuum filtered with acetone to remove excess coating solution, and heated in the oven for 1 h at 100 °C. This procedure was repeated three times for a complete coating. To coat the membranes using the vapor deposition method, the membranes and a dish of 97% PFS solution were placed in a vacuum desiccator for 48 h, then heated in an oven for 1 h at 100 °C.

Hydrophobicity was measured with a Kruss Easy Drop contact angle goniometer using DI water. The presence of PFS on the surface of the coated membranes was verified with a Krato Analytical Axis Ultra x-ray photoelectron spectrometer, and an FEI XL30 scanning electron microscope was used to visually assess if pore clogging occurred.

Membrane Stress Testing

To determine the durability of the PFS coating, the modified membranes were subjected to thermal and chemical stress tests and the average contact angle was calculated after testing to detect any changes in hydrophobicity. Resistance to high temperatures was tested by exposure to 200 °C for 2 h. To test resistance to chemical cleaning agents, membranes were exposed to 100 ppm sodium hypochlorite, pH 3 hydrochloric acid solution, and pH 11 sodium hydroxide solutions for 72 h.

Ceramic Membrane Hydrophobization

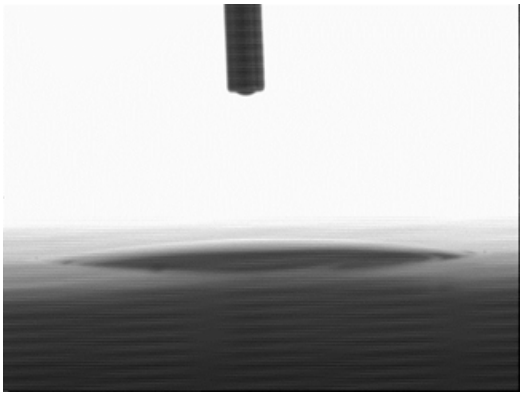

Figure 3-4. Water drop on an untreated Al X W200 membrane showing the water affinity for the surface via droplet spreading and absorption.

The first critical milestone of modifying a ceramic membrane so that it exhibited a contact angle of >120 ° was achieved. Validation of the results was conducted to confirm the persistence of the modifications. As shown in Figure 3-4, metal oxides used for ceramic membranes are hydrophilic and readily absorb water (thus making them nonstarters as MD membranes). Their surface chemistry was made hydrophobic using 1H,1H,2H,2H-perfluorodecyltriethoxysilane (PFS). The four commercially available ceramic materials modified were denoted as Al-X-S100, Al-X-W200, Ti-Al-T200, and Ti-Al-T450. The Al-X-S100 and Al-X-W200 are anodized aluminum oxide membranes from different manufacturers with average pore diameter of 0.1 and 0.2 μm, respectively. Ti-Al-T200 and Ti-Al-T450 were titanium dioxide membranes on an aluminum zirconia support from a third manufacturer with average pore diameter of 0.2 and 0.45 μm, respectively. The PFS grafting solution was prepared by dissolving the chemical in chloroform to make a 10 mM solution. The membranes were immersed in the PFS solution in a low-humidity environment for 24 h, removed and washed with acetone, then dried in an oven at 100 ± 5 °C for 1 h. The process was repeated up to a total of three times to ensure complete coverage of the membrane surface. Contact angle was measured using a Krüss Scientific goniometer and the sessile drop technique. All contact angle measurements were done using doubly deionized water (DDW).

Omniphobic MD Membrane Preparation

Two different methods were developed for the fabrication of superomniphobic membranes, and membrane characterization data were analyzed to identify characteristics that lead to increased hydrophobicity. Superomniphobicity is the ability for surfaces to repel both water and oils. Such surfaces are characterized by having a contact angle greater than 150° with water and liquids having a surface tension below 30 dynes/cm. Fabrication of superomniphobic surfaces requires creation of a nano-microscale roughness on a hydrophobic surface. In our experiments, silica nanoparticles [SiNP] were grown on the surface of cellulose acetate [CA] membranes to create the hierarchical roughness. After coating with hydrophobic perfluorodecyltriethoxysilane [PFS], the CA membranes had a water contact angle of 144 ± 4°. Additional characterizations of the fluorine percent composition (FPC) and surface roughness were conducted to analyze their effect on water contact angle. Contact angle measurements with octane (surface tension ~ 22 dynes/cm) were attempted but were not possible with the Kruss Easydrop goniometer available. Two methods were used to create the hierarchical surface roughness:

- Layer-by-layer polyelectrolyte coating

- Deposition of silica nanoparticles [SiNP] on membranes

The membranes were then hydrophobicized by coating with PFS using a previously developed vapor deposition method. The most promising method for creating the hierarchical roughness was deposition of the SiNP onto pre-treated membranes due to its high anticipated stability and hydrophobicity results.

Method 1: Layer-by-Layer [LBL] Polyelectrolyte Coating. LBL coating is a thin-film application technique where polyelectrolytes of opposite charge are deposited on the membrane surface in alternating layers. Different combinations of polyelectrolytes can be used to create surfaces of different functional groups with varying hydrophilicity, surface charge, and other properties. Polyvinylidene fluoride [PVDF] membranes were coated with SiNP-polyetherimide [PEI] / polystyrenesulfonate [PSS] polyelectrolyte solutions and treated with PFS. Different SiNP concentrations in the polyelectrolyte solutions were tested as well as different numbers of polyelectrolyte bilayers.

Method 2: Growth of SiNP on Cellulose Acetate Membranes. The methods for growing SiNP on CA membranes were adapted from an experiment by Chen et al. [13] in which a hydrophobic cellulose cloth with a contact angle of 150° was formed by growing SiNP on the cloth surface and applying a fluoropolymer coating.

Evaluating MD Performance with Volatile and Semi-Volatile Contaminants

When considering the ability of DCMD systems to treat seawater for potable water applications, organic contaminants are the primary contaminants of concern due to their volatility. Microorganisms are too large to pass through the membrane pores (typically smaller than 450 nm), inorganic contaminants typically have very low volatility and will not volatilize across the membrane, and, while seawater does not typically contain much radioactive material, DCMD has been shown to have good rejection of radioactive wastes [14]. A list of organic contaminants in the NPDWRs is included in Table 3-1.

Table 3-1. Organic contaminants regulated by the NPDWRs and maximum contaminant levels (MCLs)

Contaminant Name	MCL [mg/L]	Contaminant Name	MCL [mg/L]
Acrylamide	0.05% dosed at 1 mg/L (or equivalent)	Epichlorohydrin	0.01% dosed at 20 mg/L (or equivalent)
Alachlor	0.002	Ethylbenzene	0.7
Atrazine	0.003	Ethylene dibromide	0.00005
Benzene	0.005	Glyphosate	0.7
Benzo(a)pyrene (PAHs)	0.0002	Heptachlor	0.0004
Carbofuran	0.04	Heptachlor epoxide	0.0002
Carbon tetrachloride	0.005	Hexachlorobenzene	0.001
Chlordane	0.002	Hexachlorocyclopentadiene	0.05

Contaminant Name	MCL [mg/L]	Contaminant Name	MCL [mg/L]
Chlorobenzene	0.1	Lindane	0.0002
2,4-D (2,4-Dichlorophenoxyacetic Acid)	0.07	Methoxychlor	0.04
Dalapon	0.2	Oxamyl (Vydate)	0.2
1,2-Dibromo-3-chloropropane (DBCP)	0.0002	Polychlorinated biphenyls (PCBs)	0.0005
o-Dichlorobenzene	0.6	Pentachlorophenol	0.001
p-Dichlorobenzene	0.075	Picloram	0.5
1,2-Dichloroethane	0.005	Simazine	0.004
1,1-Dichloroethylene	0.007	Styrene	0.1
cis-1,2-Dichloroethylene	0.07	Tetrachloroethylene	0.005
trans-1,2-Dichloroethylene	0.1	Toluene	1
Dichloromethane	0.005	Toxaphene	0.003
1,2-Dichloropropane	0.005	2,4,5-TP (Silvex)	0.05
Di(2-ethylhexyl) adipate	0.4	1,2,4-Trichlorobenzene	0.07
Di(2-ethylhexyl) phthalate	0.006	1,1,1-Trichloroethane	0.2
Dinoseb	0.007	1,1,2-Trichloroethane	0.005
Dioxin (2,3,7,8-TCDD)	0.00000003	Trichloroethylene	0.005
Diquat	0.02	Vinyl chloride	0.002
Endothall	0.1	Xylenes (total)	10
Endrin	0.002		

Extraction of oil and gas generates large amounts highly saline wastewater called produced water. In 2007, 2.5 billion m^3 of produced water was generated at 2-3 times the rate of oil production in the U.S. [15, 16]. While most of the produced water was re-injected for enhanced recovery, 38.9% of the produced was reinjected into existing wells for disposal [16]. While the composition of oil and gas produced water varies greatly depending on the extraction site, produced water from the Marcellus Shale can be regulated under the Effluent Limitations Guidelines Subcategory for treatment and recovery of organics [17]. These requirements include limits for conventional parameters, metal analytes, and organic analytes. DCMD has been shown to have good rejection of nonvolatile inorganic contaminants, but the organic analytes may have sufficient volatility to accumulate in the DCMD product water. A list of the organic contaminants and their requirements is included in Table 3-2.

Table 3-2. Organic contaminants regulated by the CWT pretreatment standards for new sources for organic wastestreams (subcategory C) [18]

Contaminant Name	Monthly Average Maximum [mg/L]	Contaminant Name	Monthly Average Maximum [mg/L]
Acetone	7.97	p-Cresol	0.205
Acetonphenone	0.0562	2,3 Dichloroaniline	0.0361
Aniline	0.0164	Phenol	1.08
Butanone	1.85	Pyridine	0.182
o-Cresol	0.561	2,4,6-Trichlorophenol	0.106

Despite being acknowledged as a concern for DCMD treatment, few research groups have reported on the rejection of volatile and semi-volatile compounds by DCMD. The most comprehensive experimental analysis of organic compound removal was conducted by Wijekoon et al. [19] in their study on the rejection of trace organic compounds (TrOCs) by DCMD. In this study, a synthetic wastewater with 29 TrOCs representing a range of volatilities (the Henry's constant (H) of the compounds ranged from $5.06 \leq -\log_{10}(H) \leq 15.19$ m3·atm/mol) was treated with a DCMD system. The results showed that the rejection of the TrOCs was primarily determined by their volatility and possibly their hydrophobicity. In 24-h flux tests with a synthetic wastewater, they reported that the non-volatile compounds ($-\log_{10}(H) > 9$) were rejected by greater than 80%, and the semi-volatile compounds ($-\log_{10}(H) < 9$) had rejections between 54% and near complete rejection. Notably, a mass balance of the TrOCs at the end of the test revealed significant mass losses for many of the compounds, indicating that evaporation and adsorption of the TrOCs was a significant concern.

While this study lays important groundwork in predicting rejection trends based on the volatility of the compound, the study design measured the cumulative contaminant rejection at the end of the 24-h flux test, which may lead to underprediction of average contaminant rejection because the initial solute flux would be greater than the flux at equilibrium. Additionally, the mass losses in this study made it difficult to determine if the contaminants were rejected or lost to evaporation and adsorption and not measured in the permeate collection stream.

Another collection of studies by Gryta et al. [20-23] also analyzed the flux of volatile and semi-volatile solutes from an aqueous DCMD feed solution. These studies were conducted on the DCMD concentration of acids as well as on the extraction of ethanol and other volatile compounds from bioreactor broth. To describe the transport of these compounds, Gryta et al. developed a flux model to predict the transport of the solute and aqueous solvent based on the Stefan-Maxwell equations for multicomponent diffusion.

While this model provides valuable insight into the transport mechanisms of volatile compounds, it does not discuss how the compound concentration in the feed or permeate collection streams would change as the DCMD system runs. Additionally, the model uses the Stephan-Maxwell equations for modeling multicomponent diffusion, which create additional complexity to the model. The Stephan-Maxwell equations for multicomponent diffusion incorporate the diffusional interactions between the diffusing

species. While these interactions are important for modeling the diffusion of concentrated solutions, the relatively low concentrations of contaminants in the DCMD feed water render these interactions negligible [24].

Gryta et al. also conducted DCMD tests to enhance the separation of the ethanol from bioreactor broth and acids from spent pickling liquors in electroplating plants by varying the DCMD operating conditions. They found that ethanol separation increased with decreasing feed temperature [21], ethanol separation increased with decreasing ethanol concentration in the feed stream [20, 25], and that a maximum ethanol separation was found when varying the feed stream flow rate [20]. Salt effects on the volatile compound separation were also experimentally studied by adding 40-106 g/L iron(III) chloride ($FeCl_3$) to hydrochloric acid solutions. The addition of salts led to increased separation with increasing salt concentration [23]. While these optimization tests provide valuable information on the optimization of ethanol transport, additional research to predict the transport of different types of compounds through the DCMD system is necessary for designing DCMD systems to meet effluent requirements of different contaminants.

While the studies above provide a valuable framework for understanding the transport of multicomponent solutions in DCMD, the research here presents a novel approach to measuring the transport of volatile contaminants over the course of the DCMD flux test. During the course of DCMD operation, the flux of volatile solutes from the feed into the permeate collection stream changes the solute concentration in both the feed and the permeate collection streams. The changing feed and permeate collection stream concentrations subsequently reduce the flux of the solutes until an equilibrium state is reached. This research incorporates the changes in solute flux due to changing conditions, accounts for mass losses due to evaporation and adsorption, and enables the prediction of the equilibrium concentrations in both the feed and permeate collection stream. Because the DCMD effluent is withdrawn from the permeate collection stream, predicting this concentration is critical for understanding the performance of DCMD systems. Additionally, the model developed in this research uses a Fickian model for binary diffusion, which simplifies the model calculations. This methodology addresses gaps in prior studies and provides valuable information that enables the prediction of the DCMD effluent concentration under a wide range of conditions, which is important for the design of commercial DCMD systems.

DCMD Contaminant Concentration Model. A model for predicting the contaminant concentration in the DCMD feed and permeate collection streams was developed. The model describes the flux of contaminants based on parameters describing the physiochemical properties of the contaminants and the structure of the DCMD system.

The model description is broken into four sections: model mass balance, mass transfer in DCMD, heat transfer in DCMD, and definition of the DCMD equilibrium ratio. The model mass balance describes the contaminant concentrations during the course of DCMD operation which enables accurate calculation of contaminant concentration during the start-up phase of operation and the ability to predict when and at what stage the system will come to equilibrium. The mass transfer section describes the flux of the contaminants across a liquid-gas–liquid system. Notably, the contaminant flux depends on the vapor

pressure gradient at the liquid–gas interfaces, which varies greatly depending on the temperature at the interfaces. As a result, mass and heat transfer are inextricably linked. A DCMD equilibrium ratio has also been defined to be a measure of the accumulation of the contaminant in the permeate collection stream compared to the starting concentration at equilibrium. The equilibrium ratio is an important metric for determining the extent to which the contaminant will be rejected or magnified by the DCMD system.

To predict the contaminant concentration in the PCS during a batch DCMD process, a mass balance was developed to describe the transport of contaminants from the feed to the permeate collection stream. To write the mass balance of the feed and permeate collection streams, both the mass transfer of the contaminants and mass losses from the system were incorporated in Eqs. 8 and 9:

$$\frac{\mathrm{d}(V_f C_{c,f})}{\mathrm{d}t} = -A_m N_c - k_{l,c,f} C_{c,f} V_f \quad [8]$$

$$\frac{\mathrm{d}(V_p C_{c,p})}{\mathrm{d}t} = A_m N_c - k_{l,c,p} C_{c,p} V_p \quad [9]$$

where V is the average volume of the reservoir during the flux test, C_c is the concentration of the contaminant, t is the time since the sample was added, A_m is the area of the membrane, N_c is the contaminant flux, and k_l is the mass loss coefficient. The subscripts f and p indicate a parameter that is evaluated in the bulk feed and permeate collection streams, respectively. In the batch experiments conducted for this work, the DCMD system was not operated at high recovery, and it was assumed that the volume of the feed and permeate collection streams did not change over time. The contaminant flux depended on the concentration and temperature of the contaminants at the membrane interface, which were determined using the mass and heat transfer equations. In addition to the MD heat/mass transfer transport equations, it was necessary to account for the gas transport of volatile and semi-volatile contaminants, and this was done using the Henry's Constant and an MD equilibrium ratio. Calculating the Henry's constant is important for determining both the contaminant partial pressures and the overall mass transport coefficient. The Henry's constant was calculated at the temperatures of the membrane interfaces using the equation below [26]:

$$H_c = \gamma_c p^*_{c,T} \bar{V}_w \quad [10]$$

where γ_c is the activity coefficient of the contaminant at infinite dilution in the solution, $p^*_{c,T}$ is the pure-component vapor pressure of the contaminant at temperature (T), and $\bar{V}_w$ is the molar volume of water. The pure-component vapor pressures of the contaminants were calculated using the Antoine equation and Antoine coefficients from Yaws et al. [27] and Stephenson et al. [28].

To evaluate the activity coefficients of the contaminants, the aqueous activity coefficient at infinite dilution ($\gamma_{\infty,c}$) was used to model the contaminant activity in the permeate collection stream; while in the feed stream, the contaminant activity coefficient was modified to include the effect of salts on the solubility of the contaminants. The activity coefficient in a saline solution ($\gamma_{s,\infty,c}$) was modified using the method from Xie et al. [29]:

$$\gamma_{s,\infty,c} = \gamma_{\infty,c} 10^{0.0018 \bar{V}_c C_s} \quad [11]$$

where $\bar{V}_c$ is the molar volume of the compound in cm^3/mol, and C_s is the molar concentration of sodium chloride. The values of the aqueous activity coefficients at infinite dilution were obtained from Yaws [30].

The magnification or rejection of the contaminants in the DCMD product water was described by the equilibrium ratio (E) of the permeate collection stream concentration to the feed stream concentration (Eq. 12). Equilibrium ratio values greater than 1 indicate that the contaminant concentration is magnified in the product water, and equilibrium ratio values less than 1 indicate that the contaminant is rejected.

$$E_c = \frac{C_{c,p}}{C_{c,f}} \qquad [12]$$

A bench-scale, batch-operated DCMD system was built to test the transport in DCMD, and a schematic of this system is depicted in Figure 3-5. The membrane was held in a flat-sheet membrane module with diagonal mesh spacers to support the membrane and increase turbulent mixing. DCMD tests were conducted with Millipore membranes (GVHP, pore size 220 nm, 75% porosity) with an area of 25 cm^2.

The feed and permeate collection streams were circulated using peristaltic KNF Liquiport Lab pumps at a flow rate of 31 ml/s in both streams. The pressure in the feed and permeate collection streams was less than 20 psi, and pH of the streams was 5.5. The temperature of the feed and permeate collection streams was measured at the module inlets and outlets using Vernier Stainless Steel Temperature Probes, and the conductivity of the permeate collection stream was measured using a Vernier Conductivity Probe.

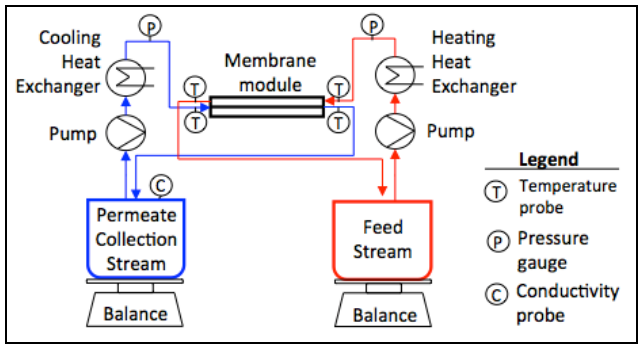

Figure 3-5. Schematic of the bench-scale DCMD system.

The feed and permeate collection streams were held in glass containers covered with Scentroid polytetrafluoroethylene gas sampling bags to reduce evaporative losses. A pair of Ohaus Adventurer Pro AV 3103 balances measured the change in mass of the feed and permeate collection streams and the balance readings were recorded every 30 s with the LoggerPro software. The reservoirs were sampled at regular time intervals, and the contaminant concentration was measured using a Shimadzu GC-2014 gas chromatograph with a flame ionization detector and Agilent HP-Innowax column.

Synthetic Wastewater Composition. A synthetic wastewater was developed to test the performance of the DCMD system when treating feed waters with salts and multiple volatile and semi-volatile contaminants. This synthetic wastewater was modeled on an industrial wastewater that has high salt concentration and high concentrations of organics.

The synthetic wastewater was made of a 0.5 M NaCl solution with seven different contaminants at a concentration around 60 mg/L each. The Henry's constant and molecular weight of the compounds were expected to influence the rate of transport, and the synthetic wastewater compounds were selected to

represent a range of industrial compounds with different volatilities and molecular weights. The characteristics of the compounds are listed in Table 3-3. Chemicals were analytical grade and obtained from Sigma Aldrich.

Table 3-3. Characteristics of the contaminants in the synthetic wastewater for DCMD flux tests

Chemical	Molecular Weight [g/mol]	Henry's Constant (25°C) [PaL/mol] Log_{10}(H)
Methyl-tert-butyl-ether (MTBE)	88.15	4.96
Pentanone	86.13	3.91
Acetone	58.08	3.76
Hexanol	102.18	3.52
Butanol	74.12	2.95
Dimethyl phenol (DMP)	94.11	2.31
Phenol	122.17	1.62

Flux and Mass Balance Tests. Flux tests were conducted by first equilibrating the feed and permeate collection streams to their respective temperatures for each run. After equilibration, the saline feed stream was spiked with the contaminants, mixed, and sampled over time to monitor the contaminant concentration. To ensure adequate mixing during the sample addition to the feed stream, the contaminant spike was well stirred and circulated through the system for 5 min before the initial concentrations in the feed and permeate collection streams were evaluated. Flux tests were conducted over 6-30 h.

The membrane integrity was monitored by evaluating the salt rejection during each flux test to ensure that the feed solution was not entering the permeate collection stream due to pore wetting of the membrane. The salt rejection of all the tests was above 99.99%, which indicated that the transport of contaminants into the permeate collection stream was due to volatilization, not pore wetting.

Mass balance tests were conducted to evaluate mass losses due to processes such as evaporation or adsorption. The mass loss coefficients for a first-order loss expression were calculated from data obtained using similar procedures to those used in the permeate flux tests. The flux test procedure was modified by replacing the membrane with an impermeable plastic sheet to isolate the feed and permeate collection streams. Additionally, both the feed and permeate collection streams were spiked with the contaminants to track the change in contaminant concentration in both loops.

Bench-Scale, Integrated FO-MD Test System

System Design

Based on the hybrid process model predictions and membrane modules available from manufacturers on the downselected FO and MD membrane candidates, a skid-mounted, integrated prototype system was designed to treat 150 gallons per day. The target system design clean-water production rate was 50 gal/day; however, to account for uncertainties in the performance of the emerging FO and MD

processes, design contingencies were incorporated, leading to ~75 gal/day (0.20 L/min) as the design water production rate. Figure 3-6 presents the initial Process Flow Diagram (PFD) of this integrated system showing major equipment and flow rates.

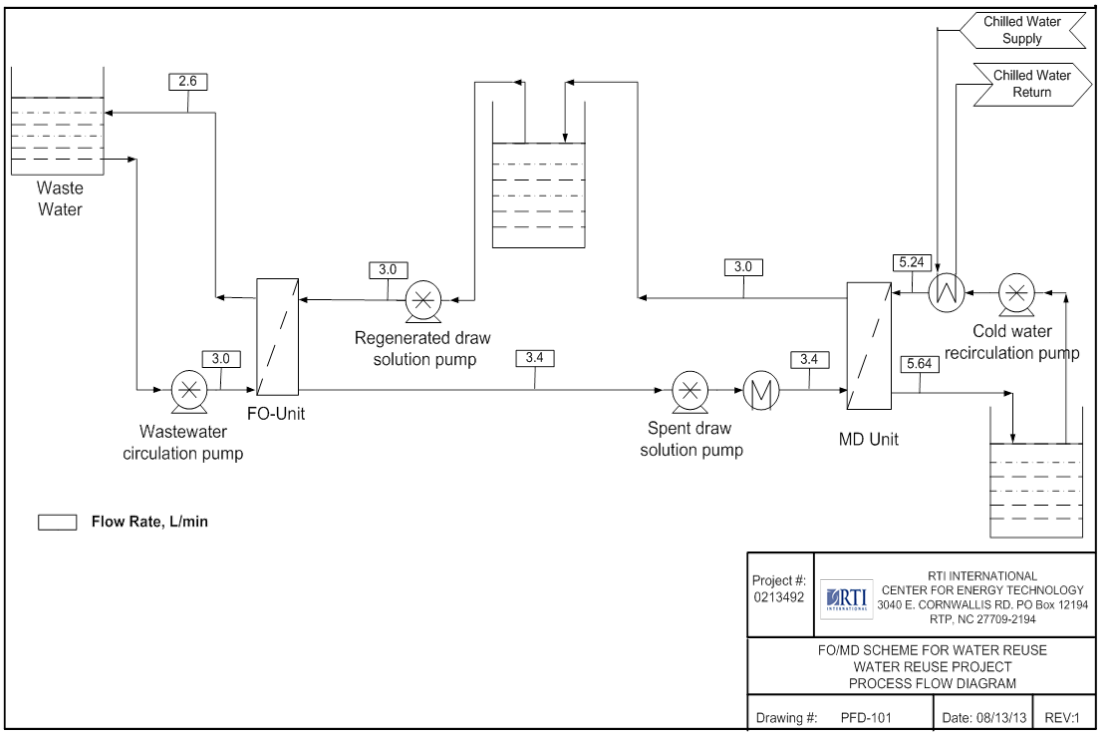

Figure 3-6. Initial PFD of the bench-scale, integrated FO-MD system.

The final, more detailed process flow schematic of the bench, integrated system is presented in Figure 3-7. The feed wastewater would be stored in vessel V-1 from which it would be pumped by pump P-01 to the FO membrane module M-1. Depending on the temperature of the incoming wastewater stream, heat exchanger HX-01 would be used to facilitate cooling of this stream when required. In the specific example case presented in Figure 3-7Figure 3-6, within the FO module, clean water at the rate of 0.2 L/min would pass through the FO membrane and into the draw-solution side. The outlet wastewater (Stream 2) would be returned to the vessel V-1 and recirculated to the FO membrane. On the permeate side of the FO membrane, 3 M NaCl draw solution (Stream 3) would be circulated from its intermediate storage vessel V-2 using pump P-02. This draw solution would pass through the FO module and become diluted by the clean water drawn through the FO membrane. This slightly diluted salt solution (Stream 4) would be sent to the intermediate holding tank V-3. From vessel V-3, the diluted draw solution would be pumped by pump P-03 and sent to heat exchangers HX-02 and HX-03 to heat up the draw solution to the required temperature for the MD step. In the example shown in Figure 3-7, the draw solution would be heated to 70 °C before it would be sent to the MD membrane module M-2. Due to the vapor pressure difference in the MD module, 0.2 L/min of water in this example case would pass through the membrane and join with the cold water stream on the permeate side of the membrane. The clean water product would then be sent to storage tank V-4. The reconcentrated draw solution (Stream 6) would be returned to

the intermediate dosing vessel V-2, where the draw-solution concentration would be monitored to make sure it was at 3 M before it was returned to the FO module M-1. If the concentration varied slightly due to any salt losses in the membrane modules, an appropriate amount of salt would be added to bring the draw solution back to 3 M.

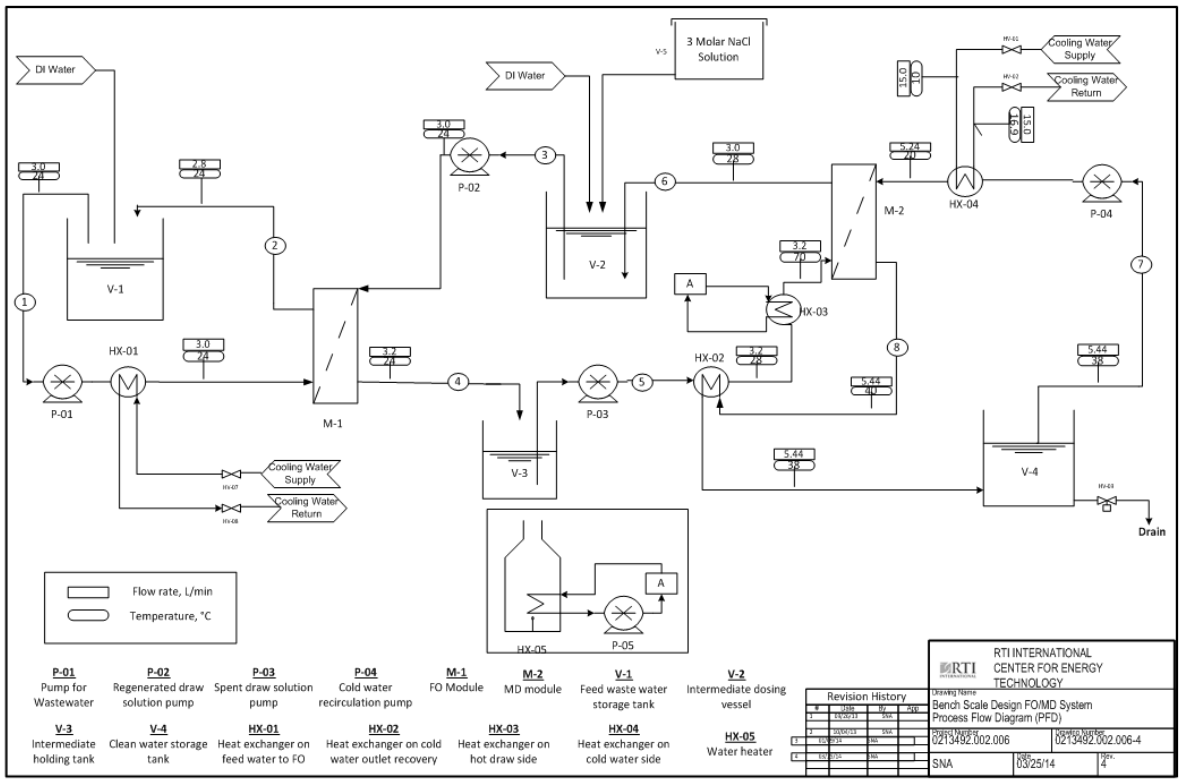

Figure 3-7. Final PFD of bench, integrated FO-MD system.

During its commissioning stage, the system performance of the bench, integrated FO-MD test unit was found to be below design expectations mainly because of a lack in heating and cooling performance by the heat exchangers. As a result, the system design was modified to improve its performance and operational flexibility. Two additional heat exchangers were therefore added to the integrated unit. For example, the maximum achievable temperature for the MD feed/FO draw loop was initially only ~60 °C. After the addition of another heat exchanger to this loop, the maximum achievable temperature improved to 75 °C. The revised P&ID for the bench, integrated unit with the new heat exchanger layout is depicted in Figure 3-8.

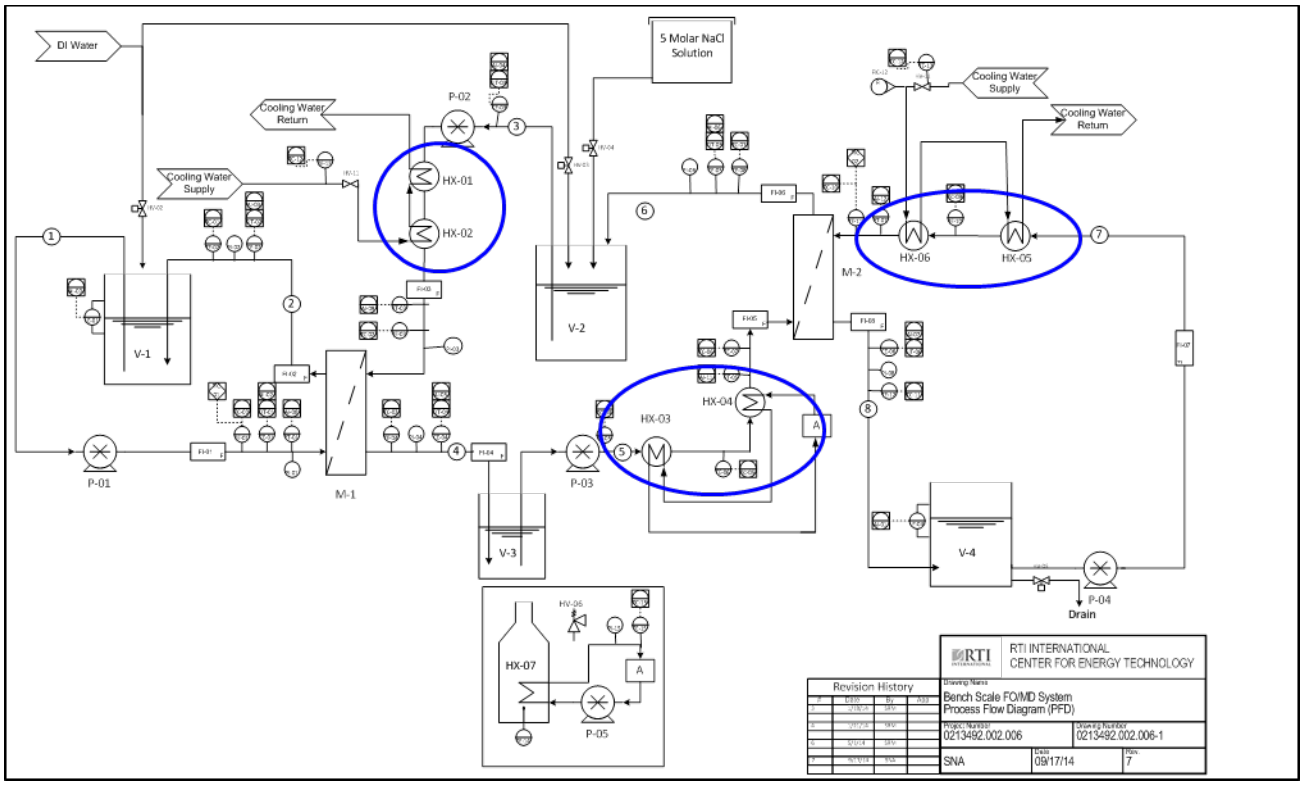

Figure 3-8. P&ID of bench, integrated FO-MD test unit, with final heat-exchanger layout indicated by the blue circles. (M-1 = FO membrane module; M-2 = MD membrane module; V-1 = Wastewater feed tank; V-2 = FO draw-solution/MD return tank; V-3 = Diluted draw-solution/MD feed tank; V-4 = Product water tank; HX-07 = Water circulation heater for MD feed).

Process Model Development

Process design and development of the integrated FO-MD process were performed using an iterative combination of the Aspen Plus® process simulation software (Aspen Technology, Inc., Bedford, MA) and the MATLAB® computing platform (The MathWorks, Inc., Natick, MA). Generic process equipment, such as heat exchangers and pumps, were readily simulated in Aspen Plus. However, Aspen Plus does not have simulation modules for emerging processes such as FO and MD. Individual models for the FO and MD membrane process components were thus developed using MATLAB programming software. The development approaches taken for these component FO and MD models are discussed below.

Forward Osmosis Model

The forward osmosis unit operation utilizes the osmotic-pressure differential across a semi-permeable membrane as the driving force for water flux, rather than the hydraulic pressure differential as in reverse-osmosis units. The aqueous feed to be treated is circulated on the side of the FO membrane with the active (selective) separation layer, while a concentrated draw-solute solution having higher osmotic potential than the aqueous feed is circulated on the other side of the FO membrane with the non-selective porous

support layer. The FO process results in concentration of the aqueous feed stream and, due to water permeation across the membrane, dilution of the draw-solution stream.

The general assumptions that were made in the development of the FO model in MATLAB were:

- No solute transfer occurs cross the FO membrane. That is, the membrane is assumed to permeate only water.
- No axial mixing occurs on the feed- and draw-solution sides of the FO membrane.
- Steady-state operation is assumed in the FO process model.

Initial development of the component FO model used the basic osmotically-driven water flux equation to compute the water permeation rate through an FO membrane:

$$J_w = A\left(\pi_{D,b} - \pi_{F,b}\right) \quad [13]$$

where J_w is the water flux [L/(m^2·h)], A is the pure water permeability [L/(m^2·h·bar)], and $\pi_{D,b}$ and $\pi_{F,b}$ are the bulk osmotic pressures (bar) of the draw and feed solutions, respectively. Eq. 13 assumes a well-mixed system so it does not account for any phenomena that would limit mass transfer across the FO membrane. Early in the model development, we found that Eq. 13 significantly overestimated the FO water flux relative to experimentally measured values, indicating that the effects of boundary layers or concentration polarization play a substantial role in the actual FO water permeation performance.

Review of the FO literature confirmed that strong concentration polarization effects have been found to occur on both the feed and draw-solution sides of the FO membrane as well as inside the porous support layer of the membrane. As solutes on the feed side are rejected by the membrane, the local solute concentration at the feed-side membrane surface becomes higher than that in the bulk feed. Additionally, as water permeates the membrane, the draw-solute concentration at the draw-side membrane surface is diluted, becoming lower than the bulk draw-solute concentration. Both of these phenomena are usually known as external concentration polarization (ECP) and could be mitigated by changing process conditions to improve process fluid dynamics. Simultaneously, draw solute also diffuses into the porous membrane support layer facing the draw side and becomes directly diluted by the water permeating the membrane active layer. Because of the inherent structural tortuosity of the porous layer and the typically slower diffusivity of draw solutes relative to that of water molecules, it is difficult to replenish and maintain the high draw-side osmotic potential inside the membrane structure itself. This phenomenon is usually referred to as internal concentration polarization (ICP) and can be affected only by membrane structural modification to reduce membrane resistance to draw-solute diffusion. The primary effect of both ECP and ICP is a reduction of the basic FO water flux in Eq. 13.

The FO model developed was subsequently revised to use Eq. 14, the modified water-flux equation presented by McCutcheon et al. and others [31, 32] that takes into consideration the ECP and ICP effects on the FO water flux:

$$J_w = A\left[\pi_{D,b}\exp(-J_w K) - \pi_{F,b}\exp\left(\frac{J_w}{k_F}\right)\right] \quad [14]$$

where K is the draw-side solute resistance to diffusion and k_F is the feed-side mass transfer coefficient. Specifically, K is an effective mass-transfer coefficient defined to account for the structural effect of the membrane porous support layer on solute mass transfer:

$$K = \frac{t\tau}{D_s\varepsilon} = \frac{S}{D_s} \quad [15]$$

In Eq. 15, D_s is the solute diffusivity in the bulk draw solution. As discussed earlier, the ratio $(t\tau/\varepsilon)$ is the membrane support structural parameter S, which was determined experimentally for the FO membranes examined according to Eq. 7. The feed-side mass transfer coefficient k_F was estimated from the feed flow rate, flow channel geometry, and solute type using Eq. 16, which had been derived by Hoek at al. for laminar flow in a thin rectangular channel [10] such as that in the SEPA CF test cell used in this project for FO membrane testing.

$$k_F = 1.62\left(\frac{QD_s^2}{2W_cH_c^2L_c}\right)^{1/3} \quad [16]$$

In Eq. 16, Q is the flow rate through the feed-side flow channel and W_c, H_c, and L_c is the flow-channel width, height, and length, respectively. In our FO modeling, the osmotic pressures of the feed and draw solutions were estimated using the OLI electrolyte thermodynamics software.

The component FO model was developed for the countercurrent flow mode, as represented by the simplified flow schematic for an FO membrane module in Figure 3-9. This representative membrane module was then further broken into a series of *N* control volumes (stages) in the axial direction (i.e., along the module length). Within each stage, mass balances were enforced. This modeling approach is equivalent to using first-order finite differential elements to develop a set of coupled differential equations from the differential mass balances in each stage. Figure 3-10 illustrates the breakdown of the membrane module into a series of *N* equal, perfectly mixed, countercurrent stages.

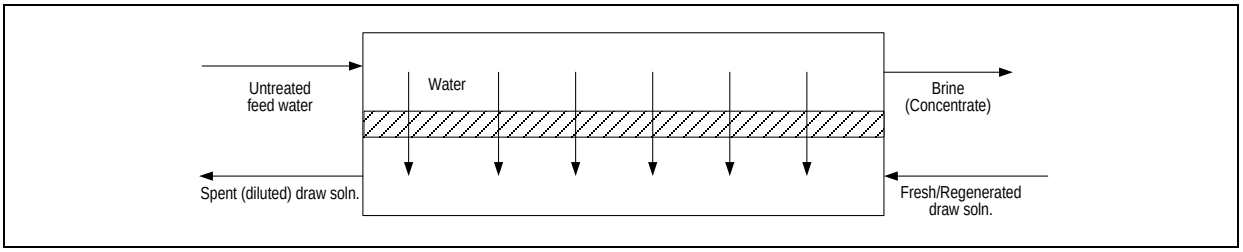

Figure 3-9. Simple FO process flow schematic.

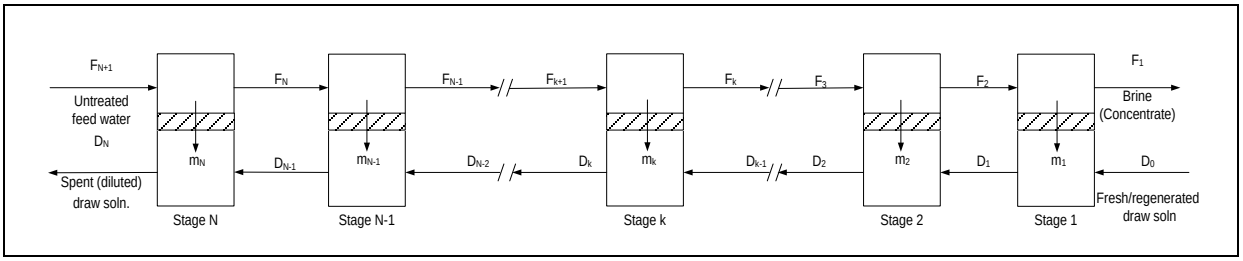

Figure 3-10. FO model broken down into series of N stages of axial control volumes.

The FO modeling was conducted by following the iterative sequence described below and as illustrated by the flowchart in Figure 3-11.

1. The membrane area of each stage *k* was computed as

$$A_k = w_k \left(\frac{L}{N}\right) \quad [17]$$

where A_k is the effective membrane permeation area of stage *k*, w_k is the membrane dimension orthogonal to the process flow, and *L* is the total length of the membrane modules flow passage.

2. The average bulk-water volume on the feed and draw-solution sides of membrane was estimated by performing a mass balance on the entire membrane module to obtain initial guess values for flow rates along the module:

$$F_{N+1} + D_0 - F_1 - D_N = 0 \quad [18]$$

3. On the basis of the initial water flows, the osmotic pressures of the bulk feed- and draw-side process streams were calculated using the OLI electrolyte thermodynamics software. The water flux was then computed from the osmotic pressures by using Eq. 14 to obtain an initial guess uniform water flux J_w and, in turn, an initial guess uniform permeation flow rate m_N for stage *N* by Eq. 19.

$$m_N = A_k \left(\frac{J_w}{N}\right) \quad [19]$$

4. Mass balances were then performed on each stage *k* to estimate the flow rates of the streams exiting on the feed- and draw sides of this stage.

$$m_k = F_{k+1} - F_k = D_k - D_{k-1} \quad [20a]$$

$$F_k = F_{k+1} - m_k \quad [20b]$$

$$D_k = D_{k-1} + m_k \quad [20c]$$

5. The flow rates from Step 4 were then used to calculate the average feed- and draw-side water volumes for the next stage. From these average water volumes, the feed- and draw-side osmotic pressures for the next stage were estimated from the OLI software. The water flux for the next stage was then computed using this new set of feed- and draw-side osmotic pressures.

6. The new calculated water flux was then used to repeat the mass balances in Step 4 to estimate the set of water volume flows to use in the next stage.

7. Steps 5 and 4 were repeated until the volume flows did not change between iterations.

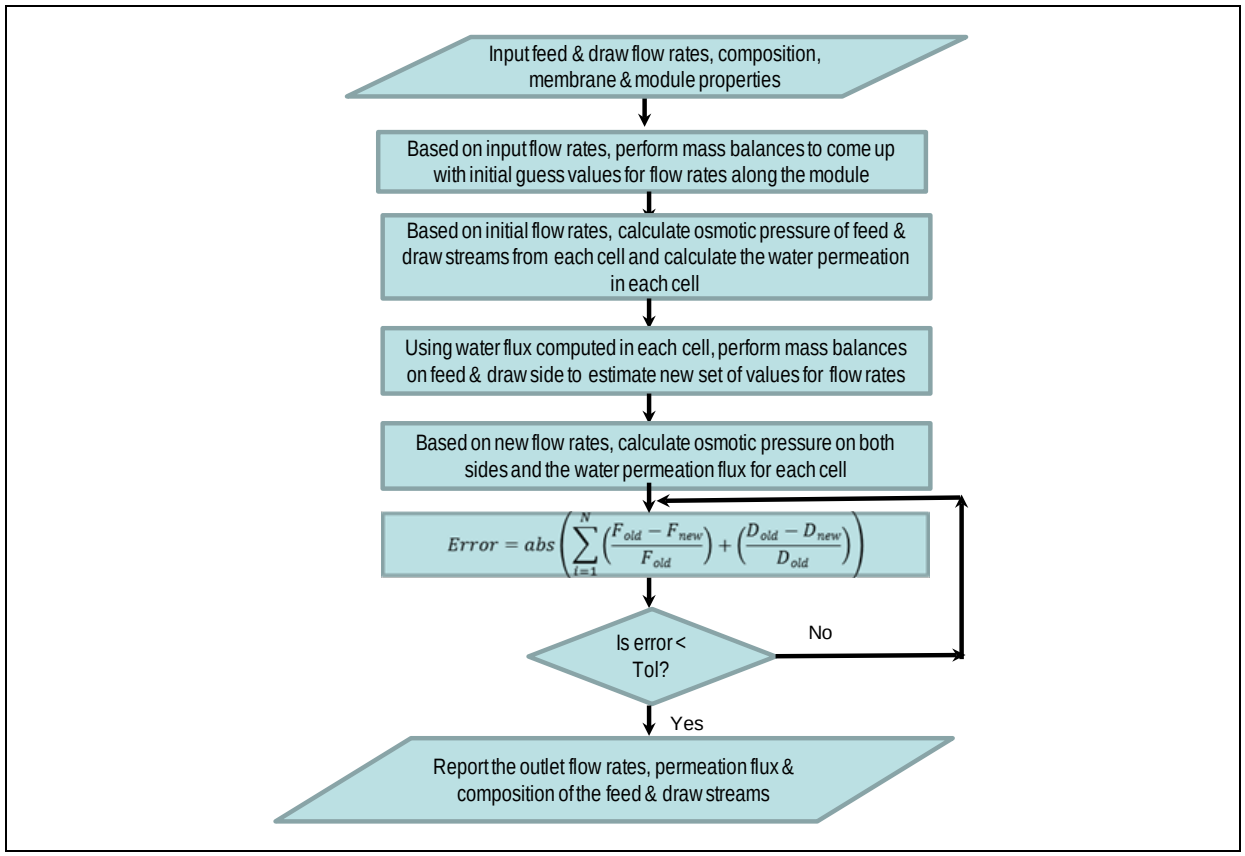

Figure 3-11. Flowchart depicting the FO modeling approach.

Membrane Distillation Model

A model for membrane distillation unit was developed on MATLAB. The developed MATLAB model was initially validated with experimental results from a flat-sheet module with a PTFE MD membrane. Throughout the project, the model was refined so that it would be applicable for multiple membrane materials and membrane geometries. At each step, the model was validated using experimental data to ensure results were relevant. The basis and underlying assumptions on the heat and mass transfer across the membrane are described below and were the same for all versions and complexities of the model.

Equations governing the model

The MD model was developed based on the procedure described by Ibrahim et. al. [33]. In this model, heat and mass balances that govern the membrane distillation process are solved simultaneously using a numerical iterative technique to determine the temperature and net water transport across the membrane module. The transport mechanism of MD can be summarized into three steps: evaporation of water on the hot feed side, penetration of water vapor through the membrane pores, and condensation of water vapor transported to the relatively cold permeate side of the membrane.

The assumptions considered in the model were:

1. No wetting occurs across the membrane, resulting in 100% rejection of the nonvolatile component in the feed.

2. Vapor and liquid phases are in mechanical equilibrium (constant total pressure) and in thermodynamic equilibrium at the interface of both feed and permeate side.

3. The entrapped air in the pores is static, and water vapor diffuses through it. The air is insoluble in water due to low solubility of air in water.

4. The pore size in the whole membrane is assumed to be uniform.

5. The water vapor is transported through a tortuous (not straight) cylinder.

The derivation of heat and mass transfer equations was based on dividing the membrane module into N elements as shown in Figure 3-12. The equations that govern the heat and mass transfer are listed below according to physical characteristics for each unit on feed, permeate and membrane side.

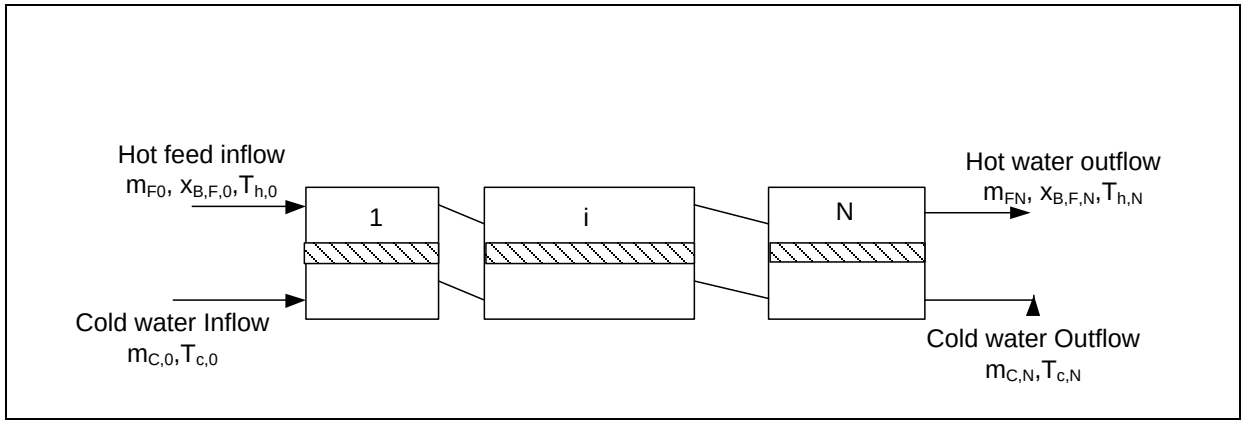

Figure 3-12. Schematic representation of the DCMD module as considered in the model development.

Feed Side

1. ***Heat Transfer*:** On the feed side, a thermal boundary layer is formed at the membrane surface because of the temperature differential between the bulk feed stream and the membrane surface temperature. The net heat transferred in the boundary layer of the membrane surface facing the feed side is by convection and water vapor leaving the boundary layer. This was expressed as:

$$Q_i^F = h_i^F A_0 \left(\bar{T}_{Bi}^F - T_{Mi}^F\right) - N_i A_0 H_i^{FV} \tag{21}$$

where $\bar{T}_{Bi}^F = \frac{T_{Bi}^F + T_{Bi-1}^F}{2}$, *i* represents the cell number, N_i is the volatile component mass flux across the boundary layer of *i* cell, based on available surface area, A_0 of the membrane on the feed side. The heat transfer coefficients were estimated from empirical correlations expressed in terms of dimensionless numbers such as Reynolds, Nusselt, Prandtl, and heating/cooling correction factors.

Based on the inlet and outlet stream enthalpies, the energy balance on the feed side was expressed as:

$$Q_i^F = m_{i-1}^F H_{i-1}^L - m_i^F H_i^L - N_i A_0 H_i^{FV} \tag{22}$$

where *H*, enthalpy of water liquid and vapor, in kJ/kg can be estimated by Eqs. 23 and 24. In this expression, *T*, the temperature of the corresponding stream is in K and the expression is valid in the temperature range of 273-373 K.

$$H^L = -1117.8 + 4.0312T + 2.0\times10^{-4}T^2 \quad (23)$$

$$H^V = 1850.7 + 2.8273T + 1.6\times10^{-3}T^2 \quad (24)$$

2. ***Mass Transfer:*** The overall mass transfer in DCMD process can be split into two steps: the first step in which the volatile component passes through the concentration boundary layer on the feed side of the membrane and the second step in which the volatile component passes through the microporous membrane to the permeate side.

   The mass flux of the volatile component through the concentration boundary layer of the nonvolatile component was calculated by the following equation.

$$N_i = -k_i^F C_T Mwt_w ln\left(\frac{x_{Mi}^F}{\bar{x}_{Bi}^F}\right) \quad (25)$$

$$\bar{x}_{Bi}^F = \frac{x_{Bi}^F + x_{Bi-1}^F}{2} \quad (26)$$

   where C_T is the total concentration at the feed bulk, x^F is the mole fraction of the nonvolatile component at the feed side and k_i^F is the mass transfer coefficient usually estimated from empirical correlations expressed in terms of dimensionless numbers such as Sherwood, Schmidt, and Prandtl numbers and correction factors.

   Based on the assumption that no wetting and 100% rejection of the nonvolatile component occurs, a component material balance on the nonvolatile component on the feed side was expressed as:

$$\frac{m_i^F}{(Mwt_{sol})_i} x_i^F = \frac{m_{i-1}^F}{(Mwt_{sol})_{i-1}} x_{i-1}^F \quad (27)$$

$$x_i^F = \frac{m_{i-1}^F}{m_i^F (Mwt_{sol})_i} \frac{(Mwt_{sol})_i}{(Mwt_{sol})_{i-1}} x_{i-1}^F \quad (28)$$

   The total mass balance on the feed side was expressed as:

$$m_{i-1}^F = m_i^F + N_i A_0 \quad (29)$$

Permeate Side

1. ***Heat Transfer:*** On the permeate side, the heat is transferred by convection and mass transfer contribution in the thermal boundary layer. The net heat transferred in the thermal boundary layer was expressed as

$$Q_i^P = h_i^P A_0 \left(T_{Mi}^P - \bar{T}_{Bi}^P\right) + N_i A_0 H_i^{PV} \quad (30)$$

   where T_{Mi}^P is the temperature of the membrane surface on the permeate side, h_i^P is the heat transfer coefficient in the thermal boundary layer, and $\bar{T}_{Bi}^P$ is the average bulk temperature on the permeate side and given as $\bar{T}_{Bi}^P = \frac{T_{Bi}^P + T_{Bi-1}^P}{2}$.

The overall energy balance on the permeate side is based on the enthalpies of the inlet and outlet streams for each cell 'i' and was expressed as:

$$Q_i^P = m_{i-1}^P H_{i-1}^L - m_i^P H_i^L + N_i A_0 H_i^{PV} \quad (31)$$

2. ***Mass Transfer:*** Based on the assumption of 100% rejection of the nonvolatile component, the overall mass balance for the permeate side was written as

$$m_{i-1}^P = m_i^P - N_i A_0 \quad (32)$$

Membrane Side

1. ***Heat Transfer:*** The heat transfer in the membrane is mainly by conduction across the membrane material and water vapor transport across the membrane through its pores. The net heat transferred in the membrane was expressed as

$$Q_i^M = h_i^M A_0 \left(T_{Mi}^F - T_{Mi}^P\right) + N_i A_0 \left(H_i^{FV} - H_i^{PV}\right) \quad (33)$$

where h_i^M is the heat transfer coefficient of the hydrophobic membrane and $T_{Mi}^F$and T_{Mi}^P are the temperatures at the membrane surface on the feed and permeate sides, respectively.

2. ***Mass Transfer:*** The mass transfer was expressed as the mass flux through the membrane, and was described by the water vapor pressure difference between the feed and permeate sides and the membrane distillation coefficient K_i^M.

$$N_i = K_i^M \left(p_{Mi}^F - p_{Mi}^P\right) \quad (34)$$

where p_{Mi}^F and p_{Mi}^P are the partial pressures of water at the feed and permeate sides, respectively, and given as

$$p_{Mi}^F = \left(1 - x_{Mi}^F\right)\alpha_i P^{VF} \quad (35)$$

$$p_{Mi}^P = P^{VP} \quad (36)$$

where P^V is the water vapor pressure estimated by the Antoine equation at temperatures T_{Mi}^F and T_{Mi}^P for feed and permeate, respectively, as follows:

$$P^V = exp\left(23.328 - \frac{3841}{T-45}\right) \quad (37)$$

where P^V is in Pascal and T is in Kelvin. This equation is valid over a temperature range of 273-373 K.

Eqs. 21, 22, 25, and 28-34 were simultaneously solved for each cell using a numerical iterative technique to determine the mass flows and temperature profiles across the membrane on the feed and permeate sides.

Hybrid FO-MD Process Modeling

To perform process modeling of the hybrid FO-MD process, component FO and MD process blocks were configured in Aspen Plus and then linked to their respective MATLAB subroutines discussed above. Specifically, the process data from the influent streams to the FO and MD process blocks were transferred

to the corresponding MATLAB subroutines using an Excel interface in order to compute the predicted water flux and performance of the FO and MD membrane modules. The resulting MATLAB output data were then relayed back to the Aspen Plus through the Excel interface. In other words, the Aspen Plus model contained and simulated the complete water treatment process that would be integrated into an industrial process application, and the MATLAB subroutines developed for the component FO and MD processes were used to perform the back-end performance computations for these technologies. This hybrid FO-MD modeling approach is illustrated in Figure 3-13.

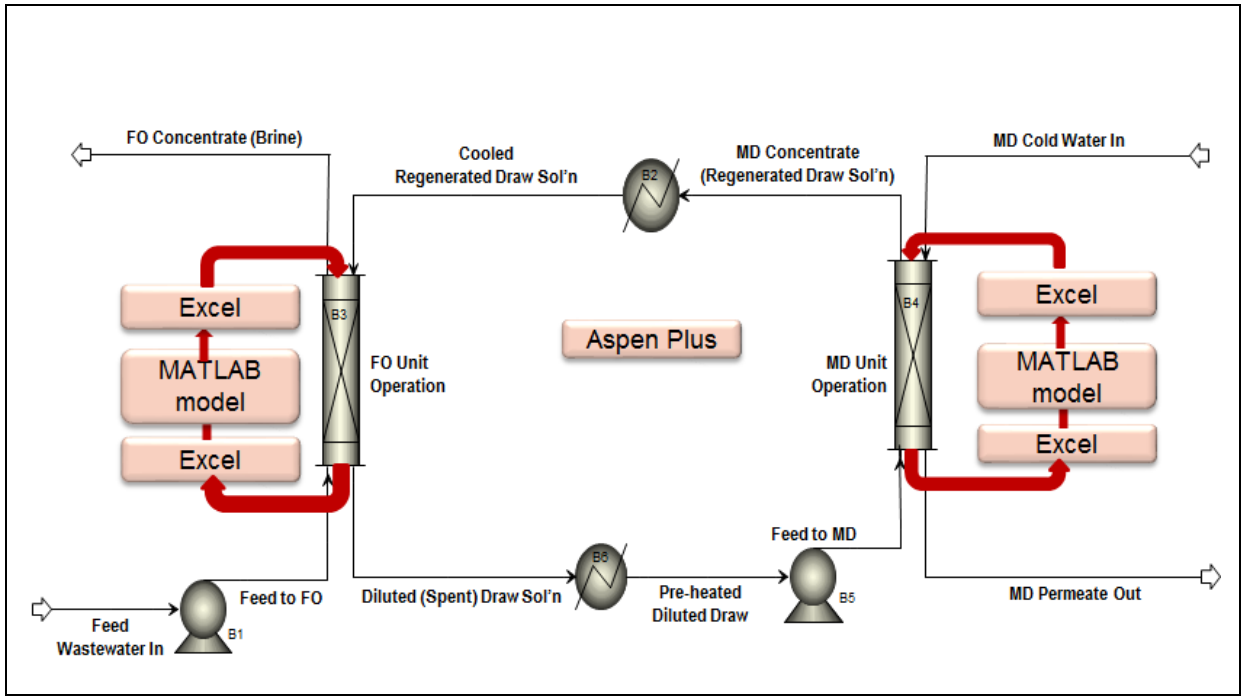

Figure 3-13. Schematic of integration of MATLAB-based component FO and MD models with auxiliary system components in Aspen Plus.

Process techno-economic analysis of the integrated (hybrid) FO-MD process was completed using the the MATLAB-based component FO and MD models in combination with heat and mass balances (HMBs) generated with Aspen Plus simulations, equipment sizing based on these HMBs, and equipment costs estimated with the in-plant cost estimator tool Aspen Icarus.

Techno-Economic Modeling and Evaluation

The goal of this analysis was to provide estimated costs and environmental impacts of the forward osmosis/membrane distillation (FO-MD) hybrid water treatment process. This analysis was performed early in the project and refined at each state. Our initial comparison used state-of-the-art membrane technology (e.g., membrane filtration / reverse osmosis[MF-RO]), which can treat wastewater with TDS levels approaching 50,000 mg/L but later design, performance, economic data and with input from our industrial partner we determined that a more appropriate comparison was higher TDS water that utilize thermal evaporation technologies, or water that has already undergone RO treatment and is unsuitable for further treatment using RO. The overall goal of the technology development project was to develop a

FO-MD water treatment system to improve the energy efficiency associated with industrial wastewater treatment and reuse in the U.S. manufacturing sector by at least 50% relative to the current comparable technology and enable the U.S. manufacturing sector to become more water sustainable, reduce wastewater discharges towards zero, reduce greenhouse gas emissions, and beneficially utilize waste heat energy.

Preliminary Techno-Economic Evaluation (RO Comparison)

Process techno-economic analysis was completed using heat and mass balances (HMBs) generated with AspenPlus simulations, equipment sizing based on these HMBs. To make an accurate comparison, cost estimates were developed for both the FO-MD and the MF/RO treatment systems. Based on empirical data, the FO-MD integrated process model, linked to the Aspen Plus, was used to aid in the development of the heat/material streams, equipment sizing, and cost estimations. In addition, US Bureau of Reclamation's (USBR) Water Treatment Estimation Routine (WaTER) [34] was utilized to determine August 2013 capital and operating costs for the MF/RO system as well as components of the FO-MD systems. A 20-year equipment lifetime was assumed for both technologies and an annual discount rate of 6% was used to calculated the Net Present Value (NPV) and the total water cost (TWC) for each technology. The sensitivity analysis included two model industrial wastewater streams; (1) low TDS (e.g., petroleum refining, pulp and paper, iron and steel, etc.) and (2) high TDS (e.g., oil and gas production, food and beverage, etc.). The environmental analysis consisted of the greenhouse gas equivalence comparison based on electricity consumption.

Estimate Quality

The accuracy of a cost estimate is a function of the stage or definition of a project. As a project progresses towards completion the cost estimate becomes more accurate. This progression has been defined by a cost estimate classification system ranging from 5 (>0% to 2% project definition) to 1 (50% to 100% project definition). Based on the current stage of this project, a Class 4 estimate was deemed appropriate and is defined as:

- CLASS 4 ESTIMATE (Study or Feasibility)
- (Typical level of project definition required: 1% to 15% of full project definition.)
- (Accuracy Range: L=-15% to -30%, H=+20% to +50%)

Class 4 estimates are generally prepared based on limited information and subsequently have fairly wide accuracy ranges. They are typically used for project screening, determination of feasibility, concept evaluation, and preliminary budget approval. Class 4 estimates are prepared for a number of purposes, such as but not limited to, detailed strategic planning, business development, project screening at more developed stages, alternative scheme analysis, confirmation of economic and/or technical feasibility, and preliminary budget approval or approval to proceed to next stage.

Hybrid FO-MD System Description. A process flow diagram (PFD) enables a better understanding of the process layout and the material flow in a process. For the integrated FO and MD system, a PFD is

presented in Figure 3-14 below. In this system, distilled-quality water is recovered from a waste water stream that would otherwise be discharged as plant effluent. As shown in the figure, waste water first enters the forward osmosis (FO) unit. This feed water is circulated on one side of the membrane while concentrated draw solution which has a high osmotic pressure is circulated on the other side of the membrane. Due to the osmotic pressure differential between the feed water and the draw solution, water permeates through the FO membrane into the draw solution. Impurities in the effluent stream are concentrated while water transfers to the draw solution side. The concentrated effluent stream exits the FO module and is sent for waste treatment/disposal. The dilute draw solution that contains the additional permeated water exits the FO module and is routed to a heat exchanger, where it is heated. The heat duty required by the dilute draw solution is provided by low grade waste heat. The hot dilute draw solution is sent to the membrane distillation unit for water recovery and simultaneous draw solution regeneration. Similar to heat exchanger configuration, the hot dilute draw solution is circulated on one side of the membrane while cold water is circulated on the other side. Due to the relatively higher vapor pressure on the draw solution side, water on this side of the membrane will pass into the vapor phase. The lower vapor pressure on the cold side of the membrane enables the vapor phase water to condense into the cold side water, thus setting mass transport of pure water between the hot and the cold sides. The regenerated draw solution coming out of the MD unit is recycled to the FO unit for water purification and marks the completion of a cycle. The recovered water in the MD system is present on the cold side which is sent for reuse in the plant.

The inputs to the treatment unit are the wastewater stream, a waste heat stream and the cold water stream. Draw solution is circulated within the treatment unit and therefore, is not considered an input stream. The outgoing streams from this system are the clean water stream that also contains the water recovered, the waste heat return stream and a liquid effluent stream that is sent for disposal.

The techno-economic analysis was based on the results of the integrated process model that was developed using Aspen Plus process simulation software. The PFD in Figure 3-14 shows the overall process flow of the integrated FO-MD system. The FO and MD process blocks were configured in Aspen Plus and were linked to the respective MATLAB subroutines. Data from the inlet streams flowing to the FO and MD process blocks is transferred to the corresponding MATLAB subroutines for computing the membrane module performance and resulting fluxes and this information is transferred back to the Aspen Plus interface.

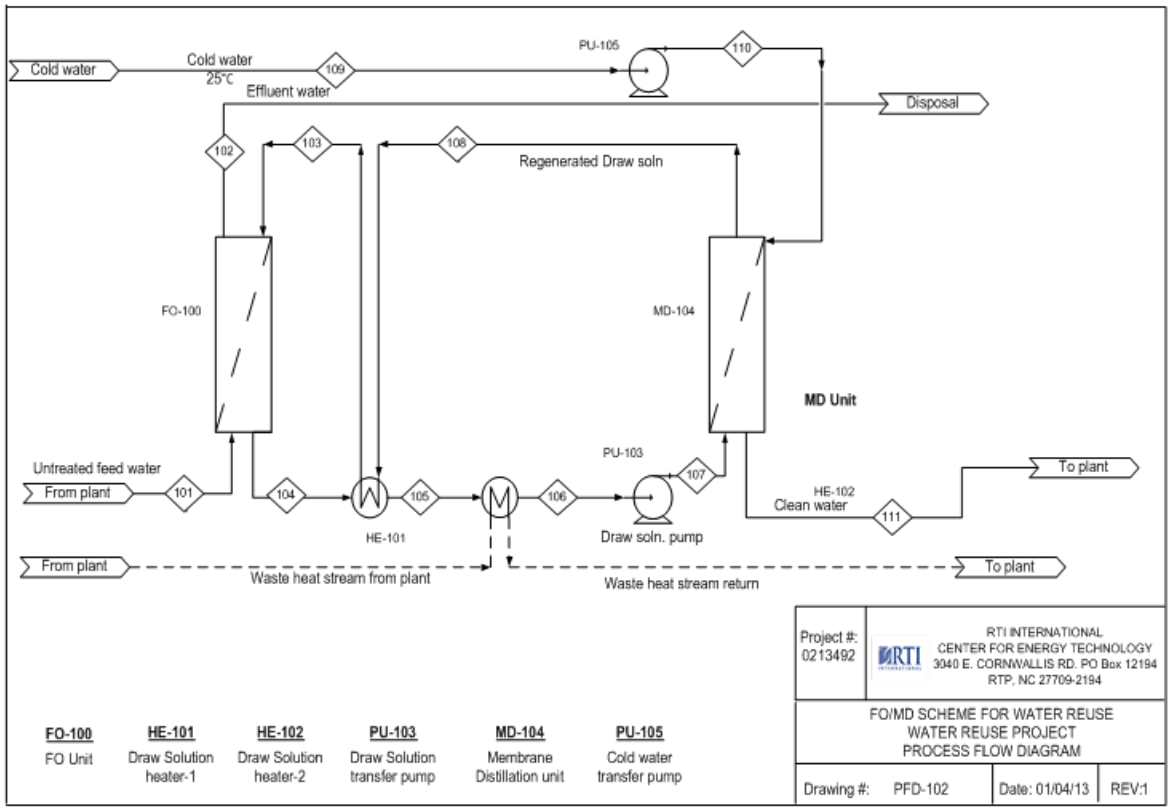

Figure 3-14. PFD of the integrated FO-MD water treatment system.

Two model wastewater streams were developed to represent the complete range of potential industries. Model wastewater streams were determined based on osmotic pressure (i.e., total dissolved solids) and included a low and high case scenario, representing industries like petroleum refining and produced water, respectively. Presented in Tables 3-4 and 3-5 are the flow rates and water quality of the model wastewater streams.

Table 3-4. Model Wastewater composition for low TDS case.

PARAMETER	VALUE	BASIS
Flow rate, average	3,854 gpm	EPA [35]
Chemical oxygen demand	115 mg/L	EPA [35]
Biochemical oxygen demand	14 mg/L	EPA [35]
Total organic carbon	33 mg/L	EPA [35]
Total suspended solids	26 mg/L	EPA [35]; API [36]
Total dissolved solids	2,170 mg/L	API [36]
Water temperature	80 °F	Professional judgment
pH	7.7	Professional judgment
Alkalinity	200 mg/L as $CaCO_3$	Professional judgment
Ammonia	1 mg/L as N	Professional judgment

PARAMETER	VALUE	BASIS
Calcium	165 mg/L	API [36]
Chloride	700 mg/L	Professional judgment
Fluoride	6 mg/L	Professional judgment
Hardness	639 mg/L	Calculated
Iron	<1 mg/L	API [37]
Magnesium	55 mg/L	Professional judgment
Nitrate	21 mg/L as N	Professional judgment
Phosphate	0.1 mg/L as P	Professional judgment
Sodium	451 mg/L	Calculated
Sulfate	400 mg/L	Professional judgment
Arsenic	0.005 mg/L	API [37]
Chromium	0.068 mg/L	API [37]
Copper	0.018 mg/L	API [37]
Mercury	0.0009 mg/L	EPA [35]
Nickel	0.010 mg/L	API [37]
Selenium	0.0172 mg/L	EPA [35]
Zinc	0.061 mg/L	API [37]
2,2,4-Trimethlypentane	0.000015 mg/L	API [37]
Benzene	0.0586 mg/L	Estimated; RTI [38]
Biphenyl	0.000035 mg/L	Estimated; RTI [38]
Cresols	0.002193 mg/L	Estimated; RTI [38]
Cumene	0.000373 mg/L	Estimated; RTI [38]
Ethylbenzene	0.003429 mg/L	Estimated; RTI [38]
Hexane	0.000653 mg/L	Estimated; RTI [38]
Methyl tertiary-butyl ether	0.1280 mg/L	Estimated; RTI [38]
Naphthalene	0.001928 mg/L	Estimated; RTI [38]
Phenol	0.006037 mg/L	Estimated; RTI [38]
Styrene	0.034476 mg/L	Estimated; RTI [38]
Toluene	0.0287 mg/L	Estimated; RTI [38]
Xylene	0.015430 mg/L	Estimated; RTI [38]
1,3-Butadiene	0.000081 mg/L	Estimated; RTI [38]

Table 3-5. Model Wastewater composition for high TDS case.

PARAMETER	VALUE	BASIS
Flow rate, average	3,854 gpm	EPA [35]
Total organic carbon	42 mg/L	EPA [35]
Total suspended solids	277 mg/L	EPA [35]; API [36]
Total dissolved solids	59,475 mg/L	API [36]
Water temperature	80 °F	Professional judgment
Alkalinity	381 mg/L as $CaCO_3$	Professional judgment
Ammonia	1 mg/L as N	Professional judgment
Calcium	165 mg/L	API [36]
Chloride	23,900 mg/L	Professional judgment
Hardness	5,838 mg/L	Calculated
Iron	22 mg/L	API [37]
Phosphate	12 mg/L as P	Professional judgment
Sodium	14,600 mg/L	Calculated
Sulfate	104 mg/L	Professional judgment
Barium	30 mg/L	API [37]
Strontium	186 mg/L	API [37]
Silica	47 mg/L	API [37]
Mercury	0.0009 mg/L	EPA [35]
Manganese	1.3 mg/L	API [37]
Potassium	436 mg/L	EPA [35]
Boron	13 mg/L	API [37]

The target product water composition was based on the requirements for intermediate pressure boiler feed water. This quality was selected because of its high-value in industrial processes and its broad application for use as process water as well as cooling tower makeup. Presented in Table 3-6 are the target water quality requirements for the techno-economic analysis.

Table 3-6. Target product water quality.

PARAMETER	INTERMEDIATE PRESSURE (10-50 bar)	BASIS
Aluminum	0.1 mg/L	EPA [39]
Ammonia	0.1 mg/L	EPA [39]
Bicarbonate	120 mg/L	EPA [39]
Calcium	0.4 mg/L	EPA [39]
Chloride	As received	EPA [39]
Copper	0.05 mg/L	EPA [39]
Hydrogen sulfide	As received	EPA [39]
Iron	0.3 mg/L	EPA [39]
Manganese	0.1 mg/L	EPA [39]
Magnesium	0.25 mg/L	EPA [39]
Silica	10 mg/L	EPA [39]
Sulfate	As received	EPA [39]
Zinc	0.01 mg/L	EPA [39]
Alkalinity	100 mg/L	EPA [39]
Carbon tetrachloride extract	1 mg/L	EPA [39]
Chemical oxygen demand	5 mg/L	EPA [39]
Dissolved oxygen	0.007 mg/L	EPA [39]
Dissolved solids	500 mg/L	EPA [39]
Suspended solids	5 mg/L	EPA [39]
Hardness	1.0 mg/L	EPA [39]
Methylene blue active substances	1 mg/L	EPA [39]
pH	8.2-10.0	EPA [39]
Temperature, °C	As received	EPA [39]

Assumptions used in Techno-economic Analysis. The assumptions used in this analysis are presented in Table 3-7 and were required for the WaTER cost model. Details about the use of these assumptions are given in the WaTER User's Manual [34].

Table 3-7. Assumptions used in the economic analysis.

PARAMETER	UNITS	VALUE
Equipment life	Years	20
Operating hours	Hours/day	24
Operating days	Days/year	329
Power Cost	$/kWh	0.1
Sulfuric Acid	$/dry ton	140
Scale Inhibitor	$/dry ton	4,400
Citric Acid	$/dry ton	2,500
Sodium Hydroxide	$/dry ton	825
Sodium EDTA	$/dry ton	1,260
Phosphoric Acid	$/dry ton	550
Sodium Chloride	$/dry ton	80
Membrane Replacement Frequency	years	3
Annual Discount Rate	%	6
Maintenance and Repair Allowance	% of equipment cost	3
Contingency	%	6

The estimation of total costs incurred for a project during its lifetime in operation is essential to evaluate or to compare a process against any other. The total costs incurred on the project in its lifetime can broadly be classified into the total capital costs and total operating costs. The project lifetime was considered to be 20 years, and the annual discount rate was assumed to be 6%. The estimation procedure for the capital and operating expenses for the two technologies are described below.

Capital Costs. The total capital cost is the sum of material equipment costs, the installation cost for the process equipment, and the total indirect capital costs. The total indirect capital costs account for the construction overhead costs, contingency, project management fees, and the working capital required for the project. These were considered to be factors of the total direct costs, and the details are listed in Table 3-8.

Table 3-8. Indirect cost components multiplier.

Indirect cost component	Factor	
Construction Overhead	4%	of Total Direct Capital costs
Contingency	6%	of Total Direct Capital costs
A&E fees; Project Management	12%	of Total Direct Capital costs
Working Capital	4%	of Total Direct Capital costs

The installation costs for all membrane modules, such as FO and MD as well as the RO and MF in the conventional technology, were estimated using the Water Treatment Estimation Routine (WaTER), which was developed as part of a joint effort between the EPA, the Bureau of Reclamation, and the National Institute of Standards and Technology. WaTER is an Excel workbook [34] developed for estimating the cost of new water treatment facilities and comparing different technological alternatives using the following design inputs: water influent composition, plant production capacity, desired treated water quality, and cost indices/reports. The cost model used in WaTER is suitable for Class 5 cost estimates as defined by Association for the Advancement of Cost Estimating (AACE). In addition, we utilized membrane supplier estimates whenever possible to increase the accuracy of the final estimate, resulting in a Class 4 estimate. The various cost component indices used on the WaTER methodology are outlined in Table 3-9. All indices were updated to August 2013 dollars for the economic analysis.

Table 3-9. Cost component categories and their associated indices used in the WaTER cost model.

Cost Component	Index (1967 = 100)
Excavation and site work	ENR Skilled Labor Wage Index
Manufactured equipment	BLS General Purpase Machinery & Equipment Commodity Code 114
Concrete	BLS Concrete Ingredients Commodity Code 132
Steel	BLS Steel Mill Products Commodity Code 1017
Labor	ENR Skilled Labor Wage Index
Pipes and valves	BLS General Purpose Equipment Producer Price Index 1149
Electrical equipment and instrumentation	BLS Electrical Machinery & Equipment Commodity Code 117
Housing	ENR Building Cost Index
Energy requirements	U.S. Department of Energy ($/kWh)
Maintenance material requirements	BLS Producer Price Index for Finished Goods Code SOP3000

Operational Costs. The total cost for operating the processes can be further split based on the cost of utilities required to run the process and the labor costs involved with the project operation. In this study, the operating costs were further split into the following categories

- Electricity
- Labor
- Chemicals (acid, caustic, antiscalant, and chlorine)
- Membrane replacement
- Cleaning chemicals

- Cartridge filters
- Repairs and replacement
- Salt makeup costs for FO systems

The salt makeup costs for FO systems were based on determining the salt flux in these systems from the process model and, therefore, estimating the annual salt makeup requirement. For the remaining operating cost components, the correlations presented in the WaTER User's Manual were utilized Wilbert, 1999 #45}. As presented in the assumptions, all membrane modules (FO, MD, MF, and RO) were assumed to last for a period of 3 years. Based on the material membrane module costs, the membrane replacement costs were estimated for each case.

Updated Techno-economic Analysis. The Class IV (+/-40%) preliminary techno-economic analyses was revised in the middle of the project. These preliminary analyses had been done for two model industrial wastewaters that represent most of the U.S. manufacturing sector with respect to TDS content. One wastewater had low TDS concentration of 2,170 mg/L; the other had high TDS concentration of 44,442 mg/L.

Final Techno-Economic Evaluation (Evaporator Comparison). Based on results from the preliminary model and after discussion with industrial project partners and the project steering committee, it was determined that a better comparison for process performance would be a thermal evaporator system. This updated techno-economic evaluation included refined performance data using data obtained from the 500-gpd system during the treatment of real industrial wastewater. These updated values on FO and MD membrane flux performance, salt consumption, and heat utilization allowed for a refined estimation of the expected economic cost of treating water at commercial scale with this technology and will also provide areas of need for future technology innovation.

Pilot-Scale, Integrated FO-MD Test Prototype

To test the concept that was developed at the bench and self-standing lab scale, an integrated prototype skid was designed, constructed and installed in a commercial-size trailer. A process flow diagram (PFD) was prepared to select appropriate equipment sizes. Figure 3-15 shows the finalized PFD for the FO-MD prototype system. Mass and heat balances were calculated for two feed conditions: 30,000 ppm and 60,000 ppm TDS. The flow conditions at a feed condition of 30,000 ppm is shown in the Figure 3-15, and the flow condition at a feed condition of 60,000 ppm is shown in Table 3-10.

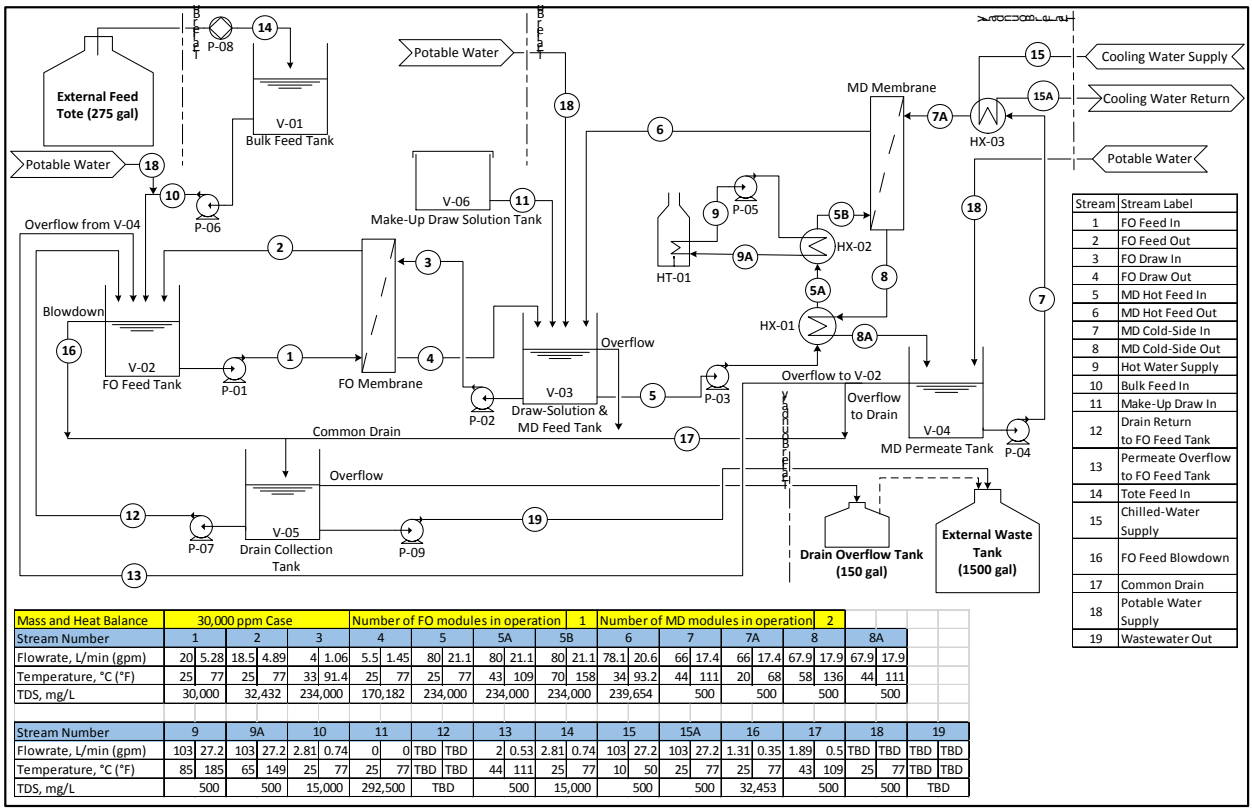

Stream	Stream Label
1	FO Feed In
2	FO Feed Out
3	FO Draw In
4	FO Draw Out
5	MD Hot Feed In
6	MD Hot Feed Out
7	MD Cold-Side In
8	MD Cold-Side Out
9	Hot Water Supply
10	Bulk Feed In
11	Make-Up Draw In
12	Drain Return to FO Feed Tank
13	Permeate Overflow to FO Feed Tank
14	Tote Feed In
15	Chilled-Water Supply
16	FO Feed Blowdown
17	Common Drain
18	Potable Water Supply
19	Wastewater Out

Mass and Heat Balance	30,000 ppm Case				Number of FO modules in operation	1			Number of MD modules in operation	2				
Stream Number	1	2	3	4	5	5A	5B	6	7	7A	8	8A		
Flowrate, L/min (gpm)	20 5.28	18.5 4.89	4 1.06	5.5 1.45	80 21.1	80 21.1	80 21.1	78.1 20.6	66 17.4	66 17.4	67.9 17.9	67.9 17.9		
Temperature, °C (°F)	25 77	25 77	33 91.4	25 77	25 77	43 109	70 158	34 93.2	44 111	20 68	58 136	44 111		
TDS, mg/L	30,000	32,432	234,000	170,182	234,000	234,000	234,000	239,654	500	500	500	500		
Stream Number	9	9A	10	11	12	13	14	15	15A	16	17	18	19	
Flowrate, L/min (gpm)	103 27.2	103 27.2	2.81 0.74	0 0	TBD TBD	2 0.53	2.81 0.74	103 27.2	103 27.2	1.31 0.35	1.89 0.5	TBD TBD	TBD TBD	
Temperature, °C (°F)	85 185	65 149	25 77	25 77	TBD TBD	44 111	25 77	10 50	25 77	25 77	43 109	25 77	TBD TBD	
TDS, mg/L	500	500	15,000	292,500	TBD	500	15,000	500	500	32,453	500	500	TBD	

Figure 3-15. PFD of integrated FO-MD system.

Table 3-10. FO-MD Flow condition at 60,000 ppm Feed TDS

Mass and Heat Balance	60,000 ppm Case								Number of FO modules in operation: 2					
Stream Number	1		2		3		4		5		5A		5B	
Flowrate, L/min (gpm)	40	10.6	38	10	8	2.11	10	2.64	80	21.1	80	21.1	80	21.1
Temperature, °C (°F)	25	77	25	77	33	91.4	25	77	25	77	43	109	70	158
TDS, mg/L	30,000		32,432		234,000		184,594		234,000		234,000		234,000	
	Number of MD modules in operation: 2													
Stream Number	6		7		7A		8		8A		9		9A	
Flowrate, L/min (gpm)	78	20.6	66	17.4	66	17.4	64	16.9	64	16.9	103	27.2	103	27.2
Temperature, °C (°F)	34	93.2	44	111	20	68	58	136	44	111	85	185	65	149
TDS, mg/L	239,654		500		500		500		500		500		500	
Stream Number	10		11		12		13		14		15		15A	
Flowrate, L/min (gpm)	2.81	0.74	0	0	TBD	TBD	2	0.53	2.82	0.75	103	27.2	103	27.2
Temperature, °C (°F)	25	77	25	77	TBD	TBD	44	111	25	77	10	50	25	77
TDS, mg/L	15,000		292,500		TBD		500		15,000		500		500	
Stream Number	16		17		18		19							
Flowrate, L/min (gpm)	0.67	0.18	1.89	0.5	TBD	TBD	TBD	TBD						
Temperature, °C (°F)	25	77	43	109	25	77	TBD	TBD						
TDS, mg/L	63,408		500		500		TBD							

Using the flow conditions of both high (60,000 ppm) and low (30,000 ppm) TDS feed conditions, a P&ID (Piping and Instrumentation Diagram) was prepared to direct construction and control logic preparation. Due to system complexity, the system was divided into four subsections: Feeding system, FO system, MD system, and Discharge system. P&IDs of each section are presented in the Appendix.

System Configuration

The integrated FO-MD system consisted of four major loops: FO loops, MD loops, a heating loop, and a cooling loop. The entire system, except the cooling loop, was mounted on a skid. A 53-foot commercial trailer was modified for the test and then the skid was mounted inside the trailer.

The FO loop has six pressure vessels (AXEON 200530, MHPVC-4040-12Q-KIT) for FO membranes, a FO Feed water circulation pump (Iwaki, MX403HCV6, 3hp), and a FO draw solution circulation pump (Iwaki, MX-251CV6, 1hp). The MD loop has 3 MD membranes (Membrana, 1" ports), a hot side recirculation pump (Iwaki, MX402CVR, 2hp), a cold side recirculation pump (Iwaki, MX402CVR, 2hp), and 3 heat exchangers for: MD hot side inlet, MD hot side outlet, and MD cold side (Alfa Laval, plate and frame type). The heating loop was installed to supply heat to the MD hot side inlet. The heating loop was composed of a heater (Watlow, CFRN773D5XS) and a heater recirculation pump (Iwaki, MXM-2212-CFVH, 1hp). The cooling water line was connected to the cold side of the heat exchanger to cool down the cold side recirculation line before entering the MD membrane. The cooling was line consisted of a heat exchanger (Alfa Laval, plate and frame type) and a recirculation pump (B&G, Inline series 90, ¾hp).

Five 50-gallon tanks were also installed for the storage/collection of: raw wastewater, FO Feed, FO draw/MD feed, MD permeate, and generated wastewater (drain tank). A tote was used to transport wastewater samples from the oil production site where the produced water was generated to the trailer site. The tote was located outside trailer and fed to the raw wastewater tank by the bulk feed pump (Iwaki, SMX-221CAYYU). Similarly, the feed transfer pump (Iwaki, MX-251CV6) was used to transfer the feed from the raw wastewater tank to the FO feed tank. A level transmitter was installed in the tank to control the corresponding transfer pump. The generated wastewater from the FO-MD system was collected in the drain tank and transferred by a pump (Iwaki, MXM-22, ½hp) to the Waste collection tank (1,500 gallons), which was located outside the trailer.

Flow transmitters, pressure transmitters, temperature transmitters, and level transmitters were installed and connected to the PLC system to control and monitor the system performance. pH and conductivity sensors were also installed and connected to the PLC system to monitor water quality. These sensors were used to protect the system from over-pressurization, overfilling, and overheating.

P&IDs were prepared and sent to an outsourcing company for the physical construction of the skid. The 3-D drawing was prepared for review. The final 3-D drawing is presented in Figure 3-16.

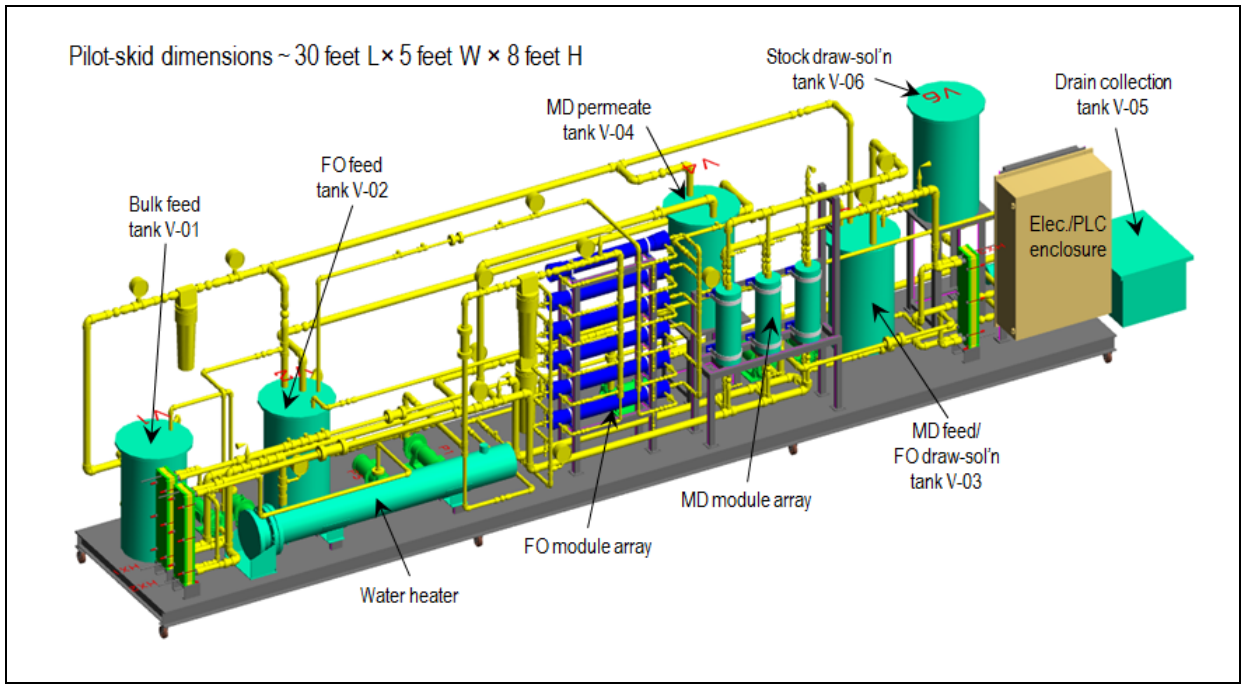

Figure 3-16. Final 3-D layout for the integrated FO-MD system.

Using the final 3-D drawing, the skid was constructed at the warehouse of the outsourcing company. Photographs of the integrated FO-MD system skid are presented in Figure 3-17. After the construction work was completed, the skid was moved into the 53-foot-long mobile trailer and a power line was connected to the trailer's main panel. The trailer was prepared for this project by having an electric transformer, two power distribution panels, an air conditioner with a heating function, and a small laboratory area for simple testing such as pH, conductivity, and Hach test kits. The trailer with the skid successfully installed inside was then transported to the test site. Pictures of the trailer are presented in Figure 3-18. The trailer was parked in front of a local facility building that featured a cooling water supply system because the trailer did not have an independent cooling system. The building's cooling water supply was therefore connected to the trailer to provide an immediate source of cooling water. Figure 3-19 shows the secondary cooling-water loop set up at the facility building. The cooling water temperature was 53 °F and the recirculation flow rate was approximately 18 gpm.

Figure 3-17. Photographs of the integrated FO-MD system skid

Figure 3-18. (a) The mobile water trailer, (b) Pilot-scale, integrated FO-MD prototype skid and (c) small laboratory area inside the trailer.

Figure 3-19. Secondary cooling-water loop set up at the test site to support field-testing of integrated FO-MD prototype

Three FO membranes were installed in the FO membrane pressure vessel after commissioning work was completed. The type of FO membrane (FO4040) used was a spiral-wound thin-film composite with polyamide coating and had an area of $3m^2$ ($32ft^2$). The physical diameter of the membrane was 4 inches and the length was 40 inches, which is equivalent to the size used at commercial scale. The MD membrane arrived from its source in existing housing, so an additional vessel was not required. A key difference between the membranes was that the MD membrane could be dried after hydro-testing, which is not possible for FO membranes (because drying would damage the FO membrane); the MD membrane was installed before hydro-testing in the manufacturing facility. The outer size of the MD membrane (8 × 20 Industrial extra-flow with center baffle) was 8.6 inches (dia) x 26.3 inches (length) and the membrane/potting material was polypropylene/epoxy. The operating flow range was 5–50 gpm. The original housing material was PVC, but was changed to CPVC in order to operate at high temperatures. The known maximum service temperature of CPVC is 200 °F (93 °C). After commission was completed, MD membranes with PVC housing were replaced with MD membranes with CPVC housing.

A secondary containment (L Bracket spill berm) was installed under the trailer to collect any potential leakage during operation. The size of the berm was 12 feet (W) x 60 feet (L) x 12 inches (h) and came with L-brackets for wall support. The feed tote (250gallon), waste collection tank (1500gallon), and drain collection (150gallon) tank were located outside the trailer. The waste collection tank came from the source equipped with a secondary containment attachment. The set-up of the trailer and relating tanks are shown in Figure 3-20.

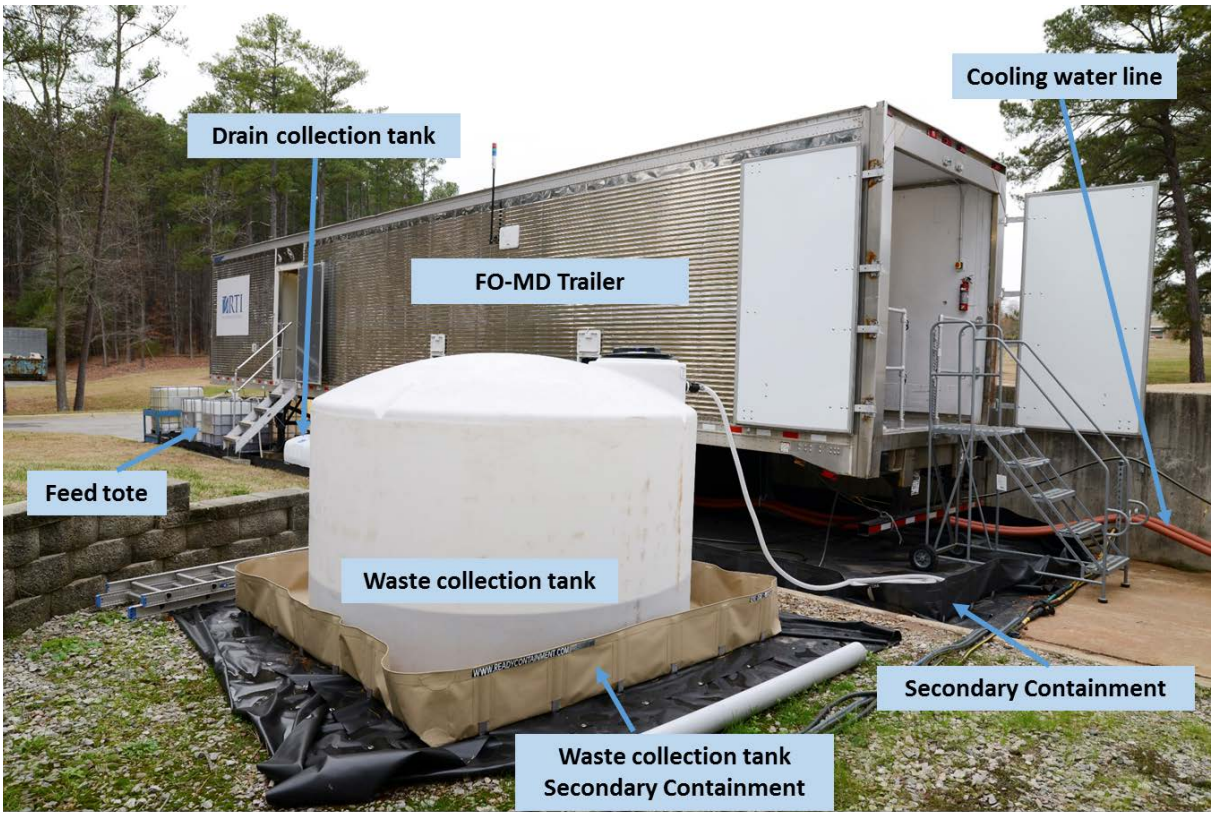

Figure 3-20. FO-MD trailer and tanks set-up

Control logic

The team developed a process control philosophy that was used to guide the PLC layout and programming. The process control philosophy consists of five preprogrammed operation modes for the prototype. 1) FO-MD once-through mode, 2) FO-MD recirculation mode, 3) Concentration only mode, 4) MD once-through mode and, 5) MD recirculation mode. Additional control logic was also added at the beginning of the control logic to select the operation mode. The operation mode selection flow chart is shown in Figure 3-21. System parameter settings for tank levels, flows, temperatures, pressures (minimum and maximum), alarm settings, and data logging, trending, and display specifications are also provided in the control philosophy document. The engineering fabricator prepared the PLC program for the prototype based the control philosophy developed in-house.

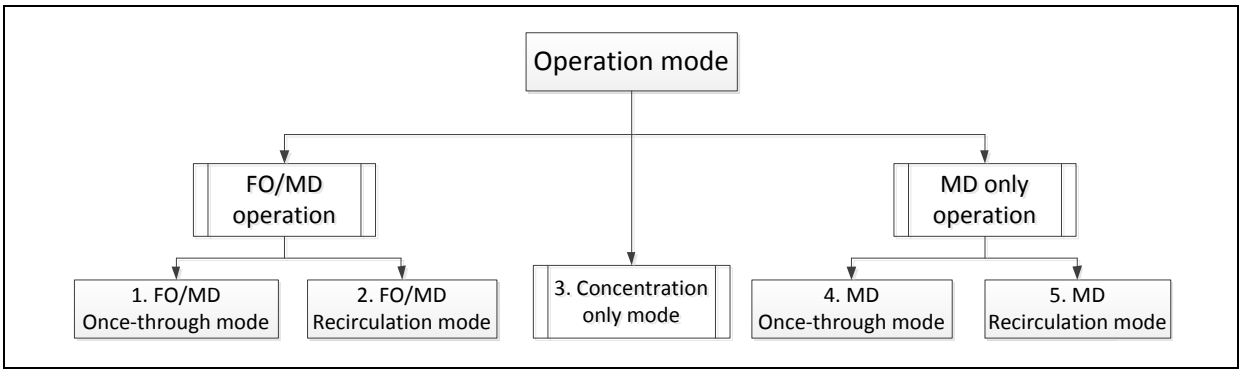

Figure 3-21. Operation mode selection flow chart

Each operation mode has a corresponding unique control mode. The once-through mode was designed to operate the system without any recirculation of permeate or brine when the feed water supply is sufficient. The once-through mode is similar to that of actual operating integrated FO-MD system. The recirculation mode was designed for long-term fouling testing and draw solution back-diffusion testing when the feed water supply becomes limited. In the recirculation mode, the overflow permeate from the MD permeate tank is returned to the FO feed tank and all material collected in the drain tank is pumped to the FO feed tank so that there is no discharge from the system. The system was also designed to operate with each membrane process decoupled, so that only the MD system is used with either once-through or recirculation. Concentration-only mode was added to concentrate the feed to the pre-set conductivity for testing purposes. A detailed flow chart of the FO-MD once-through mode is presented in Figure 3-22. Other flow charts can be found in the Appendix. The main difference between the once-through mode and the recirculation mode is the drain tank operation. All water collected in the drain tank is transferred to the waste collection tank during the once-through mode, but would be returned to the FO feed tank during the recirculation mode to maintain a near-constant concentration for the FO feed.

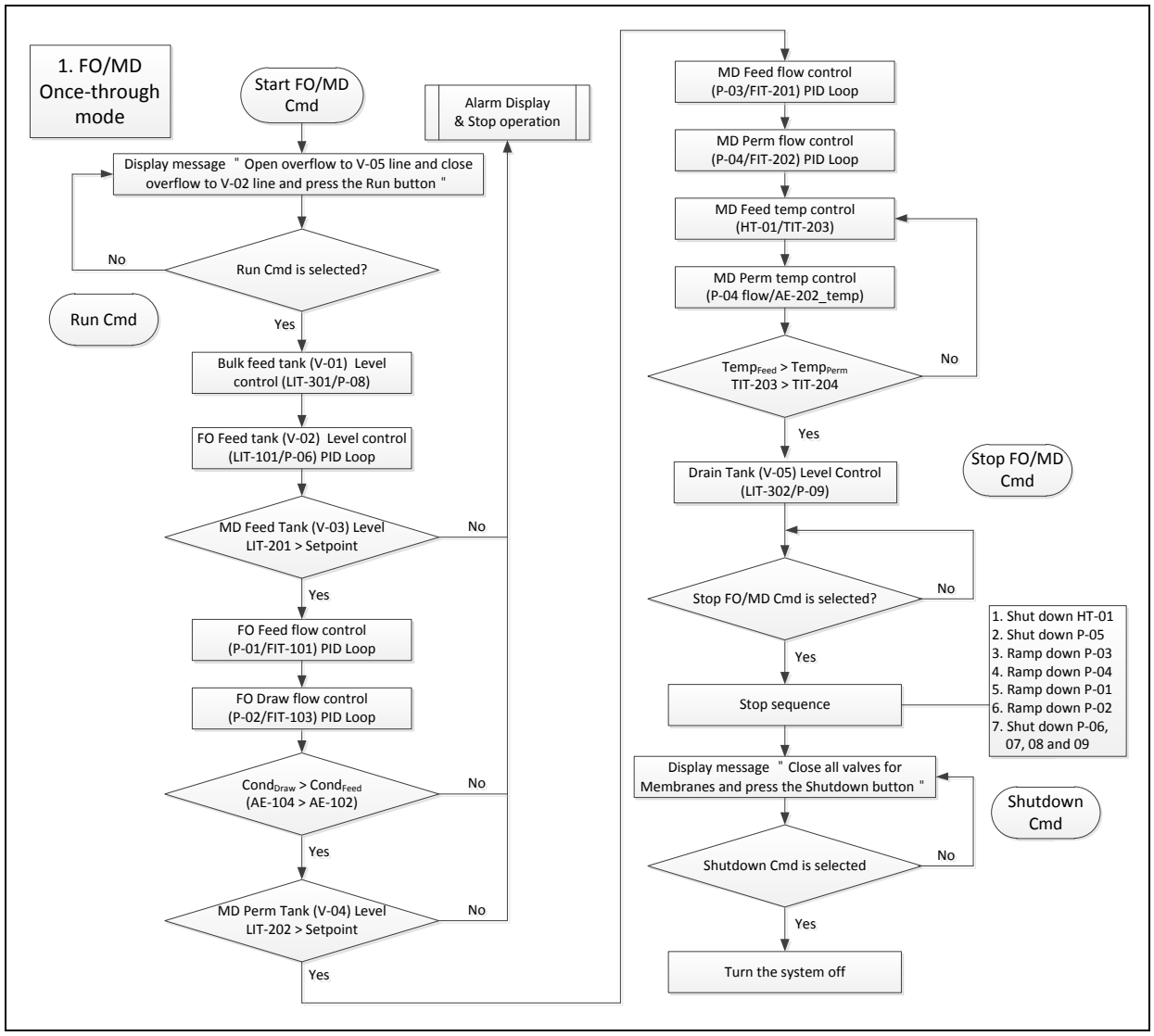

Figure 3-22. FO-MD Once through mode flow chart

Operating program

The control logic and the P&ID were used by the outsourcing company to design and manufacture the control panels (main control panel and heater control panel) for the system. The operating program was also prepared by the outsourcing company to meet the required specifications.

The main control panel consisted of control processer (Allen-Bradley), HMI (Human Machine Interface, Schneider), I/O modules (Input/Output modules), VFDs (Variable Frequency Drives) and other electrical parts such as terminal blocks, switches and contactors. The VFDs control the frequency of main pumps. Signals from installed instruments (flow, pressure and temperature) were collected in the control processer through I/O modules. The heater control panel consisted of the heater VFD and a terminal block. The operator can control the system through the HMI screen (touchpad). The screen shot of HMI and related part in the FO-MD system are shown in Figure 3-23, Figure 3-24, and Figure 3-25. Data is

displayed in real time on the HMI screen and the data graphs are shown in Figure 3-26. To enable remote monitoring and control for unattended operation through the night, a license was purchased for the Vijeo Designer v6.2 HMI configuration software installed by the engineering fabricator. This software has the Web Gate remote access function through which an interactive mirror view of the HMI application running on the skid can be set up on a remote computer. Since this software has been set up to communicate with the skid's Allen-Bradley Compact Logix PLC system, process operating variables on the skid can also be controlled (adjusted) remotely if needed. In addition, all collected data can be transferred to the remote computer and transferred to the operator's computer in the office for further processing.

Figure 3-23 HMI interface and photograph of Feed System of the FO-MD prototype in operation.

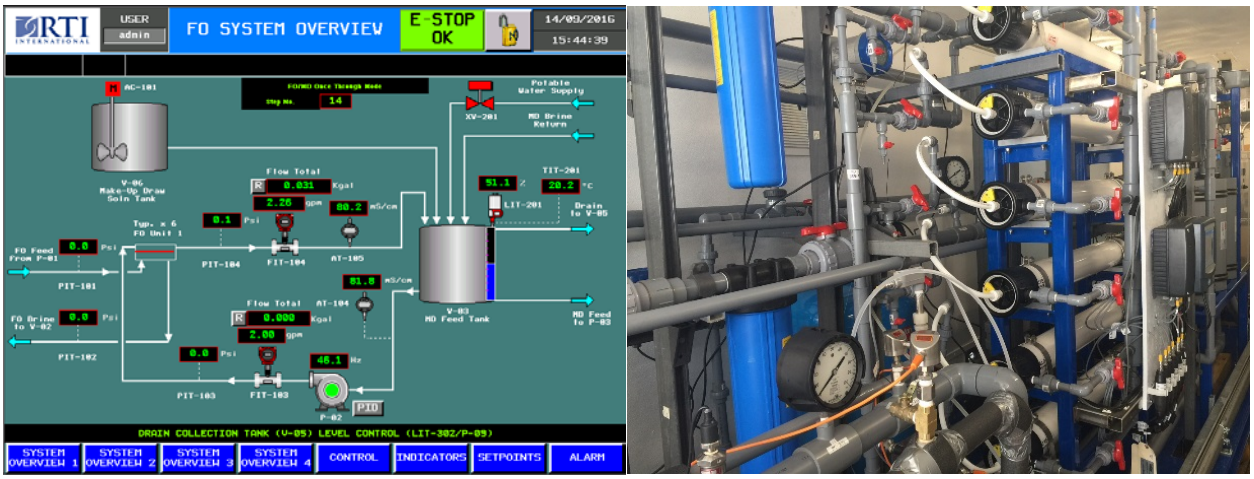

Figure 3-24. HMI interface and photograph of FO System of the FO-MD prototype in operation.

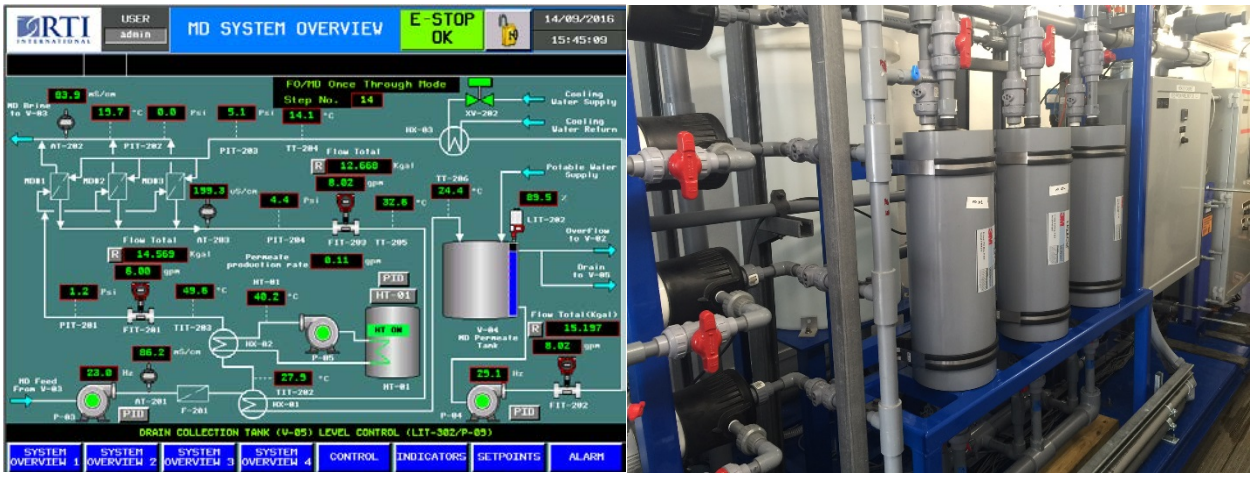

Figure 3-25. HMI interface and photograph of MD System of the FO-MD prototype in operation.

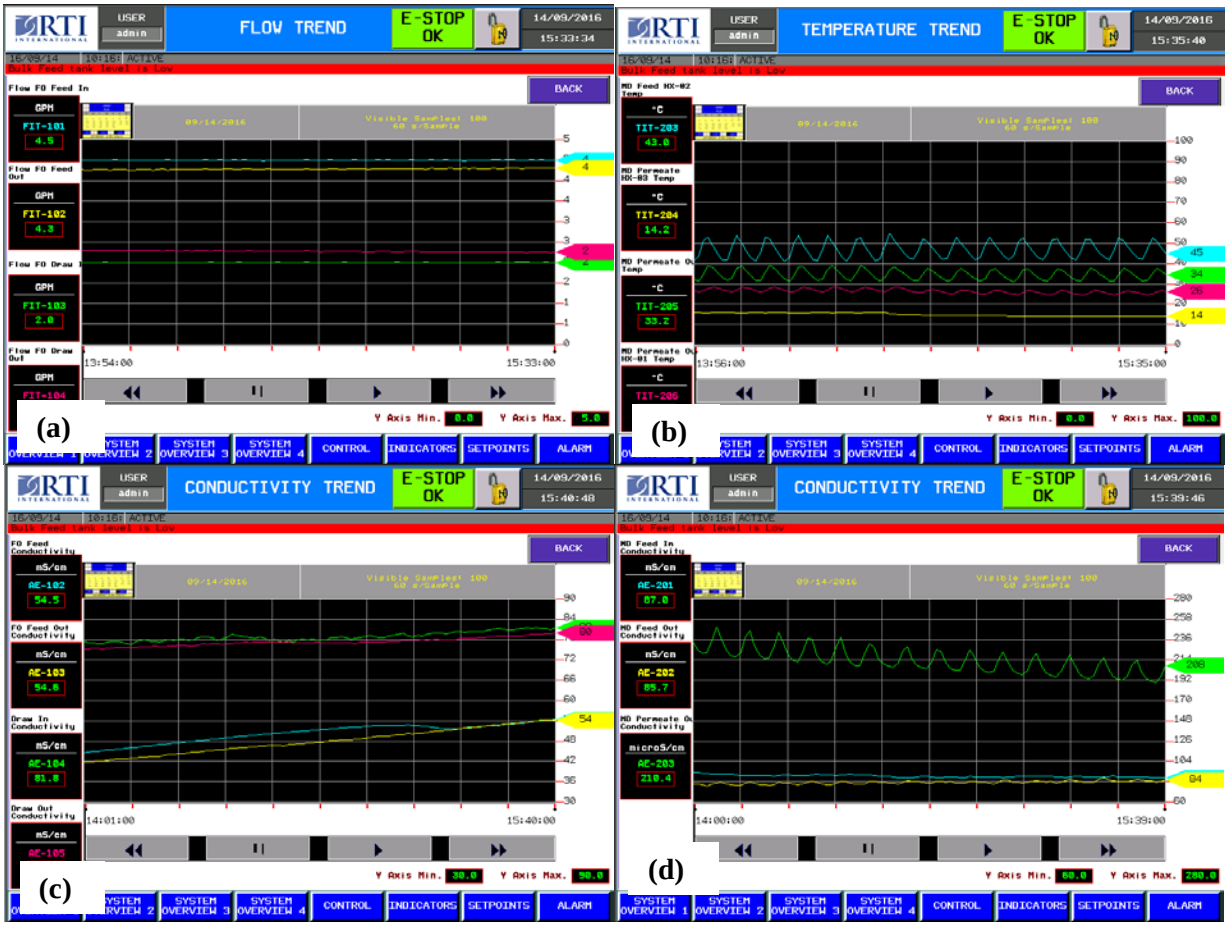

Figure 3-26. Example trend plots monitoring FO-MD prototype operation: (a) FO feed- and draw-side influent and effluent flow rates; (b) MD feed- and permeate-side influent and effluent temperatures; (c) FO feed- and draw-side influent and effluent conductivities; and (d) conductivities of MD feed- and permeate-side influents and MD permeate-side effluent (i.e., product water).

Wastewater characteristics

There were two test plans for operating the prototype FO-MD system: onsite and offsite operation. Onsite operation could supply sufficient raw wastewater and processed water discharge was relatively convenient. However, this option presented several safety, permitting, and utility (power and cooling) supply issues because the site was located at an active oil or gas production site. Challenges for the offsite operation option included a limited supply of raw wastewater (requiring regular shipments replenish supply) and required an individual wastewater disposal plan. However, power and cooling water could be more readily supplied and guaranteed for the offsite option, and there was fewer safety issues. Based on test schedule and test site availability, the test was decided to be operated off-site. Therefore, the integrated FO-MD trailer was located at the local test site in Research Triangle Park, North Carolina. Real industrial wastewater (i.e., RO brine) from the site of an oil and gas production company in California, was shipped to the test site as a feed supply for field-testing the pilot scale, integrated FO-MD prototype. The real wastewater quality is presented in Table 3-11. The stability of the site RO brine during the 7-day shipping period was determined. The stability of the RO brine was evaluated by having a third-party environmental test laboratory measure key water-quality parameters of the brine directly after collection and after a 7-day holding period at ambient conditions.

Table 3-11 compares the water-quality data measured for the “fresh” industrial RO brine of the site and the same brine after a 7-day hold period. The results show that the RO brine wastewater was essentially stable with respect to physical water quality [i.e., pH, total dissolved solids (TDS), and conductivity], metals, alkalinity, ammonia, and oil and grease. Similarly, the very polar organic compounds (acetone, methyl ethyl ketone, methyl isobutyl ketone, phenolics) also appeared to be stable in this wastewater. In contrast, the wastewater showed significant loss (>50%) of nonpolar, volatile organics such as BTEX and the lighter gasoline-range organics (C4-C12) after the 7-day hold. However, it was determined that it was not feasible to control such fugitive losses of volatiles from the wastewater in actual process testing or operation. Since the integrated FO-MD process is primarily TDS-driven, the loss of the nonpolar volatile compounds was deemed not a critical aspect for the prototype field-testing.

Table 3-11. Water-Quality Characteristics of Industrial Wastewater as Collected (Fresh) at the site and after 7-Day Holding Period*

Parameter/Constituent	Fresh wastewater	Wastewater after 7-day hold
pH	12.21	12.15
Conductivity [µS/cm]	21,400	22,300
Total Dissolved Solids [ppm]	14,000	14,000
Na [ppm]	3,950	4,500
K [ppm]	140	160
Ca [ppm]	0.33	0.72
Mg [ppm]	Not detected	Not detected
Total Alkalinity (as $CaCO_3$) [ppm]	4,700	4,900
Total Ammonia (as NH_3) [ppm]	18	17
Total Oil & Grease [ppm]	230	240
Chemical Oxygen Demand [ppm]	2,300	1,900
Biochemical Oxygen Demand [ppm]	470	470
Total Organic Content [ppm]	560	450
Gasoline-Range Organics (C_4-C_{12}) [ppm]	4.2	1.7
Diesel-Range Organics (C_{12}-C_{24}) [ppm]	34	30
BTEX [ppb]	212	111
Phenolics [ppb]	3,290	3,040
Acetone [ppb]	5,800	5,800
Methyl Ethyl Ketone [ppb]	2,600	2,800
Methyl Isobutyl Ketone [ppb]	130	180

* Water-quality tests were done by BC Laboratories (Bakersfield, CA). BC Labs performed the 7-day hold of wastewater at ambient conditions.

4. RESULTS AND DISCUSSION

Water Separation Properties of FO Membranes

FO Membranes Investigated. Eight different flat-sheet FO membranes that were at various stages of development in the FO technology sector were identified for baseline evaluation in the laboratory-scale water-test system. The CTA-NW and CTA-ES membranes are cellulose triacetate (CTA)-based and considered to be the first-generation FO membranes. The CTA-NW was CTA cast onto a weldable, non-woven polyethylene-coated polyester support. The CTA-ES was CTA made with an embedded polyester mesh support. The other six candidates identified were X-TFC, W-TFC, Y-T, HF, Z-US, and Z-S and are considered to be next-generation FO membranes. The X-TFC, W-TFC, Y-T, and Y-HF are polymeric composites likely comprising a polyamide-based selective layer on top of a porous substrate of another polymer material. The Z-US and Z-S are biomimetic membranes. These next-generation membranes have been reported to have markedly higher water fluxes, improved salt rejection, and/or broader operating pH range than the CTA-based ones.

Baseline FO Water Separation Performance

FO Water Flux. Figure 4-1 compares the FO water fluxes J_W measured with DI water feed in the different FO membranes as a function of draw-solution concentration and draw-salt type. For each draw-solution type, as salt concentration (i.e., osmotic pressure) increases, the water flux increases because of the increase in osmotic gradient across the membrane. Furthermore, a closer comparison of the results shows that, at a given draw-solution concentration, different water fluxes are obtained with different draw salts. For all the membranes in Figure 4-1, the draw salts studied can be generally ranked with respect to water flux performance as KCl > NaCl, $CaCl_2$ > $MgCl_2$. This ranking is seen more clearly in Figure 4-2, which replots the Figure 4-1 data in a different way. Draw osmotic-pressure differences alone do not explain this flux trend. Rather this trend is predominantly attributed to ICP within the membrane. The ICP effect decreases the apparent osmotic-pressure driving force seen by the active membrane layer facing the feed side and is dependent on the effective draw-solution diffusivity, which, in turn, depends on the type and size of the draw salt used. The ICP effect should be more pronounced as draw-solution diffusivity becomes lower, and the experimental data support this. Furthermore, instead of plotting as a function of draw-solution concentration as in Figure 4-1 and Figure 4-2, another way of illustrating the effect of draw-salt type on FO water flux was to graph the data as a function of the osmotic-pressure driving force. A representative plot against the osmotic-pressure difference is given in Figure 4-3 for the CTA-ES data, and the trends seen in this figure is consistent with the ICP explanation.

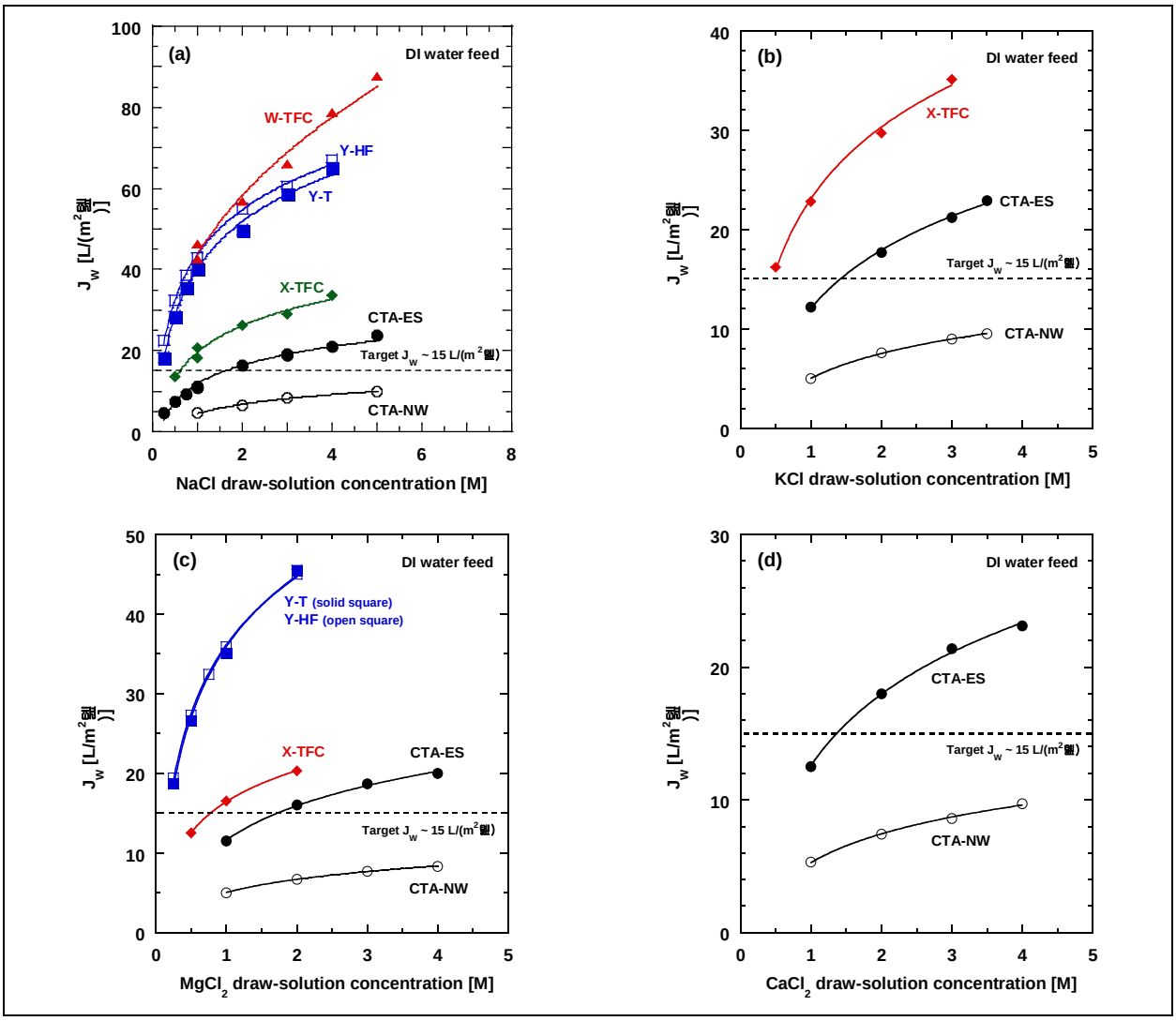

Figure 4-1. FO water fluxes J_W measured in the first-generation CTA-ES and CTA-NW membranes and the next-generation X-TFC, W-TFC, Y-T, and Y-HF membranes using (a) NaCl draw solutions, (b) KCl draw solutions, (c) $MgCl_2$ draw solutions, and (d) $CaCl_2$ draw solutions of different draw-salt concentrations. Feed: DI water. T = 23 °C.

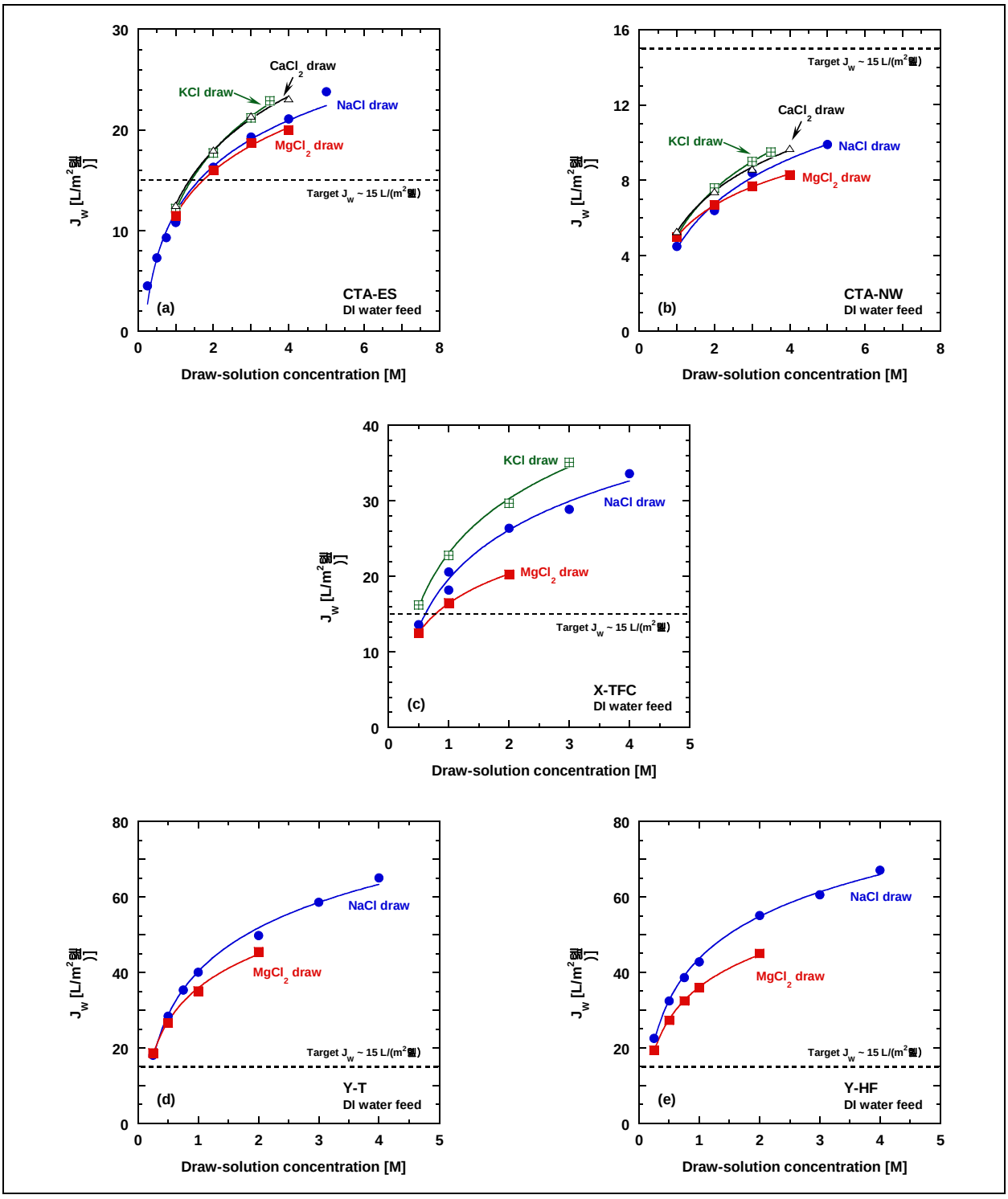

Figure 4-2. FO water fluxes J_W of the first-generation (a) CTA-ES and (b) CTA-NW membranes and the next-generation (c) X-TFC, (d) Y-T, and (e) Y-HF membranes as a function of draw-salt type and draw-solution concentration. Feed: DI water. T = 23 °C.

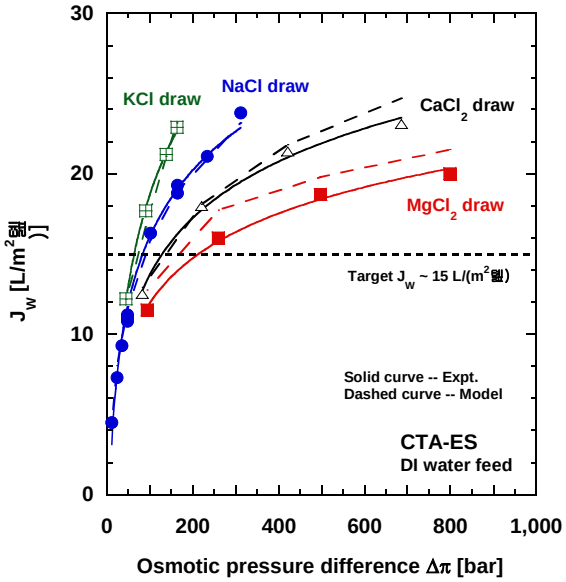

Figure 4-3. FO water fluxes J_W of the CTA-ES membrane as a function of draw-salt type and osmotic-pressure driving force $\Delta\pi$. Solid curves serve as visual guides for the experimental data. Dashed curves are FO model predictions. Osmotic pressures of feed salt concentrations used were taken from the OLI software for electrolyte solutions. Feed: DI water. T = 23 °C.

Of the two first-generation membranes, the Figure 10 graphs show that the CTA-ES had about 2.3-2.5 times higher water flux than the CTA-NW. For example, with a 3.5 M KCl draw solution, the water flux was 23 L/(m^2·h) for the CTA-ES relative to only 9.5 L/(m^2·h) for the CTA-NW. Moreover, the results show that the CTA-NW clearly cannot meet the target flux of 15 L/(m^2·h) even under these ideal test conditions and has been eliminated as a membrane candidate for this project. On the other hand, if draw-salt concentrations of 2 M or higher are used, the commercial CTA-ES could still meet the 15-L/(m^2·h) flux target.

All four next-generation membranes X-TFC, W-TFC, Y-T, and Y-HF exhibited higher water fluxes than the CTA-ES (the best first-generation membrane) and can thus more easily achieve the 15-L/(m^2·h) flux target. Relative to that of the CTA-ES, the water flux was about 1.5-2 times higher for the X-TFC and 3-4 times higher for the W-TFC, Y-T, and Y-HF. For example, with a 4 M NaCl draw solution, the measured FO water flux was greater than 60 L/(m^2·h) for Y-T and Y-HF and about 79 L/(m^2·h) for the W-TFC, while the CTA-ES had a flux of only ~20 L/(m^2·h). Additionally, because of their higher water fluxes, the next-generation membranes can meet the 15-L/(m^2·h) flux target using lower draw-solution concentrations than the CTA-ES. As shown in Figure 4-1, the X-TFC membrane could achieve the target flux with a minimum draw-salt concentration of 1 M, and the Y-T and Y-HF membranes with 0.25 M as a minimum. Based on its behavior in Figure 4-1, the W-TFC should also achieve the target flux at a minimum draw-salt concentration similar to that for the Y-T and Y-HF membranes.

The Z-type membranes are not shown in Figure 4-1 as they had very low J_w ~ 4-6 L/(m^2·h).

Reverse Salt Flux. The corresponding reverse draw-salt fluxes measured in the first- and next-generation membranes in the tests with DI water feed are presented in Figure 4-4. Like the water flux behavior, the reverse salt flux also increased with increasing draw-solution concentration (i.e., osmotic pressure) due to the resulting higher salt concentration gradient across the membrane. Of the two first-generation membranes, the CTA-ES, which had the higher water flux, also displayed higher reverse salt flux than the CTA-NW. The next-generation X-TFC generally had salt fluxes comparable to those seen in the first-generation membranes, particularly the CTA-ES in the case of the monovalent NaCl and KCl draw-salt solutions. The next-generation Y-T and Y-HF membranes, which exhibited among the highest water fluxes, have the highest monovalent salt fluxes relative to the other membranes (Figure 4-4a), with the Y-HF usually showing higher monovalent salt flux than the Y-T. For divalent salts such as $MgCl_2$, the Y-HF membrane still showed much higher salt flux than the Y-T (Figure 4-4c). It is also noted that, unlike its monovalent salt flux, the divalent salt flux of the high-flux Y-T was somewhat lower than that of the CTA-ES but comparable to that of the CTA-NW and X-TFC. For the W-TFC membrane (Figure 4-4a), which had the highest water flux, its monovalent NaCl salt flux was lower than that of the Y-T at 3M and lower NaCl draw concentrations but comparable to that of the Y-T at 4 M and higher NaCl concentrations.

Furthermore, from a comparison of Figure 4-4a and Figure 4-4b to Figure 4-4c and Figure 4-4d, the reverse salt fluxes were observed to be much lower for the divalent salts than for the monovalent salts. More specifically, the draw salts can be ranked in order of increasing salt flux as $MgCl_2 < CaCl_2 << NaCl < KCl$ for all the membranes studied. This ranking was also more easily seen by plotting the reverse salt flux as a function of the osmotic-pressure driving force for a given membrane, as in Figure 4-5 for the CTA-ES data.

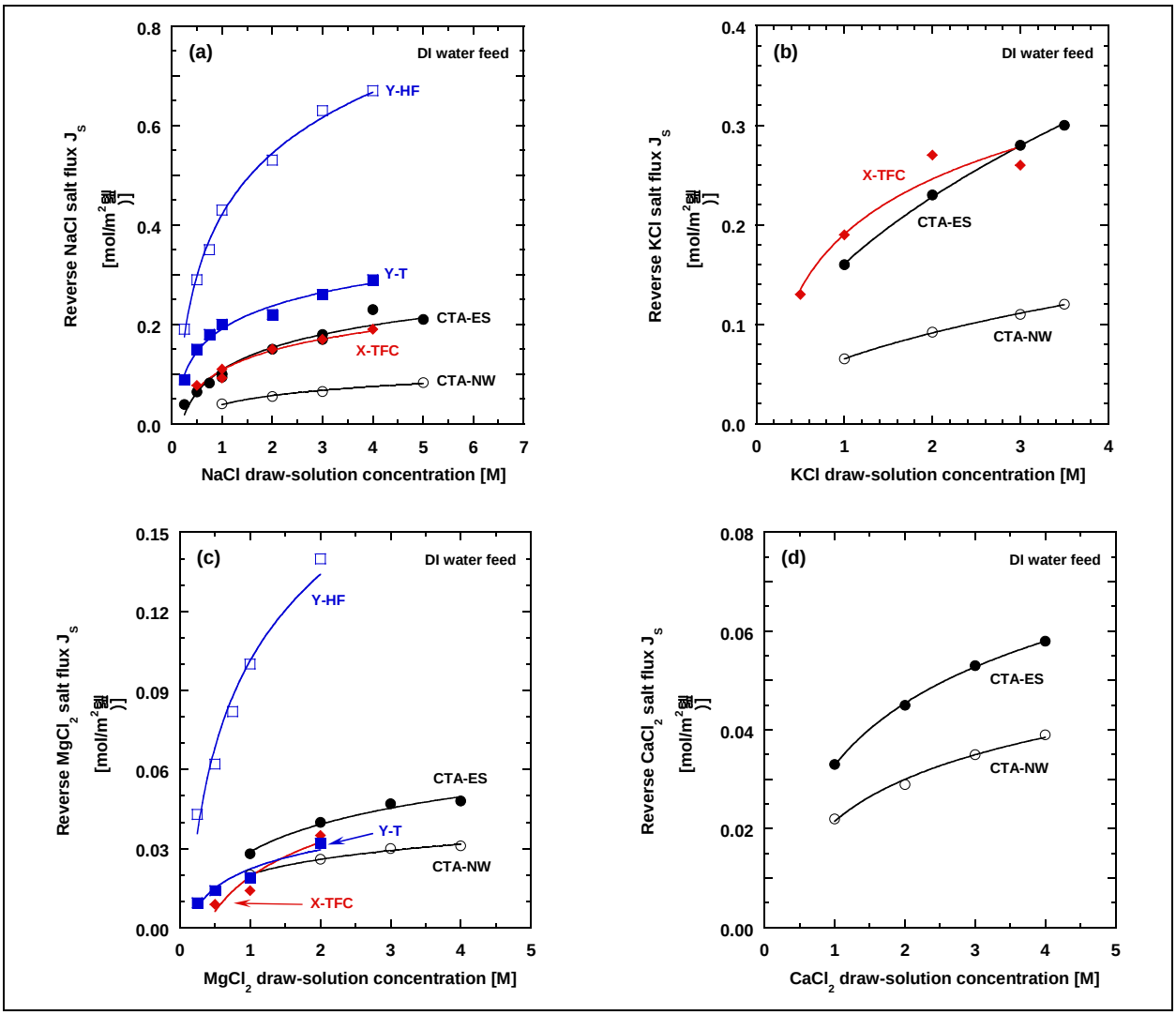

Figure 4-4. Reverse salt fluxes J_S measured in the first-generation CTA-ES and CTA-NW membranes and the next-generation X-TFC, W-TFC, Y-T, and Y-HF membranes as a function of draw-solution concentration: (a) NaCl salt flux, (b) KCl salt flux, (c) $MgCl_2$ salt flux, and (d) $CaCl_2$ salt flux: Feed: DI water. T = 23 °C. The Z-US and Z-S membranes are not included here because their reverse-salt flux was markedly higher [3-12 mol NaCl/(m^2·h)] than the other membranes.

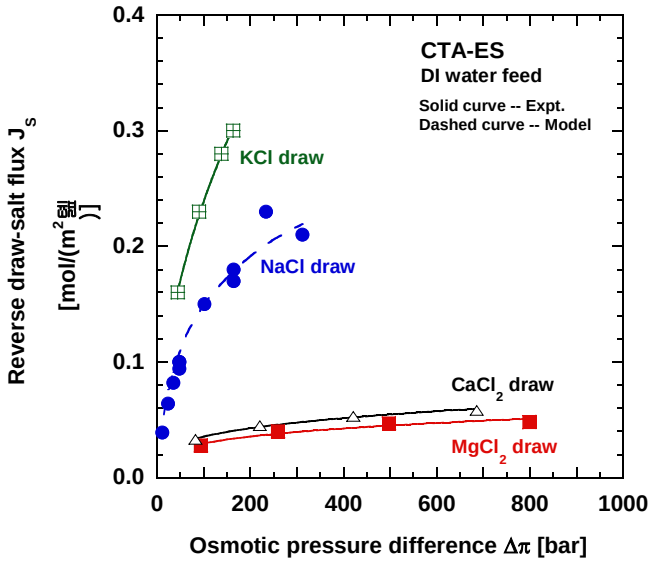

Figure 4-5. Reverse salt flux J_S as a function of osmotic pressure difference across the membrane for the CTA-ES membrane in FO mode. Solid curves serve as visual guides for the experimental data. Dashed curve for the NaCl draw represents the J_S values theoretically predicted from the intrinsic membrane properties of CTA-ES for NaCl draw. Feed: DI water. T = 23 °C.

The salt-flux trend for the chloride salts is mainly attributed to the size of the hydrated cation. For example, of these cations, K^+ has the smallest hydrated size (3 Å) and the highest salt flux and, at the largest hydrated size of 8 Å, the Mg^{2+} ion typically exhibits the lowest salt flux. As hydrated cation size becomes larger, not only is its permeation in the membrane hindered by the larger physical size but also by the lower diffusivity associated with a larger ion. As an example, Figure 4-6 shows the dependence of the measured reverse salt flux in CTA-ES on hydrated cation size for different draw-solution concentrations. The salt flux appears to level off when the hydrated ion size becomes larger than 6-7 Å, suggesting possibly that the reverse salt may not decrease much more if even larger solutes are used in the draw solution. From a process economics viewpoint, a low reverse salt permeation rate is also more attractive because less draw-salt is lost to the feed side, leading to lower make-up draw-salt cost.

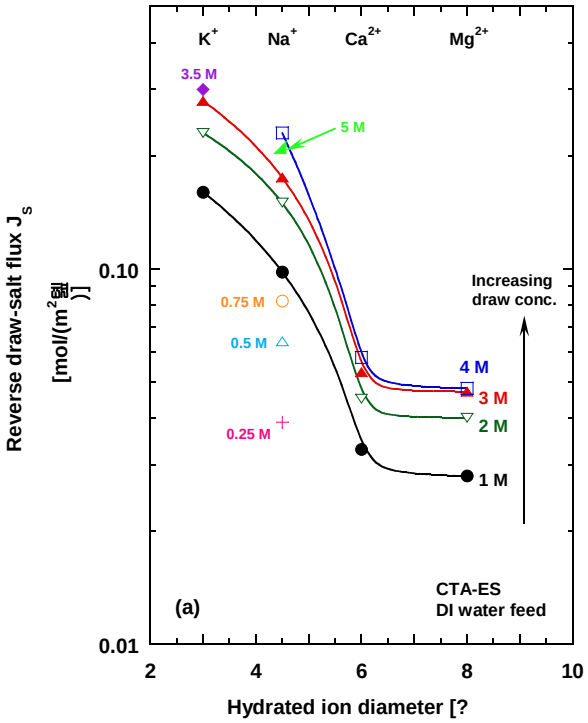

Figure 4-6. Effect of hydrated cation size of chloride draw salts on reverse salt flux J_S in the CTA-ES membrane. Feed: DI water. T = 23 °C.

Water/Salt Selectivity (J_W/J_S). In addition to water and salt fluxes, another key measure of FO membrane performance is the "water/salt selectivity," which indicates the degree to which water preferentially permeates the membrane over the salt. This selectivity is defined to be the ratio of the water flux J_W to the reverse draw-salt flux J_S and is thus denoted as J_W/J_S. The ideal FO membrane should combine a high J_W/J_S selectivity with a high J_W. Table 4-1 summarizes the average J_W/J_S selectivity values measured for the different FO membranes evaluated with DI water feed. Though they have different J_W/J_S selectivities, the membranes in Table 4-1 showed 98+% simple salt rejection in our laboratory FO testing, except for the Z-type membranes which had either very low salt rejection of 30-66% or even negative salt rejection.

The J_W/J_S selectivities of the first-generation CTA-based membranes are similar for NaCl and KCl but different for $MgCl_2$ and $CaCl_2$. Because these membranes have the same selective material layer but different membrane structure/morphology, the lower water/$MgCl_2$ and water/$CaCl_2$ selectivities in the CTA-NW are due to more severe concentration polarization effects on these larger divalent salts in this membrane's internal structure.

Relative to the CTA-ES, the next-generation X-TFC and Y-T membranes had improved J_W/J_S selectivity in addition to higher water flux. The X-TFC had water/NaCl and water/KCl selectivities roughly 1.6 times higher and water/$MgCl_2$ selectivity 2.7 times higher than those in CTA-ES. For the Y-T membrane, the water/NaCl and water/$MgCl_2$ selectivities were 1.8 and 4.9 times higher, respectively, than that in CTA-ES. In the case of the Y-HF, its J_W/J_S selectivity was lower than the X-TFC and Y-T and more

comparable to the CTA-based membranes because its high water flux (Figure 4-1a and Figure 4-1c) was also accompanied by a moderately high salt flux (Figure 4-4a and Figure 4-4c). Based on the separation data collected using only the NaCl draw salt, the W-TFC displayed the highest J_W/J_S selectivity. Though NaCl salt flux in the W-TFC was comparable to the Y-T, its resulting water/salt selectivity was better mainly because it had much higher water flux. From a process perspective, a high salt flux is not desirable typically because it translates to more draw salt lost to the feed side and, in turn, a quicker loss of osmotic-pressure driving force for water permeation.

Table 4-1. Water/Salt Selectivity (J_W/J_S) of First- and Next-Generation FO Membranes Tested

Membrane	Average J_W/J_S [L/mol] (rel. to indicated salt in FO mode)			
	NaCl	**KCl**	**$MgCl_2$**	**$CaCl_2$**
First-generation				
CTA-ES	110	76	410	400
CTA-NW	120	80	260	250
Next-generation				
X-TFC	180	120	~1,100	—
Y-T	200	—	~2,000	—
Y-HF	100	—	390	—
W-TFC	300-400	—	—	—
Z-US and Z-S	0.5-2	—	—	—

As an example of the effect draw-salt concentration on the water/salt selectivity, Figure 4-7 plots this selectivity as a function of the concentration for NaCl draw salt. From the trend lines, the J_w/J_s selectivity seems to be fairly independent of draw-solution concentration (i.e., osmotic pressure difference) for all FO membranes, except the W-TFC. The water/NaCl salt selectivity of the W-TFC decreased gradually with increasing NaCl draw content and appeared to level off at 275-300 beyond 3 M NaCl. A quick retest with the 1 M NaCl draw concentration after the test with 5 M draw gave a slightly lower water/salt selectivity of ~360, relative to the initially measured selectivity of 400. This gradual selectivity decrease in the W-TFC may be due to membrane conditioning during the course of testing.

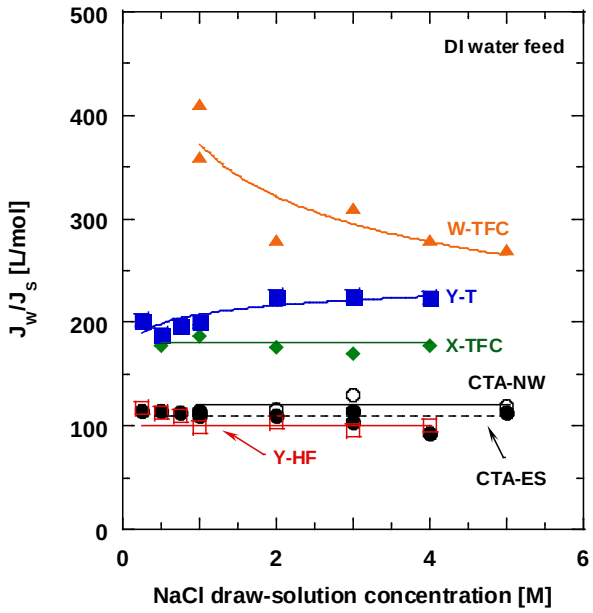

Figure 4-7. Water/NaCl salt selectivities (J_w/J_s) measured in the various FO membranes as a function of NaCl draw-solution concentration. Feed: DI water. T = 23 °C.

Thus, on the basis of the baseline J_W, J_S, and J_W/J_S selectivity data, the most promising FO membrane candidates are the Y-T, X-TFC, and CTA-ES. These three membranes should be able to meet the target water flux of 15 L/(m^2·h) in industrial wastewater applications by using a draw solution with a suitable concentration of a simple salt. They also possess good J_W/J_S selectivity, indicating that salt and other dissolved solids should not be excessively transported through these membranes.

Intrinsic Membrane Characteristic Parameters. To provide intrinsic membrane property values for process modeling, the characteristic water permeability *A*, salt permeability *B*, and structural parameter *S* of the FO membranes tested were determined in RO- and PRO-mode tests as described in Section 3. The resulting intrinsic membrane characteristic parameters measured in the various membranes are presented in Table 4-2.

In terms of intrinsic water permeability *A*, the membranes ranked in this order: W-TFC > Y-HF > Y-T > X-TFC > CTA-ES > CTA-NW. This water-permeability ranking agreed well with their observed FO water flux performance. It was also noted that, though Y-HF had higher water permeability than Y-T, the water flux measured for Y-HF in FO mode was found to be only marginally higher than the FO water flux of Y-T. In terms of salt permeability *B*, the membrane ranking was Y-HF ≈ W-TFC > Y-T >X-TFC ≈ CTA-ES > CTA-NW, which was also generally consistent with the reverse salt flux trends discussed earlier.

Table 4-2. Intrinsic Membrane Characteristic Parameters of First- and Next-Generation FO Membranes Tested

Parameter	Membrane							
	CTA-ES	CTA-NW	X-TFC	W-TFC	Y-T	Y-HF	Z-US	Z-S
Water permeability A [L/(m^2·h·bar)]	0.74-0.87	0.41-0.50	1.5-2.1	9.0-9.5	3.0-4.0	4.9-7.8	~1,500-1,600	~300-500
Salt permeability B [L/(m^2·h)]	0.32-0.39	0.13-0.19	0.28-0.48	2.0-2.3	0.75-1.9	2.0-3.7	—	—
Structural parameter S [μm]	580-600	950-1,860	480-630	~270	180-200	240-280	—	—

As discussed in Section 3, the structural parameter *S* is related to the membrane support layer and characterizes the degree of internal concentration polarization. When the *S* value is large, concentration polarization usually affects FO separation performance more. Hence, development of an FO membrane with a low *S* value is typically targeted by FO membrane developers to minimize boundary layer effects in the internal membrane structure. As shown in Table 4-2, the CTA-NW had the highest *S* value, which explains why its experimental water/$MgCl_2$ and water/$CaCl_2$ selectivities were lower than those obtained in the CTA-ES, a membrane made of the same selective material but with a different membrane structure (morphology). That is, concentration polarization effects with the divalent draw solutions were more significant in the CTA-NW than in the CTA-ES, leading most probably to a reduced osmotic gradient for water permeation in the CTA-NW. The next-generation Y-T membrane had the lowest *S* value to date, suggesting that internal concentration polarization in this membrane should be minimal. This is consistent with the excellent FO performance (i.e., high water flux coupled with high water/salt selectivities) obtained with the Y-T membrane in laboratory testing. The *S* values of W-TFC and Y-HF were also comparable to that of the Y-T.

Thus, on the basis of the baseline J_W, J_S, and J_W/J_S selectivity data and the intrinsic membrane characteristics, the most promising FO membrane candidates were the Y-T, X-TFC, W-TFC, and CTA-ES. These four membranes should be able to meet the target water flux of 15 L/(m^2·h) in industrial wastewater applications by using a draw solution with a suitable concentration of a simple salt. They also possessed good J_W/J_S selectivity, indicating that salt and other dissolved solids should not be excessively transported through these membranes. The first-generation CTA-based membrane is most suitable for treating waters with pH in the range of 3-8. For wastewater feeds having pH outside this range, the Y-T, X-TFC, and W-TFC would be more robust because they have an operating pH range of 2-11.

FO Membrane Performance with Synthetic Aqueous Feeds

To determine the effect of feed total dissolved solids (TDS) content on FO water flux, FO tests were performed with simple aqueous saline feeds and 1, 3, and, in one test series, 5 M NaCl draw solutions at room temperature on the CTA-ES membrane. As mentioned in Section 3, the feeds were aqueous NaCl, KCl, $MgCl_2$, and $CaCl_2$ solutions with salt content in the range of 500-12,000 mg/L, which encompasses the representative TDS content typically found in conventional industrial effluents.

As summarized in Figure 4-8, which plots the measured FO water flux against the osmotic pressure of the feed solution, the water flux through the CTA-ES declined gradually with increasing feed osmotic pressure [i.e., increasing TDS (salt) content] at a given draw-solution concentration. This flux decline was due to the reduction in osmotic-pressure driving force $\Delta\pi$ across the membrane due to the presence of salt in the feed. The effect of $\Delta\pi$ reduction on water flux also diminished as draw-solution concentration increased. For reference, the baseline water fluxes obtained with DI water feed (π_F = 0) under the same test conditions are also included in the plots. For example, using 1 M NaCl draw solution, the water flux decreased by 15-28% as TDS content increased from 0 to 12,000 mg/L, which corresponded to a 14-20% decrease in $\Delta\pi$. With 3 M NaCl draw, the observed water flux reduction was smaller (7-14%) because the $\Delta\pi$ driving force only decreased by 4-6% over this same TDS range. Additionally, the Figure 4-8 results also indicate that, to achieve the threshold 15 L/(m^2·h) water flux target in the project, at least a 2 M draw solution must be used with the CTA-ES membrane.

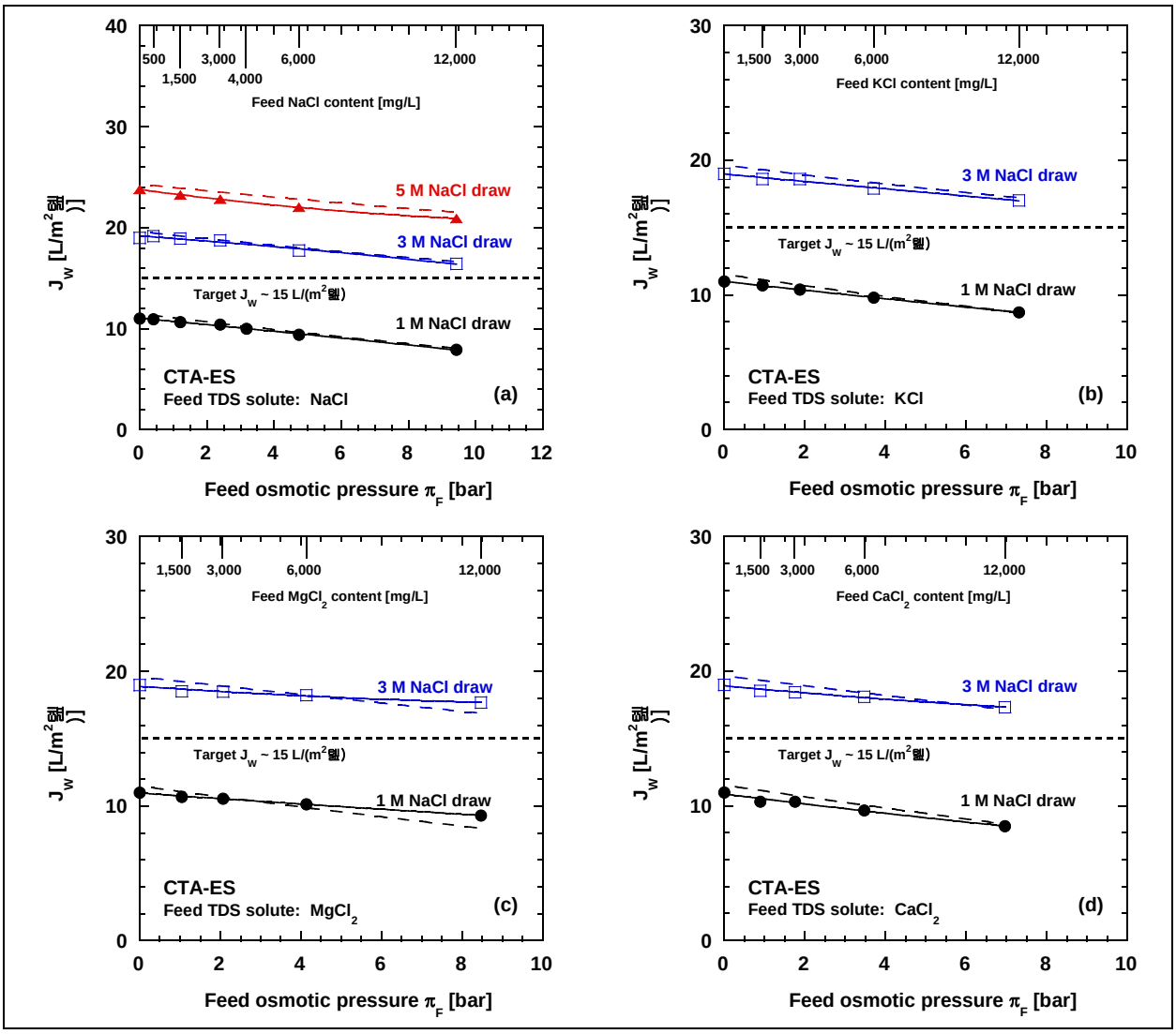

Figure 4-8. FO water flux J_W of the CTA-ES membrane at room temperature as a function of feed-solution osmotic pressure π_F or, equivalently, feed salt concentration: (a) NaCl feed, (b) KCl feed, (c) $MgCl_2$ feed, and (d) $CaCl_2$ feed. Solid curves serve as visual guides for the experimental data. Larger dashed curves are predictions by the FO model developed and discussed in Section 4.4.1 below. Osmotic pressures of feed salt concentrations used were taken from the OLI software for electrolyte solutions. The data point at π_F = 0 was obtained with DI water as feed.

FO Membrane Performance with Real Wastewater Feeds

AnMBR Effluent as FO Feed

On the basis of their baseline FO separation properties, three FO membrane candidates—CTA-ES, X-TFC, and Y-T—were downselected for testing with an actual, aqueous AnMBR effluent as feed. As noted in Section 3, the AnMBR effluent used had low contaminant concentrations of organics (120-140

mg/L COD) and suspended/dissolved solids (0-2 mg/L TSS; 2.8-3 mS/cm conductivity due dissolved species).

CTA-ES Membrane. Evaluation of the CTA-ES membrane with real AnMBR effluent as FO feed was conducted as a semi-continuous, 4-day run with a 3 M NaCl draw solution. The total cumulative time-on-stream achieved for the CTA-ES was 24.6 h. Roughly every few hours during the work-day testing, the spent (diluted) draw solution was replaced with a fresh reservoir of 3 M NaCl draw to keep the osmotic-pressure driving force as reasonably constant as possible. On the feed side, the FO feed reservoir was replenished during the first two days of testing with additional AnMBR effluent to replace the water lost to the draw side due to permeation. This procedure, though, resulted in the gradual accumulation of the AnMBR contaminants on the feed side. To avoid this undesirable accumulation of contaminants and maintain the original level of feed contaminants as much as possible, the FO feed reservoir was diluted every 1-2 h with DI water during the final two days of testing.

As shown in Figure 4-9a, the water flux J_w of the CTA-ES was quite stable, averaging ~19 L/(m^2·h) during the test run with the AnMBR effluent-based feed. For comparison, the J_w measured with clean DI water feed and 3 M NaCl draw on this membrane sample was 20 L/(m^2·h). As an additional comparison, the 2.8-3 mS/cm conductivity of the AnMBR effluent-based feed corresponded roughly to the presence of 1,400-1,500 mg/L as NaCl-equivalent, dissolved solids in the AnMBR effluent. By referencing back to the Figure 4-8 plots, the average water flux of 19 L/(m^2·h) measured with the AnMBR effluent-based feed was seen to be consistent with that obtained using an aqueous 1,500-mg/L-TDS feed and 3 M NaCl draw. Thus, the presence of low levels of feed COD and solids contaminants did not much diminish water flux of the CTA-ES. Furthermore, the use of the 3 M NaCl draw solution under the given contaminated feed conditions easily allowed the CTA-ES membrane to exceed the target water flux of 15 L/(m^2·h) in the project.

A second round of testing on the CTA-ES membrane was also performed to *concentrate* the AnMBR effluent used as FO feed. That is, the "AnMBR effluent" feed volume was allowed to gradually decrease and concentrate due to permeation of water to the draw side. Like the 4-day test run, this testing was also "semi-continuous" and used a 3 M NaCl draw solution. To maintain a stable draw-side osmotic pressure, the draw-solution concentration was kept constant throughout the test by dosing with small quantities of a 5 M NaCl draw solution with a peristaltic pump set to a pre-determined pump flow rate.

As shown in Figure 4-9b, the CTA-ES continued to have a stable water flux J_w of 19 L/(m^2·h) on average during the concentration of the AnMBR effluent-based feed. By the end of the semi-continuous 2-day concentration test run (total cumulative time-on-stream of 12.9 h), it was demonstrated that 95% water removal from the contaminated feed (or, equivalently, more than 20-fold concentration of the contaminated feed) was achieved in FO mode with the CTA-ES membrane. That is, as long as a sufficient osmotic pressure gradient across the membrane existed, water continued to permeate in the FO process. In fact, Figure 4-9b suggests that the osmotic pressure gradient did not start to diminish much until 86+% water removal, as evidenced in the water flux decreasing below19 L/(m^2·h). The high level of water

removal (or concentration of the feed) would not typically be possible with reverse osmosis because the osmotic back pressure would ultimately limit (stop) the water transport.

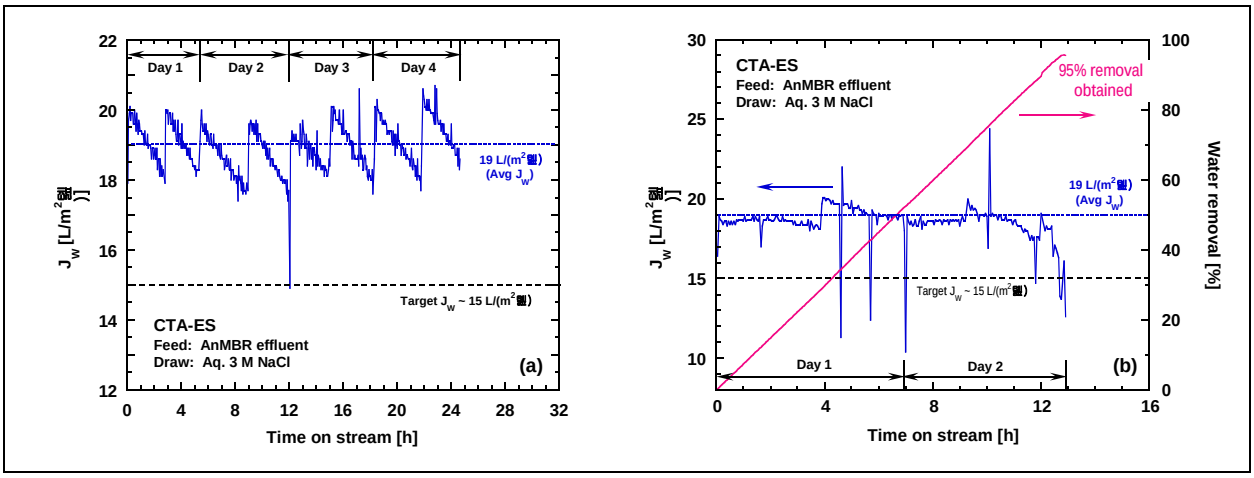

Figure 4-9. Water flux in CTA-ES as a function of time-on-stream in semi-continuous FO testing with real aqueous AnMBR effluent as feed. (a) Extended 4-day test. (b) 2-day feed concentration test (water removal percentage also plotted). Draw solution: 3 M NaCl in water. T = 23 °C.

As shown in Figure 4-10, the resulting concentrated AnMBR effluent ("FO reject") had a much darker amber brown color than the AnMBR effluent before concentration ("FO feed"). The concentrated AnMBR effluent had higher COD of 1,130 mg/L, higher TSS of 330 mg/L, and higher conductivity of ~30 mS/cm relative to the effluent before concentration.

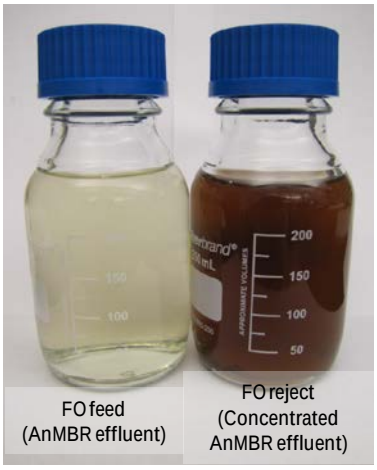

Figure 4-10. Photos comparing the AnMBR effluent before concentration ("FO feed") and after >20-fold concentration ("FO reject") with the CTA-ES membrane and 3 M NaCl draw solution.

X-TFC Membrane. The X-TFC membrane was tested with the AnMBR effluent-based feed in a semi-continuous, 4.5-day run with a 3 M NaCl draw solution. The total cumulative time-on-stream

achieved for the X-TFC was 36 h. To maintain a stable draw-side osmotic pressure, instead of replacing the spent draw solution with a fresh reservoir of 3 M NaCl draw as done in the CTA-ES test, the draw-solution concentration was kept constant in the X-TFC test by dosing with small quantities of a 5 M NaCl draw solution with a peristaltic pump set to a pre-determined pump flow rate. As before, on the feed side, the FO feed reservoir was diluted every 1-2 h with DI water to keep the feed-side conductivity and, in turn, the original level of feed contaminants as constant as possible.

As shown in Figure 4-11, the water flux J_w of the X-TFC was quite stable, averaging ~23-24 L/(m^2·h) during the test run with the AnMBR effluent-based feed. For comparison, the J_w measured with clean DI water feed and 3 M NaCl draw on this membrane sample was 24 L/(m^2·h). A post-check of the X-TFC membrane with DI water feed after exposure to the contaminated feed indicated that the low levels of feed COD and solids contaminants did not adversely affect the X-TFC water flux. Interestingly, the post-check also showed that the NaCl salt flux of the X-TFC had decreased a little after exposure, resulting in an increase in J_w/J_s selectivity from ~170-180 to 200-220. Furthermore, the use of the 3 M NaCl draw solution under the given contaminated feed conditions easily allowed the X-TFC to exceed the project's target water flux of 15 L/(m^2·h).

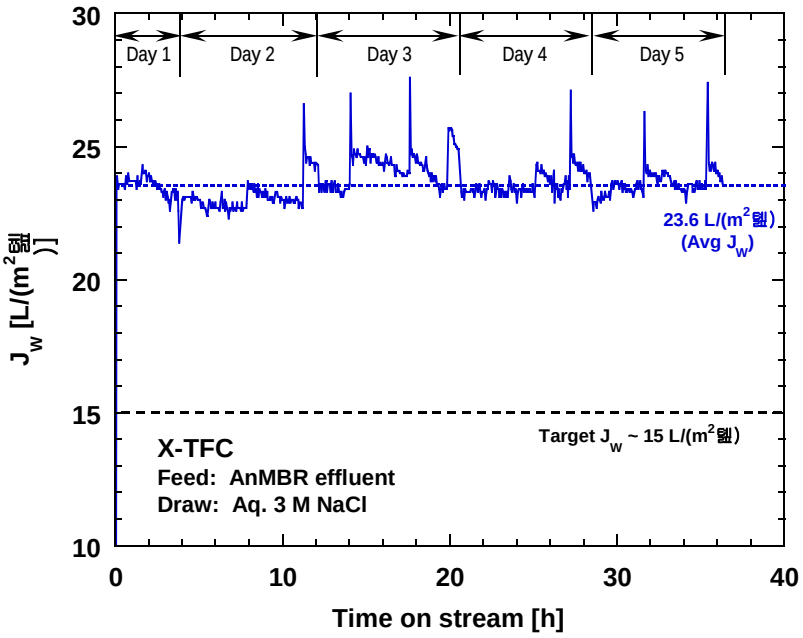

Figure 4-11. Water flux in X-TFC as a function of time-on-stream in semi-continuous FO testing with real aqueous AnMBR effluent as model contaminated feed. Draw solution: 3 M NaCl in water. Cumulative time-on-stream: 36.3 h. T = 23 °C.

Y-T Membrane. Evaluation of the Y-T membrane with the AnMBR effluent as FO feed was conducted in a semi-continuous, 3-day run with a 3 M NaCl draw solution. The total cumulative time-on-stream was ~25 h for the Y-T. As in the X-TFC test run, the draw-solution concentration was kept constant throughout the test by dosing with small quantities of a 5 M NaCl draw solution, and the FO feed

reservoir was diluted every 1-2 h with DI water to keep the feed-side conductivity and the original level of feed contaminants as constant as possible.

A similar plot is presented in Figure 4-12 for the water flux J_W of the Y-T membrane during its test run with the AnMBR effluent as FO feed. The observed average Y-T water flux was ~45 L/(m^2·h). For comparison, the J_W obtained with clean DI water feed and 3 M NaCl draw on this membrane sample before testing with the AnMBR effluent was 58 L/(m^2·h). The plot also shows that the Y-T water flux exhibited a gradual decline of ~21% from the start to the end of the test run. A post-check of the Y-T membrane with DI water feed after exposure to the AnMBR effluent indicated that the membrane's FO water flux had decreased to 49 L/(m^2·h), which is 16% lower than the pre-exposure flux value. Likewise, the post-exposure NaCl salt flux had comparably decreased so that the Y-T water/salt selectivity remained at least as good as that measured pre-exposure. From this test, it is not clear if the decrease in Y-T water flux is due to fouling by the model contaminated feed, membrane compaction, or another cause. The results can even possibly be attributed to an artifact of the test setup because the much higher water flux of the Y-T made it more challenging to keep the feed- and draw-side experimental conditions constant. On the basis of raw feed and draw conductivity values measured, it seems possible that the J_W decrease with time could be associated partly with a diminishment in osmotic-pressure driving force over the course of the test.

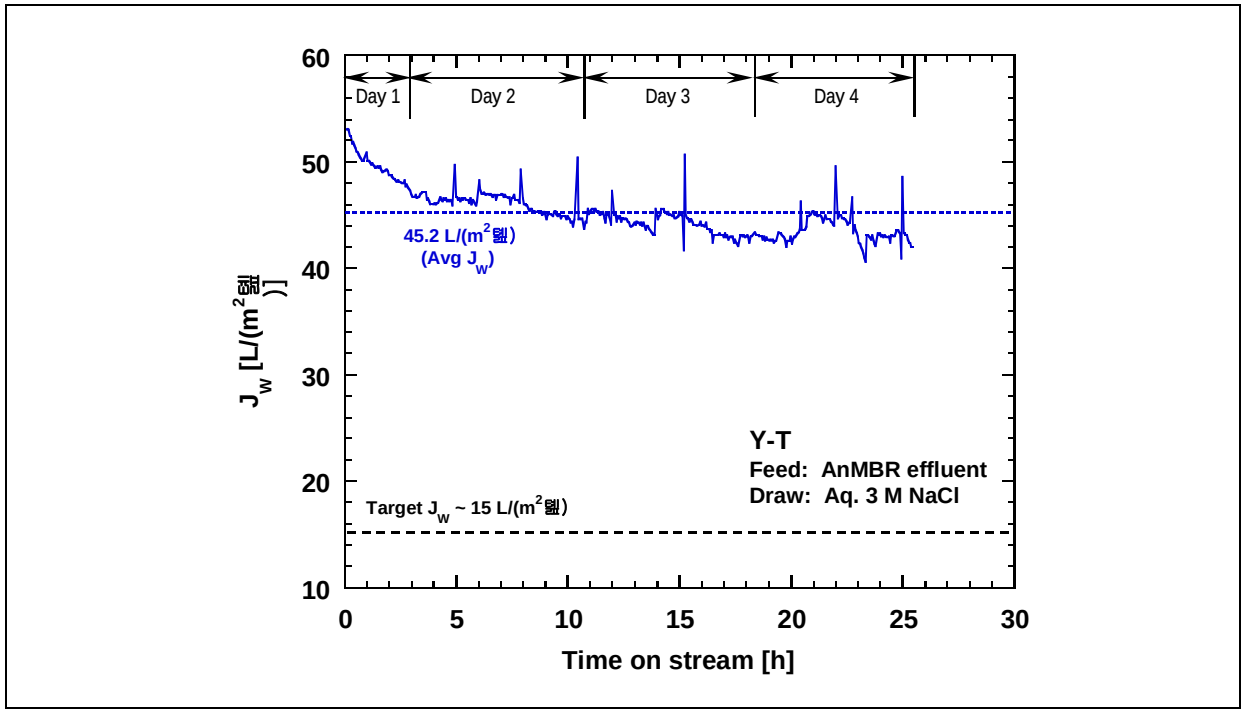

Figure 4-12. Water flux in Y-T as a function of time-on-stream in semi-continuous FO testing with real aqueous AnMBR effluent as model contaminated feed. Draw solution: 3 M NaCl in water. Cumulative time-on-stream: 25.4 h.

Industrial Wastewaters as FO Feed

FO performance testing with more complex, real wastewaters sourced from industrial processes was conducted on the laboratory water test-bed system to identify any immediate membrane performance issues that might occur during long-term operation. The objectives of the real-wastewater testing were to (i) evaluate fouling behavior of the FO membranes in the presence of actual wastewater and (ii) conduct preliminary cleaning/recovery tests to identify appropriate cleaning protocols for operation. These tests would also indicate whether the FO membrane has a so-called "critical flux." In pressure-driven membrane systems, the critical flux is the operational pressure point at which fouling is accelerated and is used as an important operating guideline. Once critical flux is established for a membrane/wastewater system, the operational setpoint can be set at a pressure point (an osmotic-potential point in the case of FO) *below* this to reduce the need for downtime due to cleaning, thereby extending the overall system performance and reducing operational costs.

Site 1 Wastewater. Two fouling studies were completed on the downselected Y-T FO membrane with the Site 1 wastewater as the feed and aqueous 3 M NaCl solution as the draw. (As mentioned in Section 3, the Site 1 wastewater had high scaling potential.) The feed-and draw-side conditions were kept as constant as possible in these tests. In both studies, severe water flux decline of 50-70% was observed after on-stream run times of 19-30 h, as shown in Figure 4-13 and Figure 4-14a. This flux decline was attributed primarily to precipitation of carbonate-based scalants. Additionally, several membrane cleaning approaches were tried to determine how much water flux recovery could be obtained in this fouling situation. Mild cleaning methods such as DI water flushing and osmotic backwashing were found to be not effective on the fouled Y-T membranes. Chemical cleaning with dilute aqueous acidic solutions, though, worked well and was able to recover 85-86% of the initial baseline membrane water flux measured with DI water feed and 1 M NaCl draw solution before exposure to real wastewater. Furthermore, as shown in Figure 4-14a, acid cleaning essentially returned the water flux obtained with Site 1 wastewater feed and 3 M NaCl draw back to its starting value of 25 L/(m^2·h). Baseline post-checks also indicated that the Y-T membranes kept their properties after using the various cleaning methods. That is, baseline water fluxes, though a little lower, stayed consistent with starting values (Figure 4-13 and Figure 4-14b), and membrane salt rejection was maintained.

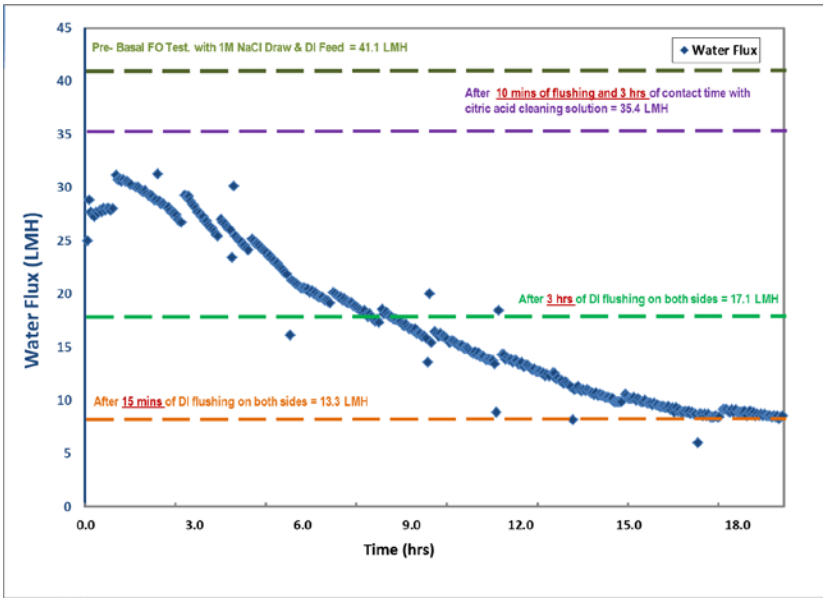

Figure 4-13. FO water flux obtained in Study #1 on Y-T membrane with real Site 1 wastewater feed and 3 M NaCl draw solution as function of on-stream run time. Shown also are the *baseline* FO water fluxes measured with DI water feed and 1 M NaCl draw solution before and after real wastewater testing and after each membrane cleaning method used.

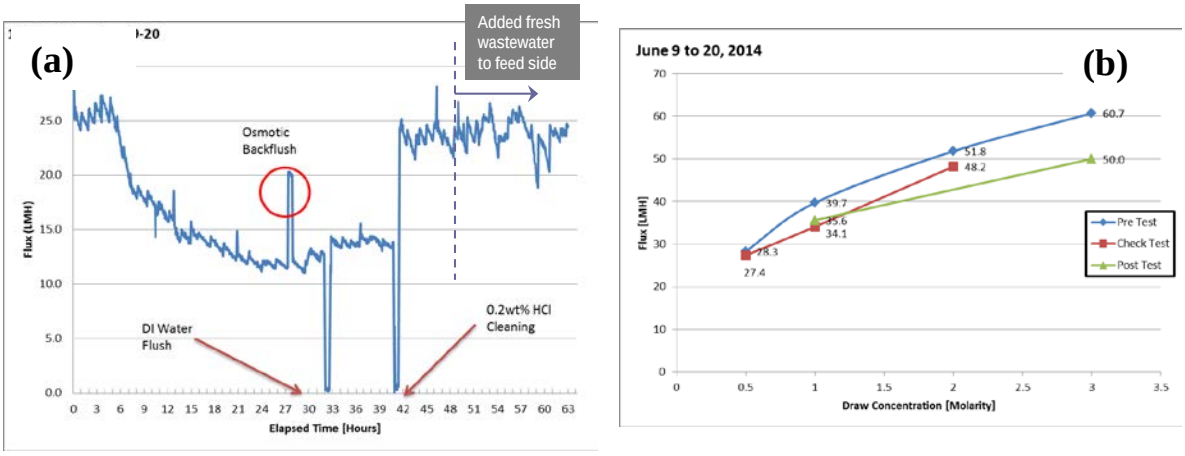

Figure 4-14. (a) FO water fluxes obtained with real Site 1 wastewater feed and 3 M NaCl draw solution as function of on-stream run time in Study #2 on Y-T membrane. [Points at which membrane cleaning was done are also shown.] (b) *Baseline* water-flux checks done in Study #2 with DI water feed at different NaCl draw concentrations before and after real wastewater testing and after the acid cleaning step.

Site 2 Wastewater. Fouling and water recovery tests were also run with the Site 2 wastewater (described in Section 3) as the feed on the Y-T FO membrane for a short time period (7-8 h). The draw solution used was aqueous 3 M NaCl solution. In the fouling test run, feed- and draw-side conditions were kept as constant as possible. As indicated by the stable FO water flux of 50-52 L/(m^2·h) over the 8-h test run in Figure 4-15a, no fouling of the Y-T membrane was seen. In the water recovery test, the 3 M NaCl draw

was maintained to keep the draw-side condition constant, while the wastewater feed was allowed to concentrate on the feed side as water permeated the membrane to the draw side. As shown in Figure 4-15b, the FO water flux was stable at 50-52 L/(m^2·h) up to an elapsed test time of ~3.5 h, which corresponded roughly to ~50% water recovery. Beyond this elapsed time, the water flux gradually decreased down to ~34 L/(m^2·h) at the end of the roughly 7-h test. This flux decline was mainly due to decreasing water permeation driving force as feed-side contaminant concentration increased rather than any membrane fouling issue. The final water recovery achieved in this test run was 91-92%. Baseline post-checks also indicated that the Site 2 wastewater did not adversely affect the membrane as its baseline properties (water flux, salt rejection) were maintained after the short-term exposure to this real wastewater.

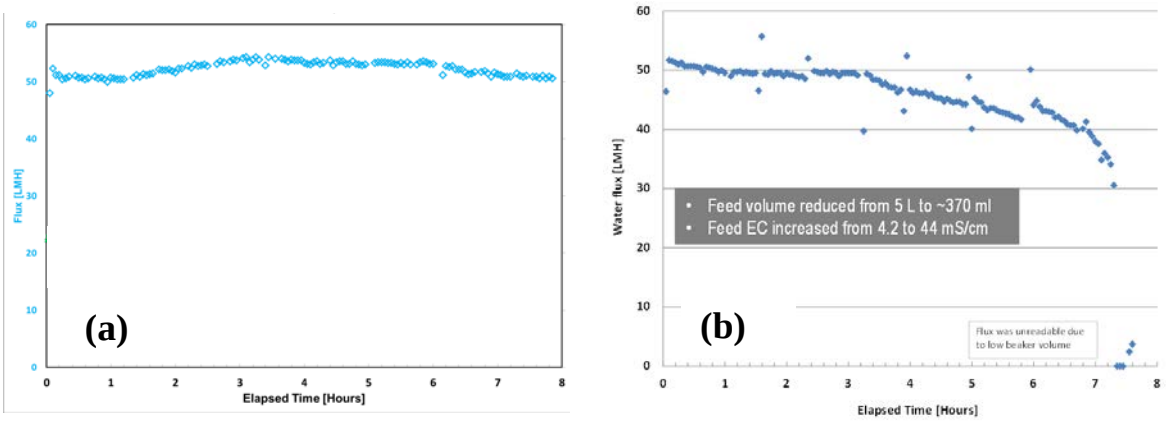

Figure 4-15. FO water fluxes obtained in Study #3 with real Site 2 wastewater feed on Y-T membrane as function of on-stream run time: (a) fouling test and (b) water recovery test. Draw: Aqueous 3 M NaCl solution.

Critical-Flux Testing of FO Membranes. For each test, the water flux of the FO membrane was first measured in a pre-check with 1 M NaCl draw to determine baseline performance. The FO membrane was then used to treat the real wastewater at different draw solution concentrations until the target cumulative time on-stream of 24 hours was reached. The wastewater feed concentration was kept pseudo-constant in these tests by the addition of DI water via a dosing pump. Water flux and electrical conductivity were monitored, and the critical flux was noted by a sharp drop in flux during operation. Upon completion of the 24-h test, the membrane was cleaned, followed by a post-check for performance. FO cleaning methods evaluated included (i) osmotic backwash, (ii) high-salinity backwash, (iii) DI flushing on both sides of membrane, and (iv) clean-in-place (CIP) with dilute aqueous 0.2 wt% HCl solution.

Figure 4-16-Figure 4-20 present the FO water-flux data obtained with the Site 1 wastewater on the Y-T membrane at different draw-solution concentrations for each of the 24-h critical-flux tests as well as results from the pre-check and post-check cleaning tests.

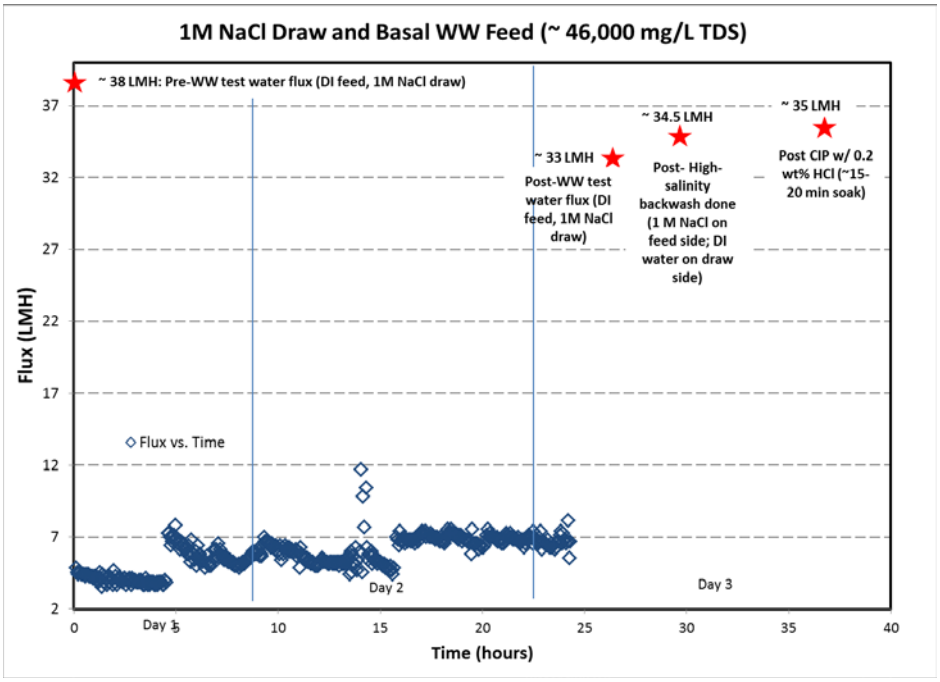

Figure 4-16. FO critical flux (Y-T membrane) obtained during the treatment of real Site 1 wastewater feed and 1 M NaCl draw solution as function of on-stream run time. The red stars indicate the average flux values of the pre-check and the different post-check cleaning/recovery values.

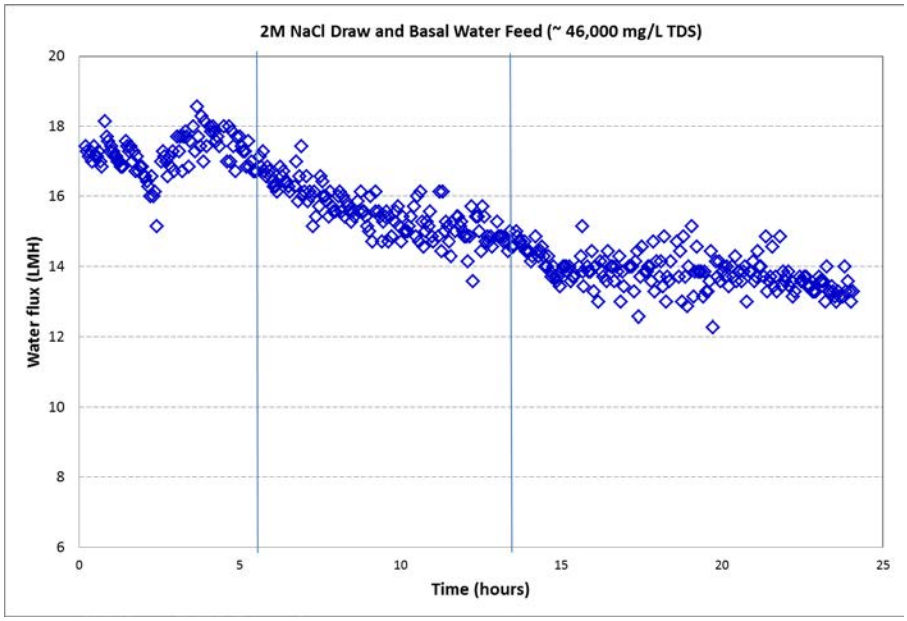

Figure 4-17. FO critical flux (Y-T membrane) obtained during the treatment of real Site 1 wastewater feed and 2 M NaCl draw solution as function of on-stream run time.

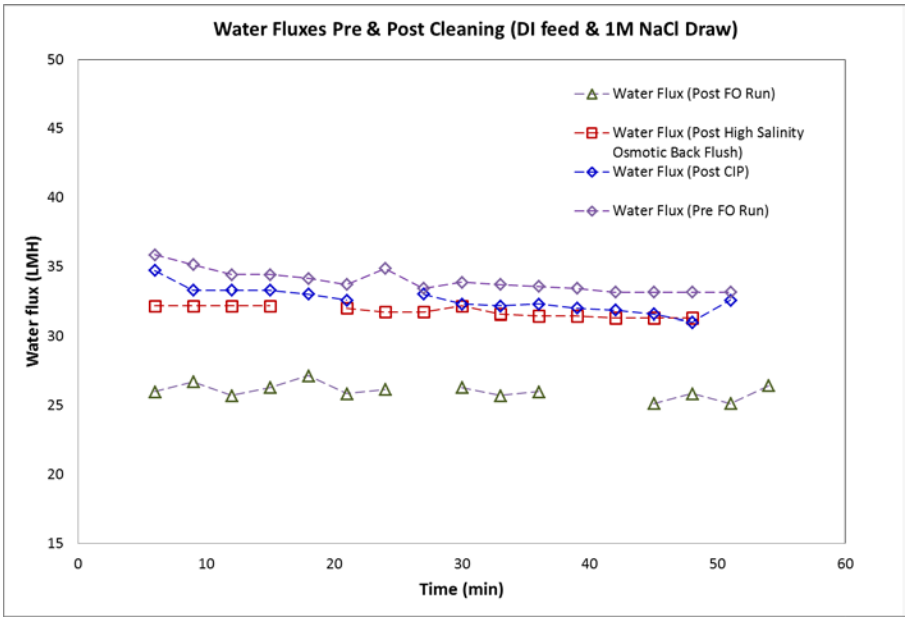

Figure 4-18. FO flux values (Y-T membrane) that show flux performance against time before treating real Site 1 wastewater feed with 2M draw, after wastewater testing without cleaning, and after high-salinity backwashing and post-CIP cleaning approaches.

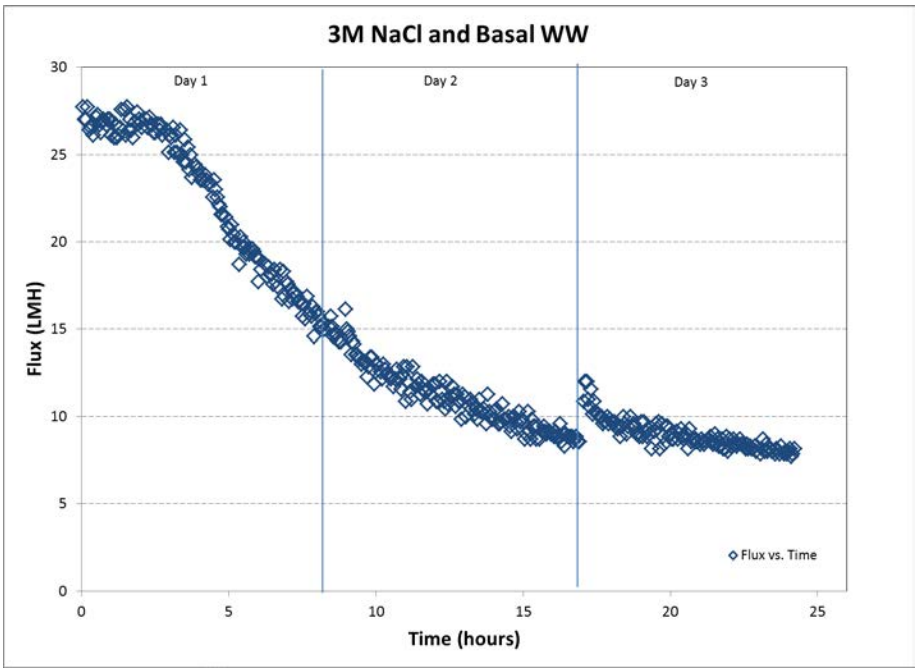

Figure 4-19. FO critical flux (Y-T membrane) obtained during the treatment of real Site 1 wastewater feed and 3 M NaCl draw solution as function of on-stream run time.

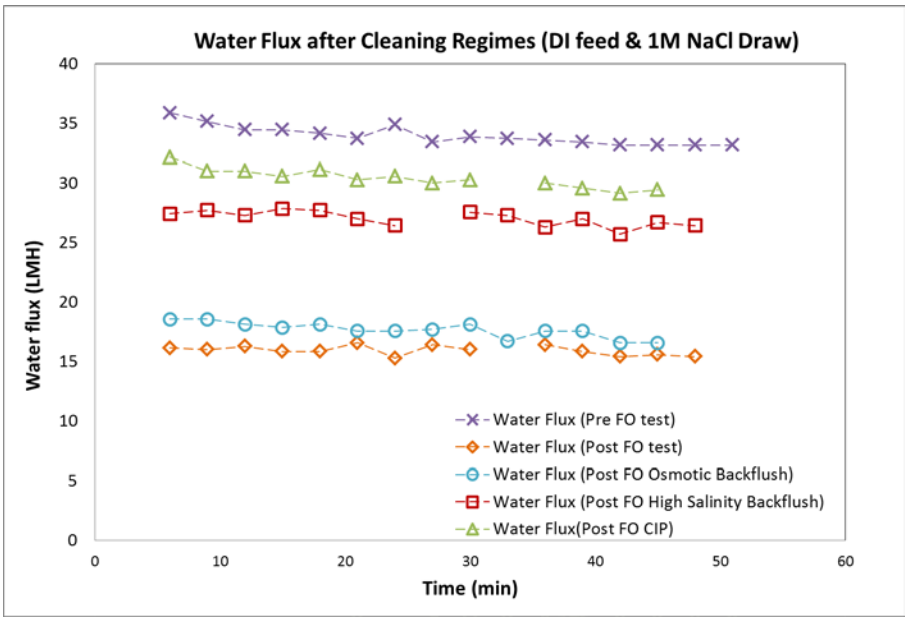

Figure 4-20. FO flux values (Y-T membrane) that show flux performance against time before treating real Site 1 wastewater feed with 3M draw, after wastewater testing without cleaning, and after various cleaning approaches.

Figure 4-16 shows that the FO membrane attained stable operation during the 24 hours of testing, clearly indicating that the critical flux was not reached for 1 M draw. However, the post-check resulted in a flux value of 33 L/(m^2·h), indicating that some level of fouling was occurring on the membrane surface [pre-check flux was 38 L/(m^2·h)]. The high-salinity backwash and post-CIP cleaning approaches recovered some of the original flux [35 L/(m^2·h) for 92% flux recovery]. A modest flux decline was observed for the 2 M NaCl draw, as shown in Figure 4-17, after approximately ~5 hours of operation. The high-salinity backwash and post-CIP cleaning resulted in about ~96% flux recovery relative to the pre-check flux values [~34 L/(m^2·h) pre-check vs. ~32.5 L/(m^2·h) post-CIP] (Figure 4-18). At 3 M draw (Figure 4-19), the onset of critical flux was clearly evident 3-4 hours into the test as shown by a significant decrease in flux. Figure 4-20 shows that the post-CIP cleaning resulted in final recovery of ~90% of the original flux [~33.5 L/(m^2·h) pre-check vs. ~30.5 L/(m^2·h) post-CIP]. There was not sufficient wastewater sample to accurately complete the critical flux testing at 4 M draw, but this test is not critical at this time, especially because operation at the lower 3 M draw concentration already showed clear critical-flux behavior. Thus, these results suggest that, for treating the moderately high-TDS Site 1 wastewater feed, the Y-T FO membrane should be operated with a NaCl draw-solution strength below 3 M. The test results also show that both high-salinity backwash and CIP with dilute 0.2 wt% HCl solution are comparably effective cleaning options for the FO membrane.

Water Separation Properties of MD Membranes

Membrane Modification and Characterization

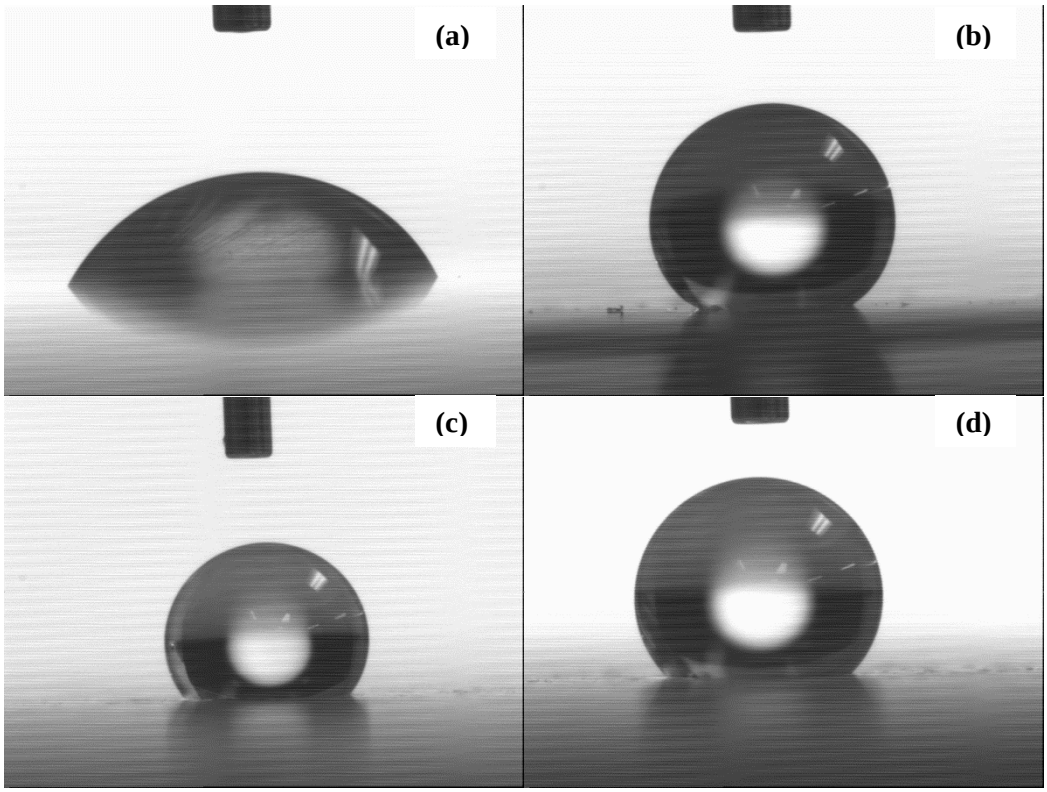

Figure 4-21. Contact angle measurements of PFS-treated ceramic membranes: (a) Al-X-S100 C.A. = 68.4 ±12.2º, (b) Al-X-W200. = 141.3 ±5.2º, (c) Ti-Al-T200 C.A. = 117.9 ±8.4º, and (d) Ti-Al-T450 C.A. =136.5 ±3.7º.

Only two of the four membranes, the TI-Al-T450 and the Al-X-W200 membranes exceeded the threshold of 120°, with measured contact angles of 136.5° ±3.7° and 141.3° ±5.2°, respectively. The failure of the other two membranes to obtain higher contact angles was unexpected, given their relatively similar metal oxide surfaces. Although both the Al-X-S100 and Al-X-W200 membranes were anodized aluminum oxide, the former was amorphous boehmite, which is an aluminum oxide hydroxide, AlO(OH), whereas the latter is γ-phase alumina oxide, Al_2O_3, so the difference in affinity with PFS might be attributed to this difference in the crystal lattice structure or possibly different fabrication methods used by the different manufacturers. However, it was more difficult to explain the diverging results for the titanium-based membranes because, other than the pore size, the support, active membrane layer composition, and manufacturer were identical. However, because the titanium dioxide active layer was formed from the deposition of spheres, with smaller spheres used for smaller pore size membranes, it was possible that the reactive nature of titanium dioxide (and the dependence of reactivity on surface area) limited the PFS coating effectiveness for the smaller pore-size membranes.

Table 4-3. Membrane characteristics and coating results for both liquid deposition (LD) and vapor deposition methods (VD). Membranes highlighted in bold are the membranes and coatings that reached the threshold contact angle and were selected for further testing.

Membrane referenced as	Membrane material	Membrane brand and model	Pore size	Membrane thickness	Porosity	Average contact angle of modified membrane
Al-S100[a]	AlO_2	Synkera Unikera Standard Membranes	0.1µm	50µm	15%	LD: 68±12°
						VD: NA
Al-W200[b]	**AlO_2**	**GE Whatman Anopore Inorganic Membranes**	**0.2µm**	**60µm**	**25-50%**	**LD: 141±2°**
						VD: 146±3°
Ti-T200[c]	TiO_2-ZrO_2	TAMI Ceramic Membranes	0.2µm	250µm/400µm support layer	Not available	LD: 118±8°
						VD: 85±15°
Ti-T450[c]	**TiO_2-ZrO_2**	**TAMI Ceramic Membranes**	**0.45µm**	**250µm/400µm support layer**	**Not available**	**LD: 136±4°**
						VD: 137±3°

[a] ("Synkera Unikera Standard Membranes," 2011)

[b] ("Anopore Inorganic Membranes (Anodisc)," 2009)

[c] (Blasi & Grospelly, 2012)

ks

The PFS coating increased the hydrophobicity of all of the ceramic membranes, but the increase in hydrophobicity was dependent on the membrane material. The PFS was bound to the metal-oxide surface via a condensation reaction. The two alumina membranes Al-S100 and Al-W200 were manufactured using different processes. SEM imaging techniques were used to visually assess if clogging was present and examine the pore structure of the membranes. The images showed differences in the pore geometry between the membranes, and no clogging was evident.

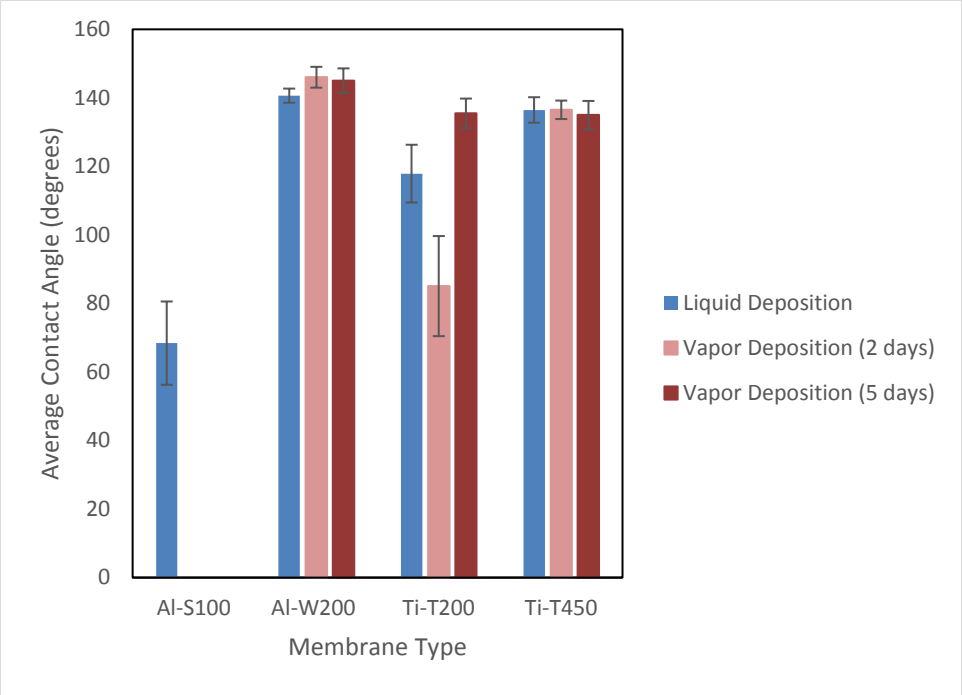

Figure 4-22. Contact angle comparison for different ceramic membrane substrates coating using both liquid deposition and vapor deposition hydrophobic modification techniques.

XPS Data

The presence of the coating on the membranes was verified by XPS. The Al-W200, TiT200, and TiT450 showed high percent composition of fluorine on the membrane surface.

Al-S100 was prepared via liquid deposition, whereas everything else was via vapor deposition.

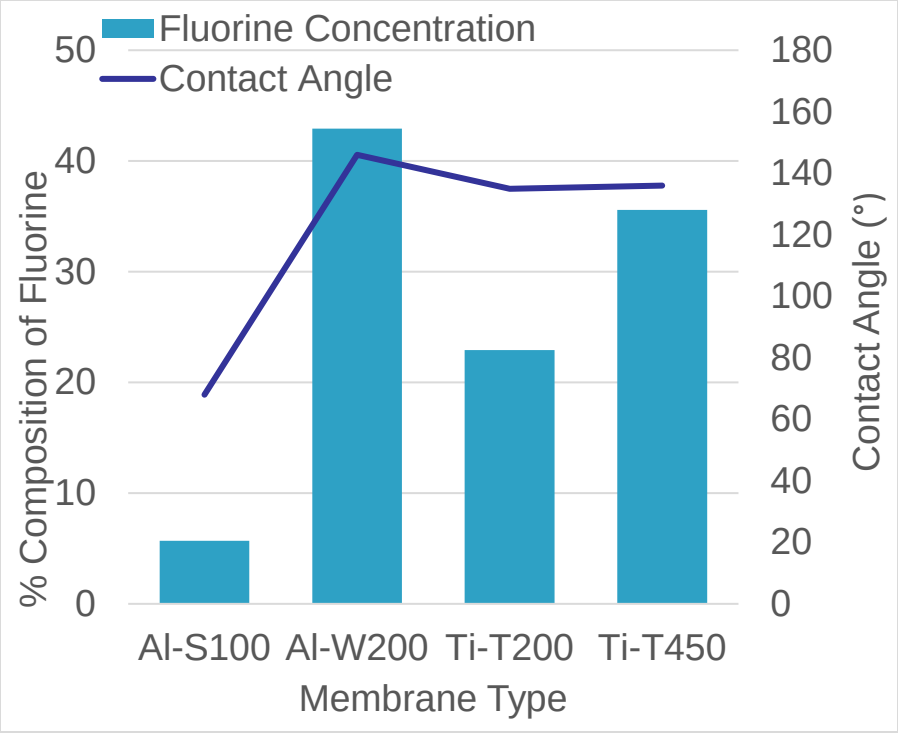

Figure 4-23. Membrane water drop contact angle measured via goniometer for different percent of fluorine deposition on the surface.

SEM Images

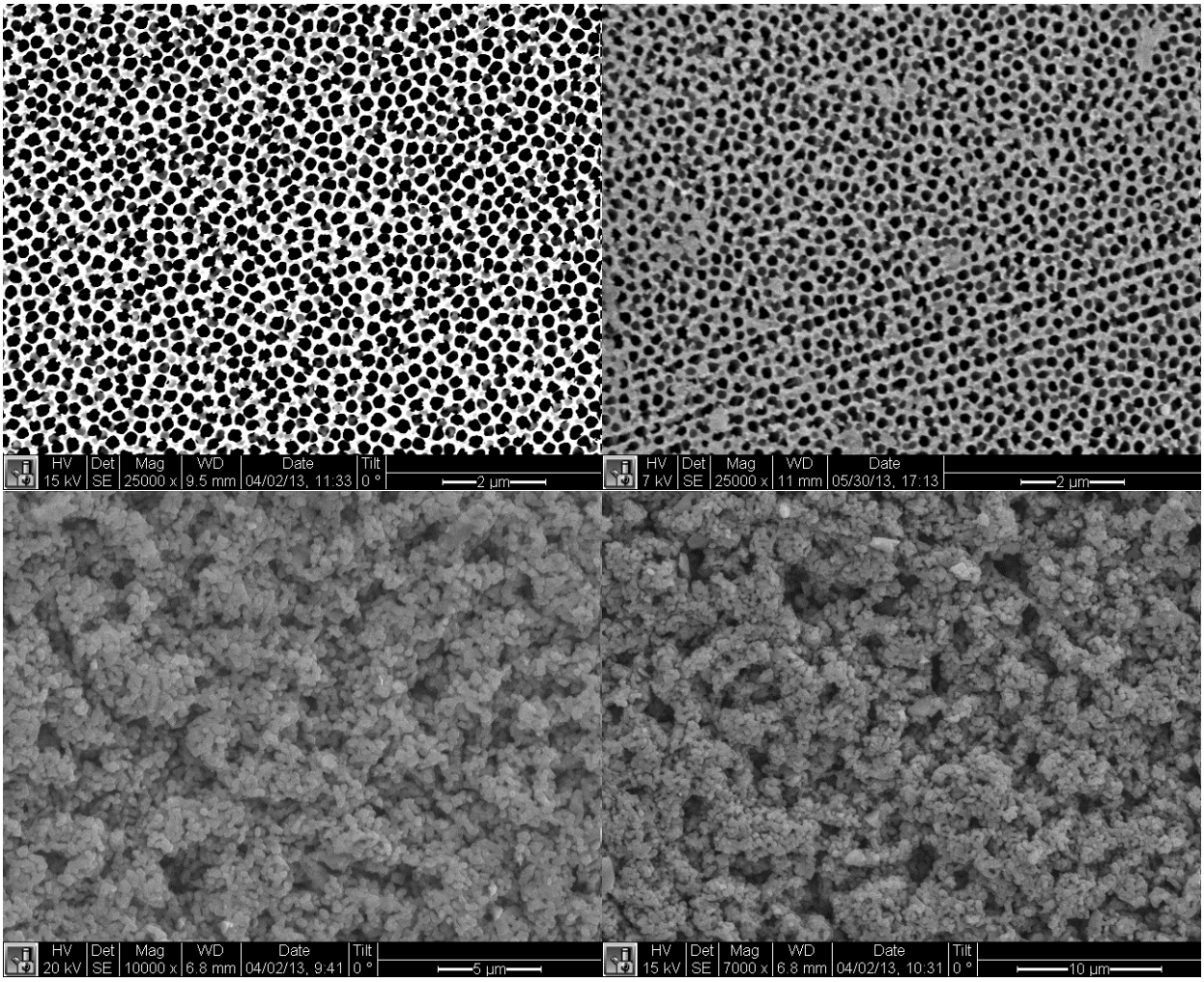

Figure 4-24. SEM Pictures showing membrane surface before coating (left) and after coating (right) of Al-W200 (top) and Ti-T450 (bottom)

Omniphobicity

The results show that the LBL coating was successful in modifying the PVDF membranes (Figure 4-25) and in increasing the membrane roughness (Figure 4-26, Figure 4-27,and Table 4-4). However, the PFS coating did not greatly increase the hydrophobicity of the membranes. This could be attributed to the lack of available functional groups to which the PFS molecules can bond on the PEI/PSS surface. The highest contact angle was reported for membranes with four bilayers of 0.5% SiNP-PEI/PSS solution (Figure 4-25), but the contact angle for these membranes was still lower than that of the unmodified membrane. Subsequent attempts with the LBL coating method focused on using polyelectrolytes with more reactive functional groups for the PFS coating and optimization of the number of bilayers and SiNP concentration.

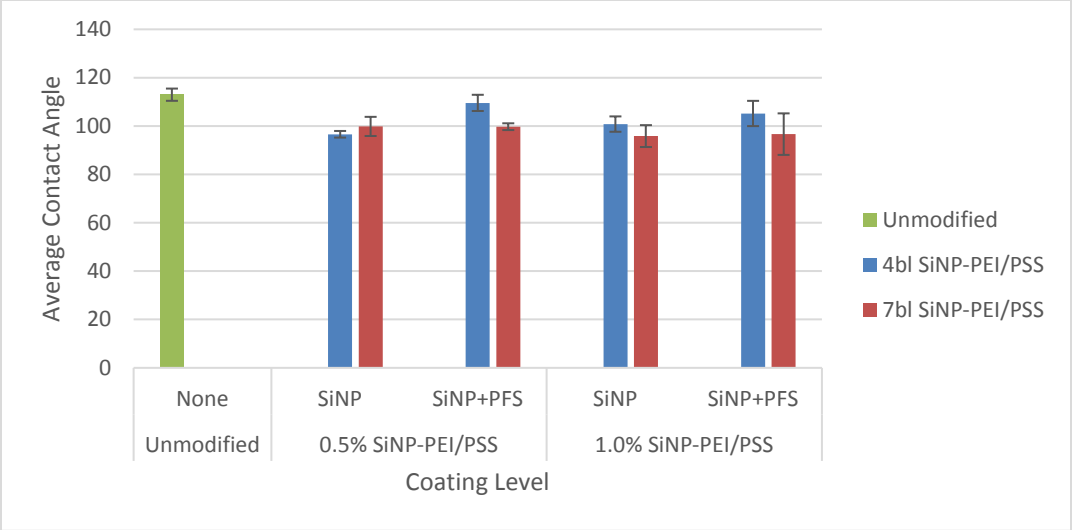

Figure 4-25. Average contact angle for SiNP-PEI/PSS-modified PVDF membranes compared to the unmodified PVDF membrane. The lower contact angle after the SiNP-PEI/PSS coating compared to the unmodified membranes shows that the PVDF membranes were successfully modified. The final contact angle after the PFS coating for all the membranes is still lower than the contact angle of the control membranes, showing low bonding with the PFS coating.

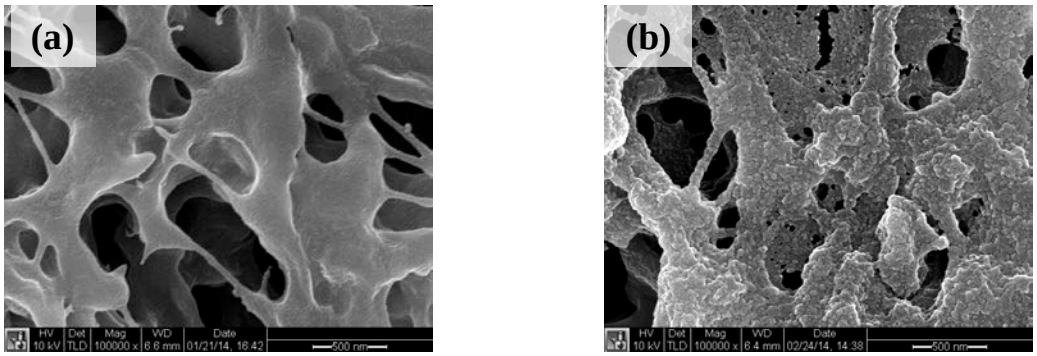

Figure 4-26. SEM images of (a) unmodified PVDF membrane, and (b) LBL-modified PVDF membrane with four bilayers of 0.5% SiNP-PEI/PSS coating. Modified membranes show increased roughness.

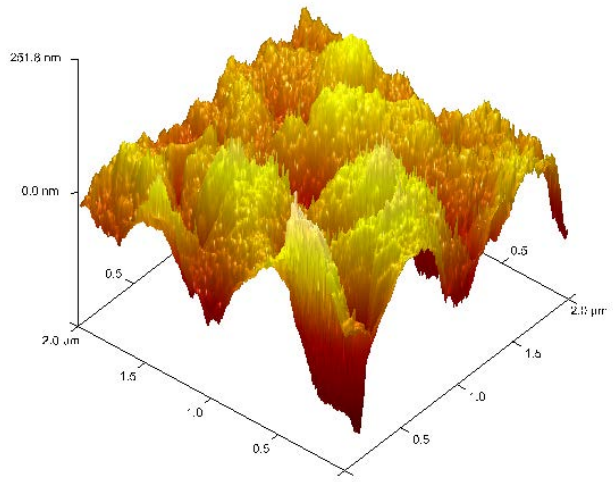

Figure 4-27. Atomic force microscopy [AFM] image of 4LBL 0.5% SiNP-PEI/PSS-modified PVDF membrane surface.

Table 4-4. AFM Roughness of Unmodified and LBL-Modified PVDF Membrane. (Modified membrane shows slight increase in roughness.)

	Unmodified PVDF	4LBL 0.5% SiNP-PEI/PSS-modified PVDF
Image Rq [nm]	33.6	52.8
Image Ra [nm]	26.9	39.3
Image Rmax [nm]	231	492

SiNP Deposition on Membranes

Other methods for coating surfaces with nanoparticles include dip-coating and spray-coating. To optimize the coating of SiNP on the membranes to create hierarchical roughness, several different parameters and coating methods are being tested to obtain the most uniform distribution of SiNP and identify the best size of SiNP to use. As shown in Figure 4-28, initial dip-coating resulted in membranes that had a relatively uneven distribution of SiNP. Additional membranes have been both dip- and spray-coated, the success of which is pending contact angle measurement and scanning electron microscopy [SEM] imaging. The highest contact angle achieved to date was 147° via deposition of 20-nm SiNP onto a PVDF membrane, followed by coating with PFS.

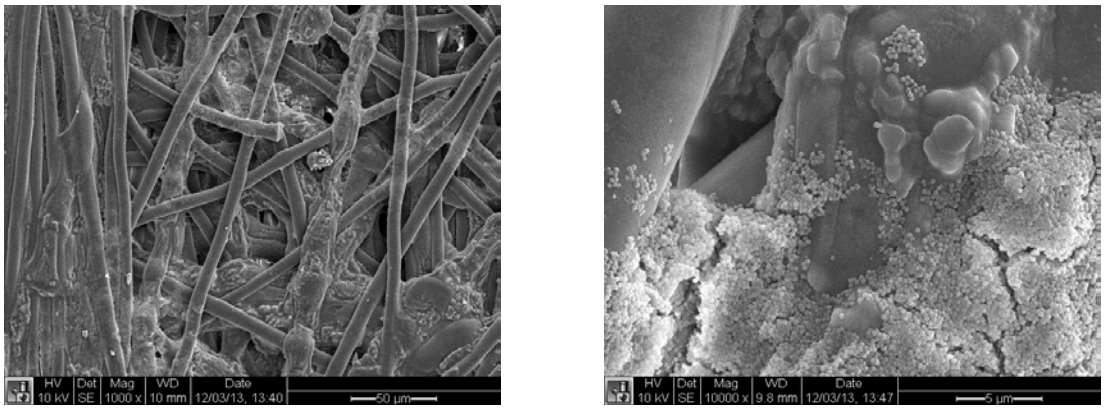

Figure 4-28. GE cellulose acetate membranes dip-coated with SiNP. The SiNP coating was applied to these membranes via in-situ growth of 400-nm SiNP on the membranes via a modified Stober process. The SiNP-coated membranes were then coated with PFS using the liquid deposition method, which resulted in some clumping.

In our experiment, the CA membranes were first conditioned in dilute nitric acid solution, followed by the addition of the silica particle precursor, methyl trimethoxysilane [MTMS]. The SiNP were then precipitated on the CA membrane by the addition of ammonium hydroxide. After one hour, the membranes were taken out of solution and rinsed. The SiNP-modified membranes were then coated with PFS by the vapor deposition method for 24 h at different temperatures (25, 50, and 80 °C). The scanning electron microscopy [SEM] images in Figure 4-29 were obtained with a FEI XL30 Scanning Electron Microscope and confirmed the presence of uniformly sized, spherical SiNP of about 250 nm. The highest water contact angle (144 ± 4°) was obtained by conditioning the membrane for one minute and applying the PFS coating at 80 °C (Figure 4-30).

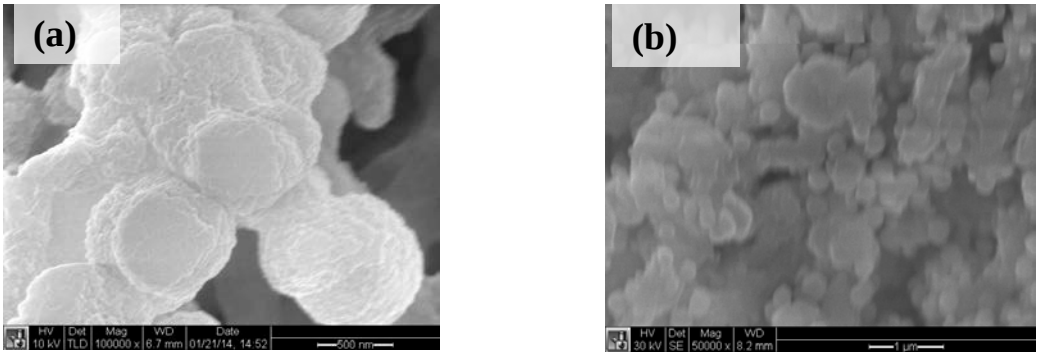

Figure 4-29. SEM images of (a) unmodified CA membrane and (b) CA membrane with SiNP (~250 nm in size) grown on it.

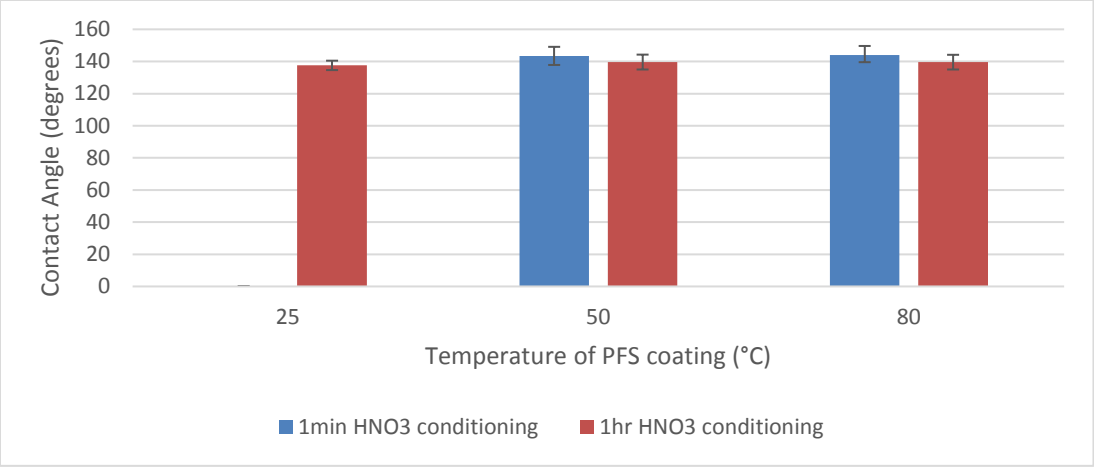

Figure 4-30. Water contact angle measured on CA membranes that were coated with SiNP and PFS under different conditions.

Effect of Fluorine Percent Composition (FPC) and Surface Root Mean Squared (RMS) Roughness on Water Contact Angle

The FPC and RMS roughness were measured on the CA membranes that were modified by the SiNP growth method above and the SiNP deposition method discussed in the previous quarterly report. FPC was measured with a Kratos analytical axis ultra X-ray photoelectron spectrometer [XPS], and RMS roughness was measured using atomic force microscopy [AFM] with a Digital Instruments Dimension 3100 scanning probe microscope.

As shown in Figure 4-31, the water contact angle of the CA membranes increased with increasing FPC up to roughly 5% FPC. For FPC greater than 5%, the water contact angle remained relatively constant at 140-145°. This result indicates that factors other than high FPC may be more important for obtaining a surface with water contact angle higher than 140°.

Figure 4-32 graphs the water contact angle of the CA membranes as a function of the RMS roughness analysis data. From these available measurements, no clear correlation between water contact angle and RMS roughness appears to exist. While prior research [40] has suggested that hierarchical structure and roughness are important in the creation of superhydrophobic surfaces, no well-developed correlation between experimentally obtained surface roughness parameters and hydrophobicity has been developed to this researcher's knowledge. Hence, it is difficult to determine how the SiNP-modified membrane structure should be adjusted to increase hydrophobicity.

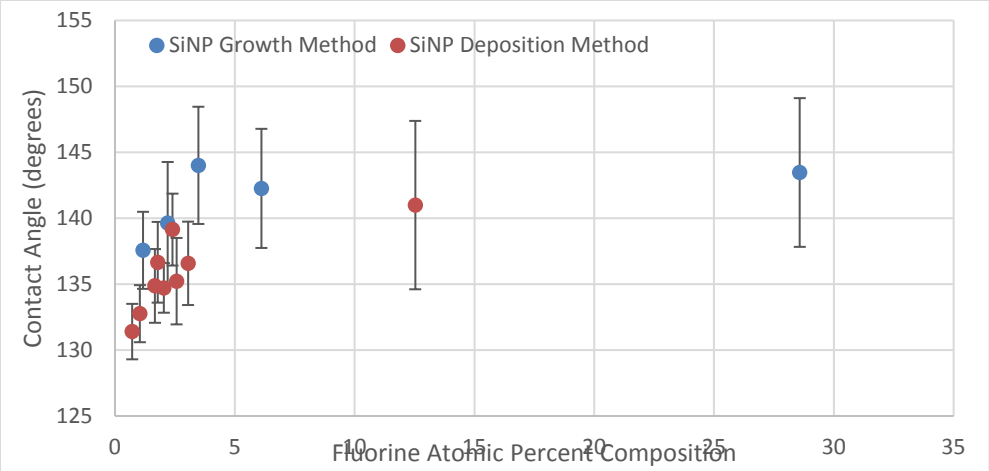

Figure 4-31. Effect of fluorine atomic percent composition on water contact angle of CA membranes modified by the SiNP growth and SiNP deposition methods of membrane modification.

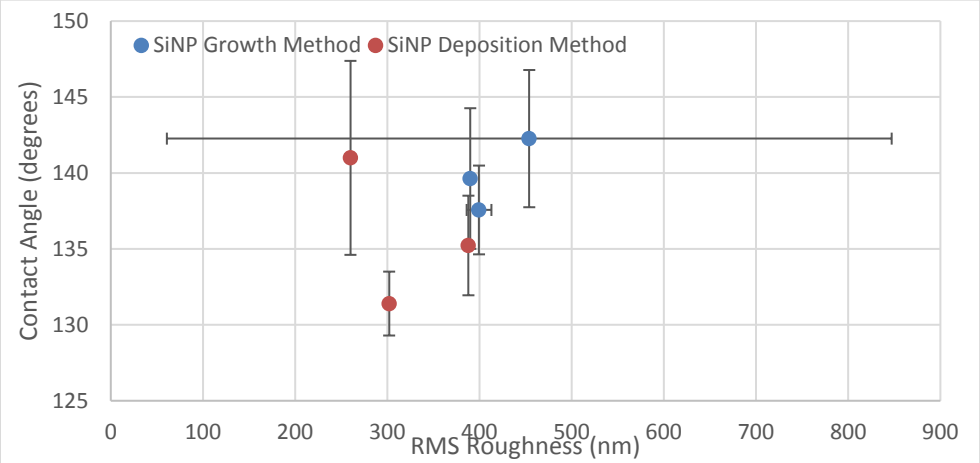

Figure 4-32. Effect of RMS roughness on water contact angle of CA membranes modified by the SiNP growth and SiNP deposition methods of membrane modification.

Membrane Stress Testing

The Al-W200 and Ti-T450 membranes that reached the threshold contact angle of 120° were subjected to thermal and chemical stress tests (Figure 4-33). Both liquid and vapor deposition coating mechanisms were resilient against degradation from thermal stresses. The coatings on the Ti-T450 membranes generally resisted chemical degradation more than the coatings on the Al-W200 membranes. Sodium hypochlorite was the cleaning agent that produced the lowest change in contact angle from all the coatings.

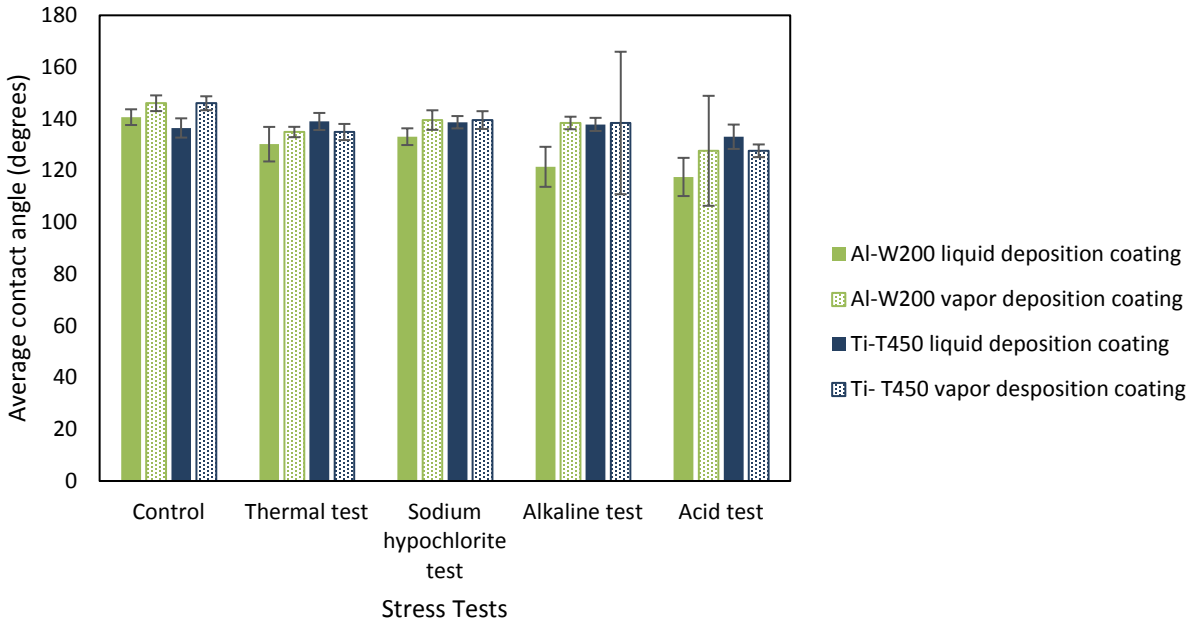

Figure 4-33. Contact angle measurements of membranes with liquid and vapor deposition coatings after thermal and chemical stress tests.

Membrane Performance Testing

The Al-W200 and Ti-T450 membranes coated by vapor deposition of PFS were selected for further flux tests due to their high contact angle and simpler coating method. Bench-scale testing showed that both of these membranes successfully produced flux in the DCMD set up. The highest flux was produced by the thin Al-W200 membranes at high temperatures and low salt feed concentrations (Figure 4-34a). The rejection values for the membranes were generally the greatest at low concentrations and at higher temperatures (Figure 4-34b). Under certain low temperature and high feed solution concentration conditions, it was not possible to produce flux through the membranes.

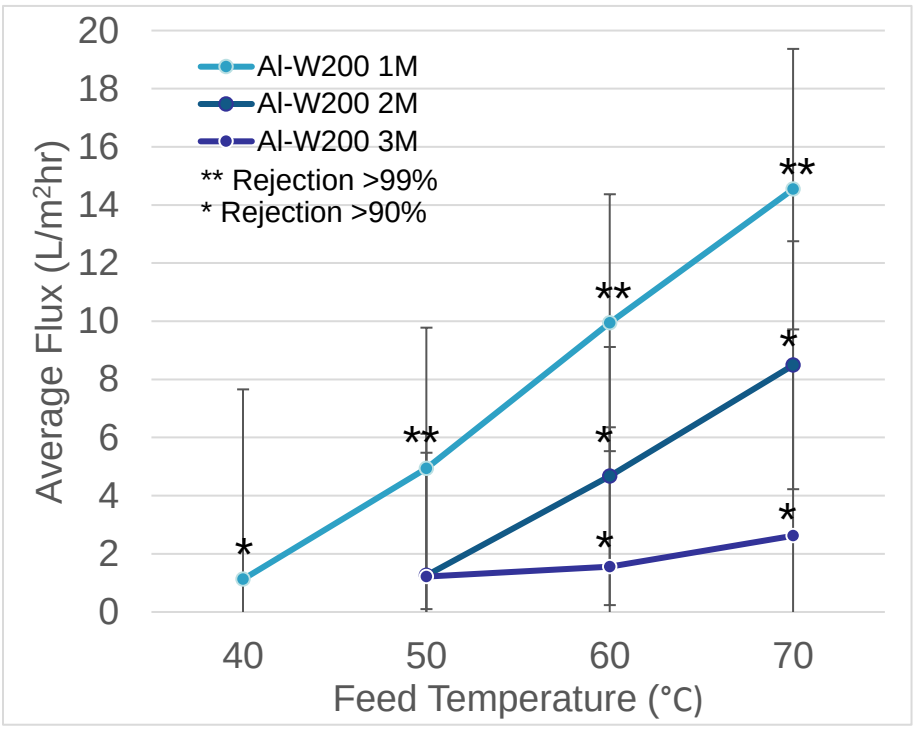

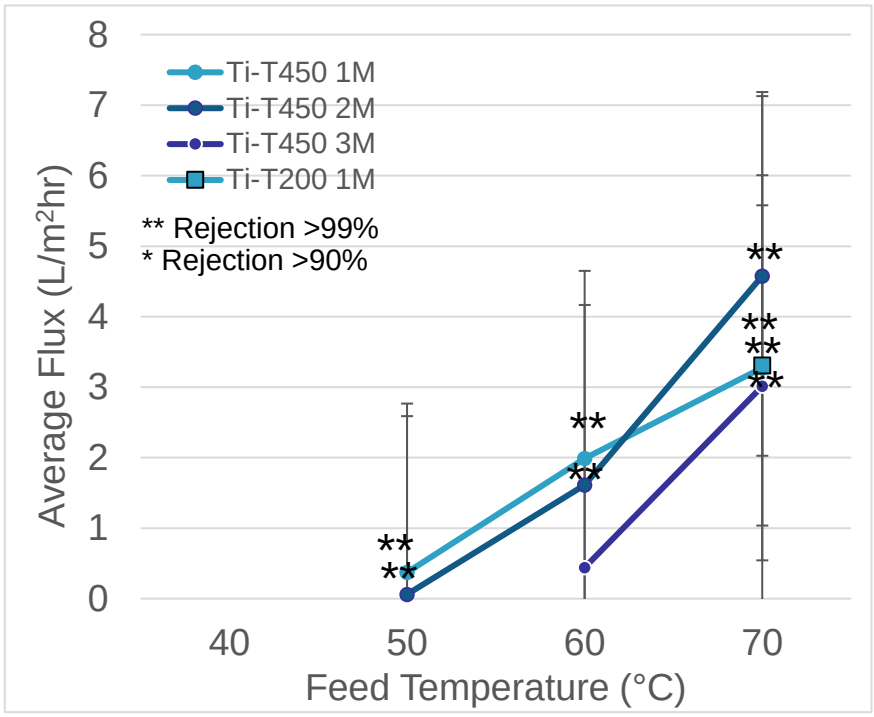

Figure 4-34. Average flux of water through a) Al-W200 and b) Ti-T450 vapor deposition coated membranes in bench scale DCMD system

The range of membranes tested showed significant differences in how the PFS coating changed the hydrophobicity of the membranes. When comparing the contact angle measurements between the two

types of anodized aluminum oxide membranes, the Al-S100 membranes had a contact angle of 68±12° and the Al-W200 membranes had a contact angle of 141±6° (Table 4-3) after liquid deposition. The coating process was expected to bind hydrophobic PFS molecules to the metal oxides in a homogenous monolayer ("Silanes, Silicone, Metal-Organic Compounds by Gelest, Inc.," n.d.). The differences in the hydrophobicity of the membranes could be due to different availability of the alumina oxide sites due to the different anodization and sealing processes from the manufacturer. The Ti-T200 and Ti-T450 membranes were produced from the same manufacturer, but showed different average contact angle measurements after the same coating procedures. Further analysis of the membrane structure with SEM showed that smaller particles were used to create the small pores of the Ti-T200 membranes. Additional manufacturing information on how the membranes are processed was relatively limited.

The modified membranes that had an average contact angle of greater than 120° were selected for stress testing and flux tests. The Al-W200 and Ti-T450 membranes showed relatively little degradation when subjected to thermal and 100ppm sodium hypochlorite stress tests when treated with both liquid and vapor deposition coatings. The PFS vapor deposition method resulted in a slightly more robust coating that had less degradation.

The flux tests showed that the ceramic membranes could be successfully modified for use in membrane distillation. The highest flux was obtained with Al-W200 membranes with a feed solution temperature of 70°C and 1M salt concentration. When comparing the characteristics of the different membrane types, the Al-W200 membranes have several physical features that make them more favorable for membrane distillation than the Ti-T450 membranes. The Al-W200 membranes are only 24% of the thickness of the Ti-T450 membranes and should have less tortuous pore channels due to the anodization process that creates almost perfectly straight pathways through the membrane ("Anopore Inorganic Membranes (Anodisc)," 2009). Both of these factors lead to an increase in flux when using the combined Knudsen-molecular diffusion model (Zachary Doubrava Hendren, 2011). Although the Ti-T450 membranes have a greater pore size, the porosity of the Ti-T450 and Al-W200 membranes is not well characterized leading to difficulties in predicting the flux from these membranes using models. Both Al-W200 and Ti-T450 membranes are can produce salt rejection rates of over 99.5% but at low fluxes the rejection rate generally decreases.

This work showed that commercially available ceramic membranes can be modified to make successful hydrophobic DCMD membranes. The coating is very durable and can withstand thermal and chemical stresses. The modified membranes were tested in a DCMD bench-scale system, and the thinner membranes with less tortuous pores had a high flux rate. The Al-W200 membranes successfully regenerated the saline feed solution and produced higher flux than the other ceramic membranes.

Laboratory-Scale MD Experimental Results

Flux and salt rejection tests for eight different polymeric membranes were completed. Polymeric materials evaluated included polytetrafluoroethylene (PTFE), polyvinylidene fluoride (PVDF), and polypropylene (PP)-based membrane materials, with pore sizes ranging from 0.2 to 0.45 μm. Both flat sheet and hollow fiber module configurations were evaluated, six of the polymeric membranes tested are

flat sheet samples, two are hollow fiber. The active membrane surface area for flat sheet module testing is 25 cm^2.; the active area for the hollow fiber modules tested is 78cm^2, using the log mean of the inner and outer diameters of the fibers. The experimental tests measure the water flux at four NaCl salt concentrations in the feed, 1, 2, 3, and 4 M at inlet ΔT values of approximately 20, 30, 40, 50 °C. All membranes exhibited a slight reduction in flux with increasing salt concentration; however, the reduction was markedly less that that typically seen in RO performance, and adequate values have been recorded and sustained at TDS concentrations >250,000 mg/L, which is well above the RO threshold of 50,000 mg/L TDS. After a membrane coupon was loaded into the test cell with its active layer facing the feed side, the pumps were started and slowly increased so that the flow velocity across the membrane reached 0.5 m/s. The flux is measured via the weight change recorded on the permeate-side balance. Figure 4-35 - Figure 4-40 summarize the experimental results of the MD baseline performance tests.

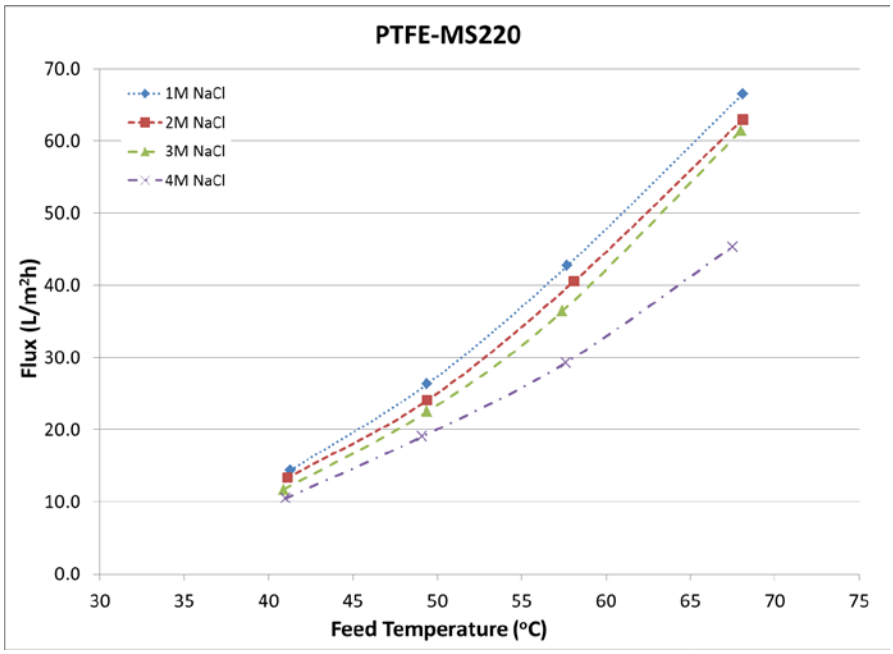

Figure 4-35. Water flux vs. feed temperature for the PTFE-MS220 membranes treating varying concentrations of NaCl. Average $R_{PTFE-MS220}$ = 99.91%.

The PTFE-MS220 membranes produced higher fluxes than their PVDF counterparts from the same manufacturer (see Figure 4-37 below), but slightly reduced salt rejection values (99.91% vs. 99.99%). PTFE-MS450 membranes with a larger pore size (0.45μm) were also tested, but complete test runs were not possible due to frequent membrane rupturing.

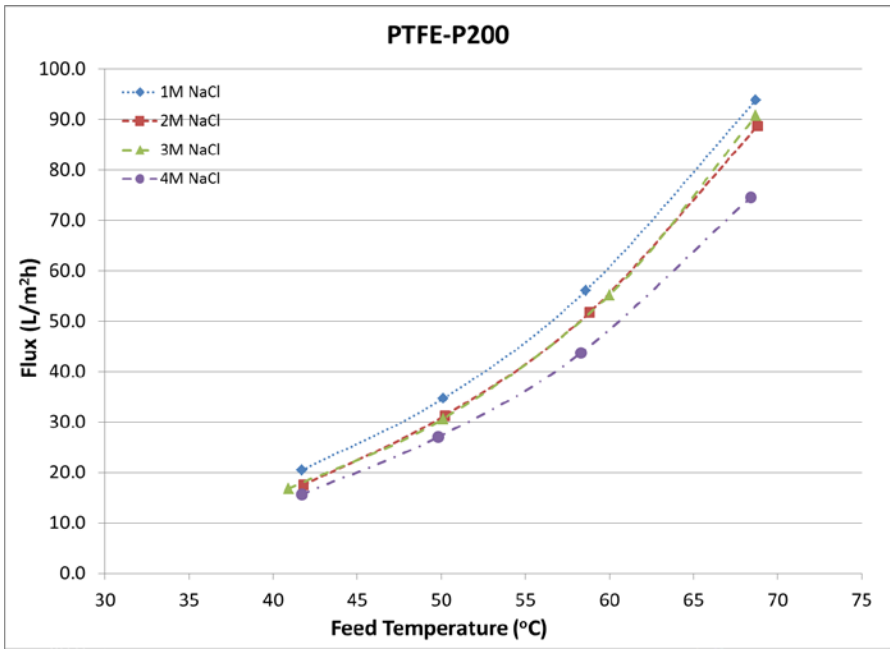

Figure 4-36. Water flux vs. feed temperature for the PTFE-P200 membranes treating varying concentrations of NaCl. Average $R_{PTFE\text{-}P200}$ = 99.99%.

The PTFE-P200 membranes showed the highest performance of all membranes tested, both in terms of flux magnitude and salt rejection. Qualitatively, they also appear to be the most mechanically robust. However, they are only available from the manufacturer in small laboratory-scale sheets, which are not large enough to be relevant for industrial MD applications. However, they demonstrate the impact of membrane structure on performance.

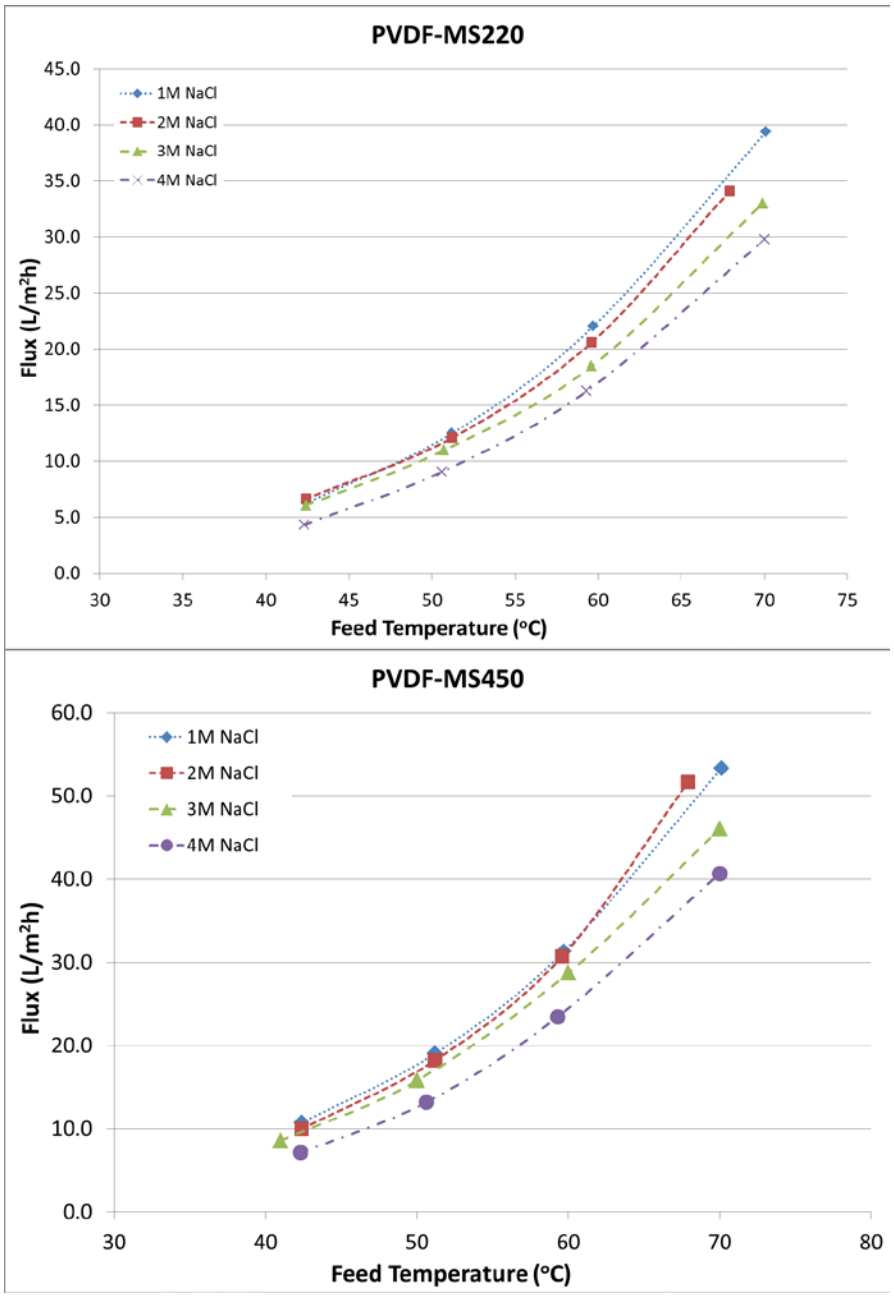

Figure 4-37. Water flux vs. feed temperature for the PVDF-MS220 and PVDF-MS450 membranes treating NaCl feeds at different concentrations. Average $R_{PVDF\text{-}MS220}$ = 99.99%, average $R_{PVDF\text{-}MS450}$ = 99.99%.

The PVDF-MS220 and PVDF-MS450 membranes have pore sizes of 0.22 and 0.45 µm, respectively, and were fabricated by the same manufacturer who made the PTFE-MS220 membranes. The larger pore-size version produced fluxes on average that were 25% higher. In both cases, the average salt rejection remained >99.99%.

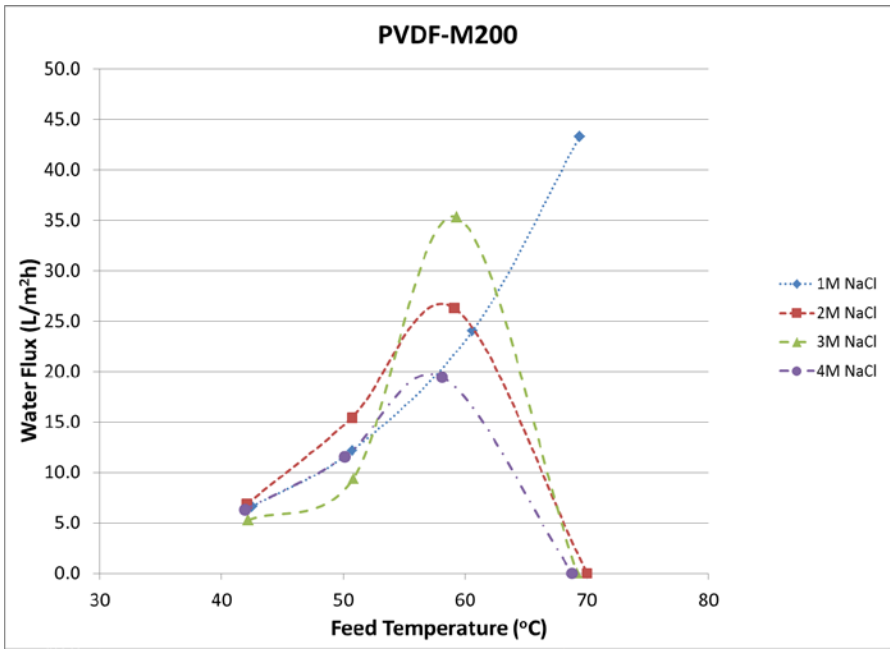

Figure 4-38. Water flux vs. feed temperature for the PVDF-M200 membranes treating varying concentrations of NaCl. Average $R_{PVDF\text{-}M200}$ = 99.94%.

Although the PVDF-M200 membranes produced fluxes similar to the other PVDF membranes tested, the membrane broke during three of the four tests as the temperature was increased to 70 °C. The breakage is shown on Figure 4-38 by the flux declining to zero at 2, 3, and 4 M NaCl concentrations. Subsequent tests started at 70 °C showed that flux and salt rejection were attainable at that high temperature, suggesting that the breakage was due in part to the degradation of membrane integrity over time. These results were not entirely unexpected because the PTFE-M200 membrane was an unsupported membrane and, thus, has reduced mechanically stability.

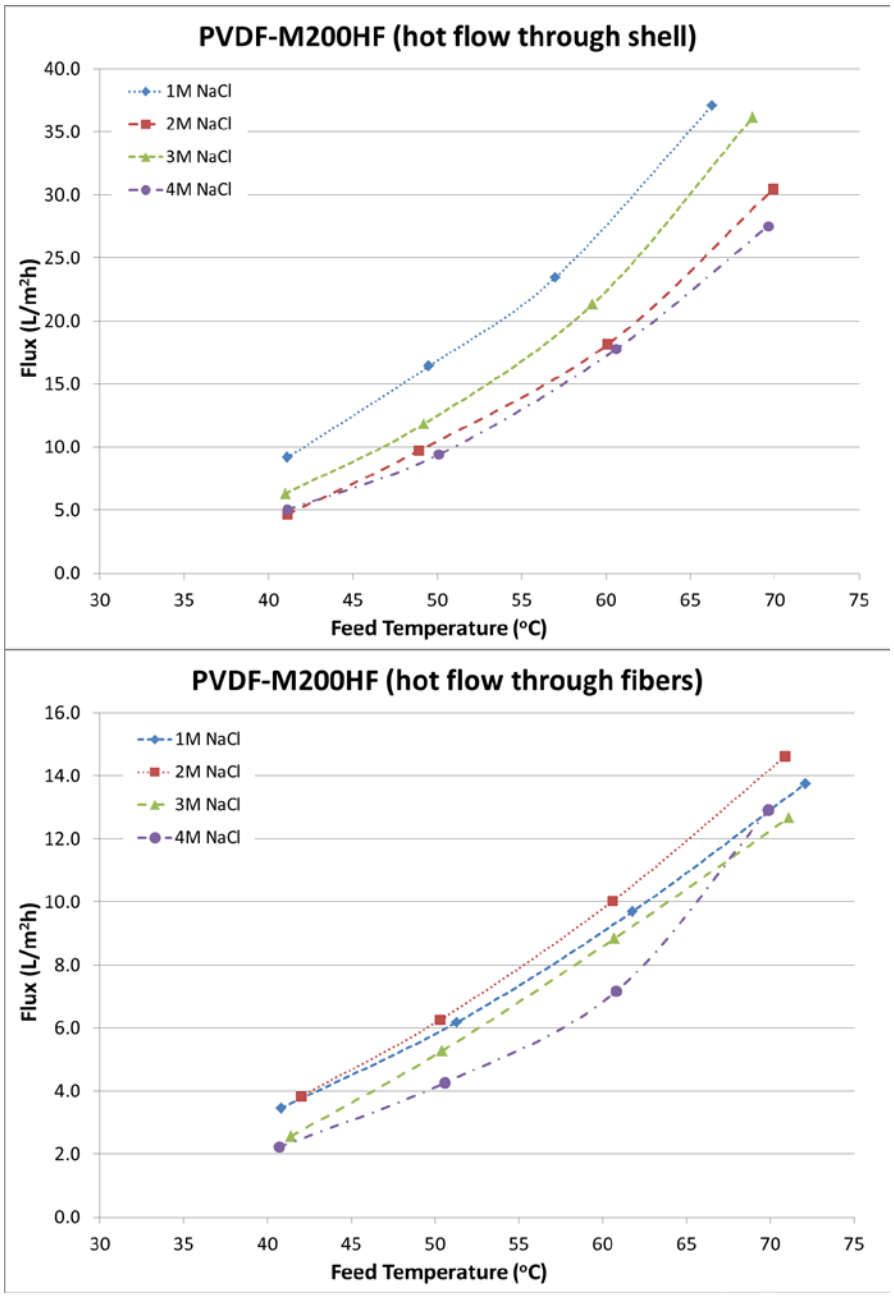

Figure 4-39. Water flux vs. feed temperature for the PVDF-M200HF hollow fiber membranes treating NaCl feeds at different concentrations. Average $R_{PVDF\text{-}M200HF}$ = 99.99%, average $R_{PVDF\text{-}M200HF}$ = 99.99%.

The hollow-fiber PVDF-M200HF membranes were run in two configurations: (i) the heated feed water flowing outside the fibers through the shell and the chilled condensing water through the fibers, and (ii) the heated feed water flowing through the fibers and the condensing stream outside the fibers through the shell. Overall, Figure 4-39 shows that the PVDF hollow fibers yielded fluxes that were slightly lower than their flat-sheet membrane versions. In addition, the flux results were lower by ~33% for the configuration with the hot flow through the fibers.

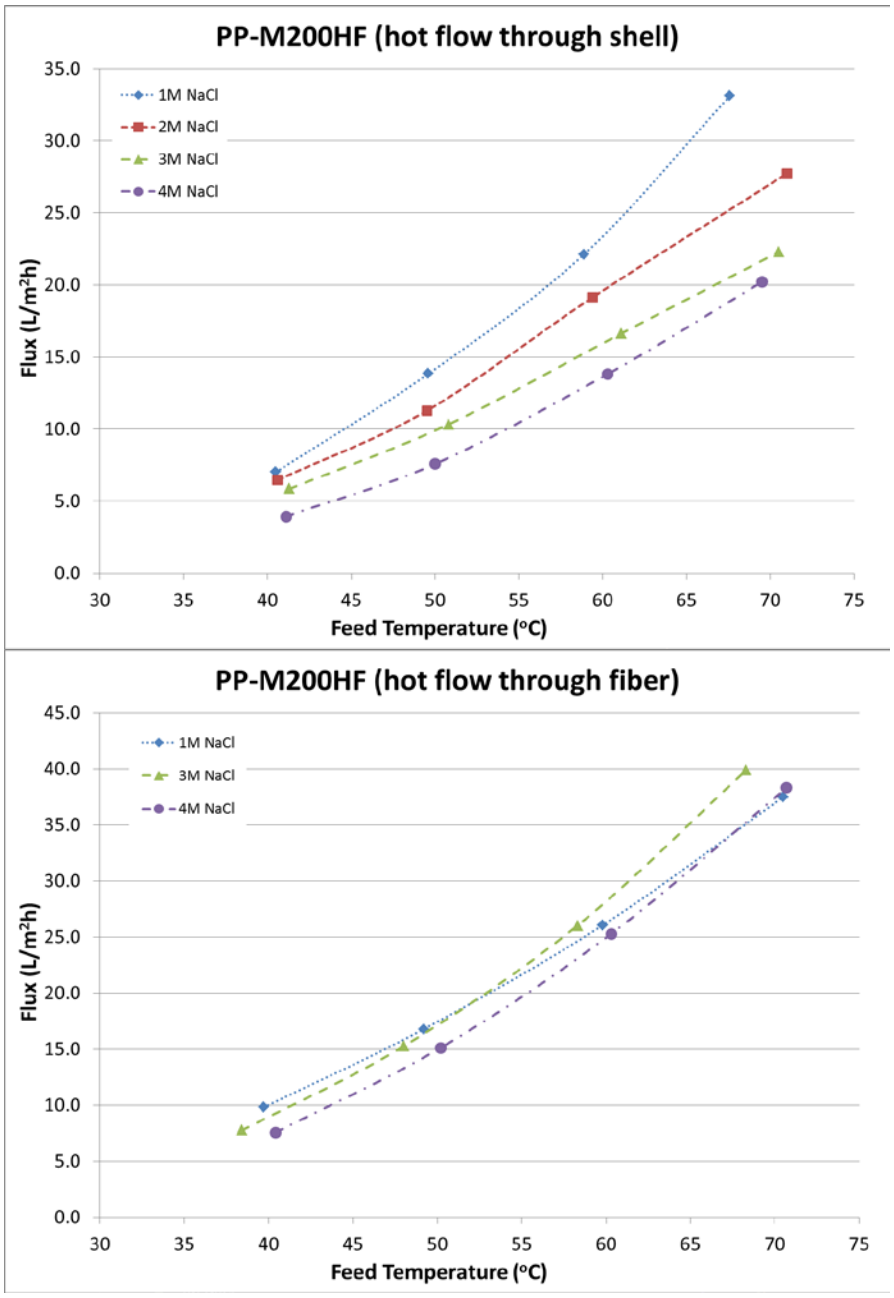

Figure 4-40. Water flux vs. feed temperature for the PP-M200HF hollow fiber membranes treating NaCl feeds at different concentrations. Average $R_{PP\text{-}M200HF}$ = 99.99%, average $R_{PP\text{-}M200HF}$ = 99.99%.

The PP hollow fiber membranes were also run in two configurations, and the results showed that the hot flow through the fibers resulted in higher fluxes than when flowed through the shell.

Ceramic MD Membrane Performance Testing

MD flux and salt rejection tests for two ceramic membranes were done. Ceramic materials evaluated included aluminum oxide- and titanium oxide-based membrane materials. Water flux was measured at

four NaCl salt concentrations (1, 2, 3, and 4 M) in the feed at inlet ΔT values of approximately 20, 30, 40, 50 °C. All membranes exhibited a slight flux reduction with increasing salt concentration. The results are shown below in Figure 4-41 and Figure 4-42.

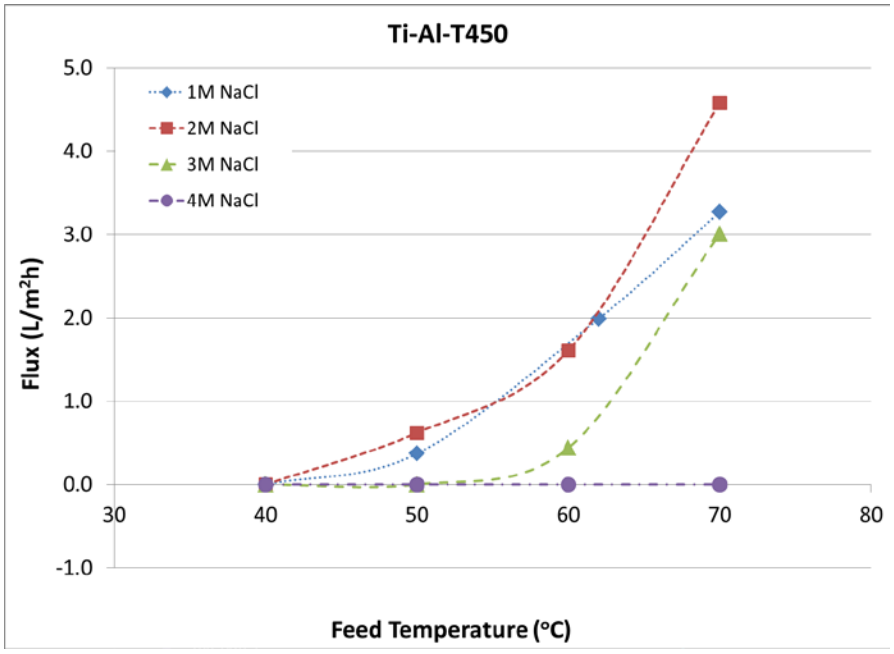

Figure 4-41. Water flux vs. feed temperature for the Ti-Al-T450 membrane treating NaCl feeds at different concentrations. Average $R_{Ti\text{-}Al\text{-}T450}$ = 99.78%.

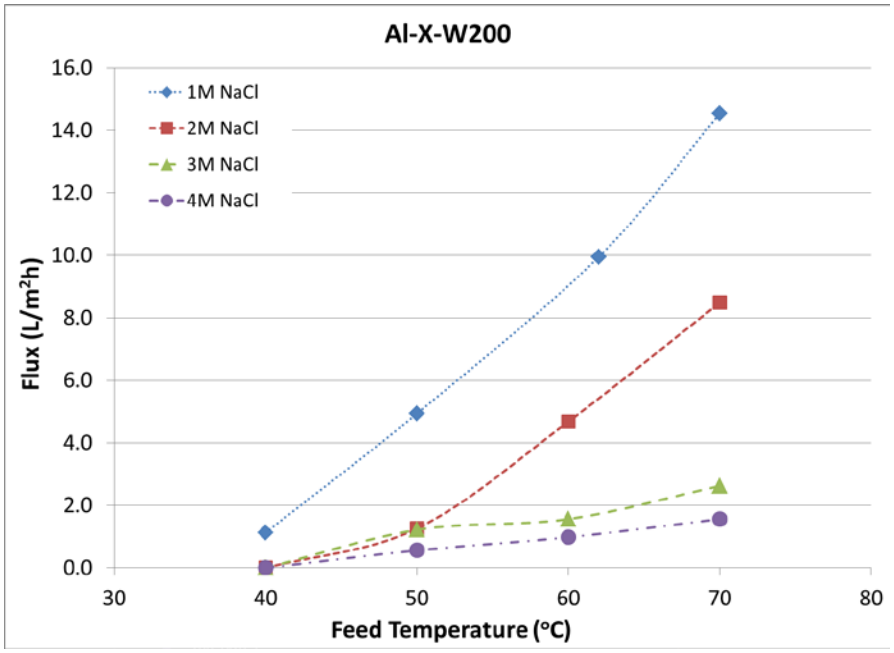

Figure 4-42. Water flux vs. feed temperature for the Al-X-W200 membrane treating NaCl feeds at different concentrations. Average $R_{TAl\text{-}X\text{-}W200}$ = 98.2%.

Figure 4-41 and Figure 4-42 show the water flux values for the two PFS-modified ceramic membranes. The overall flux values recorded were significantly less than those of the polymer membranes shown in Figure 4-35 - Figure 4-40. The likely reasons for the reduced flux values are the differences in thermal conductivity of the materials, with ceramic materials having thermal conductivity values an order of magnitude higher than the polymer membranes, which results in an overall reduced driving force across the membrane interface. In addition, the salt rejection values tended to be lower, suggesting that there may be inconsistencies in the PFS coating.

MD Membrane Extended Run Performance Testing. To evaluate the long term performance of the hollow fiber membranes, extended test runs have been incorporated into the experimental work done this quarter. In these tests the modules are run continuously to extend the typical testing time by a factor of 10. Figure 4-43 shows a typical extended run, which includes changing the water feed temperature at various points of the test.

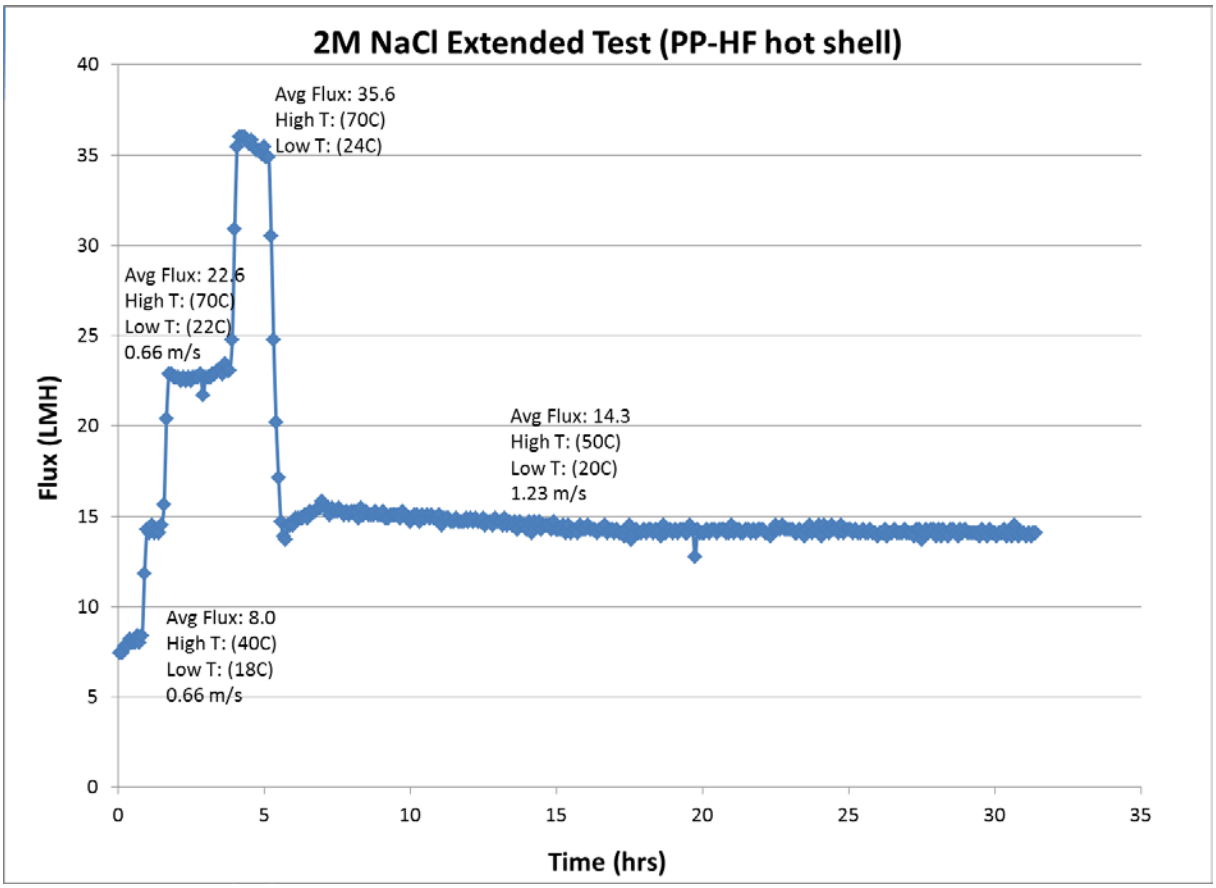

Figure 4-43. Water flux vs. feed temperature for the PP-M200-HF membranes treating 2M NaCl feed water. The rejection throughout the experiment remained above 99.9%.

Test Results from Integrated 50 GPD system

Continued MD Fouling Tests with Real Wastewater. Performance evaluation of the downselected polypropylene [PP]-based MD membrane with a real wastewater was continued this quarter. This wastewater has very high scaling potential and is supersaturated with moderately high total dissolved

solids [TDS] content. Although the MD membrane in our proposed hybrid FO-MD process technology serves mainly to regenerate the diluted FO draw solution and would not be exposed directly to the feed wastewater to be treated, it is anticipated that the MD membrane would still come into contact with some wastewater contaminants because rejection of contaminants by the FO membrane will not be perfect. Thus, this testing with a more complex, real wastewater was conducted to identify any MD performance issues that might occur during long-term operation. The objectives of the real-wastewater test was to (i) determine if there are constituents in this real wastewater that could cause pore wetting (which, in turn, could lead to poor contaminant rejection performance by the PP membrane), (ii) evaluate fouling behavior of the PP membrane hollow fibers in the presence of actual wastewater, (iii) conduct preliminary cleaning/recovery tests to begin to identify appropriate cleaning protocols for operation, and (iv) determine which feed contaminants would be poorly rejected by the PP membrane. In this quarter, specific focus was given to (ii) by determining the so-called "critical flux" of the membrane treating this moderately high-TDS, real wastewater.

Critical-Flux Testing of PP-Based MD Membranes. In pressure-driven membrane systems, the critical flux is the operational pressure point at which fouling is accelerated and is used as an important operating guideline. Once the critical flux is established for a membrane/wastewater system, the operational setpoint can be set at a pressure point (a temperature point in the case of MD) *below* this to reduce the need for downtime due to cleaning, thereby extending the overall system performance and reducing operational costs. For each test, the baseline MD performance was first determined using 2 M NaCl solution as feed. The MD module was then used to treat the real wastewater feed at a given temperature until the target cumulative time on-stream of 24 hours was reached. The wastewater feed concentration was kept pseudo-constant through the addition of deionized water via a dosing pump. Water flux, temperature, and electrical conductivity were monitored, and the critical flux was noted by a sharp drop in flux during operation. Upon completion of the 24-h test, a membrane post-check for performance was conducted.

Figure 4-44 - Figure 4-47 show the MD water flux data obtained with the Site 1 wastewater on the lab-scale PP hollow-fiber membrane module at different feed temperatures (40, 50, 60, and 70 °C) and a permeate temperature of 20 °C for each of the 24-h critical flux tests.

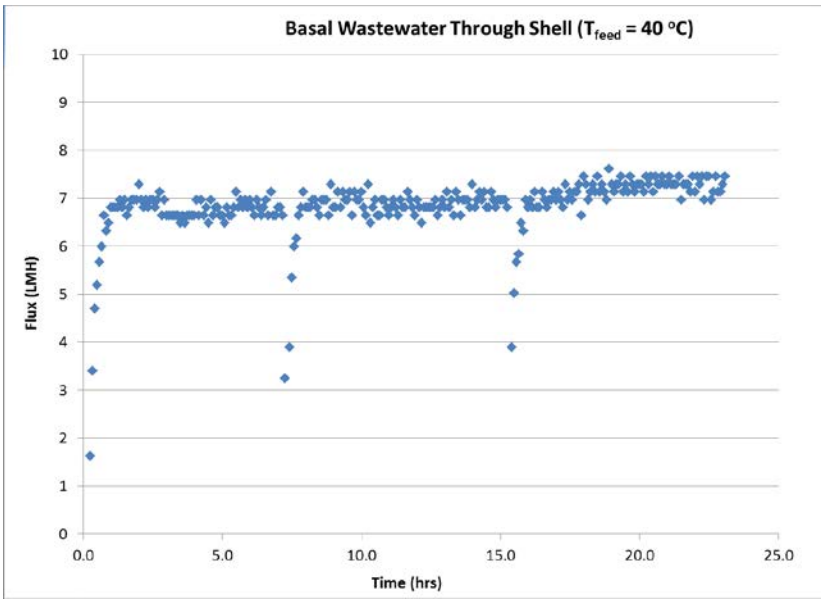

Figure 4-44. MD critical-flux test in lab-scale PP hollow-fiber membrane module treating real Site 1 wastewater at 40 ºC. Permeate temperature: 20 °C; Feed flowrate: 1.5 L/min; Permeate flowrate: 0.1 L/min. Observed TDS rejection: ~99.8%.

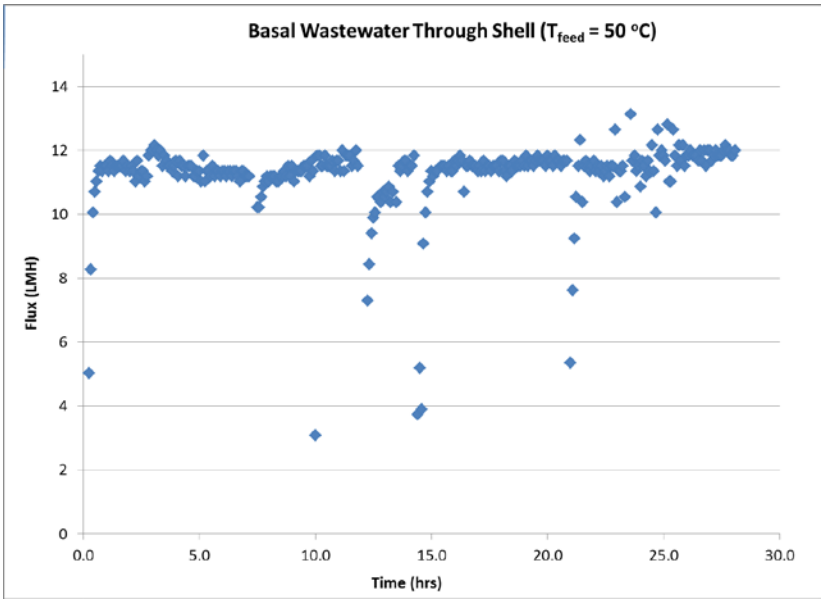

Figure 4-45. MD critical-flux test in lab-scale PP hollow-fiber membrane module treating real Site 1 wastewater at 50 ºC. Permeate temperature: 20 °C; Feed flowrate: 1.5 L/min; Permeate flowrate: 0.1 L/min. Observed TDS rejection: ~99.8%.

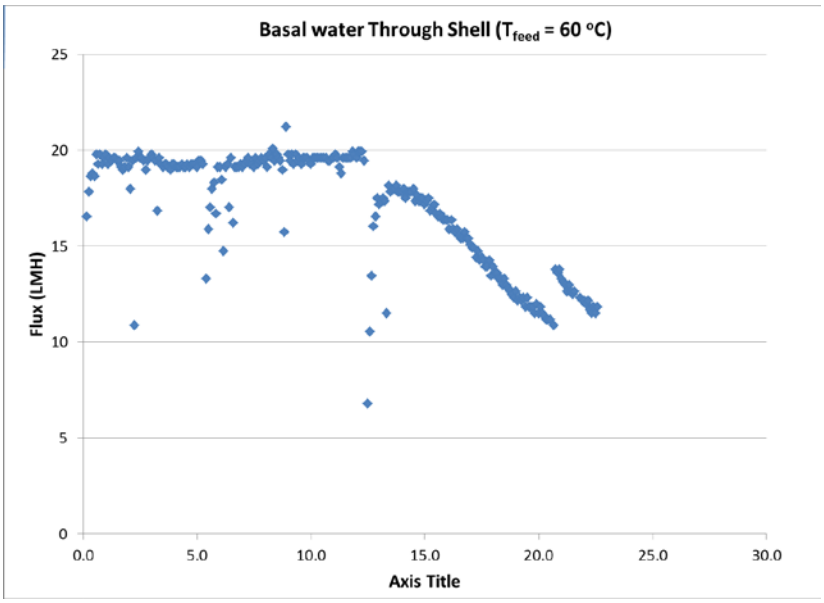

Figure 4-46. MD critical flux test in lab-scale PP hollow-fiber membrane module treating real Site 1 wastewater at 60 ºC. Permeate temperature: 20 °C; Feed flowrate: 1.5 L/min; Permeate flowrate: 0.1 L/min. Observed TDS rejection: ~99.8%.

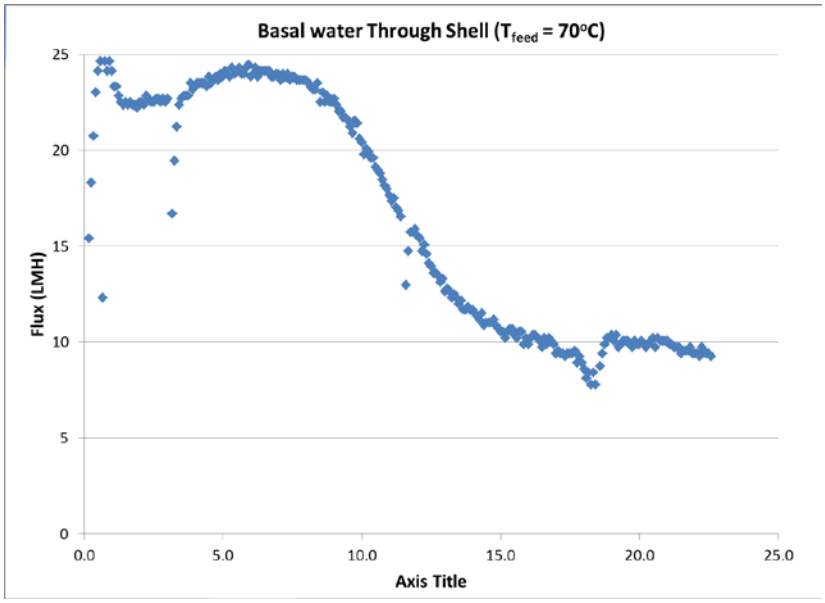

Figure 4-47. MD critical flux test in lab-scale PP hollow-fiber membrane module treating real Site 1 wastewater at 70 ºC. Permeate temperature: 20 °C; Feed flowrate: 1.5 L/min; Permeate flowrate: 0.1 L/min. Observed TDS rejection: ~99.8%.

These tests show that PP-based MD membrane operation with the Site 1 wastewater was stable at both 40 and 50 °C, as demonstrated by stable average water flux values of 7 and 11.8 L/(m^2·h), respectively, during the course of the tests (Figure 4-44 and Figure 4-45). Raising the MD feed temperature to 60 °C resulted in a sharp decline in water flux after about 11 hours (Figure 4-46). At the even higher feed temperature of 70 °C, the sharp drop in water flux was observed even earlier after only ~8 hours of

operation (Figure 4-47). These results are consistent with the concept of critical flux and confirm that critical flux will be an important operational parameter to determine during field operation of this technology. However, the results do not suggest that the MD system would need to be operated below 60 ºC because, in actual operation, the MD would be subjected to a more dilute solution (i.e., the spent FO draw solution). Continued extended testing of the integrated FO-MD system will be required to determine how the exposure of these foulants affect MD performance.

Autopsy of MD Membranes Fouled with Real Wastewater. Membrane autopsies were conducted to identify changes to the PP-based MD membrane after it had been tested with the Site 1 wastewater. The membrane autopsies consisted of high-resolution scanning electron microscopy [SEM] imaging using a FEI XL30 SEM and a lower resolution SEM imaging with elemental composition analysis using a FEI XL30 Environmental SEM [ESEM] with an Energy Dispersive X-Ray Spectrometer [EDS]. The high-resolution SEM images showed a foulant layer on the feed-side of the MD membrane in cross-sectional images as well as in images of the feed (shell)-side membrane surface (Figure 4-48 and Figure 4-49).

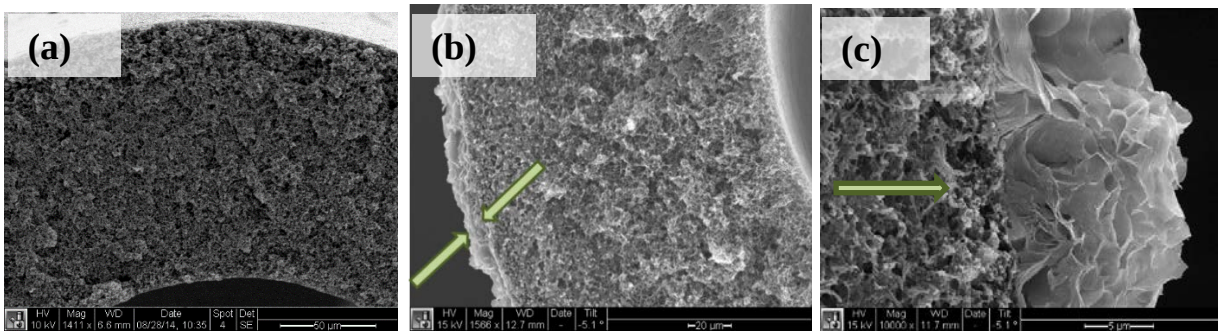

Figure 4-48. Cross-sectional SEM images of PP MD membrane fiber: (a) virgin membrane, (b) fouled membrane (foulant layer highlighted), and (c) close-up of foulant on outer edge of membrane surface.

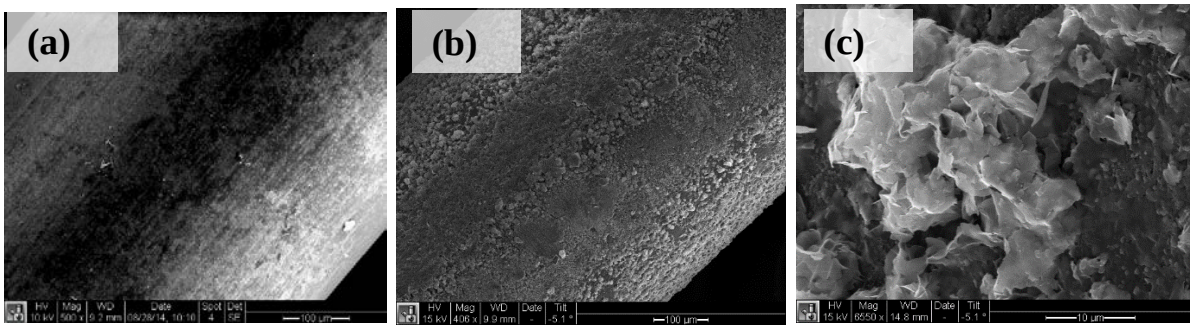

Figure 4-49. SEM images of PP MD membrane feed-side surface: (a) virgin membrane, (b) fouled membrane, and (c) close-up of foulant deposited on membrane surface.

Elemental analysis of fouled membrane cross-sections and feed-side surfaces was conducted using the EDS to scan for elements present within the image produced by the ESEM. The EDS can provide quantitative analysis for elements present and map their signal on the image. The elements searched for consisted of elements identified as present in the wastewater from prior chemical analysis and any

additional elements detected by the EDS. The list of elements from chemical analysis of the wastewater consisted of calcium, chlorine, magnesium, sodium, strontium, and sulfur. The elements associated with fouling and present in the highest concentrations included sodium, chlorine, and magnesium (Figure 4-50). Carbon and oxygen were identified as present in high concentrations as well, but these elements were not included as part of the elemental composition of the foulant because the signal from these elements could also be due to the membrane polymer.

The cross-sectional images with elemental mapping also showed a fairly localized distribution of the foulant on the membrane surface. Figure 4-51a shows the different elemental distributions in the membrane bulk and the foulant. The map shows that the membrane bulk consists of primarily carbon, while the foulant on the outer edge of the membrane shows the presence of a variety of compounds. The foulant distribution on the outer edge of the membrane can be clearly seen on individual element maps as well, and the element map for sodium is presented in Figure 4-51b as an example.

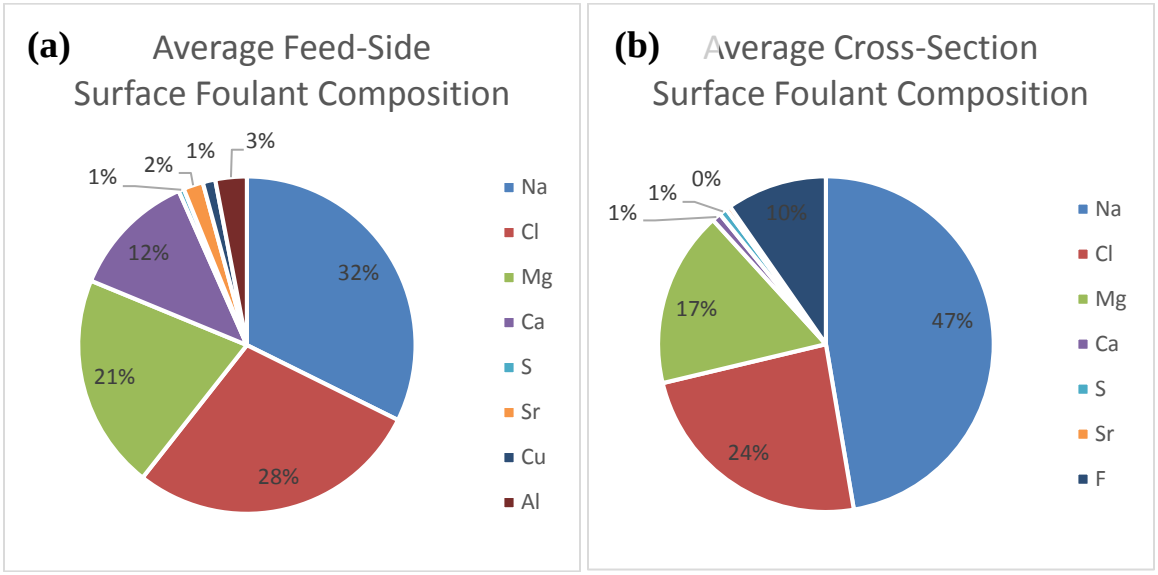

Figure 4-50. Elemental composition of foulant on images from the membrane (a) feed-side surface and (b) cross-section.

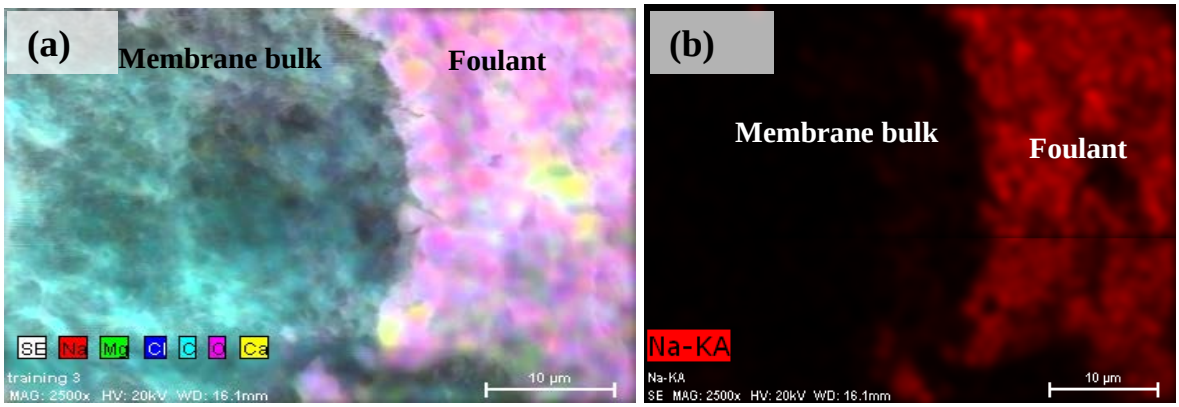

Figure 4-51. (a) Survey elemental map of elements identified on a fouled membrane cross-section. (b) Individual elemental map of sodium on the same fouled membrane.

Continued Real Wastewater Performance Testing with Integrated System. Tests were also performed using real wastewater from potential field-test site identified as Site 1. This wastewater has very high scaling potential and is supersaturated with moderately high total dissolved solids [TDS] content (~46,000 mg/L). Where prior tests focused primarily on the individual performance of either the FO or MD membrane this round of testing was conducted to assess the integrated performance of the hybrid system. The objectives of the real-wastewater test were to (i) determine if there are constituents in this real wastewater that may damage the membrane as evidenced by membrane rupture over time, (ii) evaluate fouling behavior of the FO membranes in the presence of actual wastewater, (iii) conduct preliminary cleaning/recovery tests to begin to identify appropriate cleaning protocols for operation, and (iv) determine which feed contaminants would be poorly rejected by the FO unit. Although a complete data analysis of the results is currently underway, Table 4-5 below displays the test summary of the integrated system, with a topline summary of the fluxes observed for each membrane during integrated operation.

Table 4-5. Summary of FO and MD Water Fluxes Obtained During Integrated Operation [FO membrane: Y-PFO; MD membrane: M-HF200]

Feed Solution TDS [mg/L]	Draw Conc. [M NaCl]	MD Hot feed T [°C]	MD Cold permeate T [°C]	Baseline FO Flux [L/(m^2·h)]	Typical MD Flux [L/(m^2·h)]	MD salt rejection [%]
Real WW (46,000)	1 M	~68	~24	~21	~8	>99%
Synthetic WW (46,000)	3M	~71	~24	~22.5	~8	>99%
Synthetic WW (46,000)	3M	~61	~22	~22.5	~5.1	>99%
Synthetic WW (46,000)	3M	~50	~20	~22	~3.2	>99%
Synthetic WW (46,000)	3M	~40	~19	~22	~1.8	>99%

Average MD rejection remained above 99% for all tests, independent of feed water type to FO feed. In addition to the above tests, feed water recovery tests were performed to determine the % recovery for a given feed water. A second FO module, X-TFC was installed on the integrated bench unit—however, this FO module has a significant larger area (1.5 m^2); however, the increased flow-through volume limits integrated operation with the current MD module, since the volume flow rate through the MD side is limited by the much smaller membrane area.

Volatile Contaminant Model Validation

To validate the contaminant concentration model, DCMD experiments were conducted on a bench-scale DCMD system to determine whether the model accurately predicted the feed and permeate collection

stream contaminant concentrations in a DCMD system over time. The results from the validated model were used to support Hypothesis 1 that the contaminant transport of a multicomponent feed solution in the DCMD process can be accurately described with a Fickian mass transport model. The following sections describe the subsequent results.

The results of the mass loss tests indicated that the first order loss model described the measured mass losses well. The measured results of the bench-scale loss tests showed that the feed and permeate collection stream concentrations decreased exponentially after the initial spike of contaminant solution (Figure 4-52). The loss model fit the shape of the decreasing feed and permeate collection stream concentrations, and the accuracy of the model was evaluated using the average normalized root-mean-squared error (RMSE). The average normalized RMSE was calculated by evaluating the RMSE, normalizing the RMSE by the starting contaminant concentration, and averaging the normalized RMSE over the replicates of the loss tests. The average normalized RMSE of the model ranged between 3.8-9.5% for the different compounds, indicating that the first order loss model predicted the measured losses with good accuracy.

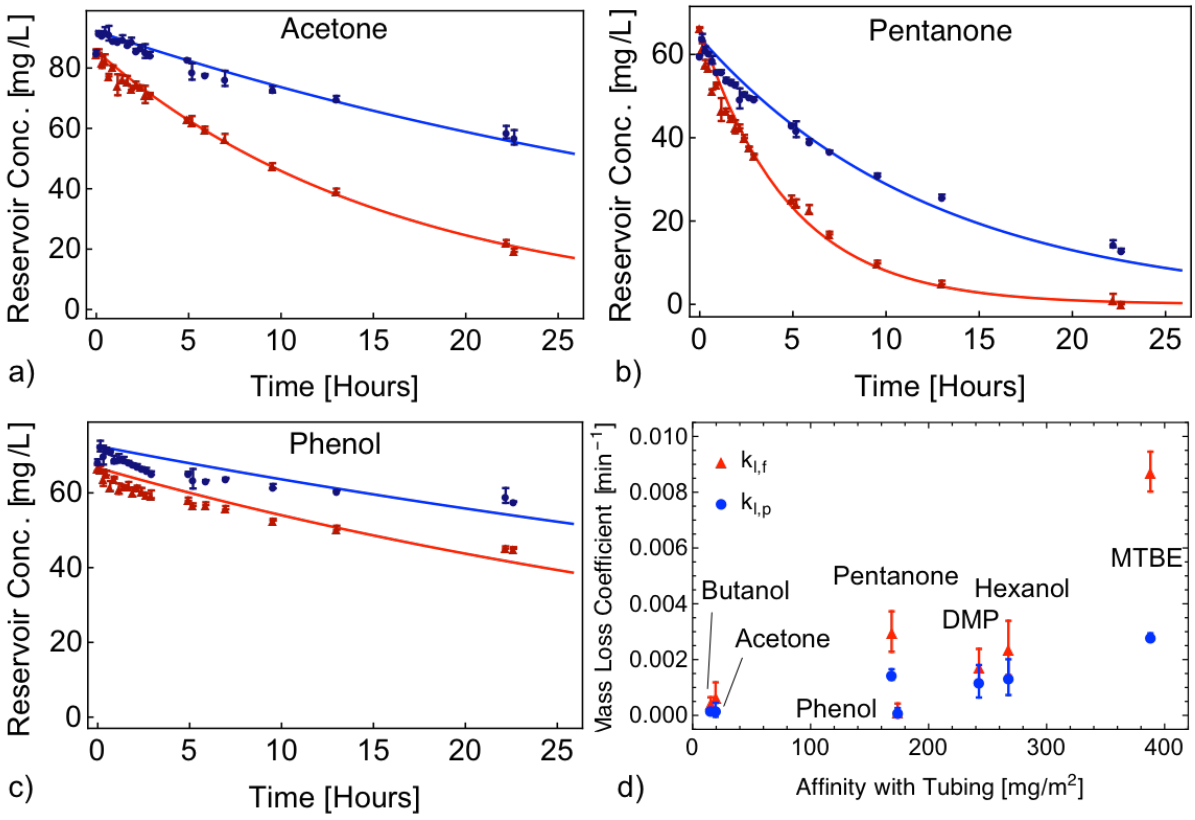

Figure 4-52. a), b), and c) depict the decrease in acetone, pentanone, and phenol concentration, respectively, due to mass losses in the feed stream (red) and permeate collection stream (blue) during a mass loss test. Data points are the averaged feed and permeate collection stream concentrations from measurements at each time point, and the error bars indicate the standard deviation associated with the measurements. Solid lines are the modeled mass losses that were modeled using the mass loss coefficients that were

fitted to the measurements. Operating conditions during testing were feed stream temperature of 313 K, permeate collection stream temperature of 293 K, and feed and permeate collection stream crossflow velocities of 31 cm/s. Figure 4-52d depicts the average feed and permeate collection stream mass loss coefficient for each compound.

The calculated mass loss coefficients were plotted in Figure 4-52d with respect to the affinity of the contaminant with the tubing. While both sorption and evaporation affected the rate of compound loss, the mass loss coefficients correlated best with the affinity to the tubing rather than to the compound's Henry's constant. This indicated that sorption to the tubing was a significant source of mass loss in the bench-scale DCMD system. The elevated temperature and presence of salt in the feed stream also led to higher contaminant loss coefficients in the feed stream than in the permeate collection stream. Higher temperatures and presence of salt generally decrease the solubility of compounds in aqueous solutions {Schwarzenbach, 2003 #38, resulting in a higher rate of mass lost from the system.

DCMD flux tests on synthetic wastewaters were conducted to monitor the transport of the contaminants from the feed stream to the permeate collection stream. The change in feed and permeate collection stream concentrations of six different contaminants during a flux test are illustrated in Figure 4-53. The concentration profiles in Figure 4-53a-e show similar feed and permeate collection stream concentration trends for compounds with relatively high values of Henry's constant [$\log_{10}(H) \geq 2.95$]. The flux test results showed that, for the volatile compounds, the measured feed stream contaminant concentration decreased over time due to both the contaminant flux into the permeate collection stream and the losses due to evaporation and adsorption. Concurrently, the measured permeate collection stream contaminant concentration initially increased due to the high contaminant flux. As the permeate collection stream contaminant concentration increased, the vapor pressure gradient between the feed stream and permeate collection stream decreased, causing the permeate collection stream concentration to plateau and reach a maximum as the contaminant flux decreased. The subsequent decrease in the permeate collection stream concentration was due to the evaporative and adsorptive losses that occurred in both the feed and permeate collection streams.

While the concentration profiles of the compounds with higher Henry's constant showed the same pattern, the phenol permeate collection stream concentration did not reach a critical point maximum within the timescale of the flux test (Figure 4-53f), illustrating that the Henry's constant of the compound affected the flux of the contaminant. The different trend in the concentration profile is due to low phenol flux and low rate of mass losses. The low phenol flux and rate of loss resulted in a relatively high phenol feed steam concentration and slow increase in the phenol permeate collection stream concentration. As a result, the concentration in the permeate collection stream had not reached equilibrium with the feed stream and reached a critical point maximum by the end of the flux test.

Notably, the measured concentration profiles in Figure 4-53a-d showed that the permeate collection stream concentrations reached concentrations higher than the feed stream concentrations. This demonstrated that the DCMD systems magnified the concentration of volatile contaminants, which could result in effluent that is unusable for certain applications.

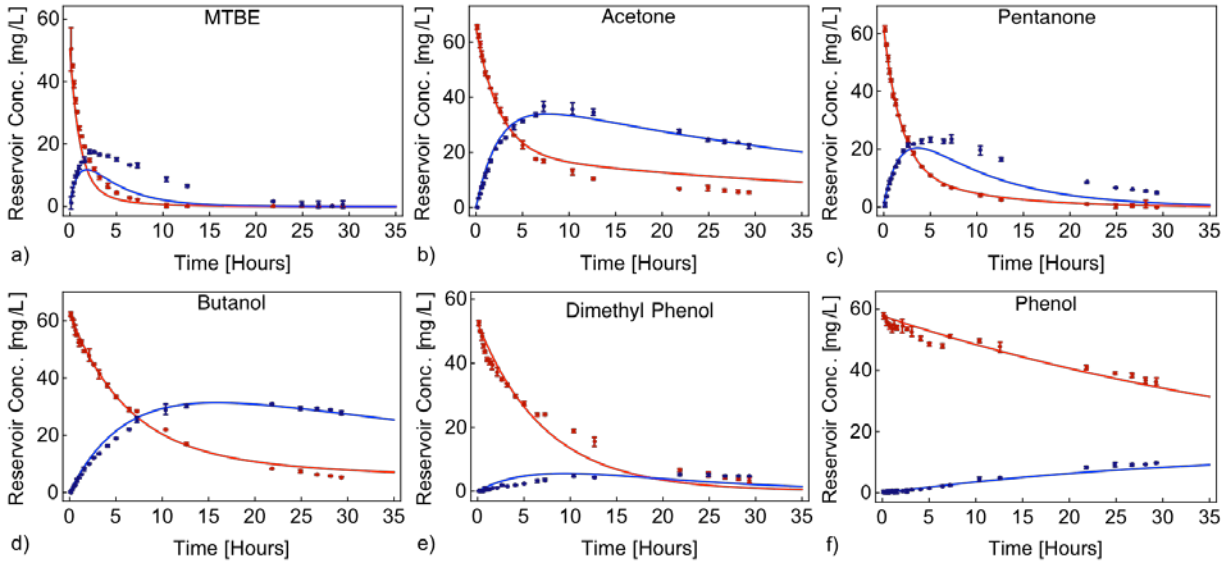

Figure 4-53. Measured and modeled contaminant concentration in the feed stream (red) and permeate collection stream (blue). Data points are averaged feed and permeate collection stream concentrations from measurements at each time point, and the error bars indicate the standard deviation associated with the measurements. Concentration profiles of contaminants are arranged in order of decreasing value of Henry's constant of the contaminants. Operating conditions during testing were feed stream temperature of 313 K, permeate collection stream temperature of 293 K, and feed and permeate collection stream crossflow velocities of 31 cm/s.

Quantifying and predicting the effluent concentrations are important for determining what applications DCMD can be used for. The contaminant concentration model was used to describe the transport of the contaminants during the DCMD treatment of the synthetic wastewater. The modeled results for each contaminant are overlaid on the measured results in Figure 4-53. The contaminant concentration model predictions described the measured contaminant concentrations during the flux test with good accuracy. For each contaminant, the modeled results described both the decrease in feed stream concentration and the initial increase and subsequent decrease in permeate collection stream concentration. The average normalized RMSE for the contaminants tested ranged between 5.7-11.5%, indicating that the contaminant concentration model was a good descriptor of the DCMD system.

While the contaminant concentration model generally described the transport in DCMD systems well, the model tended to underpredict the permeate collection stream concentration of compounds with high mass loss coefficients, such as MTBE (11.5% average normalized RMSE) and pentanone (8.2% average normalized RMSE). This trend may be due to the differences in introducing the contaminants to the permeate collection stream between the mass loss tests and the flux tests. During the mass loss tests, a spiking solution of the contaminants was prepared, added to the reservoir, and mixed vigorously to dissolve the contaminants. However, during the flux tests, the contaminants were slowly introduced to the permeate collection stream through the membrane interface. This difference in introducing the

compounds may have resulted in an overprediction of the mass loss coefficient for the more volatile compounds.

The good fit of the contaminant concentration model to the results from the DCMD flux test indicated that the contaminant mass transport was well described by the model. By accounting for the mass transport of contaminants through the membrane as well as system losses, the contaminant concentration model is a valuable tool for determining the PCS concentration in DCMD systems at any stage during the water treatment process.

Therefore, the validation of the contaminant concentration model supports the hypothesis that the contaminant transport of a multicomponent feed solution in the DCMD process can be accurately described with a Fickian mass transport model. While the Fickian model does not include the diffusional interactions between the diffusing species, the accuracy of the model shows that the contaminant concentration model adequately predicts the change in contaminant concentration in both the feed and permeate collection streams. Validation of the model enables the same mass transport mechanisms to be used in predicting the contaminant concentrations in large-scale systems as well.

Bench-Scale Integrated Test System

To conduct integrated performance evaluation and process behavior on available FO and MD membrane modules (bench or full-size) beyond membrane coupons, the bench-scale, integrated FO-MD test system described in Section 3.2 was built, shaken down, and commissioned. This skid-mounted, bench system is 4 ft. wide by 4 ft. long by 6 ft. high, and photos of it are shown in Figure 4-54 and Figure 4-55. Figure 4-56 is a screenshot of the data acquisition (DAQ) interface configured in the LabVIEW design software environment (National Instruments, Austin, TX). The DAQ interface layout followed the PFD and P&ID given in Section 3 for this bench unit. The FI, TE, and CE labels in the DAQ layout indicated the locations of the flowmeters, thermocouples, and conductivity probes, respectively, in the bench system.

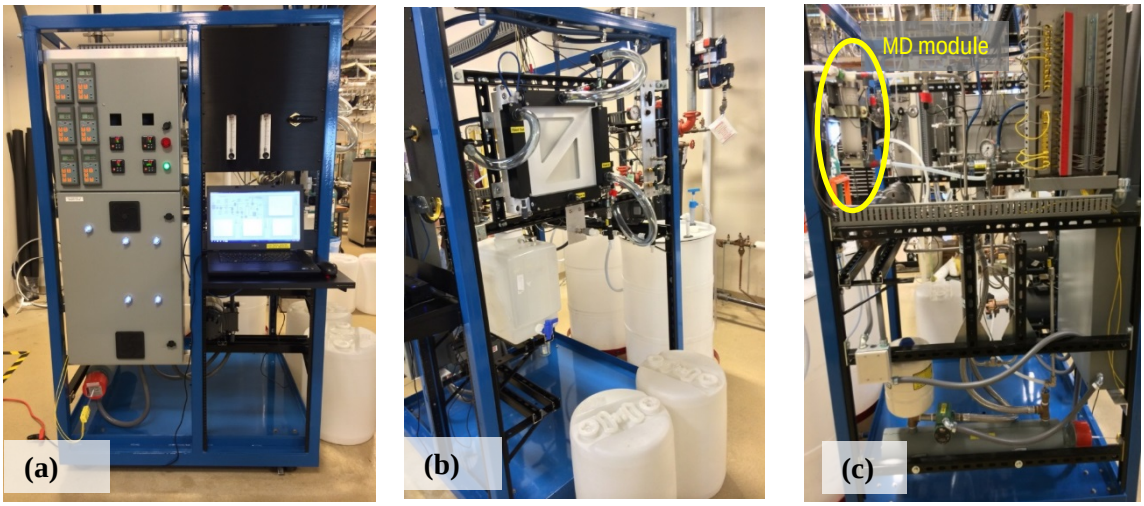

Figure 4-54. Photos of bench, integrated FO-MD system: (a) front view, (b) right-side view, and (c) left-side view with M-HF200 MD membrane module (area ~ 0.64 m^2) highlighted.

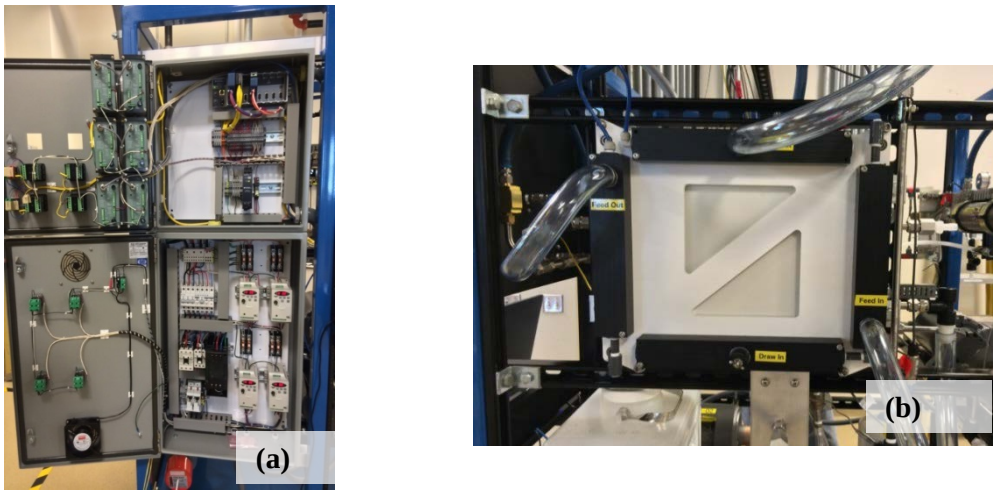

Figure 4-55. Photos of bench, integrated FO-MD system: (a) interior of electrical and DAQ enclosures and (b) close-up of FO membrane module candidate Y-PFO (area ~ 0.21 m^2).

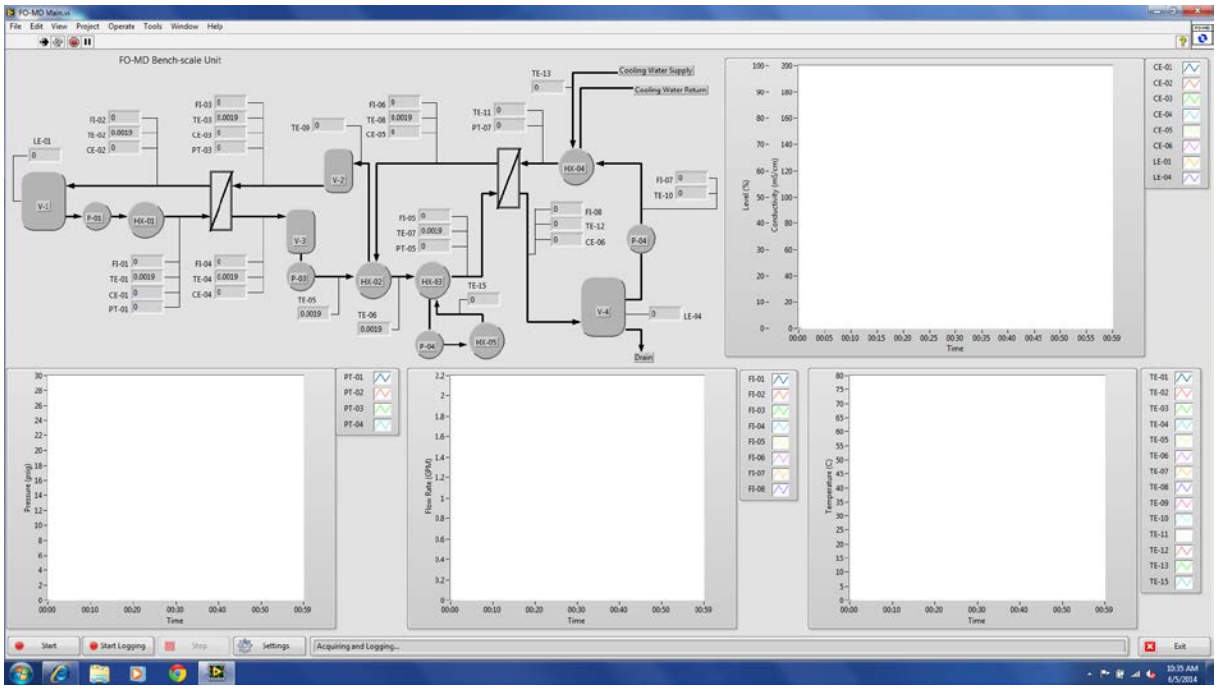

Figure 4-56. Screenshot of DAQ interface on bench, integrated FO-MD system.

Integrated Performance Testing-1. The first FO module installed on the bench, integrated test system was the Y-PFO, which had membrane area of 0.21-m^2 and was made from the first downselected FO membrane Y-T. The MD module installed was the M-HF200 (2.5 in. dia. × 8 in. long), which had membrane area of 0.64-m^2 and was made from the downselected polypropylene-based MD membrane. The FO and MD process sections were run in integrated operation mode for over 5 h with DI water feed, aqueous 0.5 NaCl draw solution, FO feed temperature of 25 °C, MD hot-side temperature of 60 °C, and MD cold-side temperature of 23 °C. The FO draw-side concentration was solely maintained by the MD section in this test; that is, no external dosing to replenish the draw-solution strength was done. The system reached stable integrated operation after roughly 1 h. Figure 4-57 shows that the measured steady-state water flux was ~23 L/(m^2·h) in the 0.21-m^2 FO module and ~7 L/(m^2·h) in the 0.64-m^2 MD module. These values were consistent with the water fluxes provided by the manufacturers for these membrane modules under the given test conditions. As also shown in Figure 4-57, these module water fluxes resulted in an overall product-water flow rate of 27-32 gal/day that the integrated system stably maintained for 4 h after reaching steady state. The water product was also high-quality, containing low dissolved-solids content, as indicated by its stable, low conductivity reading of ~3 µS/cm during the course of the test.

More importantly, the bench, integrated FO-MD system operation showed that the MD process can successfully regenerate the FO draw solution to keep a stable FO osmotic-pressure driving force. Without MD regeneration, operation of the FO process by itself resulted in a continuous decline in FO water flux with time, as shown in Figure 4-58. The data collected in the Figure 4-57 test run also demonstrated the

"self-regulating" behavior of the integrated FO-MD system, highlighting that the hybrid FO-MD process could inherently find a steady state (i.e., no "process runaway" potential).

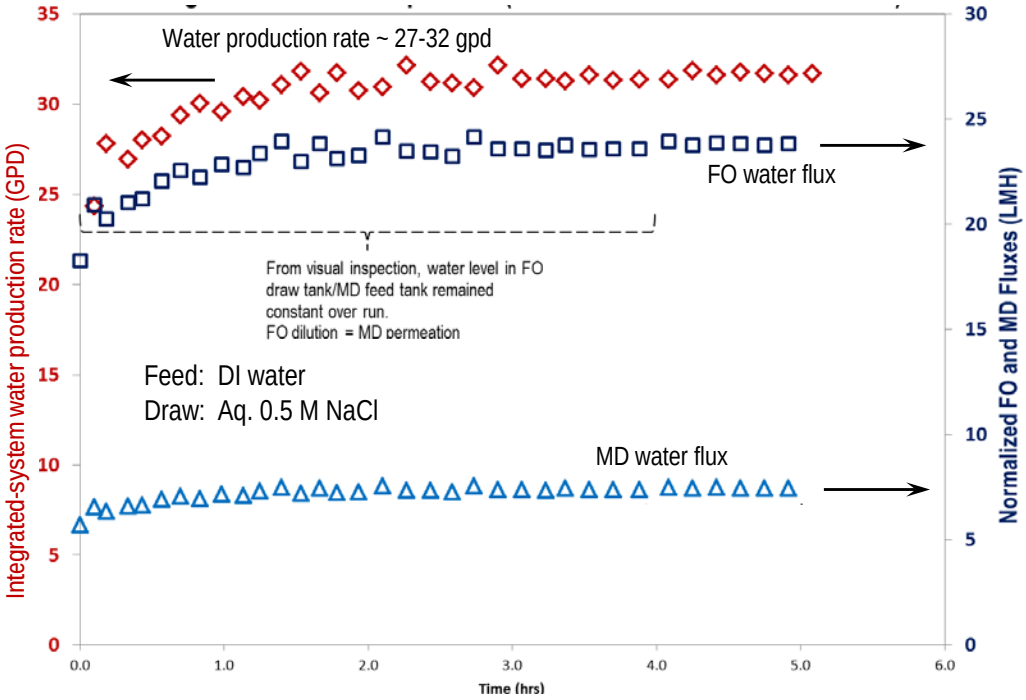

Figure 4-57. Integrated operation data obtained on the bench, hybrid FO-MD test unit, demonstrating full-system operability and stability.

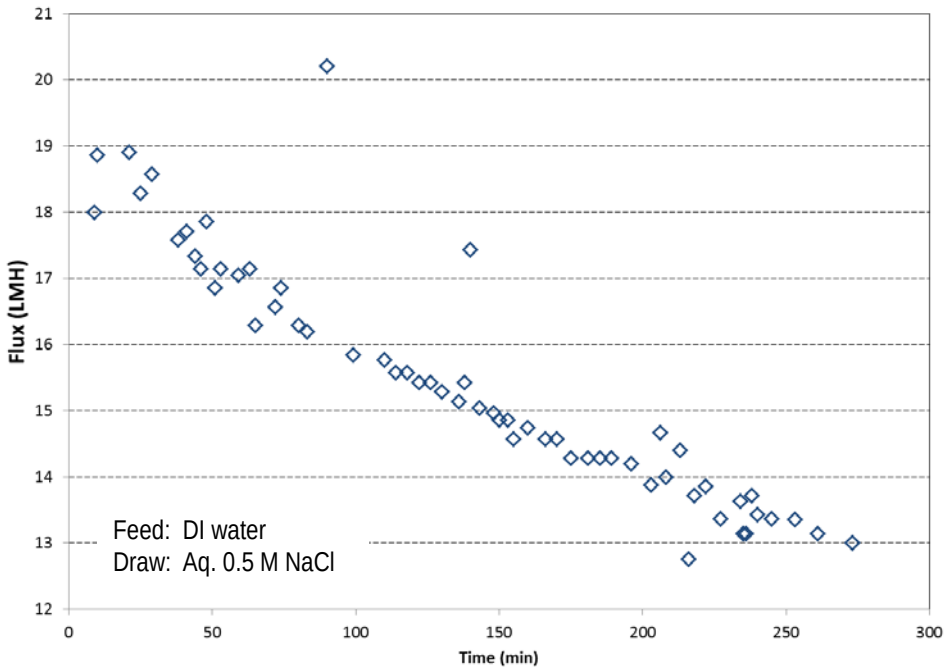

Figure 4-58. Decline in FO water flux when FO module was operated in bench, hybrid FO-MD test unit without MD regeneration of draw solution. Flux declined because of loss of draw-solution osmotic pressure due to the dilutive effect of FO permeation.

Additional bench, integrated system tests were conducted to further investigate the system behavior (e.g., approach to steady state) and performance of the integrated FO-MD process. Integrated FO-MD testing with a synthetic aqueous NaCl feed and a real raw wastewater from an oil and gas production facility identified as Site 2 was done on the Y-PFO flat-sheet FO module and the 2.5 in. × 8 in. hollow-fiber MD module installed on the test system. The synthetic feed had a moderately high TDS concentration of 46,000 mg/L as NaCl. The Site 2 raw wastewater had low TDS (~2,400 mg/L) as well as silica, hydrocarbon organics, and a variety of other contaminants. The draw-solution concentration used was 3 M NaCl for the synthetic feed and 1 M NaCl for the Site 2 raw wastewater. The MD hot-feed temperature was varied from 40 to 70 °C in the synthetic feed tests but was set to 70 °C in the Site 2 wastewater feed tests. In both synthetic and Site 2 wastewater feed tests, the MD cold-permeate temperature was essentially ambient (19-24 °C). Furthermore, in one type of Site 2 feed test, the wastewater feed TDS concentration was kept pseudo-constant by adding DI water to the feed tank with a dosing pump. In another type of test, the Site 2 wastewater feed was allowed to concentrate and then operated at a given water recovery. In both types of tests, the FO draw-side concentration was maintained by the MD process.

Table 4-6 summarizes the water fluxes measured in the FO and MD modules during integrated operation of the bench FO-MD unit. Under the given test conditions, the average Y-PFO module water flux stabilized at 21-22 L/(m^2·h). As expected, the water flux of the M-HF200 MD module decreased with decreasing hot MD feed temperature from 8 L/(m^2·h) at 68-70 °C to 1.8 L/(m^2·h) at 40 °C. Hence, at the lower MD feed temperatures, achieving steady state in the integrated system was slow because the FO

water permeation rate was outperforming that of the MD. In all tests, the average MD rejection remained above 99% and was unaffected by feed water type to the FO.

Table 4-6. FO and MD Water Fluxes Obtained During Integrated Operation with Synthetic Feed and Raw Site 2 Wastewater

Feed [TDS (mg/L)]	NaCl draw concentration [M]	MD hot-feed temperature [°C]	MD cold-permeate temperature [°C]	Water flux [L/(m²·h)]	
				FO module	MD module
Synthetic [46,000 mg/L TDS as NaCl]	3	71	24	22.5	8
		61	22	22.5	5.1
		50	20	22	3.2
		40	19	22	1.8
Raw Site 2 wastewater [~2,400 mg/L TDS]	1	68	24	21	8

FO membrane: Y-PFO module (area ~ 0.21 m^2); MD membrane: M-HF200 module (area ~ 0.64 m^2)
Measured MD salt rejection: >99% in all tests

Tests at different water recoveries (e.g., 25%, 75%) were done with raw Site 2 wastewater on the integrated system to assess performance and fouling tendencies in the modules. Figure 4-59 presents the FO and MD fluxes measured during the constant feed concentration testing as a function of run time. As indicated by the leveling off of the FO water flux, stable integrated operation was reached after ~1 h. The FO water flux stabilized at ~20-21 L/(m^2·h), and the steady-state MD water flux was ~7 L/(m^2·h). The overall product-water flow obtained on the integrated FO-MD system with the raw Site 2 wastewater feed was 27-28 gal/day, which was stably maintained for 5.5 h after reaching steady state.

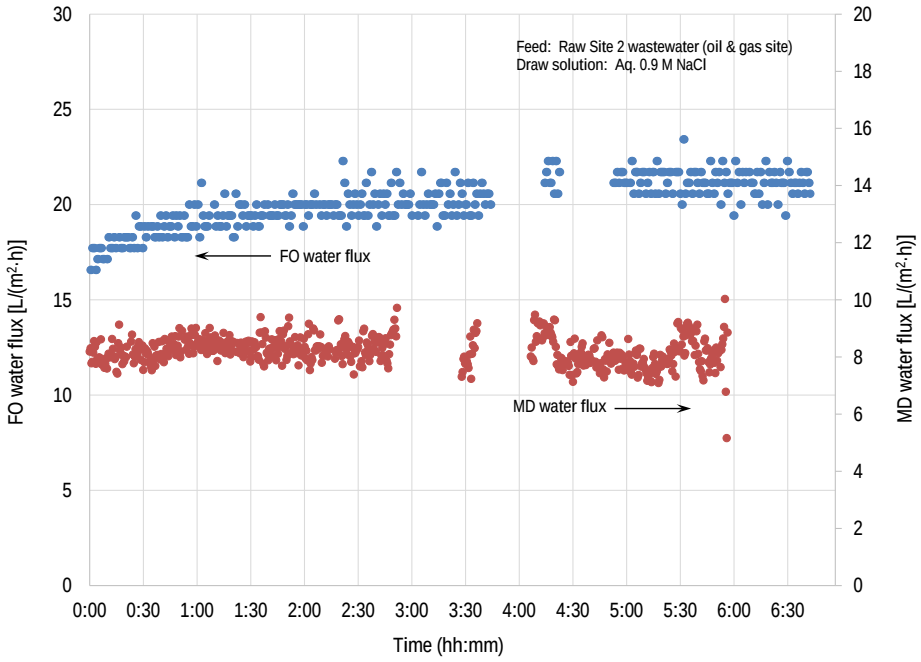

Figure 4-59. Integrated-operation water fluxes measured on bench, FO-MD system treating real raw Site 2 wastewater as function of on-stream run time. Wastewater feed TDS concentration was kept constant by addition of DI water with a dosing pump. FO draw solution: Aq. 0.9 M NaCl. MD hot-feed and cold permeate temperature = 70 °C and 20-24 °C, respectively.

In the feed concentration/water recovery testing, the raw Site 2 wastewater feed was first allowed to concentrate to reach roughly a water recovery of 25%, as reflected by conductivity in the feed wastewater tank increasing from about 5,000 to 8,000 µS/cm. The higher TDS content of the concentrated wastewater feed was then maintained by adding DI water to the feed tank with a dosing pump. The results of the first 6 h of integrated operation at 25% water recovery are shown in Figure 4-60. During the first 60-90 min of operation, the FO water flux gradually increased from 18 to 23 L/(m^2·h) in its approach to a pseudo-steady state. After 90 min of operation, however, the water flux of the FO module did not stabilize as in the previous test but began to decline slowly until it was ~15 L/(m^2·h) at the end of the 6-h test. The MD water flux, though, stayed essentially constant at ~7-8 L/(m^2·h) throughout the entire 6-h test run.

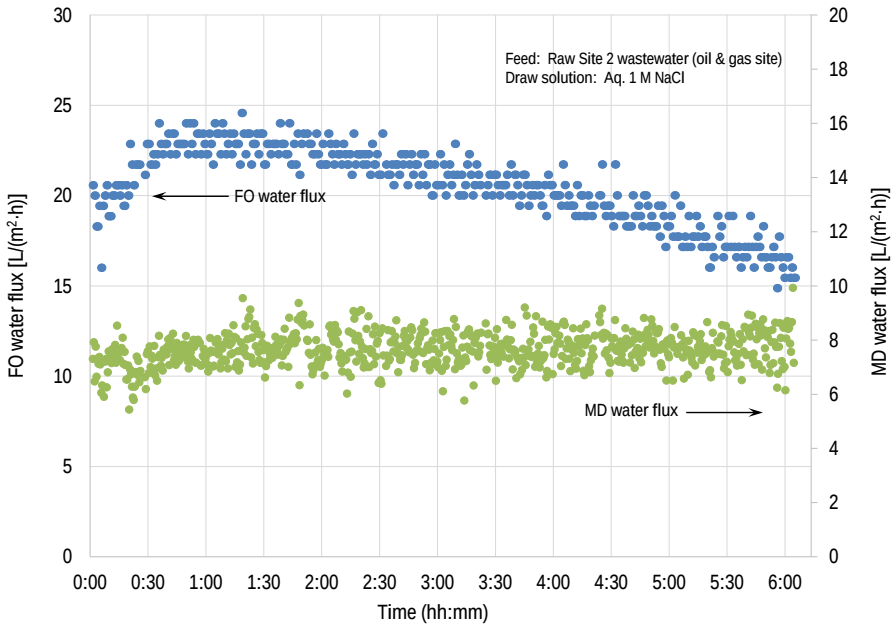

Figure 4-60. Integrated-operation water fluxes measured in feed concentration/water recovery testing on bench, FO-MD system treating real raw Site 2 wastewater as function of on-stream run time. Water recovery: 25%. FO draw solution: Aq. 1 M NaCl. MD hot-feed and cold permeate temperature = 70 °C and 20-24 °C, respectively.

To determine whether the FO water flux needed a longer time to stabilize, the feed concentration testing at 25% water recovery was resumed the next work day. As shown in Figure 4-61, the FO water flux started at ~15 L/(m^2·h), the value at which the previous testing in Figure 4-60 had ended, and slowly rose to ~18-19 L/(m^2·h) in the first hour of the test. However, after 1.5 h into the test, the FO water flux rapidly decreased until it was only 3 L/(m^2·h) at the end of the 6.5-h test run. In contrast, the water flux of the MD module again stayed stable at ~7 L/(m^2·h) throughout the test. Furthermore, the product water leaving the integrated system was high-quality, as indicated by the product water's low conductivity reading that translated to 99+% TDS rejection.

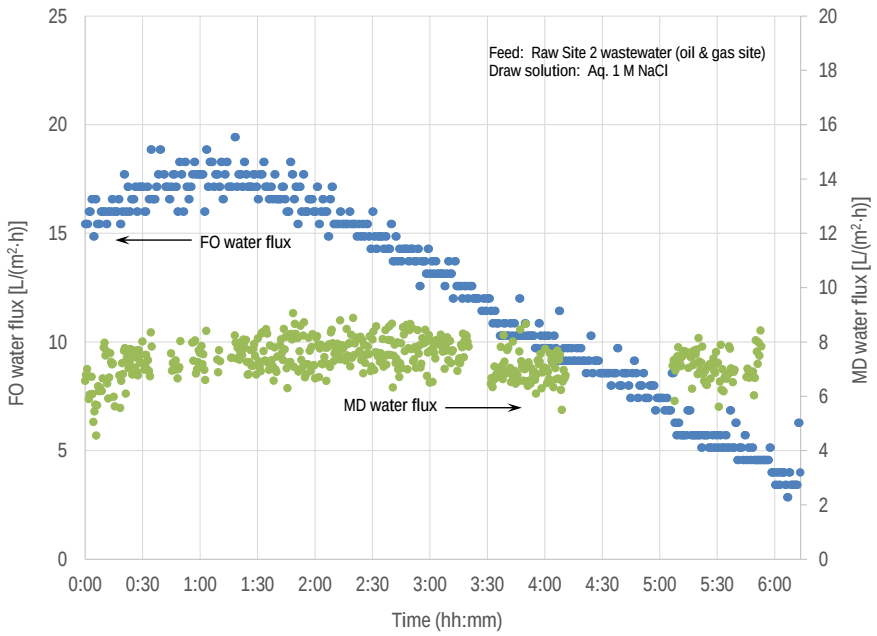

Figure 4-61. Water fluxes measured in continued feed concentration/water recovery testing on bench, integrated FO-MD system treating real raw Site 2 wastewater as function of on-stream run time. Water recovery: 25%. FO draw solution: Aq. 1 M NaCl. MD hot-feed and cold permeate temperature = 70 °C and 20-24 °C, respectively.

The continual decrease observed in the FO water flux during the course of feed concentration testing indicated that the concentration increase in the ***raw*** Site 2 wastewater feed accompanying increasing water recovery was quickly fouling the FO module. While cleaning the FO module with dilute acid and base easily returned the module's water flux to initial values before exposure to raw Site 2 wastewater, the feed concentration test results suggest that some level of feed pretreatment should be done on ***raw*** wastewater feeds to extend FO module performance stability. Because the MD membrane only saw the FO draw solution as its feed, no adverse effect of wastewater feed concentration testing was seen on the MD module.

Integrated Performance Testing-2. Next, the Y-PFO module was replaced with a module of the second downselected FO membrane candidate (X-TFC) on the integrated bench unit. Because this FO module (X-TFC-MS) had a 13-fold larger area (2.8 m^2) than the Y-PFO module, the FO feed pump and flowmeters in the FO feed line were also replaced with larger ones during installation of this second FO module. After leak-checking the modified FO section of the system, baseline tests were conducted on the X-TFC-MS module with DI water feed at different NaCl draw concentrations to check integrity. The module was run in concurrent flow configuration first and then switched to countercurrent mode.

As shown in Table 4-7, the X-TFC-MS module had water fluxes of 12-19 L/(m^2·h) and reverse NaCl salt fluxes of about 0.01-0.04 mol/(m^2·h). These values translated to salt/water selectivities (J_S/J_W) of ~0.03-0.12 g NaCl/L permeated water. Because these selectivity values are better than the J_S/J_W measured on X-TFC membrane coupons, the X-TFC-MS module was deemed good (i.e., not defective).

Comparison of the data obtained with 1 M NaCl draw also show that the module water flux appeared to be improving as it was run longer. A possible gradual conditioning effect of water on the membrane in the module could be occurring over time as the membrane became more hydrated and/or as the preservative in which the manufacturer stores the membrane was flushed out of the module.

Table 4-7. Baseline Water and Salt Fluxes Measured in X-TFC-MS FO Membrane Module Installed on the Bench, Integrated Test System

NaCl draw concentration [M]	Flow configuration	Water flus (J_W) [L/(m^2·h)]	Reverse NaCl flux (J_S) [mol/(m^2·h)]	J_S/J_W [g/L]
1	Concurrent	12	0.0064	0.031
1.5		17	—	—
2		17.4	0.025	0.084
3		19	0.040	0.12
1	Countercurrent	15	—	—
2		18	—	—
1 (repeat)		17	0.013	0.045

Membrane area: 2.8 m^2; Feed: DI water

Attempts were then made to operate the X-TFC-MS FO module in integrated fashion with the existing M-HF200 MD module (2.5 in. dia. × 8 in. long) installed on the bench system. However, we found that the larger flowthrough volume of the X-TFC-MS FO module made integrated operation with the existing MD module not practical because the flow rate on the MD side was now limited by the much smaller membrane area of the MD module. A larger MD membrane module (4 in. dia. × 13 in. long) was considered and fabricated by the selected MD manufacturer. In the end, unfortunately, design calculations showed that the existing bench, integrated test system was not able support the increased heat load needed to run the larger MD module to allow for integrated operation with the larger FO module.

Water Recovery (Feed Concentration) Tests on FO Module. FO-only tests were also done on the bench, integrated test system to determine the maximum TDS (total dissolved solids) concentration to which the X-TFC-MS module could concentrate wastewater feeds. This maximum achievable concentration is of particular interest for high-TDS feeds because the advantage of the FO-MD technology is perceived to be the treatment of high- to very-high TDS wastewaters that are either too challenging or impossible for RO to handle. As a baseline laboratory-scale comparison, an analogous test was conducted on a X-TFC membrane coupon on the FO water test-bed system. Three feed concentration (water recovery) tests were conducted:

1. Synthetic feed containing high TDS concentration of ~78,000 ppm as NaCl on an X-TFC FO membrane coupon (area ~ 140 cm^2) in the water test-bed system

2. Synthetic feed having high TDS concentration of ~57,620 ppm as NaCl on the X-TFC-MS FO membrane module (area ~ 2.8 m^2) installed on the bench, integrated FO-MD test system

3. Real RO concentrate (reject or brine) containing TDS content of ~12,960 ppm on the X-TFC-MS FO membrane module (area ~ 2.8 m^2). [The brine sample was sourced from the oil and gas production facility Site 2.]

The first test with synthetic 78,000 ppm NaCl feed utilized a 5 M NaCl draw solution, and concentration of this feed was achieved semi-continuously over a cumulative time on-stream of 30 h. The test with synthetic 57,620 ppm NaCl feed had a total continuous time on-stream of 6.6 h and used a 4 M NaCl draw. Likewise, a 4 M NaCl draw was used for the RO brine test, which had a continuous total run time of 80 min. In all tests, as more and more water permeated the FO membrane with time, the feed-side concentration gradually increased. This was accompanied by a gradual decease in FO water flux with time because of the reduction in osmotic driving force due to the increasing feed-side TDS content and the dilution of the draw solution with permeated water. The feed-concentration performance results obtained in the three tests are presented in Table 4-8.

Table 4-8. Degree of Feed-Side Concentration and Water Flux Measured Experimentally on X-TFC FO Membrane with Synthetic High-TDS Solutions and Real RO Concentrate as Feeds

X-TFC membrane	NaCl draw solution concentration	Feed TDS [ppm]		Water flux [L/(m^2·h)]		VRF[b]
		Initial	Final[a]	Initial	Final	
Coupon (140 cm^2 area)	5 M	78,000 (as NaCl)	262,750	12	1.3-1.5	3.3
Spiral-wound module (2.8 m^2)	4 M	57,620 (as NaCl)	202,250	10-11	2.7	4.1
		12,960 (real RO brine from Site 2)	60,350	17	12	5.1

[a] Determined experimentally on feed sample collected at the end of the test runs.

[b] VRF ≡ Volume reduction factor on feed side.

As shown in Table 4-8, the FO process could concentrate the FO feed up to TDS concentrations well above 200,000 ppm, which is at least 2.5 times higher than the TDS level to which RO can achieve. The apparent water recovery achieved with the degrees of feed-side concentration in Table 4-8 ranged from 70-78.5%, and the volume reduction factor for the feeds in the tests varied from 3-5. These levels of feed-side concentration and water recovery are particularly good for a membrane-based process treating high-TDS feeds and can only be achieved in the FO process if draw solutions of high enough osmotic potential are used to keep clean water permeating the membrane. As shown in Table 4-8, the water flux measured in the tests with high-TDS feeds declined by a factor of 4-8 relative to the initial flux, depending on the draw-solution strength used.

Integrated FO-MD Prototype Operation

The TDS of raw wastewater that came from the oil production site was about 14,000 ppm, and the target feed TDS to the prototype was varied from 30,000 to 180,000 ppm. To reach these target TDS values, the

raw wastewater was initially concentrated by operating the FO-MD system in once-through mode until the desired test condition TDS value was reached. The FO-MD system operation was then changed to recirculation mode to test the FO-MD system performance at that specific operating condition. The FO-MD system was operated continuously for more than 4 weeks to test the feasibility of long-term operation. The FO membrane fouling was assessed by monitoring the FO feed water flux change. An additional test using $MgCl_2$ as draw solution instead of NaCl was performed.

Preliminary Pre-concentration Test

Shipments of two 275-gallon totes filled with industrial wastewater (i.e., RO brine) from Site 2, an oil and gas production company in California, were delivered to the test site to be used as feed for the integrated FO-MD prototype testing. The first shipment arrived on July 12, 2016; the second shipment was received on September 27, 2016. A third shipment of wastewater was also delivered on October 13, 2016.

Operation of the integrated FO-MD prototype with the first shipment of wastewater feed was conducted in FO-MD once-through operation mode to first pre-concentrate this feed by a factor of 2, and the first pre-concentration test results are shown in Table 4-9, Figure 4-62, and Figure 4-63. An aqueous ~1 M NaCl solution was first used as the FO draw solution. The MD feed temperature was set to 45 °C. A trial-and-error approach, combined with observation of system behavior trends, was taken to determine the process parameters needed to balance the FO and MD processes to achieve a pseudo-steady state for prototype operation.

Table 4-9. Initial Process Water-Quality Properties Measured during Integrated FO-MD Prototype Operation to Pre-concentrate and Double TDS Content of Raw Wastewater Feed

Process sample	pH	Conductivity (mS/cm)	TDS (ppm)	COD (ppm)	TOC (ppm)
Bulk (raw) feed	11.41	16.9	12,400	2,265	855
Concentrated feed	10.95	40.3	27,700	3,835	1,130
FO draw solution	10.48	87.5	58,000	N/A*	18
MD product water	9.72	0.29	100	27	9.4

*COD could not be measured because of interference from the sample's high TDS content.

As an initial check of prototype performance, 'grab' samples for water-quality analysis were collected from four process tank locations: bulk (raw) feed, concentrated feed, FO draw solution, and MD product water. The physical water-quality properties were measured in-house at the test site on these samples and results are presented in Figure 4-62. With the 1 M NaCl draw solution, the FO-MD prototype successfully pre-concentrated the bulk feed by a factor of 2.2, as indicated by the feed TDS increasing from 12,400 to 27,700 ppm. The product water generated in this test run by the prototype also had low TDS of ~100 ppm, which is below the EPA drinking water limit of 500 ppm. Thus, under the given testing conditions, the FO-MD prototype achieved a TDS rejection of roughly 99.2%. Additionally, a comparison of COD and TOC values in the feed and product water showed that the prototype had an apparent rejection of

>98% for organic compounds in this wastewater. Furthermore, though less alkaline than the feed, the product water was still alkaline (pH ~ 9.7), indicating that one or more basic compounds in the wastewater were passing through the FO and MD membranes.

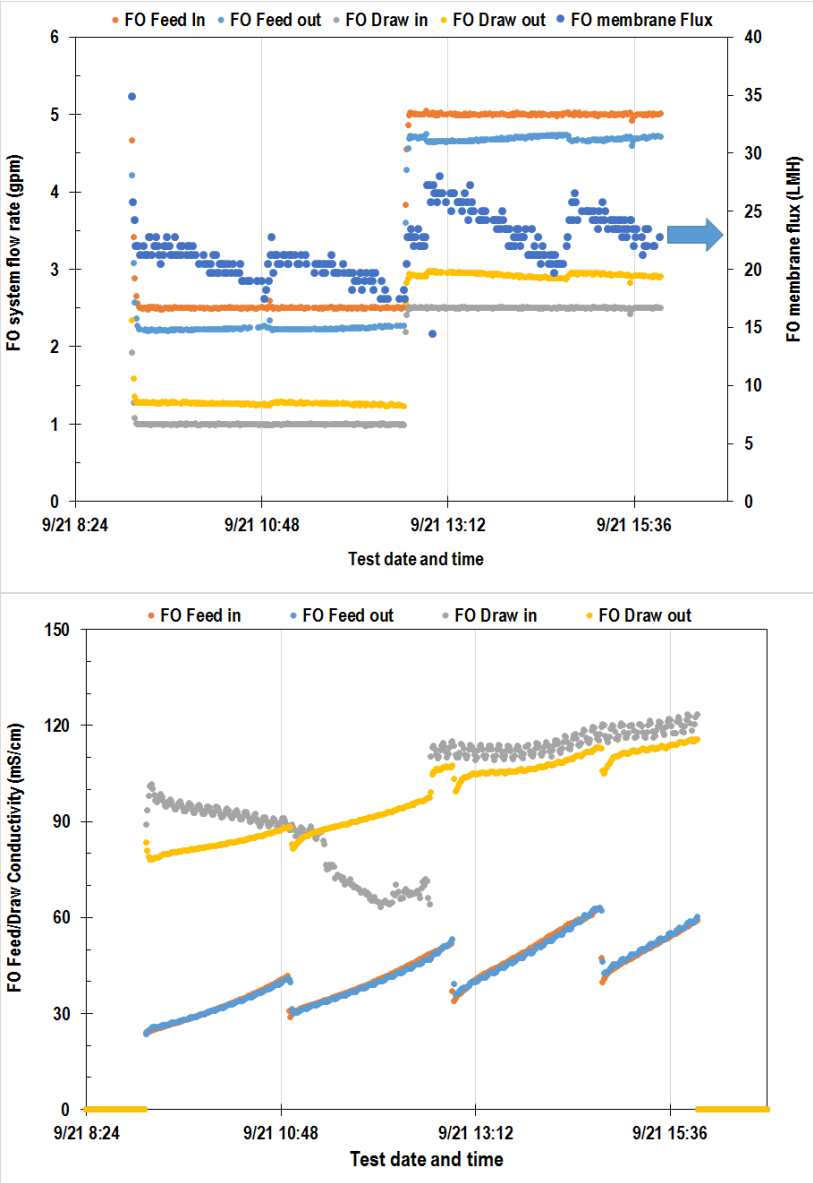

Figure 4-62. FO system pre-concentration test operating data.

Near the end of the 30,000 ppm test phase, the FO draw-solution strength was raised from 1 M to 2 M NaCl solution, and testing was resumed. The higher draw strength increased the driving force for water permeation across the FO membrane and was expected to accelerate the pre-concentration of the wastewater feed to the next-higher 80,000 ppm TDS target. However, the effective draw solution strength decreased to only 1.6-1.7 M because the draw solution tank contents became diluted by the large hold-up volume of process water in the prototype lines during system operation. To balance the increased amount of water permeating the FO subsystem, the MD feed-temperature set point was increased to 55 °C. For

this test run, wastewater samples from all process-stream sampling points on the prototype were collected and shipped to an environmental testing laboratory for a comprehensive water-quality analysis. The analysis results on the samples are discussed below.

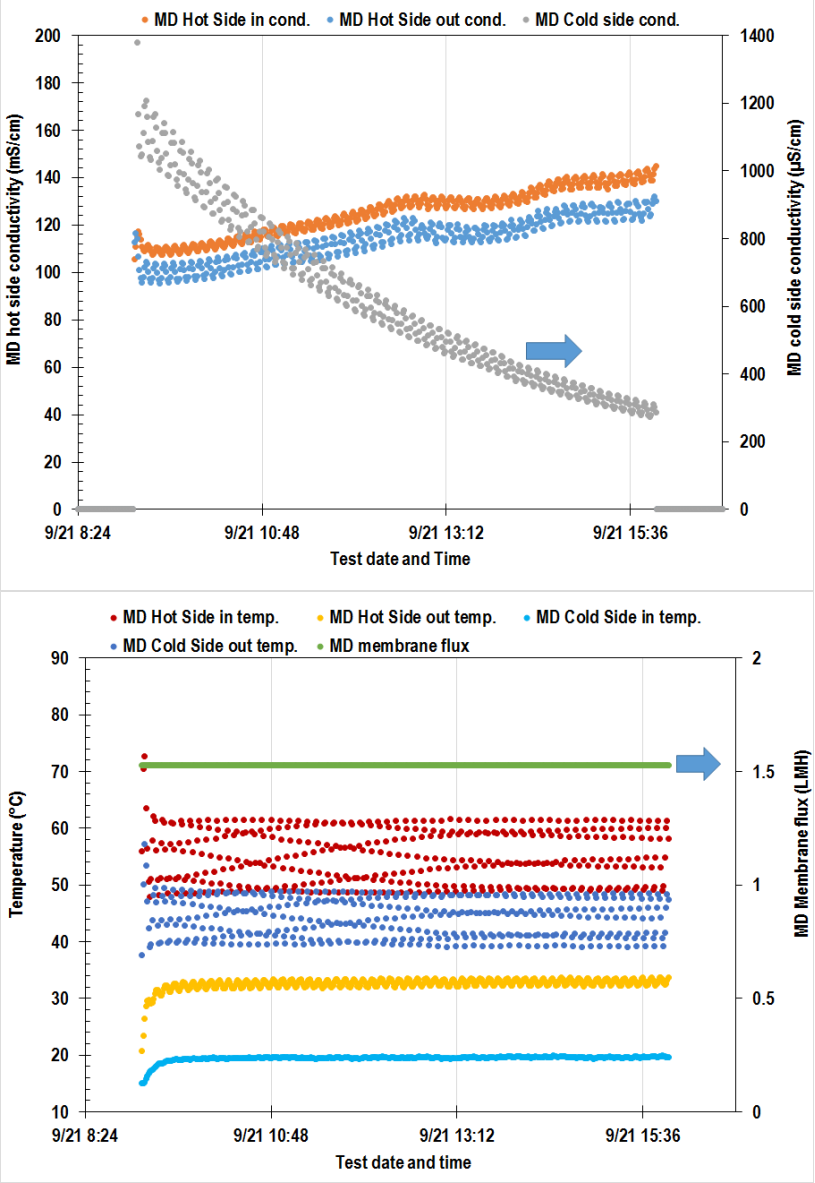

Figure 4-63. MD system pre-concentration test operation data

Prototype Operation at Different Feed TDS Levels

At the beginning, the prototype testing focused on pre-concentrating the industrial wastewater feed of RO brine from Site 2, an oil and gas production company in California, from the starting bulk TDS of 13,000-15,000 ppm to increasingly higher feed TDS levels. At each higher feed TDS concentration target reached, the FO-MD prototype was then run from several days up to a week in order to collect short-term process performance data. During this feed pre-concentration period, the FO draw-solution strength was gradually increased as needed to higher NaCl solution concentrations: from 1.5 M to 2 M to 3 M and

finally to 4.5-5 M. Increasing the draw-solution salt concentration was necessary to increase and/or maintain the driving force for water permeation across the FO membrane to maintain a practical FO water flux at each higher feed TDS levels. The objective of the step-wise pre-concentration and operation approach was to challenge the FO and MD membranes in the integrated FO-MD unit and gauge their process operational limits.

57,000 ppm Feed TDS Level

After the preliminary pre-concentrating test, the first higher feed TDS pre-concentration targeted was 30,000 ppm. In practice, the effective pre-concentrated feed TDS level achieved and used for continuous operation varied from 47,000 to 67,000 ppm (average 57,000ppm), representing a feed pre-concentration factor of 3-5. The molarity of the draw solution used was 1.6-2 M NaCl.

During operation, the MD hot-feed temperature set point was slowly decreased from 55 °C to 45 °C and then finally to 40 °C. The temperature reduction was done to balance the overall integrated FO-MD system operation. Because the FO water production rate was lower than the MD production rate under the given process conditions used, the MD hot-feed temperature was lowered to slow down the MD water permeation rate and maintain adequate working fluid level in the MD feed tank. As shown in Figure 4-64, during this campaign, the prototype's water production rate (the production rate of FO system, which is the same as the MD production rate) was slowed down from 215 gal/day (0.15 gal/min) at the 55 °C MD feed temperature to 130 gal/day (0.09 gal/min) at 45 °C and then to ~100 gal/day (0.07 gal/min) at 40 °C. The measured conductivity of the clean water produced by the prototype is presented in Figure 4-65 and was very low (~50 µS/cm), indicating high TDS removal performance of the MD membrane.

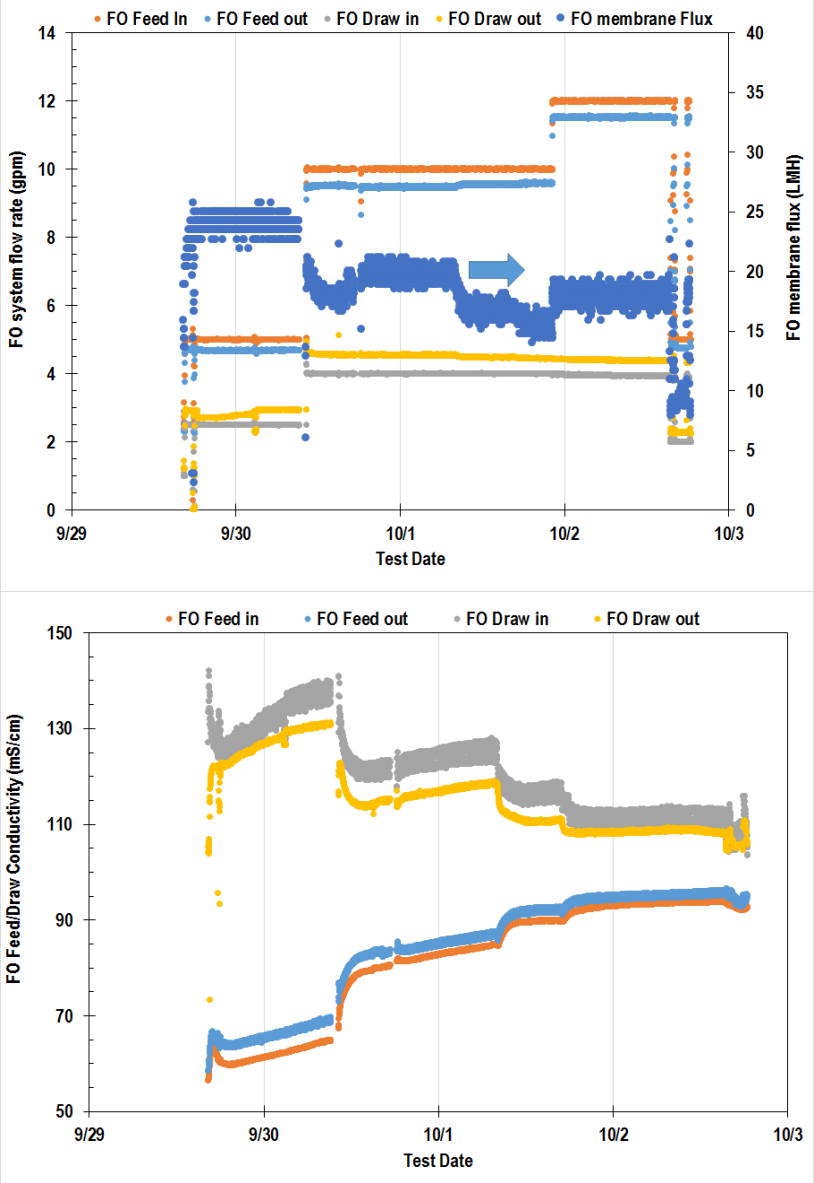

Figure 4-64. FO system operating data at feed TDS level of 57,000 ppm.

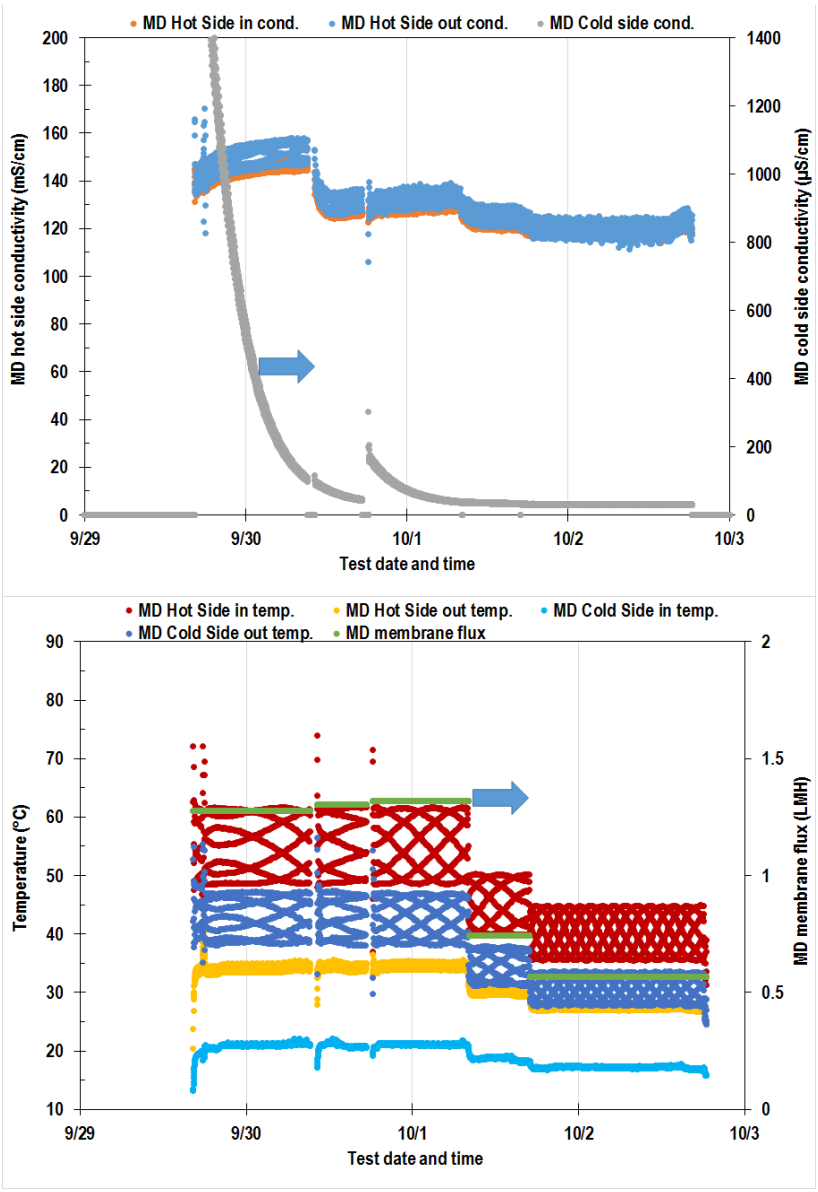

Figure 4-65. MD system operating data at feed TDS level of 57,000 ppm.

During this first test campaign, the FO-MD prototype achieved an apparent TDS rejection of roughly 99.6%. From a comparison of COD and TOC in the feed and product water streams, the prototype had an apparent 99.2-99.5% rejection of organic compounds in the wastewater feed treated. Though less alkaline than the feed (pH ~ 10.8-11.3), the product water was still alkaline with pH 9.4-9.7, indicating that some basic compounds in the wastewater were passing through both FO and MD membranes.

86,000 ppm Feed TDS Level

The level of pre-concentrated feed TDS targeted was 80,000 ppm. During prototype testing, the effective higher feed TDS concentration fluctuated between 82,000 and 90,000 ppm, which corresponded to a feed pre-concentration factor of roughly 5.5-7. The effective strength of the draw solution used in this test run was 2.5-2.6 M NaCl. This draw strength was lower than the prepared draw-solution molarity of 3 M NaCl

used because of subsequent dilution by the large hold-up volume of process water in the system lines during operation.

To balance the overall integrated FO-MD system operation, the MD hot-feed temperature setpoint was decreased from 50 to 40 °C when the FO water production rate fell below the MD production rate. The cooler MD feed temperature was utilized as a process 'lever' to slow down the MD water permeation rate and thereby maintain adequate working fluid level in the MD feed tank. Figure 4-66 shows that the prototype's water production rate was quite stable at about 137 gal/day (0.095 gal/min) in this test run. Steady-state conductivity of the resulting product water was measured to be low at 45-150 µS/cm, as shown in Figure 4-67. Apparent TDS rejection was roughly 99.7%, and apparent COD and TOC rejection was ~99.2%. The product water had pH 9.7-9.9, relative to the feed pH of 10.4-10.7.

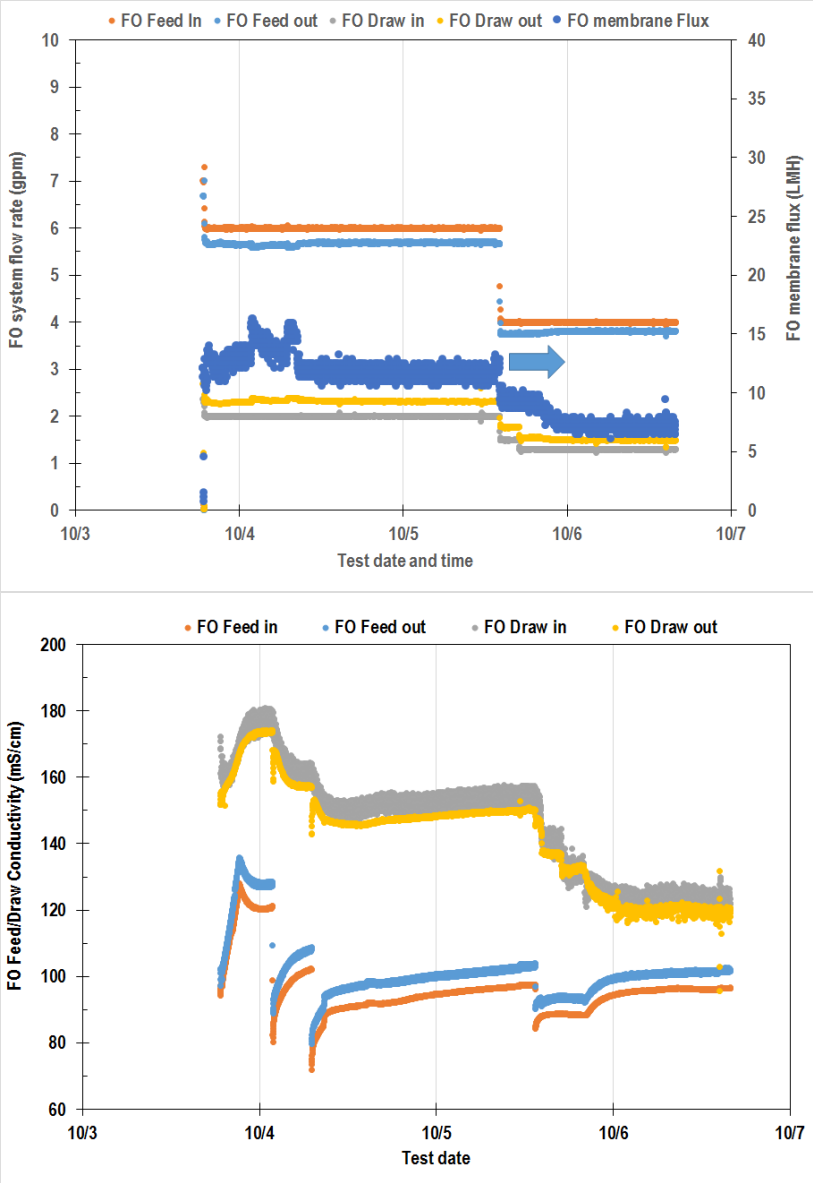

Figure 4-66. FO system operating data feed TDS level of 86,000 ppm.

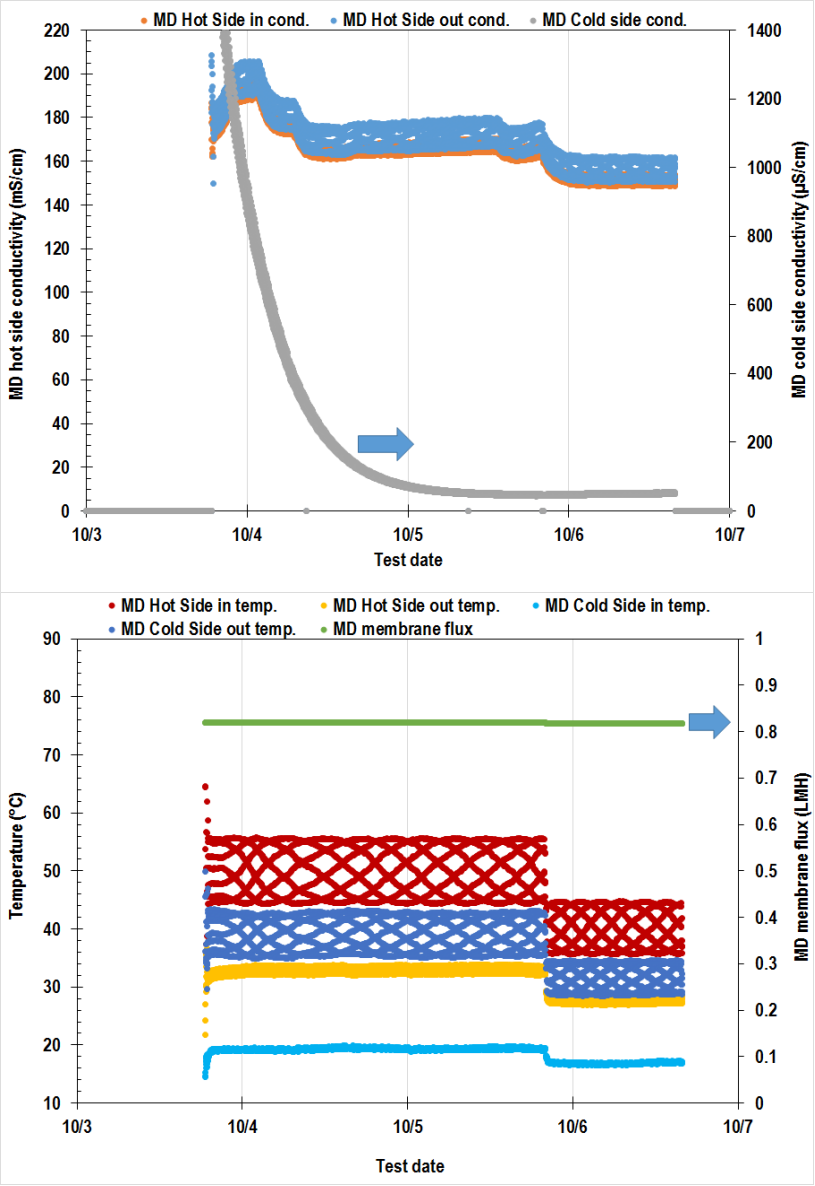

Figure 4-67. Low conductivity (gray data) of the product water from the integrated FO-MD prototype during operation with industrial feed pre-concentrated to feed-TDS level of 86,000 ppm.

190,500 ppm Feed TDS Level

The highest pre-concentrated feed TDS level targeted was 180,000 ppm. The actual feed TDS concentration during prototype operation varied between 177,000 and 204,000 ppm (average 190,500 ppm), resulting in a 13- to 16-fold feed pre-concentration factor. The FO draw solution prepared for this test run was 4.5-5 M NaCl. However, again due to dilution by the large hold-up volume of process water in the system lines, the actual draw strength in operation decreased to 4.2 M initially and then to 3.4-3.7 M in the later stages of this test run. By maintaining the high draw-solution concentration,

a practical FO water flux throughout this very high feed-TDS test run was challenging because of how quickly dilution of the draw solution occurred over time.

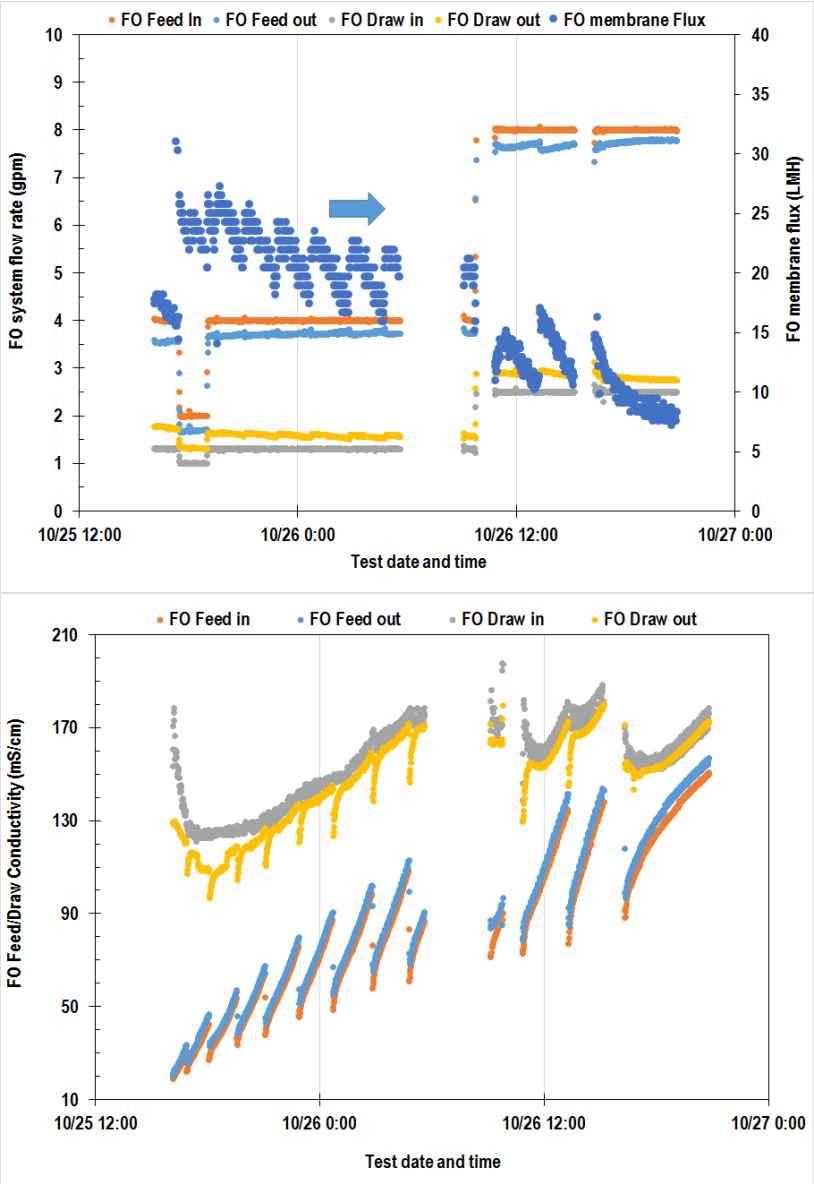

Figure 4-68. FO system operating data to concentrate feed TDS level up to 190,500 ppm.

For this test campaign, the FO water flux was low due to fouled membranes, as the FO membrane elements had been in operation with the industrial wastewater feed for 4-5 weeks. The FO membranes were replaced with new ones after the first couple of days of raw-feed pre-concentration in case the low flux was due to fouled membranes. However, the water flux of the new FO membranes with the 177,000-204,000 ppm TDS feed was still similarly low, suggesting that low osmotic-pressure driving force, rather than membrane fouling, was the likely cause of the low FO water flux. Furthermore, one of the used FO membrane elements removed from the system was sent for membrane autopsy (foulant analysis) to a third-party membrane diagnostic laboratory. The autopsy results on this used FO membrane

are discussed later in this section. The results of the pre-concentration period are shown in Figure 4-68 and Figure 4-69. Three FO membranes and two MD membranes were used in this test. FO feed and draw flow rates were 9 and 3 gpm and increased to 12 and 3.9 gpm, respectively. MD hot and cold side flow rate were both 12 gpm, and hot side temperature was changed from 50–35 °C.

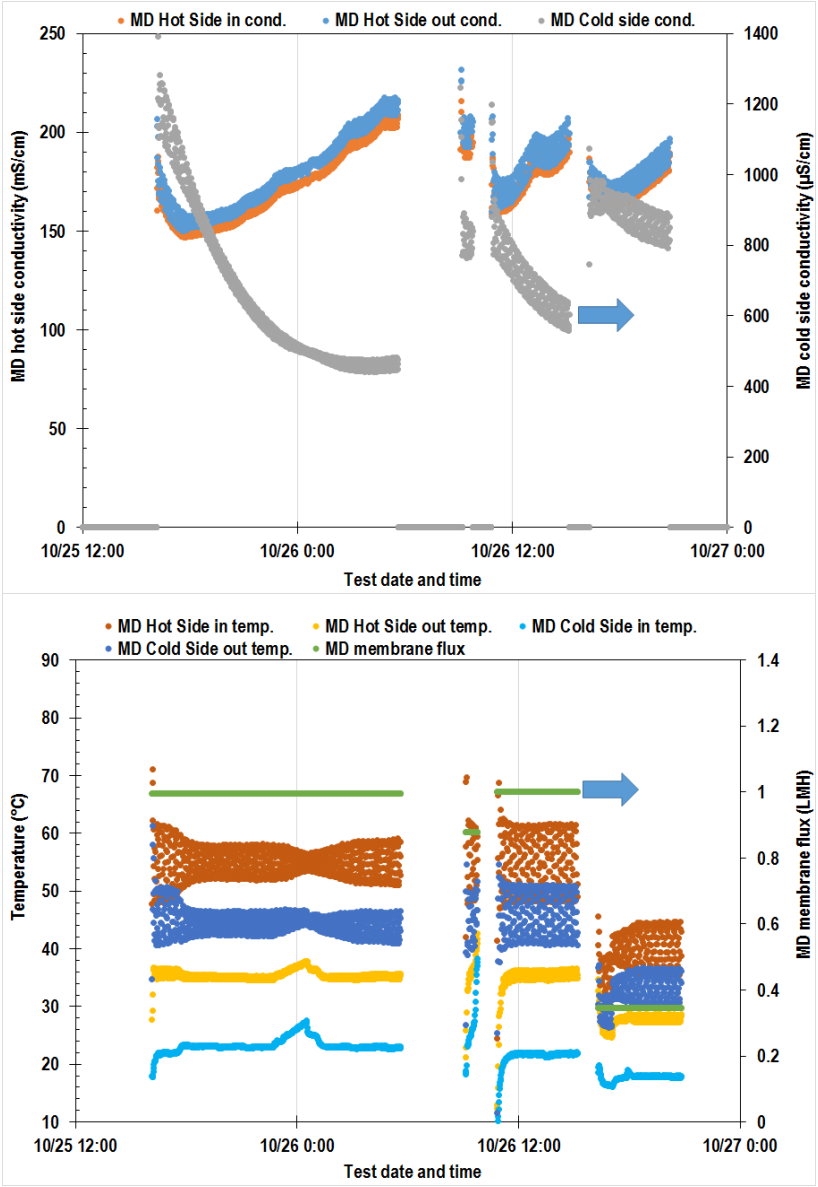

Figure 4-69. MD system operating data to concentrate feed TDS level up to 190,500 ppm.

In this very high feed-TDS test campaign that ran for over 3 weeks, the MD feed temperature was one of several process setpoints changed multiple times to try to balance the dynamically changing system process conditions. As shown in Figure 4-70 and Figure 4-71, the MD feed temperature started at 55 °C, which yielded a water production rate of ~346 gal/day (0.24 gal/min). This temperature was then decreased

to 40 °C, reducing the water production rate to 115 gal/day (0.08 gal/min). Since the FO water flux continued to gradually decrease below the MD water flux, the MD feed temperature was reduced further to 35 °C (Figure 4-71). The water production consequently fell to ~72 gal/day (0.05 gal/min). At this point, the MD water flux started slowing down too much relative to the FO water flux. Hence, the MD feed temperature was raised back to 50 °C [water production rate ~ 144 gal/day (0.1 gal/min)].

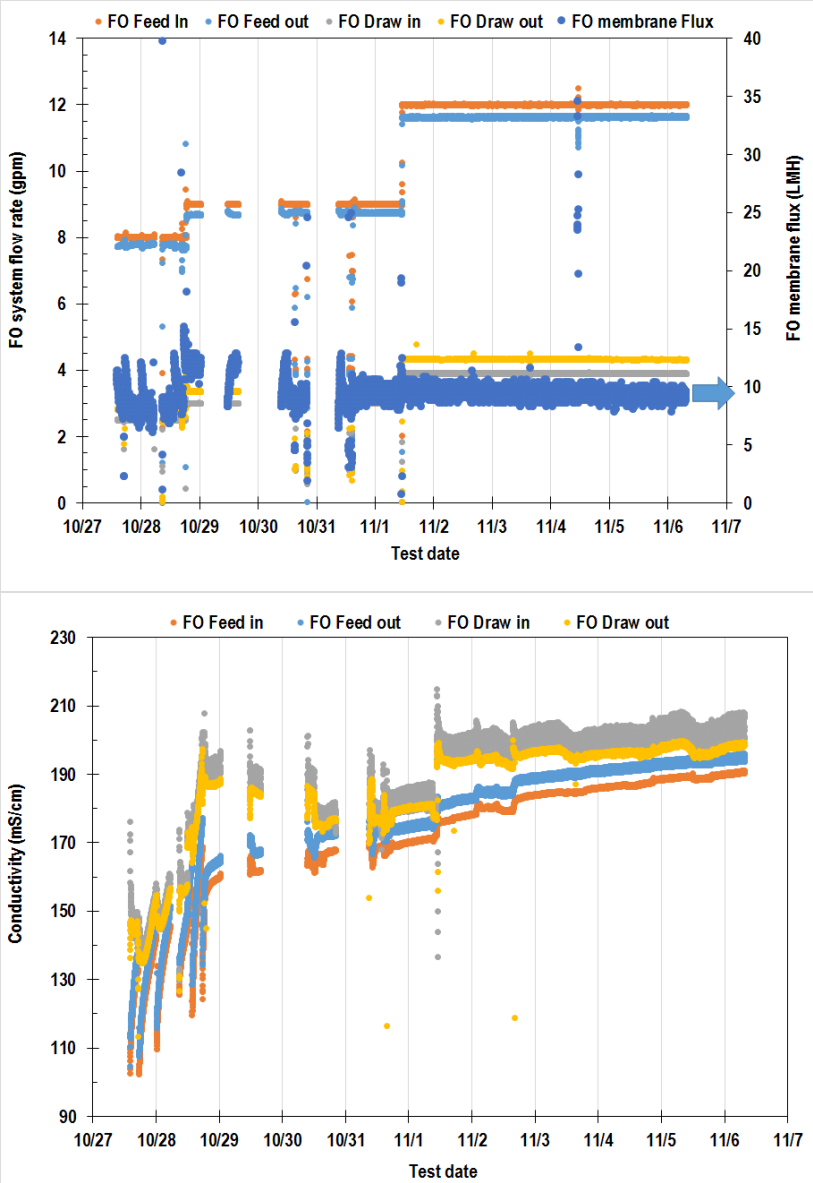

Figure 4-70. FO system operating data in recirculation mode at 190,500 ppm feed TDS level.

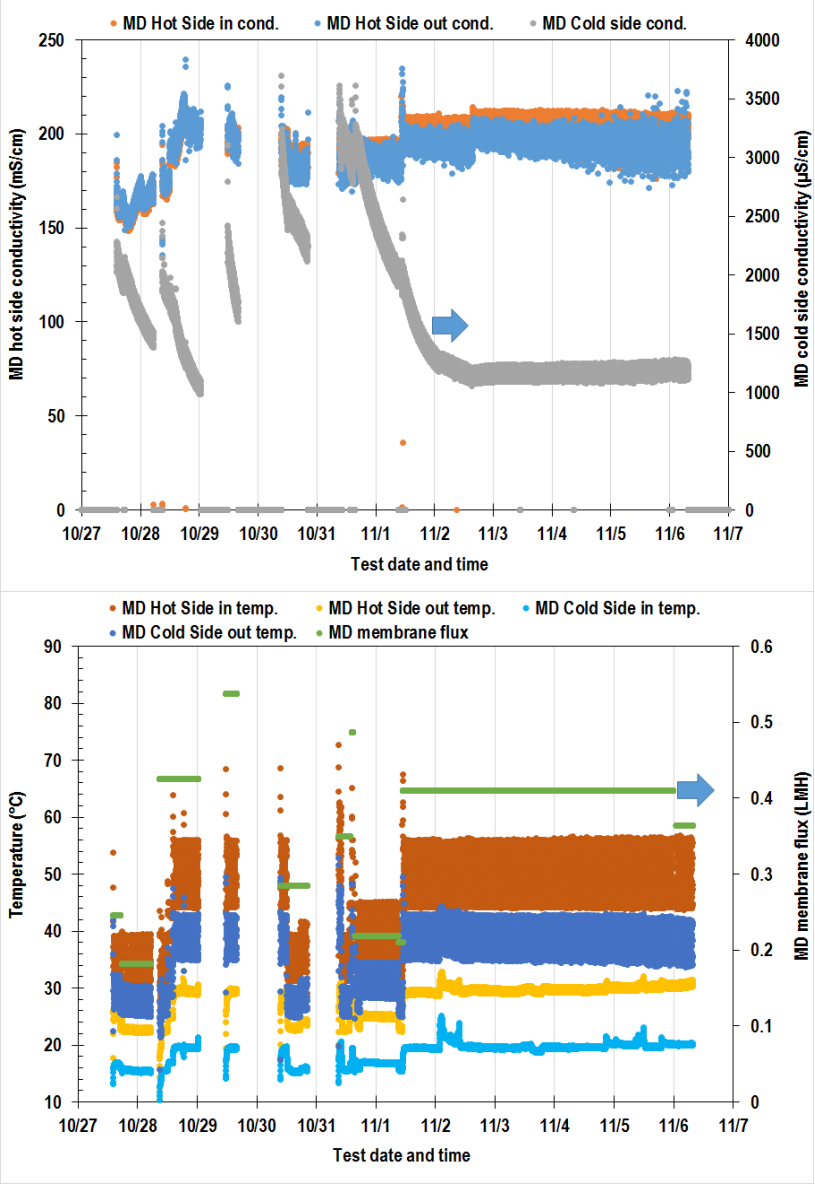

Figure 4-71. MD system operating data in recirculation mode at 190,500 ppm feed TDS level.

Figure 4-71 shows that, in this very high feed-TDS test run, the product-water conductivity was higher than that noted in previous test runs. The conductivity of the product water started at ~450 µS/cm and gradually rose to 600 µS/cm and then 800 µS/cm. After an additional 10 days of prototype operation, this conductivity continued to increase and appeared to stabilize at 1,100–1,300 µS/cm. Though the overall TDS rejection of the prototype remained at 99.6-99.7%, the conductivity increase in the product water indicated leakage of more charged species across the MD membranes, which had been in operation for more than 7 weeks by this point. This permeation of more ions across the MD membrane suggested that gradual wetting of the MD membranes may be occurring over time, possibly due to accumulation of permeated hydrocarbon organics and other low-surface-tension compounds in the FO draw tank, which was also the MD feed source. The product-water COD concentration did roughly double relative to that

measured in previous test runs, but the overall COD rejection of the prototype still seemed good at ~99.2%. Though still lower than the feed pH of 11.4–11.8, the product-water pH of 10.2-10.9 was also more alkaline in this test run than that in the earlier campaigns.

Long-Term Operation

The integrated FO-MD prototype was successfully operated up to feed TDS concentrations as high as 180,000-200,000 ppm. However, for a longer-term operational study, it was decided that an intermediately high feed-TDS level should be used to make prototype operation easier to maintain and obtain more practical water fluxes through the FO and MD process sections. A pre-concentrated feed TDS level of 130,000 ppm was selected for the long-term test run. Additionally, because of possible wetting in the MD membrane modules used thus far (as mentioned above), we switched to a new MD membrane module from the same manufacturing batch for the longer-term test run. This new MD module had not yet been exposed to any real wastewater.

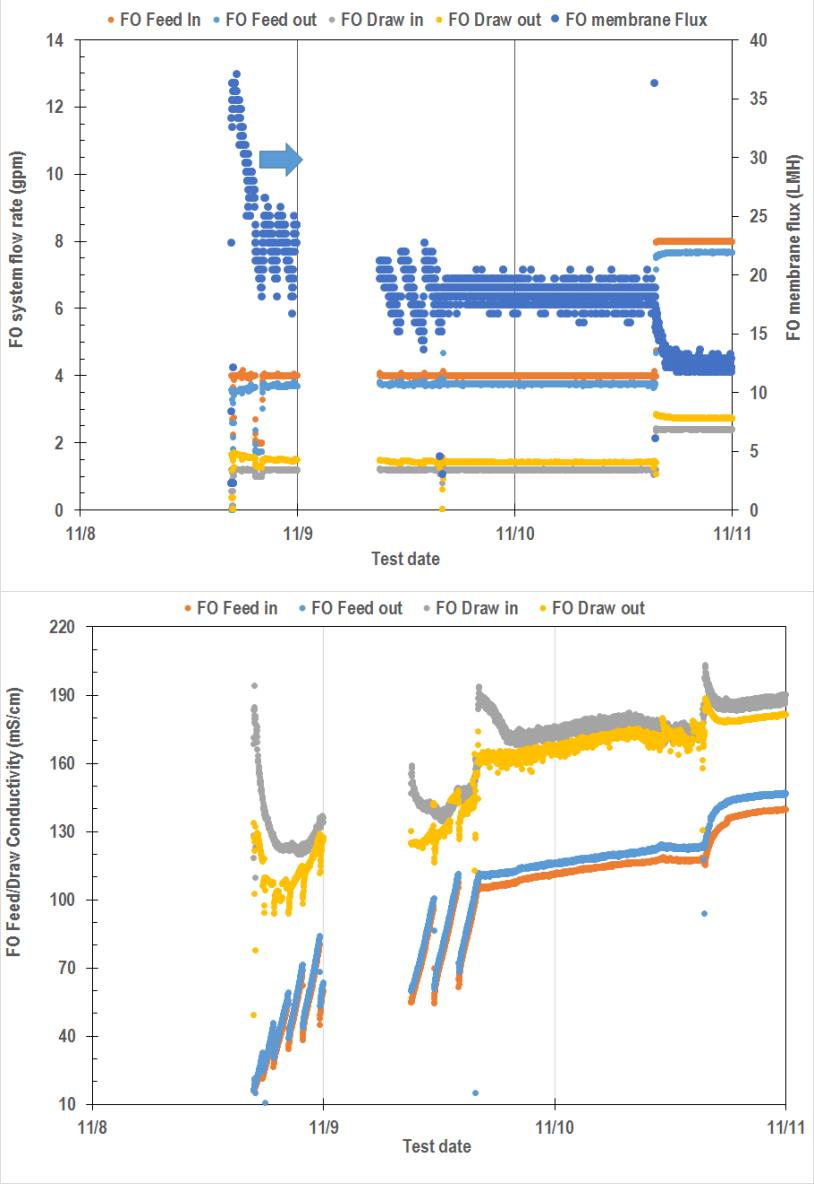

Figure 4-72. FO operating data during feed pre-concentration in preparation for long term operation.

Once-Through Operation To Concentrate FO Feed

To prepare enough of the target 130,000 ppm TDS feed, the prototype unit was run for a couple of days in the FO-MD once-through operation mode to pre-concentrate the raw industrial wastewater (Figure 4-72). A 4.5-5 M NaCl solution was prepared as the FO draw solution for this test run. However, the large hold-up volume of process water in the system lines diluted the prepared draw solution strength to ~3.5 M NaCl during much of this test campaign. For this test run, the resulting effective feed TDS concentration varied between 100,000 160,000 ppm, corresponding to a 7- to 12-fold feed pre-concentration factor.

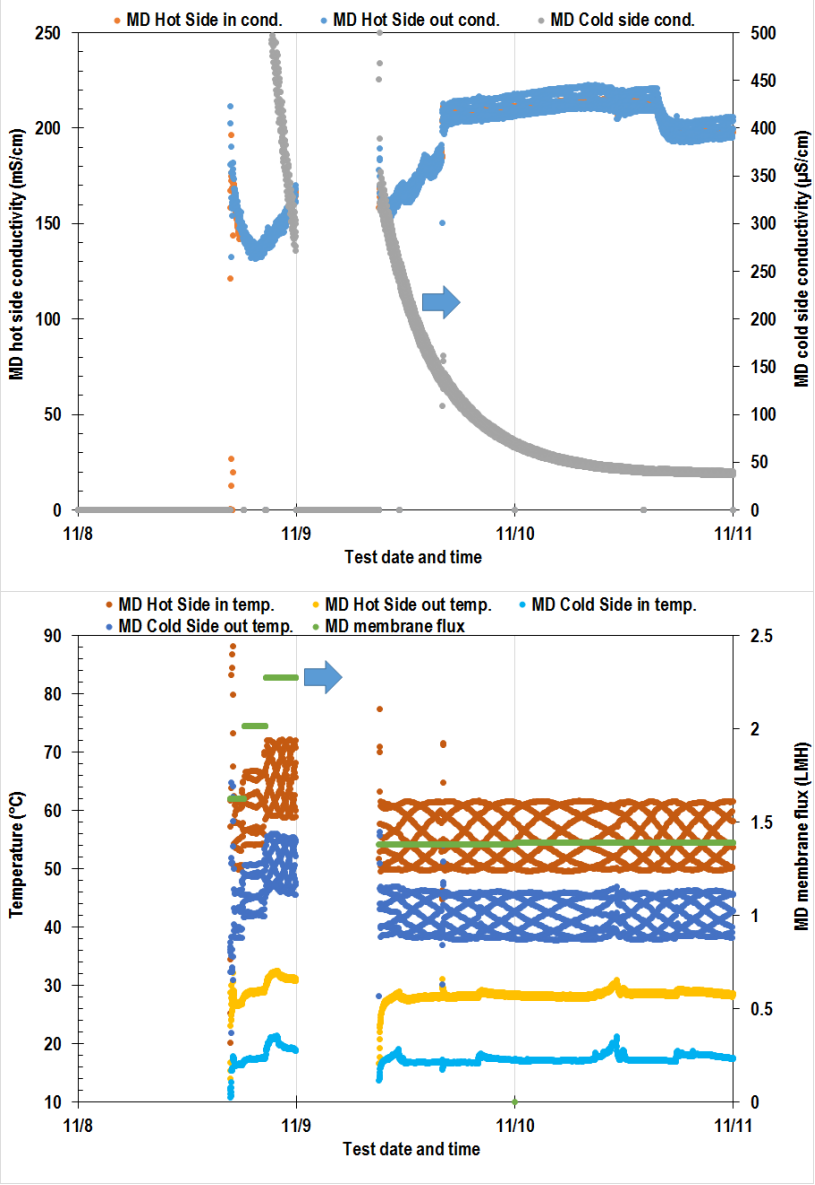

Figure 4-73. MD operating data during feed pre-concentration in preparation for long term operation.

The new MD membrane module showed much improved water quality and production flow rate of the clean water from the FO-MD prototype relative to the likely fouled MD module. At MD feed temperature of 55 °C, the water production rate in Figure 4-73 appeared stable at about 230 gal/day (0.16 gal/min). More importantly, as shown in Figure 4-73, the product-water conductivity was very low again (<40 µS/cm).

Long-Term Recirculation Mode Operation

Operation of the FO-MD prototype with the 100,000-160,000-ppm-TDS feed continued for one month. Figure 4-74 is a summary plot of the process flow rates and conditions used during this testing period. Most of the test run was conducted at 55 °C MD feed temperature. In the last week of the test, the MD

feed temperature was then more systematically changed between 55 °C and 75 °C. At 75 °C, the measured water production flow rate of the prototype was ~325 gal/day with the process conditions corresponding to this long-term test.

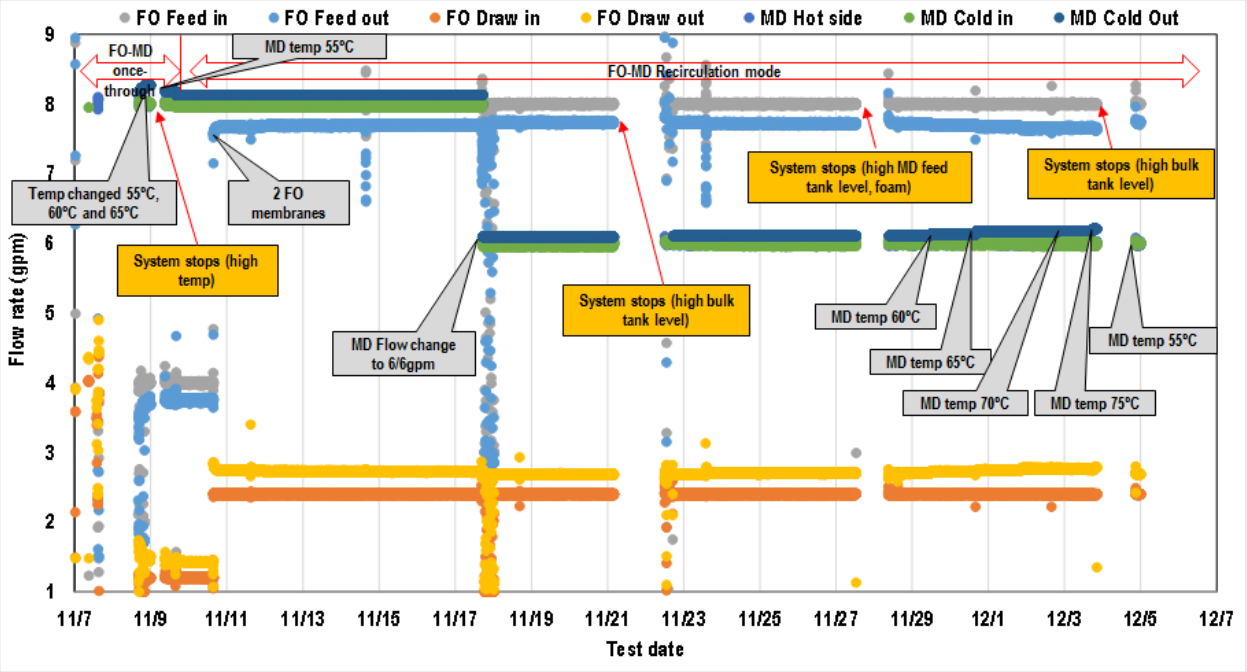

Figure 4-74. Summary plot of process flow rates and conditions during the longer-term operation of the integrated FO-MD prototype with pre concentrated industrial feed having TDS level of 100,000-160,000 ppm.

One FO membrane was used for the test, and FO feed and draw flow rates were set at 4 and 1.2 gpm, respectively, during the once-through mode where the conductivity difference was high. On November 10, 2016, to increase the FO production rate, the number of FO membranes online was increased to two, and the FO feed and draw flow rates were increased to 8 and 2.4 gpm, respectively, as well. The flow change is apparent in Figure 4-75, which presents FO feed and draw-solution flow rates and FO membrane flux during the long-term test period. The FO membrane flux was as high as 37 LMH at the start-up of concentrating and decreased to 8.7–11.4 LMH during recirculation mode. The narrow difference between the feed and draw solution conductivity (or TDS) provided a reduced osmotic driving force that resulted in this low FO membrane flux.

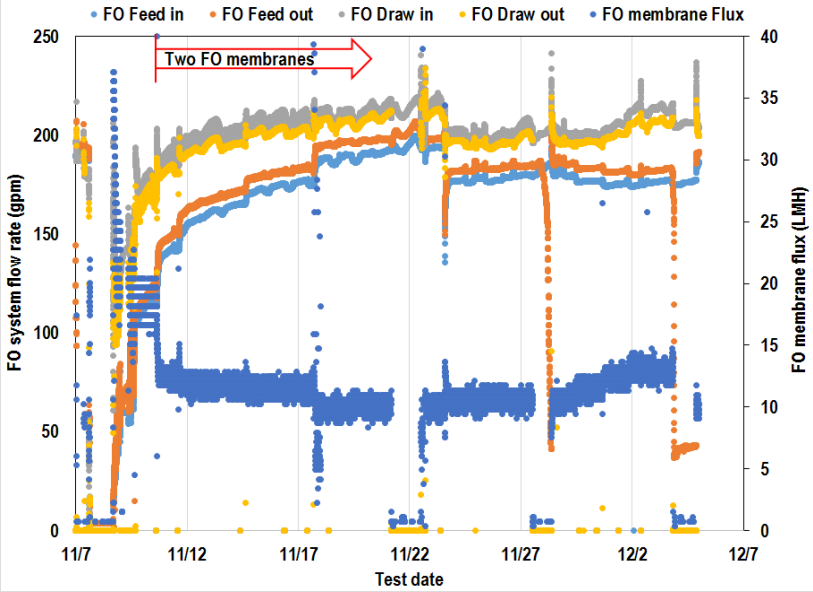

Figure 4-75. FO system operating result for long term operation test

One MD membrane module was used for the long-term test, and both the MD hot side and MD cold side flow was set at 8 gpm. The MD flux was also as high as 2.3 LMH at the start-up and decreased to 1.3–1.8 LMH when the MD hot side temperature was decreased. The MD system operating results, including MD temperature profiles, MD membrane flux, and conductivities, are shown in Figure 4-76. The MD membrane flux values are shown in both graphs to compare the effect of conductivity and temperature. The effect of conductivity on the MD membrane flux was not significant under the range of test conditions evaluated. The MD membrane flow rate drop on November 17, 2016 (Figure 4-74) decreased the flux significantly, which shows that flow rate is a major driver of flux for the MD system.

The high MD membrane flux at start-up was mainly attributed to the high temperature of MD hot side during once-through mode as seen in Figure 4-76. After the hot side temperature was stabilized during the recirculation mode, the MD hot side temperature was increased to show high MD membrane flux again. However, the MD flux was still lower than the MD flux at the start-up. The FO hot side temperature was 80 °C at start-up in the once-through mode, but the temperature could not be increased above 70 °C in the recirculation mode to protect the FO membrane because the FO membrane temperature limit is 45 °C and the residual temperature from the MD increased the FO draw feed temperature. The MD membrane exhibited wetting due to frequent stopping. The MD membrane wetting increased the MD cold side conductivity. There were two stops during the operation run and the MD cold side conductivity increased sharply for each of these events. After these two stops, the MD membrane wetting tendency was increased and the MD cold side conductivity was increased from 36 to 104µS/cm and the MD flux was lowered as well.

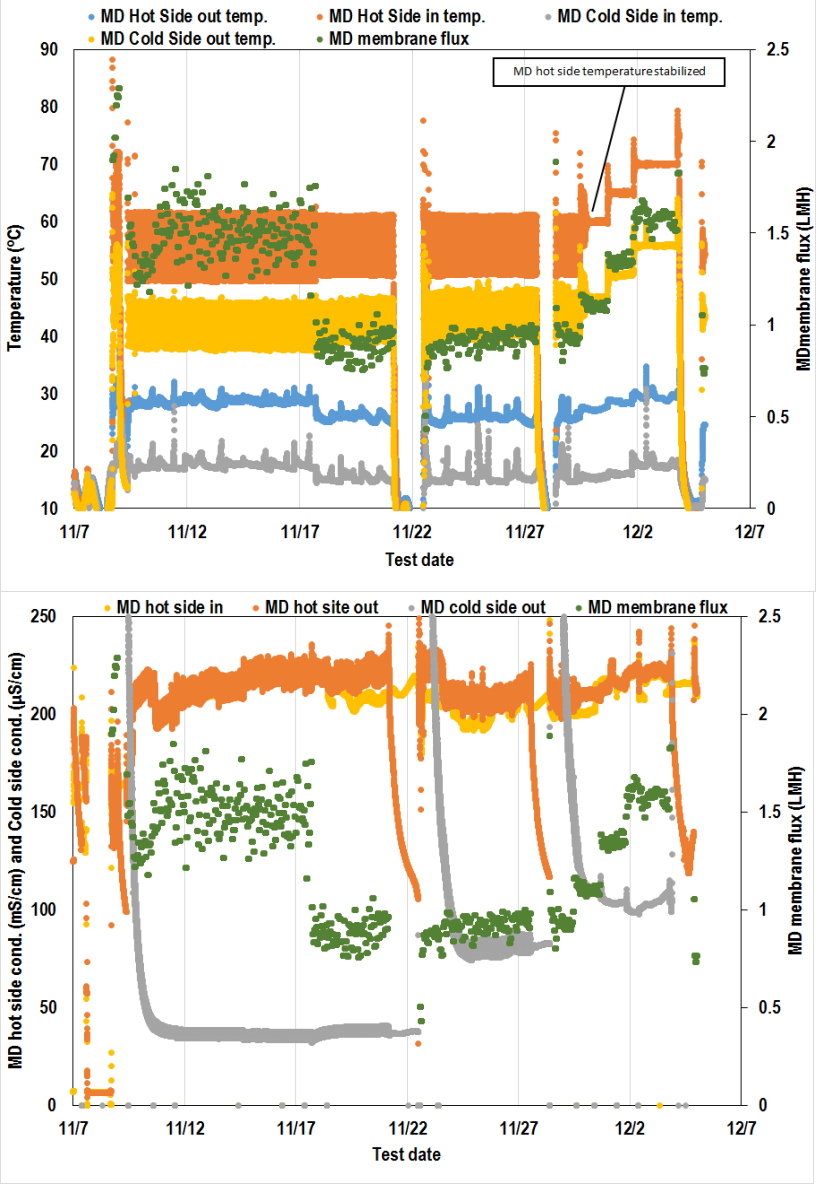

Figure 4-76. MD system operating results for long-term operation test.

A power meter was installed before the long term operation, the electricity consumption of FO-MD system was monitored during the operation period. The cooling water was supplied from the building beside the trailer so the electricity used for cooling was not included in the power consumption data. The data was processed to show the specific power consumption per produced water volume (kWh/m^3) and is presented in Figure 4-77. The change of recirculation flow rate of FO and MD membrane changed the overall power consumption but changes in MD system showed higher effect on the power consumption. The flow rate reduction increased the specific power consumption because the flow rate reduction lower the power consumption and production rate at the same time. An increase of MD hot side temperature from 65ºC to 75ºC reduced the specific power consumption by improving the MD production rate.

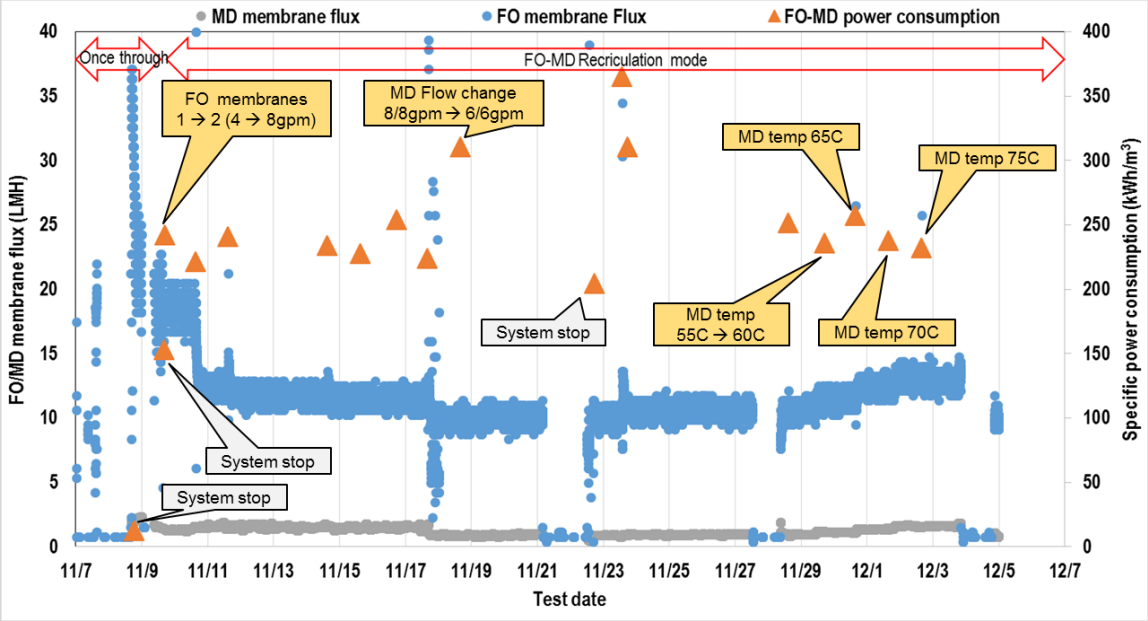

Figure 4-77. Power consumption during long term operation

Fouling Comparison and Divalent Draw Salt

FO Membrane Fouling Analysis

Membrane fouling can be quantified by monitoring pressure drop in the membrane system long-term operation or via membrane autopsy. During the test period, the FO membrane pressure drop was monitored in order to quantify the FO membrane fouling tendency but the pressure drop (and apparent operational timeframe) was too small to quantity any FO membrane fouling using this method. It was decided to repeat the FO concentrating operation to compare the FO flux with that observed during the initial concentration to that observed after the long-term operation (a month). The same conditions as the once through mode in the long-term operation (Figure 4-72) were used for this test. The FO membrane flux and conductivity results are shown in Figure 4-77. The operating conditions were similar those used on November 9, 2016, in Figure 4-72, but the flux in this test was slightly higher even after one month operation. This comparative test indicates that the FO fouling was not significant, which is a somewhat remarkable observation given that the wastewater tested was the reject from an RO plant because it was determined that it was too difficult to concentrate any further. Despite the fact that both FO and RO utilize a similar rejection mechanism at the membrane interface, the operation of the FO system was able to achieve significant additional water recovery for this wastewater.

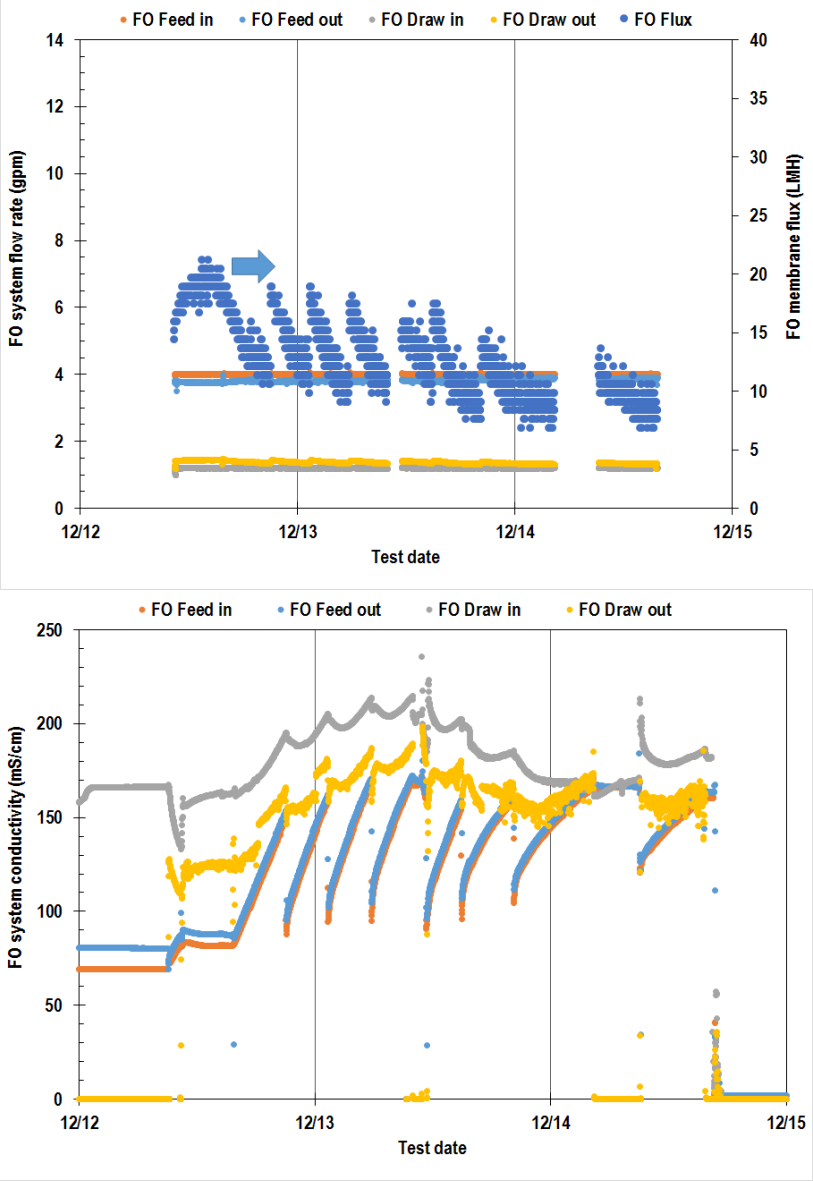

Figure 4-78. FO fouling test

Divalent Draw Salt

Before concluding operation of the integrated FO-MD prototype, the unit was run for about 6 days with ~3 M $MgCl_2$ solution as the FO draw solution. The objective of this study was to obtain process performance data for comparison to that collected with NaCl draw salt. We were primarily interested in the effect of the larger divalent Mg^{2+} cation on the reverse draw-salt flux across the FO membrane. Preliminary observations indicated that $MgCl_2$ draw caused scaling in the prototype under the given high operating pH condition. The results for this test run are shown in Figure 4-78 and Figure 4-79. The 3 M $MgCl_2$ solution was prepared as a draw solution, and one FO membrane and one MD membrane were used. The FO feed and draw flow rates were 4 and 2gpm, respectively, and was changed to 6 and 1.8gpm on December 16, 2016. The MD hot and cold side flow rates were set to 6 gpm. The MD hot side

temperature was set to 50 C. The MD hot side out temperature was maintained at 37 °C, and MD cold side in and out temperatures were maintained at 16 and 27 °C, respectively, until December 17, 2016.

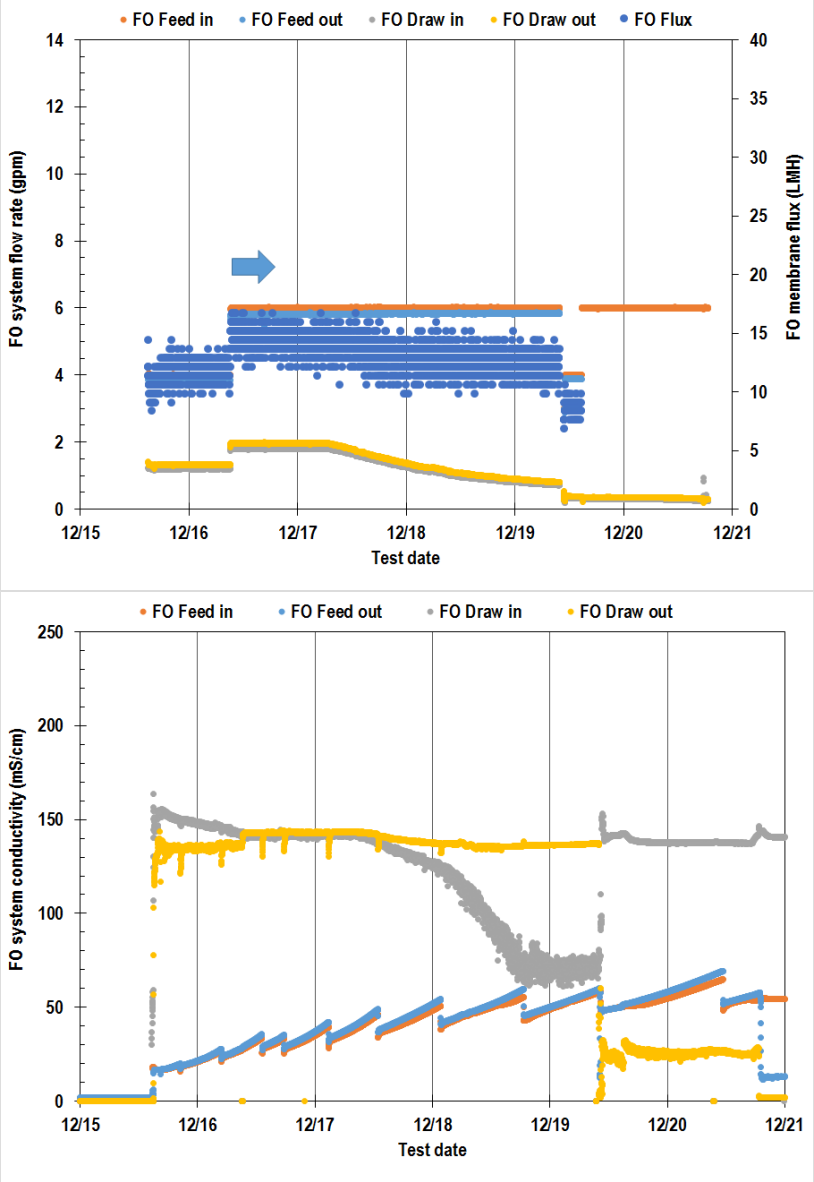

Figure 4-79. FO test result with $MgCl_2$ draw solution.

The FO feed flow increase (4 to 6 gpm) enhanced the FO membrane flux from 10–14 to 13–17 LMH. The FO membrane flux decreased during the operation period due to scaling on the membrane surface. The high feed pH (>11) increases the likelihood of precipitation when the FO feed contacts the FO draw solution because the divalent Mg^{+} ion is prone to precipitation (e.g., $MgSO_4(s)$). This test did not evaluate the effect of pH adjustment of the FO feed to prevent scaling, which would help prevent the high pH transfer from the feed to the draw. The precipitation decreased the FO draw solution conductivity, which reduced the available driving force of the draw solution.

A cartridge filter was installed in the MD hot side line to filter the magnesium precipitate and prevent fouling of the MD membrane. The differential pressure of the cartridge filter increased sharply, which lowered the MD hot side water flow rate significantly, as evident in Figure 4-79 (December 17, 2016). The temperatures of MD hot side out and MD cold side out were also decreased due to the decrease in the flow. There was a system stop on December 19, 2016 and the MD cold side conductivity was not increased that much comparing with that of NaCl solution. This also implies that the diffusion of $MgCl_2$ through the MD membrane pores is much less than that observed for NaCl. This suggests that adjusting the FO feed pH so that $MgCl_2$ does not precipitate from solution could be a strategy to use it as the draw solution in cases where an even higher water quality is needed than that attainable with NaCl as the draw solution. The test was concluded on December 20, 2016, water samples were taken for analysis. In addition, a second used FO membrane element, one used MD membrane module, and the MD feed-side filter cartridge were sent for autopsy.

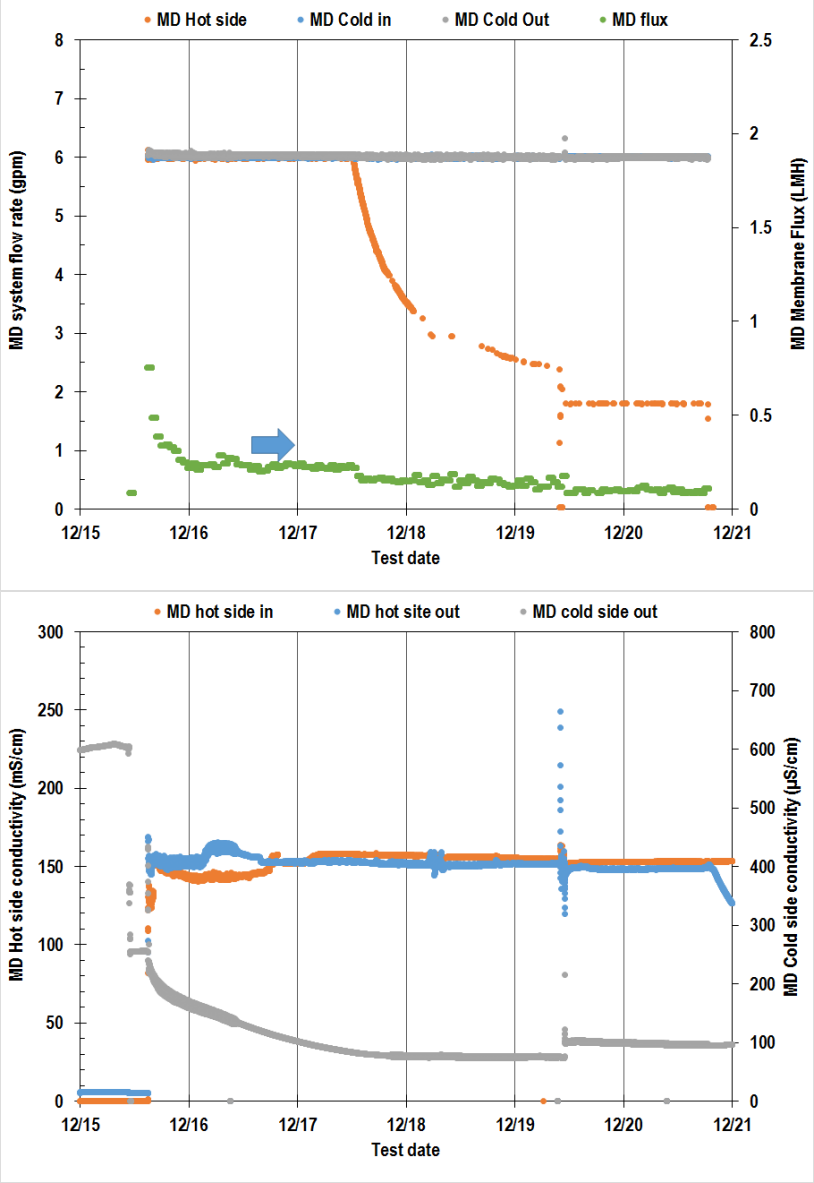

Figure 4-80. MD results with $MgCl_2$ draw solution.

Water Treatment Performance

Organics and Ammonia Removal

In addition to TDS monitoring via EC measurement, additional water quality parameters were assessed that were determined to be of interest based on the original wastewater analysis. Samples were taken from FO feed in/out, FO draw in/out, MD hot side in/out and MD cold side in/out (MD permeate) to measure TOC and ammonia. Results are shown in Figure 4-80 and Figure 4-81, for TOC and ammonia, respectively. More than 90% of the TOC was rejected by the FO membrane, therefore, the TOC in the FO feed increased during the once through mode as water was removed. Increasing contact time by recirculating all permeate to the feed during recirculation mode increased the TOC concentration in the draw solution since it accumulates over time but the MD permeate TOC showed very little TOC present during recirculation mode. When the MD system stopped, there was sharp increase in TOC on 10/31, 12/7, which is attributed to diffusion through the membrane while it was idle. The overall TOC reject for MD during operation higher than 99% for all experimental runs.

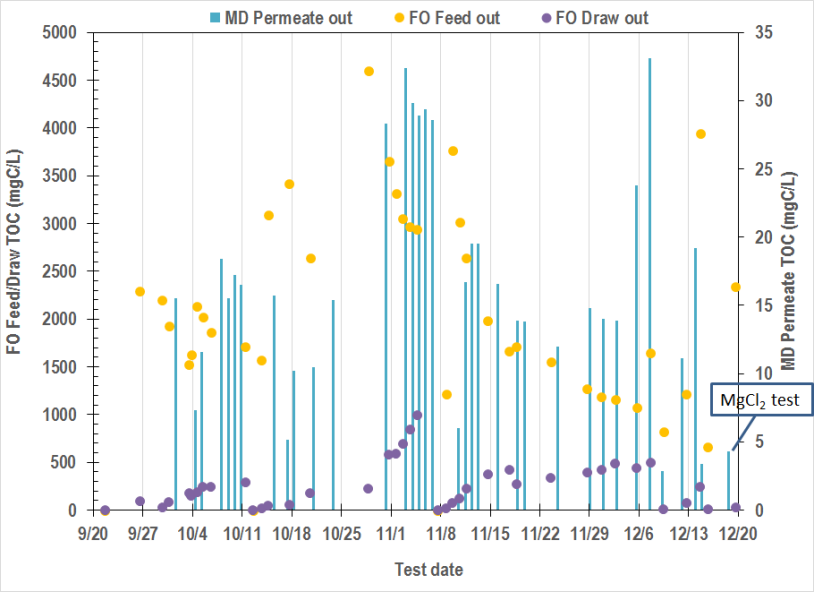

Figure 4-81. FO-MD prototype operation TOC results

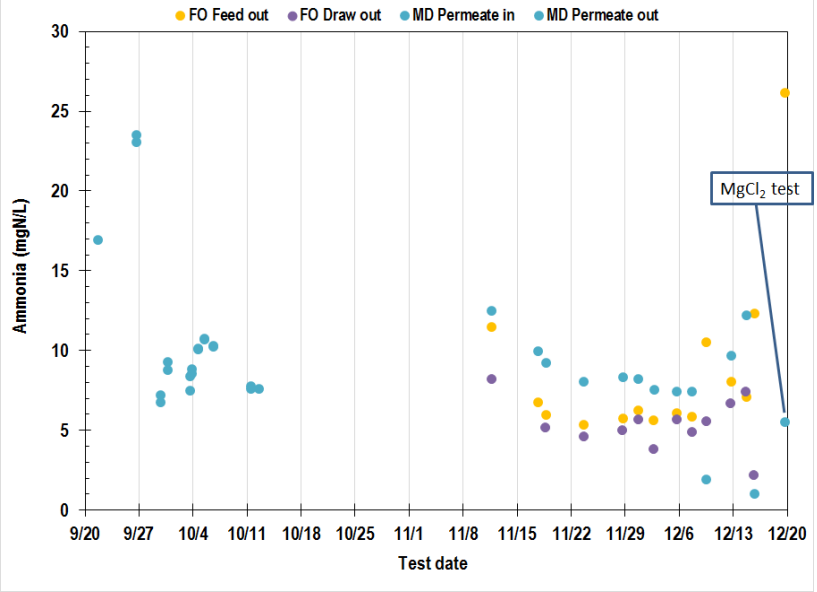

Figure 4-82. FO-MD prototype operation Ammonia results

The observed ammonia rejection was not high as for TOC. High pH in the FO feed converted most ammonium ions to ammonia and the ammonia could penetrate both the FO and MD membrane. The ammonia rejection for FO is poor since it is a small uncharged molecule and these molecules are not rejected well by FO membranes. Ammonia rejection is poor for MD since it is volatile and at elevated temperatures it will be stripped from the draw to the permeate. Thus, the ammonia level in the MD permeate was higher than that of FO feed.

Water Quality Analysis Results

Samples were collected from all process-stream sampling point and shipped to an environmental testing laboratory for a comprehensive water-quality analysis. The analysis results are summarized in Table 4-10 and Table 4-11. The FO-MD system was shown to reject most inorganic components including oil & grease, which were almost completely rejected (greater than 99%). The change of the draw solution from NaCl to $MgCl_2$ enhanced the rejection performance as seen from data on 12/20/2016.

Some VOCs (volatile organic compounds) and SVOCs (semi-volatile organic compounds) could penetrate both FO and MD membrane and accumulate in the MD permeate. VOCs rejection by the FO membrane were around 50% and those VOCs that passed through the FO membrane were not rejected by the MD membrane. Therefore, the VOCs concentrations in MD permeate showed higher value than those in the FO draw/MD feed. The FO membrane rejection of SVOCs was around 70%, which is higher than those of VOCs. And the MD membrane could reject around 90% of SVOCs in the FO feed so the overall rejection of SVOCs in FO-MD system showed more than 95%. GRO (Gasoline Range Organics) showed similar rejection trends as VOCs and the overall rejection by FO-MD system was 70%. DROs (Diesel Range Organics) showed similar rejection trends as that of SVOCs and the overall rejection was 99%. Using $MgCl_2$ as the draw solution could potentially enhance the removal efficiency (12/20 samples). However, further long term operation is required to test the performance of divalent ion draw solution on

the produced water quality under a wider range of conditions than what was observed in the limited testing run for divalent draw solutions.

Table 4-10. Detected dissolved inorganic and oil & grease

Test item	Date	Bulk feed (Raw W.W.)	FO feed (Concentrated W.W.)	FO draw / MD Feed	MD permeate
Oil & grease (ppm)	9/26	4.2	9	5.2	ND
	12/20	ND	2.4	12.8	ND
Total Alkalinity (ppm as $CaCO_3$)	9/26	ND	8,400	1,125	54
	12/20	3,600	9,600	1,300	16
Silica (SiO_2) (ppm)	9/26	100	124	70	0.67
	12/15			3.7	
	12/20	98	130	0.65	0.32
Boron (ppm)	9/26	17	63	22.8	0.21
	12/15			1.7	
	12/20	21	73	5.0	ND
Magnesium (ppm)	12/15			49,000	
	12/20	ND	44	44,000	4.2
Sodium (ppm)	9/26	3,700	18,000	27,800	200
	12/15			2,700	
	12/20	4,400	15,000	3,200	4.7
Bromide (ppm)	9/26	8.8	28.5	29.3	0.22
	12/15			57	
	12/20	ND	38	12,000	3
Fluoride (ppm)	9/26	2.3	5.6	3.8	0.05
	12/20	2.8	12	ND	0.021
Chloride (ppm)	9/26	3,600	17,500	49.000	470
	12/15			150,000	
	12/20	3400	1500	140,000	21

Table 4-11. Detected VOC, SVOC and organics concentrations

Test item	Date	Bulk feed (Raw W.W)	FO feed (Concentrated W.W.)	FO Draw / MD Feed	MD permeate
Acetone (VOC, ppb)	9/26	1,700	1700	822.9	1,450
	10/28		1950	1100	1,850
	12/20	4650		150	220
Methyl ethyl ketone (VOC, ppb)	9/26	795	835	378.6	687.5
	10/28		995	460	915
	12/20	1800	4450	40	61
Isopropanol (VOC, ppb)	9/26	1,800	2600	1050	1,650
	10/28		3,000	1,400	1,850

	12/20	3,500	5,800	47	78
Tetra-hydrofuran (VOC, ppb)	9/26	280	755	330	635
	10/28		190	120	220
	12/20	110	790	210	330
Methylene chloride (VOC, ppb)	12/20	2.4	1.5	1.6	1.2
2,4-Di-methylphenol (SVOC, ppb)	9/26	340	815	127.5	31.5
	10/28		4,600	480	64
	12/20	710	2,700	4.6	15
Phenolics (total) (SVOC, ppb)	9/26	1,600	4605	1390	130
	10/28		27,800	4,370	172
	12/20	3,370	15,600	23.9	15
GRO* (C5-C12) (PPM)	9/26	0.83	1.55	0.103	0.32
	10/28		1.6	0.089	0.78
	12/20	1.7	4.5	ND	0.036
DRO** (C12-C24) (PPM)	9/26	190	705	38	1.2
	10/28		1,200	98	2.2
	12/20	63	240	23	0.53
DRO** (C10-C28) (PPM)	9/26	220	795	46.25	3.1
	10/28		1,400	110	5.5
	12/20	68	310	32	0.87

*GRO: Gasoline Range Organics
**DRO: Diesel Range Organics

Membrane Autopsy

Fouling Analysis after Operation with NaCl Draw Solution

Due to limited project time, this task was completed as part of the operation of the pilot-scale FO-MD prototype, rather than on the smaller bench system. The task objective was to assess the resistance of the membranes and module components (glue lines, feed and permeate spacers, gaskets, etc.) to chemical contaminants found in wastewaters.

A used spiral-wound FO membrane element was sent for membrane autopsy (foulant analysis) to a third-party membrane diagnostic laboratory. This FO element had been in operation in the integrated FO-MD prototype for 4-5 weeks with pre-concentrated, real industrial wastewater feed containing trace amounts of organic compounds. The information for this analysis was used to help determine if the low FO water flux observed during the test campaign with the pre-concentrated wastewater feed having very high TDS of 177,000-204,000 ppm could be attributed to fouling of the membrane surface.

According to the membrane autopsy report, the used FO membrane element was in very good condition. The fiberglass casing, end caps, brine seal, draw-solution tube, and internal components (i.e., feed- and draw-side spacers, membrane envelopes) were intact and free of visual foulants. Likewise, the exposed membrane surfaces on both the feed and draw sides were free of visual foulants (Figure 4-82). Though small amounts of tan particles were noted on the membrane glue lines on every membrane leaf, the

membrane glue lines were also in good condition, and the tan particles did not extend to the active membrane surfaces.

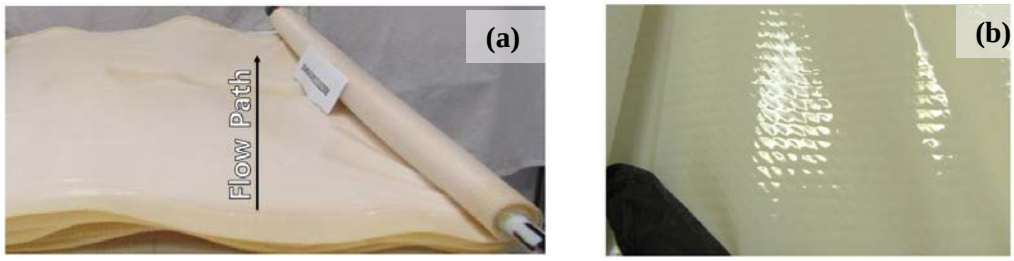

Figure 4-83. Photos of the used FO membrane surfaces on the (a) feed side and (b) draw side

Chromatic Elemental Imaging (CEI) was done on the feed-and draw-side membrane surfaces and a cross-section of the FO membrane. On the feed-side membrane surface, CEI identified only dendritic NaCl crystals and granular particles of colloidal silica (Figure 4-83 (a)), which are both present in the industrial wastewater feed. On the draw-side membrane surface, only NaCl crystals were found (Figure 4-83 (b)), which is expected because NaCl solutions had been used as the FO draw solution during prototype operation. As shown in Figure 4-84, CEI imaging of a membrane cross-section detected only NaCl crystals. Though most NaCl remained on the membrane surfaces, some areas in the interior of the membrane cross-section appeared slightly orange (see Figure 4-84), suggesting migration of the NaCl salt through the FO membrane.

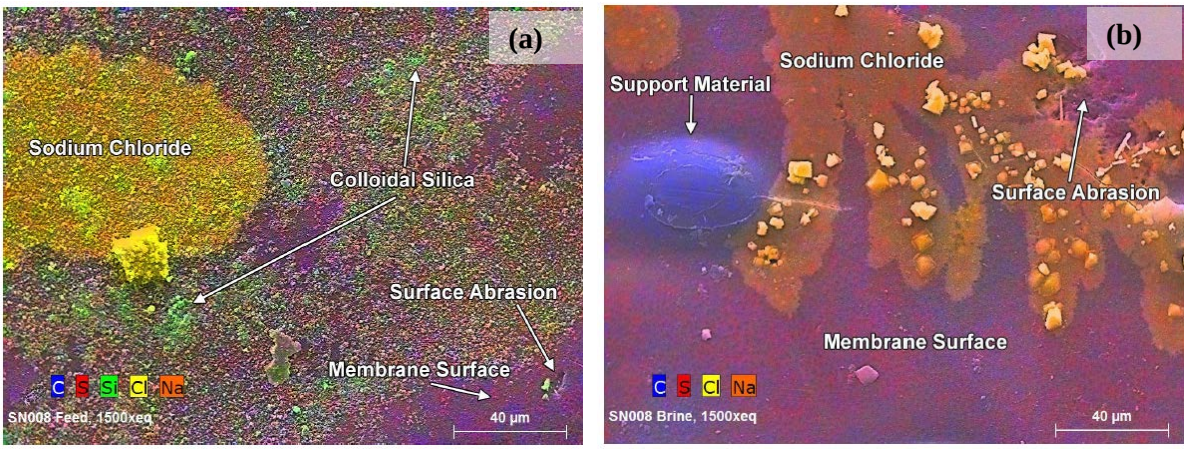

Figure 4-84. CEI images (1,500x) of the (a) feed side and (b) draw side membrane surfaces of the used FO element autopsied

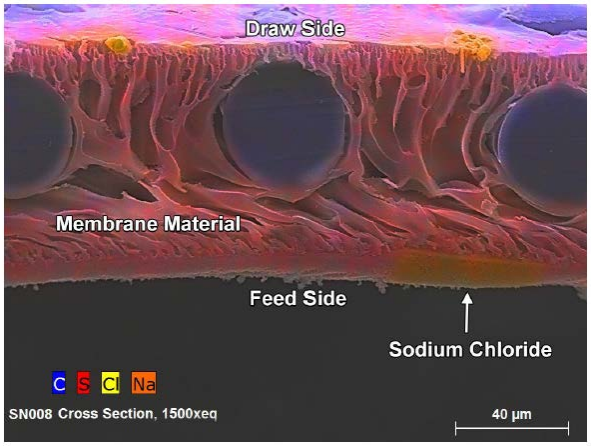

Figure 4-85. CEI image (1,500x) of a cross-section of the used FO membrane autopsied

The autopsy results demonstrated minimal foulant on the used FO membrane that was exposed to the pre-concentrated industrial wastewater feed. During the 4- to 5-week exposure time to the trace levels of chemical (organic) contaminants in the wastewater feed, no degradation of external or internal components of the FO membrane element was also observed. Thus, these results indicate that the low FO water flux observed in the prototype at very high TDS feeds was attributed mainly to low osmotic-pressure driving force, rather than membrane fouling.

Fouling Analysis after Operation with $MgCl_2$ Draw Solution

At the end of the testing with $MgCl_2$ draw-solution testing, a second used FO membrane element, one used MD membrane module, and the MD feed-side filter cartridge were removed from the system and shipped for autopsy (foulant analysis) on December 22, 2016, to a third-party membrane diagnostic laboratory.

The FO membrane was operated for 6–7 weeks with the NaCl draw solution and then for 1 week with the $MgCl_2$ draw solution. The membrane autopsy report indicates that the used FO membrane element was in good condition because the end caps, brine seal, and draw solution tube exhibited good mechanical condition. Brown, granular foulant was observed randomly on the feed scroll end (brine seal end). The membrane surfaces were lightly coated with a white, powdery foulant that was more predominant on the feed side (brine seal end) of the element. Fine, brown, granular material was also visible on the feed end glue line. Patches of brown discoloration were observed throughout the membrane. The discoloration was more prevalent on the concentrate end of the element and was present on both the feed and draw sides of the element. The fouling pattern was similar on all the membrane leaves. There was a strong hydrocarbon odor upon dissection.

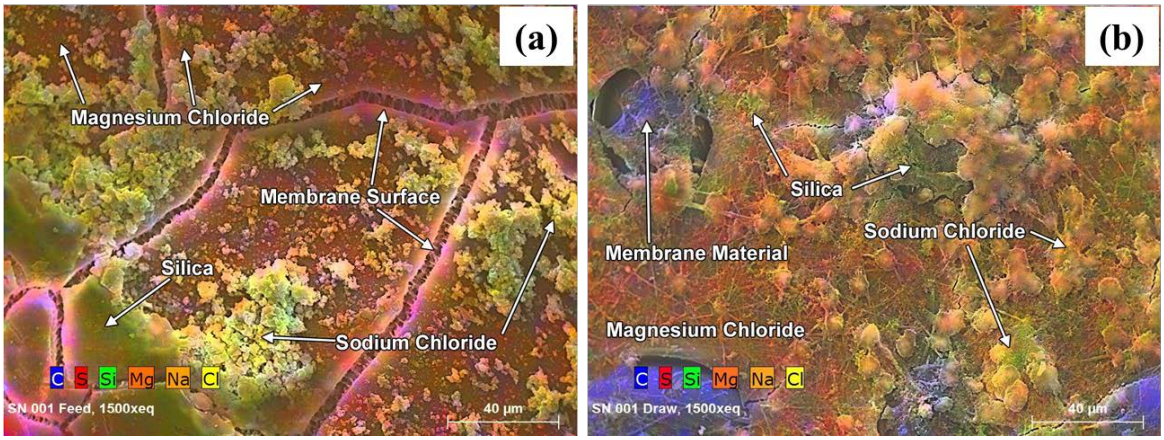

Figure 4-86. CEI images (1,500x) of the (a) feed side and (b) draw side membrane surfaces of the second FO element autopsied

CEI imaging of the feed side of the membrane surface identified the bulk of the granular material as a mixture of silica (green) and salts (magnesium chloride, sodium chloride—combination of orange and yellow) (Figure 4-85a and Figure 4-86). The CEI of the draw side of the membrane surface identified the granular foulant as primarily salts, sodium and magnesium chloride (yellow-orange), with isolated areas containing silica (green) (Figure 4-85b). The membrane material (carbon-blue) was visible in random areas where the foulant was absent. CEI imaging of a cross section of the fouled membrane showed the bulk of the foulant was isolated to the feed side of the fiber. Sodium and magnesium salts were visible migrating through the fouled fiber (Figure 4-86).

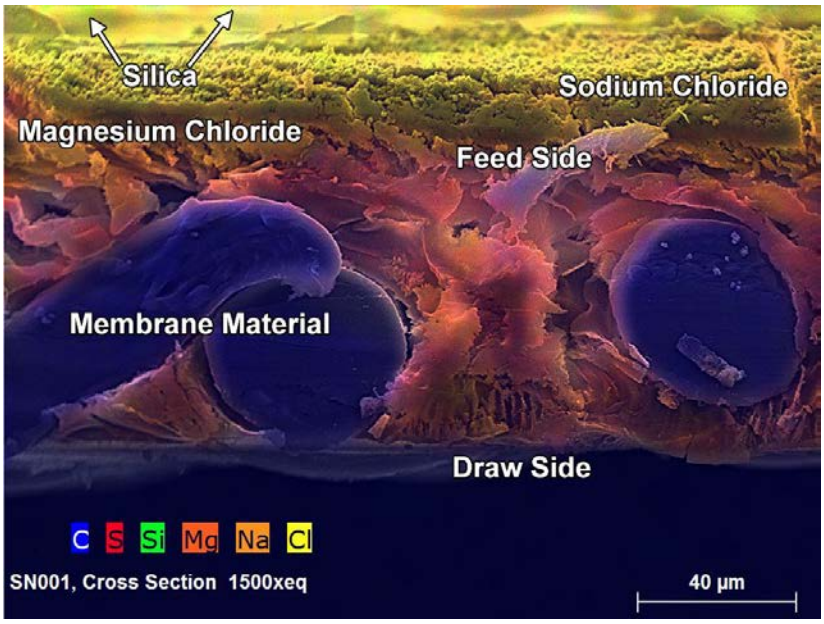

Figure 4-87. CEI image (1,500x) of a cross-section of the second FO membrane autopsied

The cartridge filter was installed in the MD feed line and had been in operation for 12 weeks. The cartridge filter was a 10-µm AMI cartridge filter (Model H-F20BB10CF) with a high-consistency, melt-blown polypropylene sediment filter. The CEI image from the autopsy results is shown in Figure 4-87.

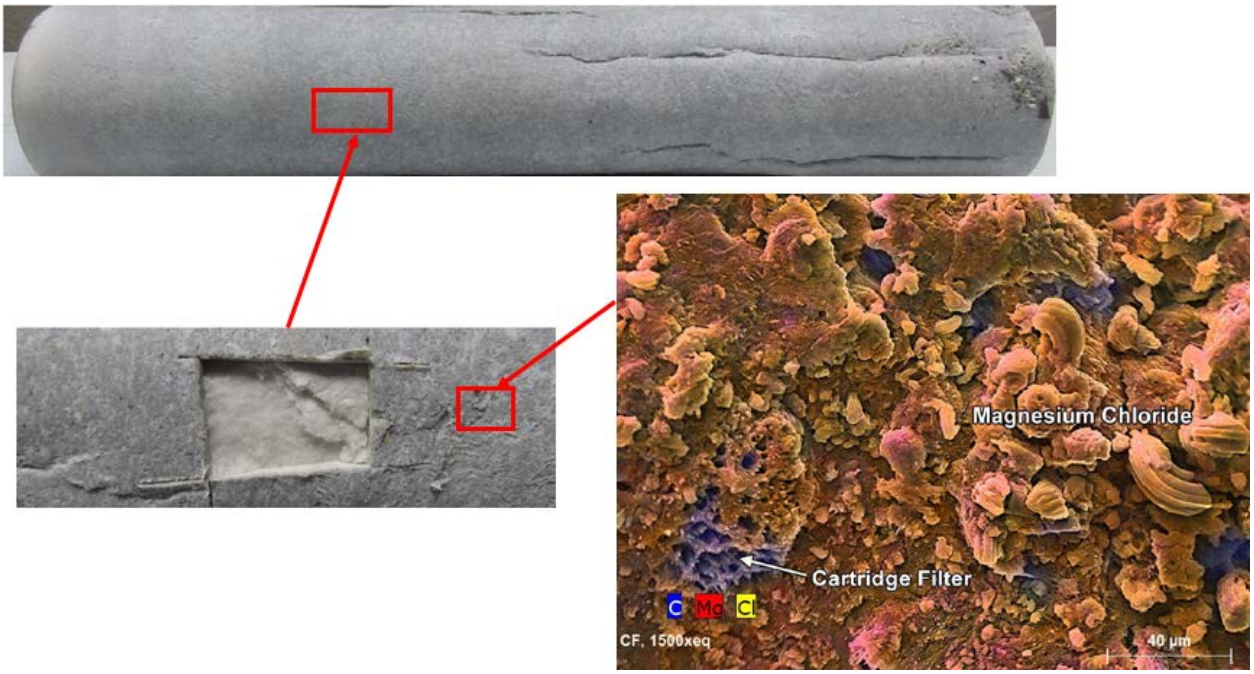

Figure 4-88. Cartridge filter autopsy including CEI image (x1500).

The exterior of the cartridge filter was gray in color, and the foulant could not be scraped from the cartridge filter surfaces. Multicolored debris (black, white, brown and gray) was observed on and closest to one end of the filter. Dissection of the filter showed that the inner layers closest to the core tube were free from visible foulant material. CEI of the exterior of the cartridge filter identified the granular material as magnesium chloride (orange). Some areas containing higher concentrations of magnesium (red) were detected throughout the magnesium chloride layer. The foulant covered most of the cartridge filter so that the fiber material (carbon-blue) was only visible in isolated areas. CEI imaging also confirmed the lack of organic material.

The MD module #1 was sent for autopsy after 8 weeks of operation, which included 7 weeks with NaCl as the draw solution and 1 week with $MgCl_2$ as the draw solution. The external casing of the distillation fiber module was in good condition and free of foulant material and physical damage. One end of the module was coated in white, granular foulant, while the other end was free of any visual contamination. The module dissection pictures are presented in Figure 4-88. A window was cut in the module and the fibers inspected. The fibers of the module were relatively free of visual foulant, and the fibers closest to the end of the module showed a slightly tan discoloration. There was a strong petroleum odor upon dissection.

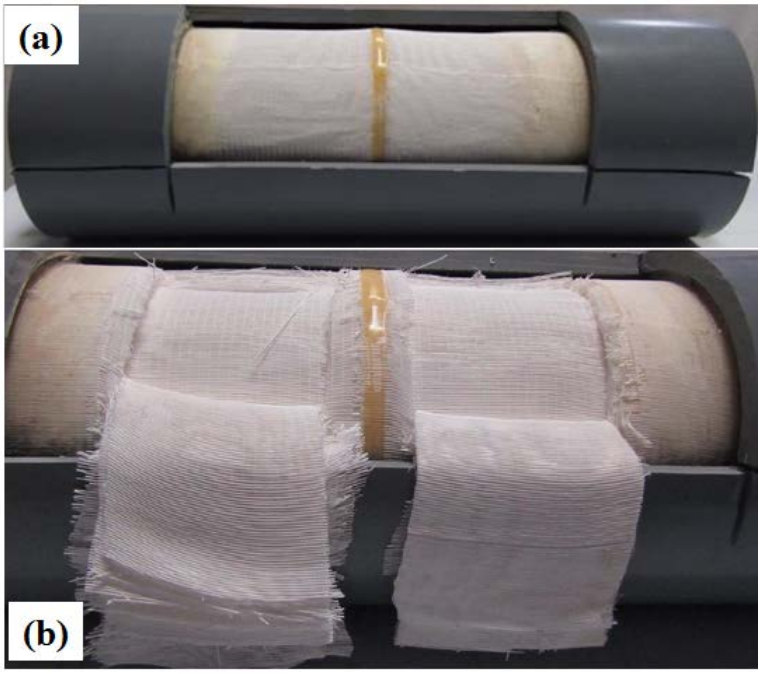

Figure 4-89. Dissection of used MD membrane: (a) exposed fibers (b) dissected fibers.

CEI image analysis identified the particles as sodium chloride salts (orange-yellow). The fiber material (carbon-blue) was largely visible confirming the virtual lack of foulant material. The interior of both the fouled and new fiber showed only the fiber material (carbon-blue). A cross-section of the fouled and new fiber showed similar thickness to the fiber material. Additionally, no obvious contaminants were observed migrating through the fouled fiber. The CEI images for the MD hollow fibers are presented in Figure 4-89.

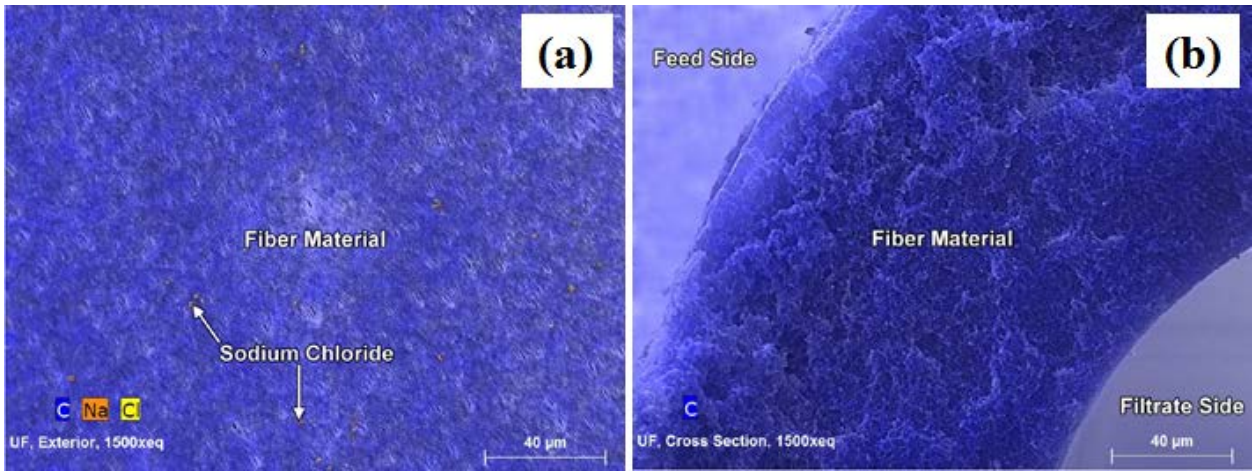

Figure 4-90. CEI image (1,500x) of the used MD membrane: (a) membrane surface and (b) cross section.

Integrated FO-MD Prototype Testing Summary

The integrated FO-MD prototype was operated successfully for over 15 weeks. Due to pumping capacity, the number of FO membranes used during testing was between one and three in order to balance the production rate with MD system, where between one and two modules were used simultaneously during testing. Produced wastewater from an oil production site was transferred to the test site and used as the feed water for the tests. The raw wastewater was concentrated up to 190,500 ppm TDS level to evaluate the removal efficiency and fouling changes to membrane performance. The integrated FO-MD prototype was shown to exhibit successful stable operation over long time periods.

Membrane fouling and membrane integrity were assessed throughout the testing. No chemical cleaning was applied during the test period. The system was flushed with dechlorinated tap water between each new test condition. A membrane autopsy was conducted to assess the fouling and membrane integrity. Even though the feed was concentrated more than 10 times, membrane fouling was unnoticeable, and there were no defects on the surfaces of the FO and MD membranes.

The FO membrane rejected most inorganic contaminants, oil&grease (including GRO and DRO) and SVOCs in the wastewater. The removal efficiency was more than 99%, except for sodium and chlorine which were used for the draw solution. Ammonia and VOCs were shown to pass through the FO membrane and MD membrane could not reject either ammonia or VOCs. Therefore, post treatment to remove ammonia or VOCs after the FO-MD system is required when the raw wastewater contains high level of ammonia or VOCs.

Additional testing using a divalent salt as draw solution was conducted during the piloting phase. A concentration of approximately 3 M $MgCl_2$ solution was used for draw solution. The treated water quality was improved by using the divalent ion draw solution, but the high pH of the wastewater facilitated the precipitation of divalent ion on the FO draw side and the MD feed cartridge filter. The divalent ion scaling decreased the available dissolved salt in the draw solution, which resulted in a drastic decrease of the FO-MD system performance due to decreased available osmotic driving force. The use of divalent salt ($MgCl_2$) as draw solution may improve the removal efficiency of the FO-MD system, but pH adjustment would be required to prevent any precipitation, scaling, and loss of osmotic driving force.

Process Modeling and Validation

Forward Osmosis Model

Validation with Laboratory Data

The initial FO model validation was performed using experimental FO permeation data obtained with DI water feed and draw solutions having different concentrations of various chloride salts of alkali and alkaline earth metals. Membrane-related input to the model were the experimentally determined intrinsic water permeability A and the support structural parameter S of the membrane. A representative model validation plot is presented in Figure 4-90 for the CTA-ES membrane. The coefficient of determination

(R^2) was >0.93 for almost all the solutions for this membrane and served as a good indicator of model validity.

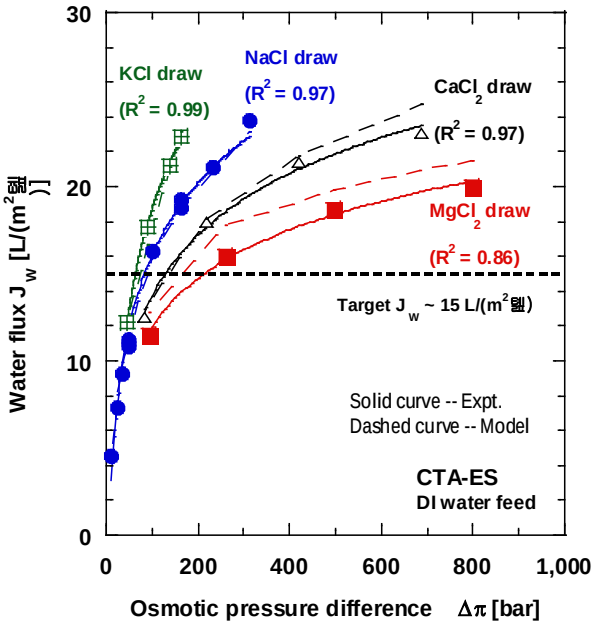

Figure 4-91. Model versus experimental water flux as function of draw-salt type and draw-solution osmotic-pressure difference for the CTA-ES membrane with DI water feed in FO operating mode at room temperature. Solid curves serve as visual guides for the experimental data. Larger dashed curves with R^2 values are the FO model predictions. Osmotic pressures of feed salt concentrations used were taken from the OLI software for electrolyte solutions.

The FO model was also validated with experimental water flux data obtained on the CTA-ES membrane with synthetic, aqueous feeds containing low concentrations of various salts to mimic wastewater on the feed side and therefore a realistic reduction in the osmotic pressure differential across the FO membrane. The saline solutions used as feeds were NaCl, $MgCl_2$, $CaCl_2$ and KCl solutions in the concentration range of 1,500-12,000 mg/L. The resulting FO model predictions obtained with these saline feeds have been presented earlier with the experimental water-flux data in Figure 4-8. The dashed lines representing the model predictions in the Figure 4-8 plots are in good agreement with the data values and trends. The FO model developed does account for the reduction in osmotic pressure differential (due to the presence of feed salinity) in the corresponding water flux calculation.

The summary of the FO model validation results in Table 4-12 shows a strong correlation between the model-predicted values and the observed experimental results, as measured by the R^2 value. The water flux values of the FO membranes were shown to be accurately predicted by the model, with R^2 values >0.95.

Table 4-12. First-Round FO Model Validation Summary

FO membrane	Key control variables	Observed output	Number of data points	Model R^2 value (goodness-of-fit)
CTA-NW	Feed and draw solution osmotic pressures & flow rates	Water flux	16	0.94
CTA-ES	Feed and draw solution osmotic pressures; Flow rate	Water flux	16	0.95
X-TFC	Feed and draw solution osmotic pressures; flow rate	Water flux	12	0.97

Validation with Bench-Scale Data. Second-round FO model refinement/validation was completed using experimental baseline performance data obtained on an FO membrane module installed in the bench, integrated FO-MD test system. The data were collected on FO module having an effective membrane area of 0.21 m^2. Relative to that of the laboratory-scale FO membrane coupons used for the first-round model validation, the membrane area of the flat-sheet FO module was 15 times larger. Hence, this sizable increase in active membrane area provided a useful assessment of model performance at the next larger scale.

The baseline experimental performance data obtained on the 0.21-m^2 FO module were determined at room temperature using DI water feed at different aqueous NaCl draw-solution concentrations up to 3 M. These experimental data were then compared to the water fluxes predicted by the FO model developed and validated previously with laboratory data on membrane coupons. Key FO model inputs, in addition to the effective membrane area of the module, were intrinsic membrane characteristics such as water permeability A and membrane support structural parameter S. From a parameter sensitivity analysis, the FO model appeared to be most sensitive to the S value. While the A value used in the model was consistent with that provided by the FO membrane manufacturer, the S value ultimately used to obtain the best model fit, though, was ~1.9 times larger than the manufacturer's value. With the manufacturer's S value (245 μm), the FO model consistently overpredicted the module's water flux. However, with the larger S value (463 μm), the model water fluxes agreed very well with the experimental data (coefficient of determination R^2 ~ 98%), as shown in Figure 4-91 and Figure 4-92. The larger S was not unreasonable because this FO module was found to possess lower water flux than that given by the manufacturer. The lower flux indicated that the composite structure of the production FO membrane packaged in this module has greater resistance to water transport than the laboratory versions of the membrane studied previously, and the greater water-transport resistance is usually captured as a higher S value for the membrane. Thus, the existing FO model was validated by the experimental data for a larger FO module.

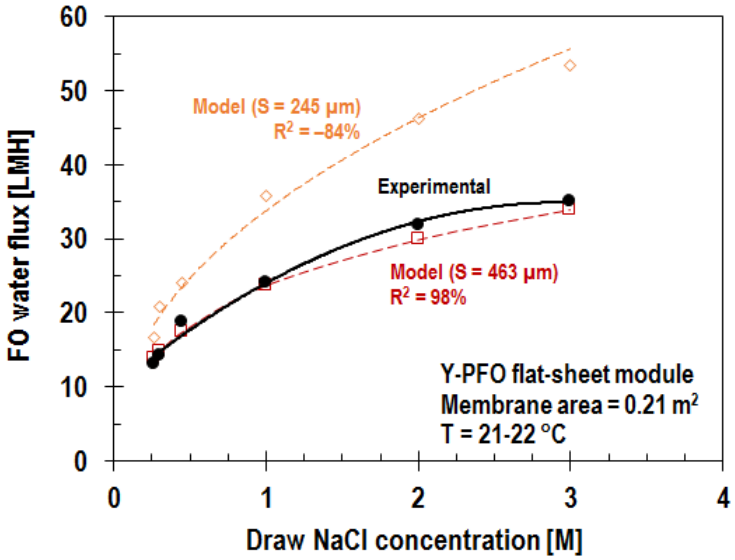

Figure 4-92. Comparison of model-predicted water fluxes to fluxes experimentally measured in the FO membrane module Y-PFO as a function of NaCl draw concentration in the bench, integrated FO-MD test unit.

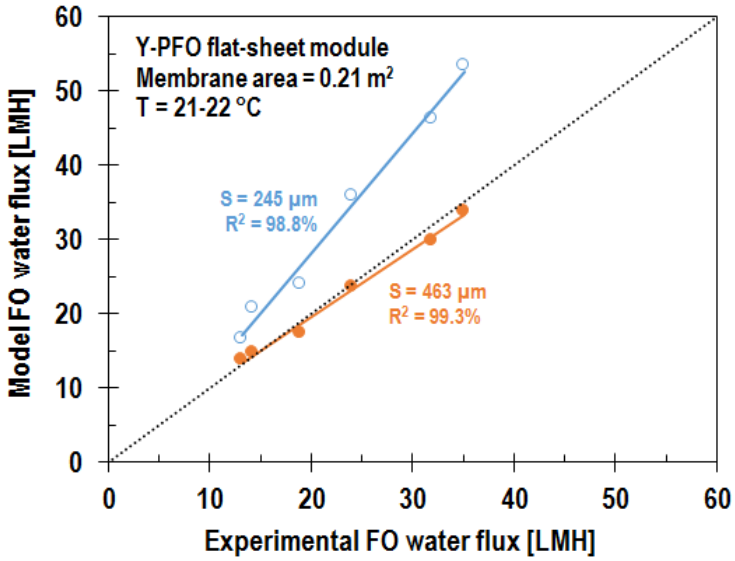

Figure 4-93. Parity plot comparing model-predicted water fluxes to fluxes experimentally measured in the FO membrane module Y-PFO in the bench, integrated FO-MD test unit.

Membrane Distillation Model

MD Initial Model Validation

The model was validated with experimental data available for a DCMD module with PTFE as the membrane. The experiments were run with 0.1 M NaCl solution on the feed side and DI water on the

permeate side. The water flux across the membrane was noted for each run. To evaluate the effect of the temperature differential on the water flux across the membrane, the hot feed side was maintained at a constant temperature; while the cold permeate side temperature was varied to achieve the set temperature differential. The first experiment was run with a constant feed temperature of 28 °C for different ΔT values achieved by varying the cold stream temperature. The second experiment was run with a constant feed temperature of 50 °C and at the set ΔT values. To evaluate the performance of the model, the list of feed and membrane parameters that were considered as an input to the model are summarized in Table 4-13.

Table 4-13. List of Input values used for the PTFE DCMD module

Input Values		
Area	0.0004524	m^2
Temperature of feed, Tf(in)	depending on the case	
Temperature of cold stream,Tp(in)	depending on the case	
Mass flow inlet of feed stream	2.3	g/s
Mass flow inlet of cold stream	2.3	g/s
Concentration of salt in inlet feed stream,C_T	100	$gmol/m^3$
Molecular weight of feed solution	18.02	g/gmol
Mole fraction of salt in bulk feed	0.0018	
Heat transfer coefficient of the membrane, h^M	350.36	W/m^2K
Porosity, ε	0.7	
Tortuosity, τ	1.59	
Thickness, t	325	µm
Pore radius, r	1.60×10^{-7}	m

The model solves for the water flux, heat flux, temperature, salt concentration and mass flow profiles along the membrane. For the same conditions considered in the experimental runs, the model was evaluated and the results are plotted in Figure 4-93.

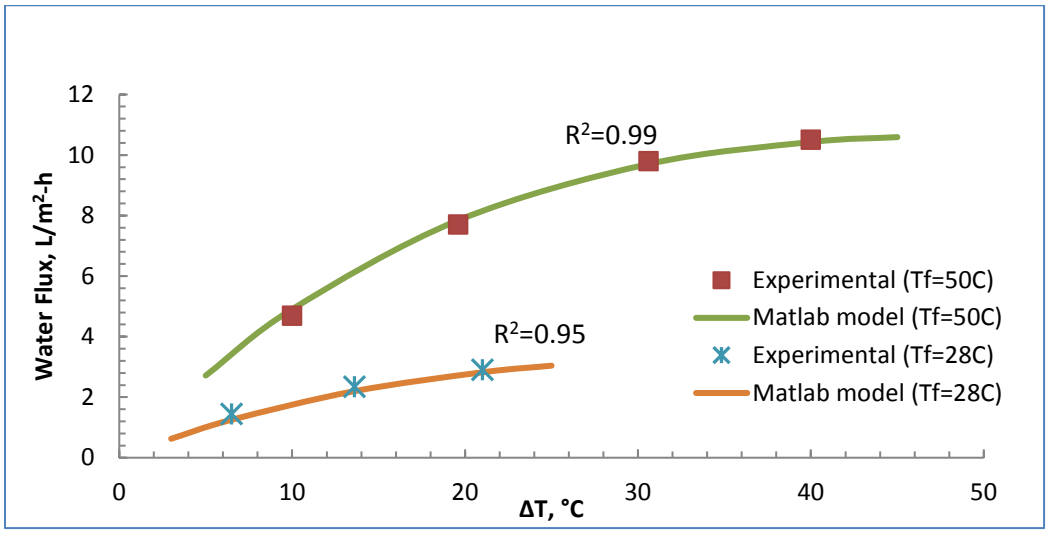

Figure 4-94. Model validation results: Water flux for a PTFE DCMD module at feed temperatures of 28 and 50°C and set ΔT values.

From Figure 4-93, it is evident that the water fluxes calculated by the model align very well with the experimental water flux values. The R^2 values for both the data sets was found to be greater than 0.95.

MD Model Validation Using 2.5 in. × 8 in. Hollow-Fiber Module

The model was validated with experimental data available from the 50-gpd system which utilizes a 2.5" x 8" hollow fiber module with PP as the membrane. Second-round process model refinement/validation was completed using experimental baseline performance data obtained on the MD membrane module installed in the bench, integrated test system. The membrane area for the MD module used for the testing was 0.64 m^2. The approximate order of magnitude increase in active membrane area over what was used in the initial model validation provides for a useful assessment of model performance at larger scales.

The validity of the component MD model was further checked with additional experimental water permeation data obtained by the manufacturer of the MD hollow-fiber membrane module (2.5 in. dia. × 8 in. long) designated as PP-M200-HF. The membrane in this device comprised polypropylene hollow fibers. The manufacturer's membrane parameters and different shell- and bore-side flow conditions were used in the RTI MD model to predict the MD water fluxes for this module. The model fluxes obtained are compared to the manufacturer's experimental fluxes in Table 4-14. It was noted that the permeate water flux of this MD module was quite low [0.73-2.98 L/(m^2·h)] because the manufacturer's tests had been conducted using very low shell- and bore-side fluid flow rates (0.20-0.75 gpm).

The MD water fluxes predicted by the MD model were found to be in good agreement with the third-party experimental values measured, further validating the RTI model. Furthermore, examination of the model predictions indicate that higher water flux can be obtained from the MD module by increasing the shell- and bore-side fluid flow rates, which effectively reduces temperature polarization effects on the feed and permeate sides.

Table 4-14. Comparison of MD Water Fluxes Predicted by MD Model and Experimentally Measured by Membrane Manufacturer for Hollow-Fiber MD Module PP-M200-HF

Test no.	Module shell-side			Module bore-side			Water flux [L/(m^2·h)]	
	Flow [gpm]	Inlet T [°C]	Outlet T [°C]	Flow [gpm]	Inlet T [°C]	Outlet T [°C]	Experimental	Model [RTI]
1	0.20	59.8	25.2	0.20	14.8	43.4	1.03	0.89
2	0.25	50.9	21.4	0.25	15.8	30.2	0.74	0.73
3	0.25	60.2	27.4	0.25	15.0	46.2	1.28	1.28
4	0.50	55.8	34.1	0.50	15.8	39.6	2.02	2.32
5	0.75	52.5	37.1	0.50	15.6	41.8	2.05	2.98

The model fluxes obtained are compared to the experimental fluxes on the 50-gpd unit in Figure 4-94. The MD water fluxes predicted by the RTI MD model were found to be in good agreement with the experimental values measured, further validating the RTI model.

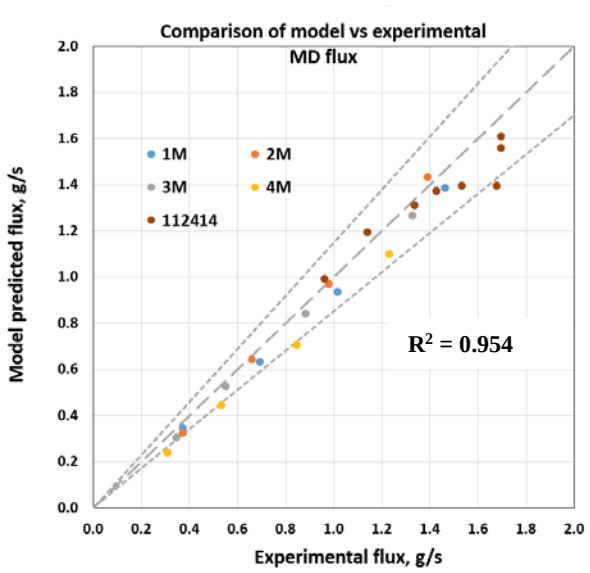

Figure 4-95. Comparison of model-predicted water fluxes to fluxes experimentally measured in the MD module in the bench, integrated FO-MD test unit. Data shows experimental/model results for real wastewater (112414) and 1, 2, 3, and 4M NaCl feeds (R^2 > 95% meets the MD aspect of the milestone).

MD Model Validation Using Commercial Scale 8" x 20" Hollow-Fiber Module

A final model validation using experimental data available from the 500-gpd system was performed. This system utilizes 8" × 20" hollow fiber modules with PP as the membrane and treated real wastewater. Final-round process model refinement/validation was completed using experimental baseline performance data obtained on the FO and MD membrane modules installed in the trailer mounted pilot, integrated test system treating real wastewater from our industrial partner. Table 4-15 shows the summary of the data used for the model validation. Twelve different process condition were used to validate the model. The conditions cover a range of flowrates, feed temperatures, and feed salt concentrations.

Table 4-15. Summary of the range of operational conditions and measured temperatures and water production values for treating industrial wastewater.

Run no.	Feed Salt	Hot Side				Cold side				Permeate Recovery		
		Feed flow		Feed temp	Outlet temp	Feed flow		Feed temp	Outlet temp			
	(mg/L)	lpm	g/s	C	C	lpm	g/s			lmh	lpm	
1	160,000	60.56	761.84	55	35.6	45.42	654.69	21.7	44	0.995157	0.886	1.46%
2	190,000	60.56	761.84	55	34.9	52.99	761.71	22.8	44	0.995157	0.886	1.46%
3	190,000	60.56	761.84	55	35.4	45.42	654.69	21.7	46	0.995157	0.886	1.46%
4	190,000	60.56	761.84	40	28	45.42	646.5	17.8	33	0.344478	0.307	0.51%
5	175,000	45.42	571.38	35	22	45.42	644.46	16	28	0.182871	0.163	0.36%
6	195,000	30.28	380.92	55	29	30.28	433.46	19	41	0.425281	0.379	1.25%
7	195,000	30.28	380.92	40	25	30.28	430.84	17	31	0.216893	0.193	0.64%
8	195,000	30.28	380.92	50	30	30.28	433.25	20	39	0.40827	0.363	1.20%
9	125,000	30.28	380.92	55	26	30.28	438.33	16.2	43	1.624573	0.723	2.39%
10	125,000	30.28	380.92	60	28.5	30.28	440.79	17.2	45	2.015831	0.897	2.96%
11	125,000	30.28	380.92	65	31	30.28	442.45	19	50	2.279506	1.014	3.35%
12	160,000	30.28	380.92	55	28	30.28	436.83	17	42	1.386416	0.617	2.04%

Results from this refinement/validation demonstrate that the MD model accurately (R^2 > 80%) predicts the performance of the pilot, integrated demonstration FO-MD system. Data from pilot system was used as the basis for the model performance assessment. The membrane areas for MD modules used for the testing was ~26 m^2. The approximate order of magnitude increase in active membrane area over what was used in the second-round model validation provides for a useful assessment of model performance at commercial scale. The MD model was checked with experimental water permeation data obtained on the 8 in. × 20 in. MD hollow-fiber membrane module in the pilot-scale unit. The membrane in this device is comprised of the same polypropylene hollow fibers tested on the stand-alone MD laboratory test bed as well as the second-round validation 2.5" x 8" module. The manufacturer's membrane parameters and different shell- and bore-side flow conditions were used in the MD model to predict the MD water recovery for this module as well as the exit temperatures for both the heated feed and chilled permeate streams exiting the module. The MD exit temperatures predicted by the MD model were found to be in good agreement with the experimental values measured, further validating the MD model and allowing for a large-scale assessment of the energy consumption of the system at larger scales.

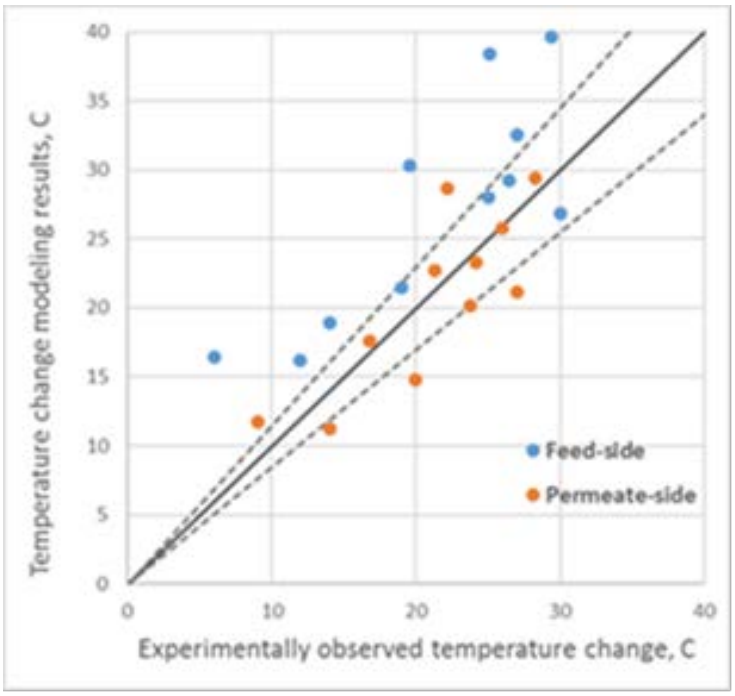

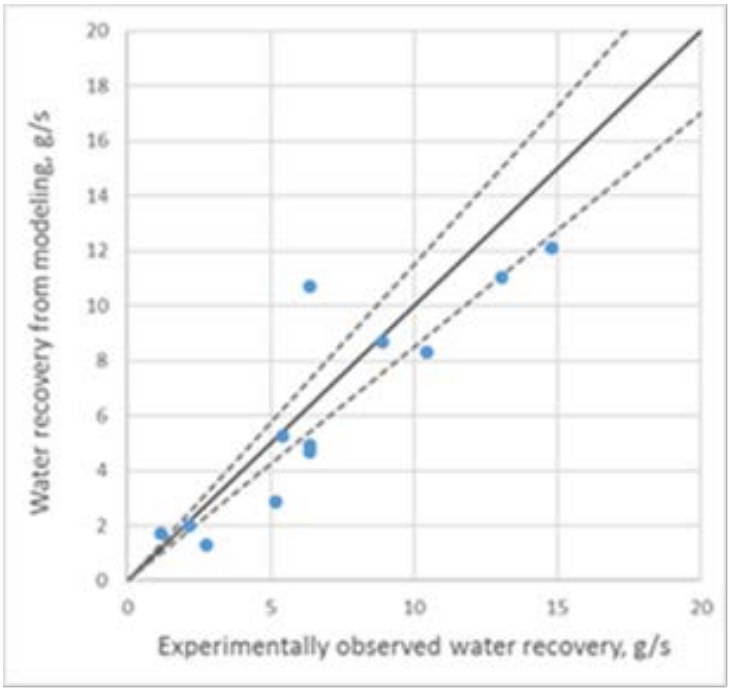

Figure 4-96. (a) Comparison of model-predicted exit temperatures for both the feed and permeate exit streams to experimentally measured values in the MD module in the demonstration FO-MD test unit and (b) Comparison of model-predicted water production rates to water production rates experimentally measured in the MD module in the demonstration FO-MD test unit. Data shows experimental/model results for real wastewater samples

Techno-economic Analysis

Preliminary Techno-Economic Evaluation Results Summary

The targeted water recovery for both the technologies (e.g., FO-MD and MF-RO) was set to 94% and was the basis for design. Based on the process calculations, the operating and capital costs for both the processes were estimated using the procedure described in detail in Section 3. As previously described, the capital costs for the two technologies are split into the direct costs and indirect costs. The direct costs include the equipment and their installation costs, while the indirect costs account for the additional expenditure for construction overhead, contingency and other additional costs.

Low-TDS Case

A summary of the costs involved in the two processes for a low-TDS wastewater are summarized in Table 4-16. As expected, the total capital costs for the integrated FO-MD technology were estimated to be 54% higher than the MF-RO. This cost increase is primarily due to the higher membrane cost associated with a 'young' technology. The integrated FO-MD technology is at a very early scale of development, and it is expected that, with the advancing development of this technology, the membrane costs will decrease substantially. Conversely, the integrated FO-MD technology had 35% lower operating costs compared to the conventional technology. This was primarily due to the low-pressure operation (<10 lbs/in^2) of the FO-MD system, resulting in lower pumping energy requirement. The MF-RO system operates at high pressures (400–1,200 lbs/in^2) and, thus, has a much higher projected electrical energy requirement.

Table 4-16. Low TDS case cost summaries for FO-MD and MF-RO.

COSTS	FO-MD	MF-RO
Capital Costs		
Direct		
Equipment	$ 6,919,372	$ 3,728,290
Building	$ 1,131,955	$ 938,865
Electrical	$ 1,427,914	$ 1,137,871
Instrumentation & Control	$ 1,020,904	$ 834,221
Piping	$ 1,502,922	$ 872,910
Other	$ 782,421	$ 775,616
Total Direct Capital costs	$ 12,785,488	$ 8,287,773
Indirect		
Construction Overhead	$ 511,420	$ 331,511
contingency	$ 767,129	$ 497,266
A&E fees Proj management	$ 1,534,259	$ 994,533
working capital	$ 511,420	$ 331,511
Total indirect capital costs	$ 3,324,227	$ 2,154,821
Total capital costs	$ 16,109,715	$ 10,442,594
Operating Costs		
Energy	$ 267,247	$ 3,201,670
Membrane replacement	$ 1,310,367	$ 275,686
Labor and Overhead	$ 1,463,076	$ 1,463,076
Spare parts	$ 55,232	$ 89,112
chemicals	$ 23,514	$ 23,514
Salt losses	$ 157,937	
other		
Total operating costs	$ 3,277,373	$ 5,053,058

Based on the capital and operating costs obtained for both the technologies, the annualized capital cost was calculated. The total water treatment costs per year are equal to the sum of the annualized capital cost and the annual operating cost. Additionally, the total water cost (TWC) was also determined for each technology approach. The TWC is the annualized capital and operating cost per unit volume of water and is a commonly used measure in the water treatment industry.

For this analysis, a technology lifetime of 20 years and a rate of interest of 6% were considered for the TWC calculation. Based on the assumption that both technologies would have similar life spans, this approach was deemed acceptable.

Presented in Table 4-17 are the summary results of the techno-economic analysis. In the low-TDS case, based on the NPV, TWC, and power consumption assessment, the FO-MD would be the technology of

choice for treating this waste water. The analysis resulted in a 21% lower NPV, 23% lower TWC, and 91% reduction in electricity consumption and associated CO_2 equivalence.

Table 4-17. Low TDS case techno-economic and environmental results summary.

LOW TDS CASE (2,170 mg/L TDS)			
METRIC	FO-MD	MF-RO	% REDUCTION
Water Recovery, %	94	94	0
Total Capital Cost, $MM	16.1	10.4	-55
Annual Operational Cost, $MM	3.28	5.05	35
NPV	53.7	68.4	21
Total Water Cost (TWC), $/m^3	0.72	0.92	22
Electrical Energy, kWh/m^3	0.41	4.47	91
CO_2 Equivalence, Metric tons	1,886	20,466	91

High-TDS Case

High-TDS wastewaters are the most difficult to desalinate with membrane technologies due to their high osmotic pressure potential. In RO systems, the hydraulic pressure force on the wastewater needs to be greater than the osmotic pressure of the waste water. This requirement results in an upper technical limit on the amount of water that can be recovered, often based on the structural properties of the membrane. FO systems rely on the higher osmotic pressure on the draw-side of the membrane to induce water flux, resulting in a much higher range of TDS waters that can be treated. Taking into account the limitations of each process, the design basis water recovery rate was set at 80% for the FO-MD system and 40% for the MF-RO system. Like the low TDS case, the total direct capital costs for the FO-MD system was 82% higher than the MF-RO system and the operating costs lower by 20%. Presented in Table 4-18 is a summary of the capital and operating costs for the high TDS case wastewater for both the FO-MD and MF-RO systems.

Table 4-18. High-TDS case cost summaries for FO-MD and MF-RO.

COSTS	FO-MD	MF-RO
Capital Costs		
Direct		
Equipment	$ 9,181,172	$ 3,839,708
Building	$ 1,131,955	$ 820,603
Electrical	$ 1,399,523	$ 1,184,568
Instrumentation & Control	$ 1,014,224	$ 624,221
Piping	$ 1,425,953	$ 996,744
Other	$ 808,462	$ 775,979
Total Direct Capital costs	$ 14,961,289	$ 8,241,823
Indirect		
Construction Overhead	$ 598,452	$ 329,673
Contingency	$ 897,677	$ 494,509
A&E fees Project management	$ 1,795,355	$ 989,019
working capital	$ 598,452	$ 329,673
Total indirect capital costs	$ 3,889,935	$ 2,142,874
Total capital costs	$ 18,851,224	$ 10,384,697
Operating Costs		
Energy	$ 240,601	$ 2,879,527
Membrane replacement	$ 1,951,000	$ 409,115
Labor and Overhead	$ 1,463,076	$ 1,463,076
Spare parts	$ 66,906	$ 70,010
Chemicals	$ 22,086	$ 22,086
Salt losses	$ 134,415	
other		
Total operating costs	$ 3,878,083	$ 4,843,813

Presented in Table 4-19 are the summary results of the techno-economic analysis. In the high-TDS case, based on the NPV, TWC, and power consumption assessment, the FO-MD would be the technology of choice for treating this wastewater. The analysis resulted in a 4% lower NPV, 52% lower TWC, and 95% reduction in electricity consumption and associated CO_2 equivalence.

Table 4-19. High-TDS case techo-economic and environmental results summary.

HIGH TDS CASE (44,442 mg/L TDS)			
METRIC	FO-MD	MF-RO	% REDUCTION
Water Recovery, %	80	40	-100
Total Capital Cost, $MM	18.9	10.4	-82
Annual Operational Cost, $MM	3.88	4.84	20
NPV	63.3	65.9	4
Total Water Cost (TWC), $/m^3	1.00	2.08	52
Electrical Energy, kWh/m^3	0.44	9.46	95
CO2 Equivalence, Metric tons	1,698	18,430	91

Updated Techno-economic Analysis Summary

The Class IV (+/-40%) preliminary techno-economic analyses done at the project start was revised. These preliminary analyses had been done for two model industrial wastewaters that represent most of the U.S. manufacturing sector with respect to TDS content. One wastewater had low TDS concentration of 2,170 mg/L; the other had high TDS concentration of 44,442 mg/L.

The project's industrial partner refined and updated the techno-economics for the RO cases to which the hybrid FO-MD case studies had been compared. In this analysis, ultrafiltration [UF] replaced the microfiltration [MF] operation as the pretreatment for RO. In the updated analysis, a three-stage RO configuration with 90% water recovery was used for the low-TDS case, and a one-stage RO design with 48% water recovery was used for the high-TDS scenario. (In the preliminary analysis, a single stage for RO had been used for both cases. RO water recovery had been 94% and 40% for the low- and high-TDS cases, respectively.) The accuracy of the industrial partner provided UF/RO process estimates was given as roughly +/-5%, which significantly improved the overall comparison.

For the FO-MD analysis, the labor formula used was very conservative and overestimated the projected labor cost according to actual industry practices. It is anticipated that labor costs for a fully mature, 'nth-generation' FO-MD system would likely be on the same order as that used for the UF-RO system in the project's industrial partner's analysis. Other assumptions in the FO-MD analysis remained the same as in the preliminary analysis, pending revision with real field data to be obtained on the field FO-MD prototype. Accordingly, the techno-economic analysis was updated for the model low- and high-TDS industrial wastewater case studies. The updated techno-economic results are presented in Table 4-20 and Table 4-21.

Table 4-20. Updated Summary of Techno-economic Assessment of Water Reuse Treatment Technologies for Model Low-TDS Industrial Wastewater (Design Feed Flow Rate = 3,854 gal/min)

LOW-TDS CASE (2,170 mg/L)			
Metric	**FO-MD**	**UF-RO (Industrial partner analysis)**	**% Reduction (FO-MD rel. to UF-RO)**
Water recovery (%)	94	90	-4.4
Total capital cost ($MM)	16.1	20.6	22
Annual operational cost ($MM)	1.88	1.24	-52
NPV (Net present value)	37.6	34.8	-8.0
Total water cost [TWC] ($/m^3)	0.50	0.44	-14
Electrical energy (kWh/m^3)	0.41	1.07	62

Table 4-21. Updated Summary of Techno-economic Assessment of Water Reuse Treatment Technologies for Model High-TDS Industrial Wastewater (Design Feed Flow Rate = 3,854 gal/min)

HIGH-TDS CASE (44,442 mg/L)			
Metric	**FO-MD**	**UF-RO (Industrial partner analysis)**	**% Reduction (FO-MD rel. to UF-RO)**
Water recovery (%)	80	48	-67
Total capital cost ($MM)	18.9	22.6	16
Annual operational cost ($MM)	2.49	2.57	3.1
NPV (Net present value)	47.3	52.1	9.2
Total water cost [TWC] ($/m^3)	0.75	1.26	40
Electrical energy (kWh/m^3)	0.44	6.08	93

With respect to capital cost, the FO-MD system ($16-19MM) was initially projected to be less expensive than that of the UF-RO system ($21-23MM) in both cases. The FO-MD system also has higher water reuse efficiency than the UF-RO system (94% for FO-MD vs. 90% for UF-RO for the low-TDS case and 80% vs. 48% for the high-TDS case). The FO-MD platform also still consumes less electricity than the UF-RO technology, requiring 0.41-0.44 kWh/m^3 for FO-MD instead of 1.1 kWh/m^3 (low-TDS) and 6.1 kWh/m^3 (high-TDS) for the UF-RO technology. It should be noted, though, that the percentage reduction in electrical consumption for the low-TDS case in the updated analysis is now smaller than the estimate of 91% in the preliminary analysis.

Comparison of the other metrics for the two technologies indicates that the potential benefit/impact of the FO-MD platform is really for the treatment of high-TDS wastewaters, not for low-TDS wastewaters. With respect to operational cost, the FO-MD is 52% higher than the revised UF-RO in the low-TDS case and

only marginally better than the revised UF/RO by 3% in the high-TDS case. For the low-TDS scenario, the updated Net Present Value [NPV] estimates were $38MM for FO-MD and $35MM for UF-RO, while the total water cost [TWC] were $0.50/$m^3$ and $0.44/$m^3$, respectively, for FO-MD and UF-RO. Hence, UF-RO is more attractive for treating low-TDS wastewaters. In the high-TDS case, FO-MD showed a slightly better NPV of $47MM than UF/MD, which was estimated to be $52MM. Furthermore, TWC was $0.75/$m^3$ for FO-MD, about 40% lower than the $1.26/$m^3$ estimate for UF-RO. On the basis of these revised techno-economic results, the advantage of FO-MD technology is in the treatment of high- to very-high-TDS wastewaters that are either too challenging or impossible for RO to handle. *The updated techno-economic analysis indicates that FO-MD should be benchmarked more to other high-TDS water treatment technologies such as evaporators and crystallizers, rather than to RO as initially assumed.* This conclusion informed both the targeted real wastewater samples for testing of the prototype system as well as final technology comparison.

Final Techno-economic Analysis Summary Based on Pilot Data. The intermediate techno-economic analyses was updated again using data from the 500 GPD pilot system and the updated model. Although the initial TE assessment included two potential industrial wastewater sources, project results as well as input from our industrial partner indicated that FO-MD would not be a practical fit for the low-TDS case. Therefore, the final TE analysis includes only the high-TDS concentration of 59,442 mg/L. Maintaining the same water recovery allows for an even comparison from prior iterations of the TE analysis and an evaluation of what parameters changed due to updated understanding of the process during the project at larger scales. The final analysis maintains the same design basis as generated before, but model results and assumptions used for parameters such as specific heat utilization for MD, salt consumption in FO, as well as membrane flux performance were replaced with values observed from the 500-GPD demonstration system. The updated analysis also considered additional cases with both the required heating and cooling streams were obtained. In the case of needing to pay for cooling, a dedicated cooling tower was designed and included in the overall capital cost total. Table 4-22 shows the updated techno-economics of the FO-MD system in comparison with the literature-based initial integration for the original projection and four updated cases: 1) an ideal best case scenario where the site can provide both free heating and cooling, 2) a scenario where heat must be purchased (low-pressure steam), cooling is available on site, and there is no heat recovery step, 3) a scenario where both heating and cooling must e purchased, and 4) a scenario where heating and cooling both must be purchased, but heat recovery is added to the process.

Table 4-22. Summary of Final Techno-economic Assessment of Water Reuse Treatment Technologies for Model High-TDS Industrial Wastewater (Design Feed Flow Rate = 3,854 gal/min)

HIGH-TDS CASE (59,442 mg/L)					
Metric	**FO-MD—Original Projection**	**FO-MD—Free Heat/Cooling**	**FO-MD—Free Cooling**	**FO-MD—Pay Heat/Cool**	**FO-MD—Pay Heat/Cool, w/Heat Recovery (40%)**
Water recovery (%)	80	80	80	80	80
Total capital cost ($MM)	18.9	48	48	80	80
Annual operational cost ($MM)	2.49	10.6	79	79	52
Electrical energy (kWh_e/m^3)	0.44	4.7	4.7	4.7	4.7
Heat energy (kWh_t/m^3)	10	900	900	900	550
Total water cost [TWC] ($/m^3$)	0.75	2.72	13.80	14.53	9.06
Total water cost [TWC] ($/bbl)	0.12	0.43	2.19	2.31	1.44

Table 4-22 shows that the projected overall cost of treatment via FO-MD has increased by approximately a factor of 2 to 16 depending on if the necessary heat must be purchased, which is a significant increase over the initial projections. The largest contribution to this cost increase is a result of the increase in heat energy required for the MD side of the system and increased electricity requirement for pumping. The initial projects were based on literature energy consumption values and used as a best-case scenario for heat utilization for MD. Literature reported values for specific heat energy consumption for MD as low as 1.25 kWh/m^3 and 6 kWh/m^3, so the initial projections of 10 kWh/m^3 was assumed [41, 42]. The experimental data also showed that the required electrical energy for pumping increased by a factor of 5 because the recirculation rate for MD is, in reality, much higher than initially anticipated. The initial projected water cost of $0.75 was also within +/- $0.50 of reported values for MD at full scale. Several experimental show that DCMD can be used to treat produced waters with high salt rejection and claimed that the DCMD treatment cost is comparable to the cost to re-inject the wastewater for disposal. An economic evaluation by Macedonio et al [43] estimated that a 100 m^3/hour DCMD plant could treat water at $1.28/$m^3$ if the produced water was fed to the plant at 20°C and $0.72 if the produced water entered the plant at 50v°C. However, based on our findings in this project, these costs at or near $1/$m^3$ are likely to be unattainable in practice when energy inputs are not completely free. The updated projections of heat required for water production is one of the major contributors to this increased cost. The increased heat

requirement increases the cost of the MD system in two ways: 1) increased heating requires additional heat exchanger surface area to obtain the heat, the cost of heat exchangers is one of the major expenditures for the capital requirements of the system; 2) the higher heat requirements result in a greater than projected heat utilization through the membrane modules, which limits the attainable flux through the membrane and increases the overall membrane area requirements and associated footprint, including piping, valves, etc. These costs are absorbed into the TWC projection and are highly dependent on the cost of the heat (waste vs. purchased). On the FO side, the prototype data showed that initial projected salt consumption of 0.0053 moles NaCl/L should be increased to 0.0095 moles NaCl/L, which had a minimal impact on the operational cost of the system (+ \$0.03/m^3 total water cost). The projected FO membrane flux of 30 LMH was demonstrated as feasible during the pilot operation. This projected Table 4-23 shows a comparison of some of the key operational parameters and how they changed as data was generated from the laboratory to the demonstration scale.

Table 4-23. Initial and final values used to develop TE analysis for the FO-MD system and their directional impact on overall system cost.

Initial Value Used	Updated Value	Impact on Cost
Salt Makeup = 0.0053 mol NaCl/L water produced	Salt Makeup = 0.0095 mol NaCl/L water produced	Minimal increase to operating cost
FO flux = 30 LMH	FO Flux = 15 LMH	No change
MD flux = 22 LMH	MD flux = 3 LMH	Increased capital cost
MD Specific Heat = 10 kWh/m^3	MD Heat Specific Heat = 900 kWh/m^3	Increased operating/capital costs

As a scenario where the waste heat is completely free obviously makes the most cost competitive FO-MD scenario with a projected cost of \$2.72/m^3. However, we note that the likelihood of ample and available waste heat that approaches a temperature of 80 °C is not a likely scenario, and it is more likely that the true cost of the FO-MD system will be closer to the \$9 per m^3 product water range where heat integration is included. This value is competitive with some of the higher end costs for deep-well injection of high-TDS wastewater, which varies from \$0.25/bbl to \$12/bbl, depending on geographic location and transportation costs from the site to the disposal well. This also suggests that FO-MD may be competitive with thermal evaporator technology if high-TDS wastewater sites are electing to pay for disposal costs rather than onsite treatment. As highlighted in Figure 4-96 the major cost driver for the FO-MD technology is from the MD side of the treatment system, with costs for MD pumps, heater exchanger, and membranes modules and piping/valves accounting for ~61% of the total required CAPEX for the non-heat integration case and ~71% of the total required CAPEX for the case where heat integration is used. Including heat integration as well as the cost of an installed cooling system more than doubles the capital expenditure of the system, but the heat integration reduces the operation cost significantly so that TWC is decreased by ~30%.

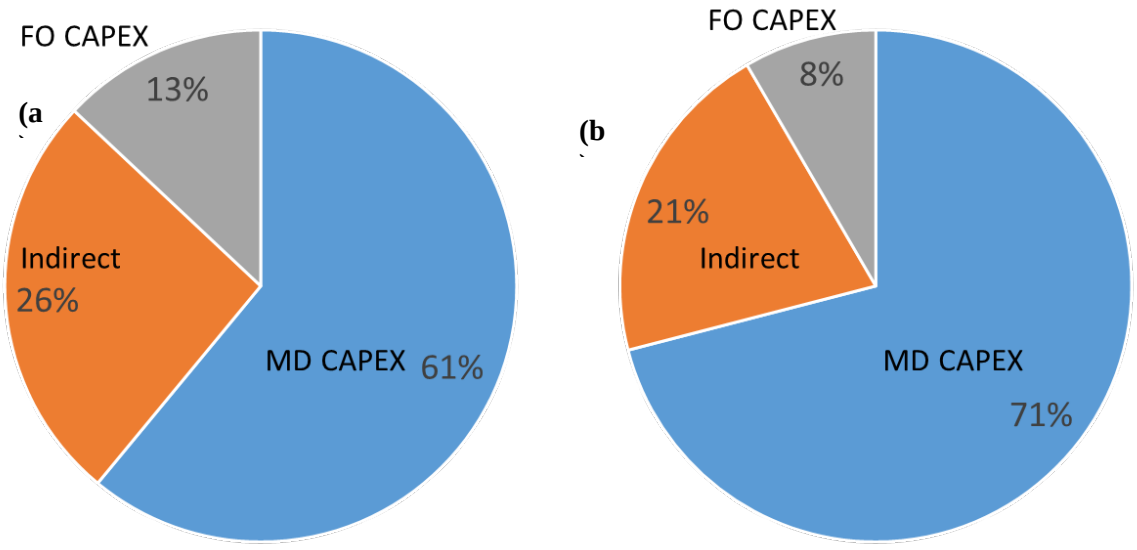

Figure 4-97. CAPEX breakdown between Indirect, FO, and MD costs for (a) non-heat integration (total CAPEX = 34 $MM) and (b) heat integration cases (total CAPEX = 74 $MM).

On the operational side, the heating requirements for MD accounts for 93% and 89% of the operational costs for the non-heat integration and with heat integration scenarios, respectively. These estimations were made assuming a heating cost of $7.2/kg for low-pressure steam. Although the fractional decrease in heating is not much lower for heat integration, the total projected annual OPEX costs decrease by ~37%, which results in a net decrease in TWC to $8.4/m^3. These TEA results demonstrate the importance of assessing improving the heating recovery and overall efficiency of the MD side of the process.

A question that this updated cost projection highlights is why there is such a difference in performance values (i.e., loss of flux at each scale-up stage). MD flux values approaching 35 LMH were recorded at the laboratory scale and ~ 10 LMH for the 50-GPD system, while the maximum flux measured on the 500-GPD system was 4 LMH. The chief reason for this drop-off was a decrease in volumetric flow rate to the MD module, which reduced the heat/mass transfer coefficients as well as the available heat reservoir near the membrane interface to drive water vapor through the membrane. Table 4-24 shows the pertinent flow conditions through the hollow-fiber modules at each stage and size scale.

Table 4-24. MD membrane volumetric flow, velocity, flux, and membrane module specific area at each experimental stage of the project.

Development Stage	Typical Feed Flow (L/min)	Module Area (m^2)	Typical Flux @60C (LMH)	Crossflow Velocity (cm/s)	MD Recirculation Ratio Velocity
Bench system	2	0.0085	30	0.37	580Q
50-GPD system	25	0.64	8	0.065	350Q
500-GPD system	30	26.7	2	0.0019	20Q

This decrease in flux performance can be directly explained by the flow velocity of the feed water at each state. The high ratio of volumetric flow to membrane surface area defines the cross-flow velocity within the module. The larger membrane modules were limited in the volumetric flow rate that they could handle because the module integrity would be compromised at higher flow rates due to pressure buildup on the seals. The 8x20 modules are rated to handle a flow rate of up to 190 L/min, but the 500-GPD system pump losses through the heat exchanger were higher than anticipated, so it was not possible to supply this maximum flow rate to the module. However, 190 L/min corresponds to a crossflow velocity of 0.012 cm/s for the 8x20 module, which is an order of magnitude improvement. Based on this and results at the 2.5" x 8" scale, our model verification suggested that a flux of ~8 LMH could be expected through the 8" x 20" module.

Potential for Further Cost Reduction of FO-MD. The results of the study show that FO technology is not the primary driver for costs of the integrated FO-MD system and that the observed performance of the FO system is adequate for near-term scale up, if the draw solution can be recovered. Although MD studies often cite the need for the development of an MD-specific membrane, results from this effort suggest that existing commercial membranes provide more than adequate fluxes and that the capital cost of the membrane modules is much less important than the cost due to heating and the overall energy efficiency of the system. This supports the idea that a more important need is the development of a larger-scale MD module that maximizes flow volume to specific surface area to reduce the specific heating requirements for MD. The second and more critical need for development in MD is the heat management and recovery. The TEA analysis illustrates that the heat efficiency of the MD process is the major driver of TWC and that even more than doubling the projected capital cost of the FO-MD system is more than offset by reducing the MD heating requirements. Future efforts for MD development should prioritize improvements to energy utilization and recovery. Small-scale thermal evaporators require a specific energy consumption of 130–400 kWh/m^3, and, although MD is not yet able to approach this low range, the polymer materials of construction would constitute a capital cost advantage and make FO-MD a clearly advantageous alternative if the heating requirements can be reduced below the 200 kWh/m^3 range. The potential impacts on price are illustrated in Figure 4-97, which shows that increasing the heat integration and finding the optimum recirculation rate would allow the TWC of FO-MD to approach \$5/m^3 (\$0.85/bbl).

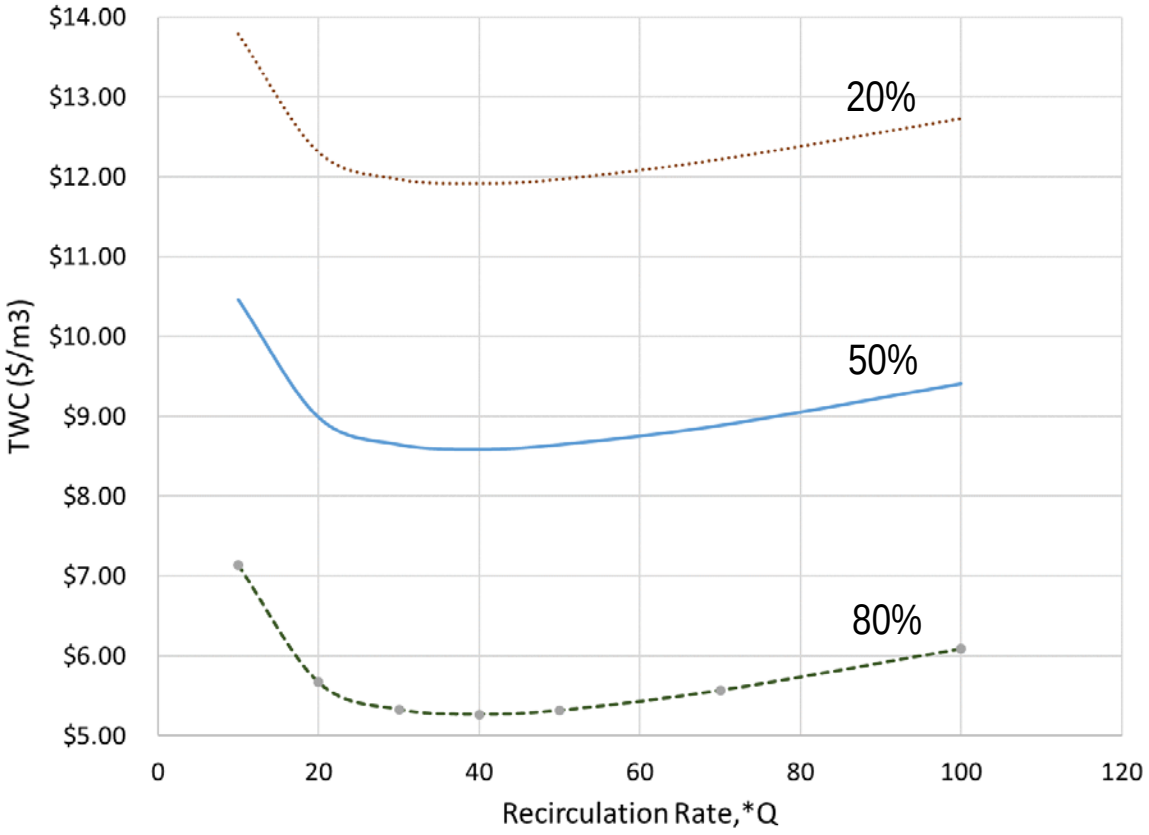

Figure 4-98. Impact of increased heat integration on the TWC for FO-MD and minimum TWC for each heat integration case as a function of recirculation rate.

5. BENEFITS ASSESSMENT

Energy Potential Benefits

The FO and MD study in this project has achieved the treatment of water with TDS that was not possible with any water treatment process, except for thermal evaporators. In the FO-MD process, low-grade heat (40-70 °C) can be used as a major source of energy. This opens a great possibility of more energy efficiency in water treatment. Most of the energy consumption in RO is electricity for high-pressure pump. Because FO-MD does not use any high pressure, any type of low-grade heat can meet most of the energy consumptions in this type of desalination system.

Total U.S. industrial and mining self-supplied water withdrawals in 2005 were 18,200 and 4,020 million gallons per day {Kenny, 2009 #28}. It was estimated that 88% of industrial water withdrawals were self-supplied, and the remaining 12% obtained water from outside sources (i.e., municipal). The total withdrawal volume utilized in this evaluation was an estimated 25,250 million gallons per day. It was assumed that 40% of the total volume was lost via evaporation and product and 20% required additional treatment to attain boiler feed requirements.

The current state of the industrial water/energy cycle utilizes 100% of the energy requirements from electricity, while adoption of FO-MD technology would result in only 8–50% of the energy coming from electricity and the remaining 50–92% coming from waste heat utilization. Assuming a sufficient quantity of waste heat can be recovered, a significant portion of electrical energy that is currently being used for high-TDS water can be saved.

Based on our preliminary evaluation, the U.S. industrial sector can potentially save up to an estimated 130 trillion BTUs per year and beneficially utilize approximately 1,886 trillion BTUs of waste heat per year by adopting the FO-MD technology versus RO utilization for water reuse.

Potential Environment Benefits

U.S. manufacturing industries are in a unique position to address the energy–water nexus by tapping into currently underutilized waste heat to drive water treatment. Relative to current technologies, there are several wide-ranging expected environmental benefits that would result from the adoption of the hybrid FO-MD membrane system to treat and reuse industrial wastewater effluent. Reductions in water withdrawals and discharges would alleviate water stress throughout the U.S and cut down on the quantity of trace contaminants released into the nation’s waterways, reduce total pollutant loads discharged, and improve the overall water quality. From a climate change standpoint, the utilization of waste heat instead of electricity as the main driver for water purification would allow industrial facilities to significantly reduce greenhouse gas emissions. The up to 26 million metric tons of CO_2 emissions eliminated as a result of reduced electricity consumption upon industry-wide adoption of this technological approach is equivalent to the annual emissions of 6 coal-fired power plants [44]. These are benefits that would be realized upon implementation of the FO-MD hybrid membrane system and expanded upon as emerging industries also employed this approach.

Additionally, the FO-MD hybrid technology would fit well with other emerging wastewater treatment technologies such as anaerobic membrane bioreactors (AnMBR). Industrial wastewaters have the potential to generate at least 160 trillion BTUs of energy per year via AnMBR. In contrast, conventional aerobic biological treatment, which is the industry workhorse in wastewater treatment facilities, generates and releases an estimated 407,000 metric tons amounts of CH_4 as greenhouse gas (8.5 million metric tons of CO_2 equivalents) [45]. The synergistic effect of combining the FO-MD system with newer-generation technologies such as the AnMBR in the industrial sector would further eliminate greenhouse gas pollutants and build upon already substantial environmental benefits.

Potential Economics Benefits

The greatest benefit of using FO-MD is that high-TDS industrial wastewater, that used to be disposed of, can be considered as a resource that can be beneficially reused. Previously, this was not possible because it was either out of range for RO or the cost of thermal evaporator was prohibitively high. FO-MD process can be built using much lower-cost material such as CPVC for the majority of the pipes. It can also treat water with feed TDS several times higher than RO. Once the benefits of industrial water reuse is realized, there will be increasingly more voluntary participation from the industry, purely based on the economical aspects of the process. The economic savings realized by reducing electricity consumption would serve as a key driver for industry to adopt this approach. Initial estimates indicate potential industry-wide savings of up to $3.8 billion per year over current approaches. This estimate is based on the relative savings in electricity consumption between the FO-MD approach and RO, assuming an electricity value of $0.10/kWh. In addition, this sustainable low-energy approach to water management has generated interest from industry leaders in emerging industries like shale gas extraction and biofuels production and has the potential for application in power generation, all of which broaden the scope for water savings and increase associated potential positive economic and environmental impacts. For example, a single shale gas well requires 1–8 million gallons of water for hydrofracturing, of which 10-40% is returned as flowback water within the first two weeks and another 190,000–770,000 gallons per year are discharged as produced water throughout the life of the well. Current practices involve off-site treatment in addition to hauling charges that bring the total cost of disposal to $2-5/bbl. This can bring water treatment costs up to $0.5 million per well on an annual basis. An innovative solution would be to utilize on-site natural gas (available in a side flare) to heat this wastewater for the hybrid FO-MD system. The over 1,000 wells drilled in Pennsylvania alone illustrate the potential economic savings that can realized by emerging industries and highlights the versatility of this transformative technology.

6. COMMERCIALIZATION

As a result of this project, one of the largest scale FO-MD pilot in existence was produced and mounted on a trailer for mobile testing. It is a very unique capability and provides a system that can be deployed to virtually anywhere in United States. The trailer-mounted FO-MD pilot system will be deployed to actual industrial sites where its benefits can be demonstrated onsite. The produced water from a steam-assisted gravity drainage (SAGD) oil production site has been successfully tested, and it is anticipated that the reduction in final volume can significantly aid in the operation of oil production wells. The process can also improve environmental protection because there will be less volume of brine that needs to be injected into deep wells. In addition, any type of water that has high levels of organic and dissolved contaminants can be a target candidate for future testing.

Once the capabilities of this concept are field proven at multiple industrial sites, it can be introduced to the industry managers, municipalities, equipment manufacturers, system integrators, consulting engineers, and various final end users from different industries. Currently, various FO-MD technology providers and potential users for the technology are being contacted by the technical leads and participating industrial partners of this project.

For full scale commercialization, it is necessary to accumulate more data from pilot-plant studies. There has also been a downturn in FO-MD membrane manufacturers over the last few years. Current generations of FO and MD membranes used in this study are good starting point for building full-scale plants, and their chemistry has been proven to be compatible with extreme conditions necessary for industrial operation. However, the overall system design needs much more development efforts, and it is still necessary to develop better membrane module design, particularly in terms of flow and heat management.

To make the FO-MD process feasible and economically competitive, current spiral-wound FO membranes and any MD membranes seem to require following critical design improvements:

- Pressure drop in the draw-solution phase. The current FO membranes designs are adaptation of RO membranes, where the permeate would not experience the driving force limitation as in FO. Additionally, the path for the draw solution through the inside of the envelop seems to be designed to minimize short-circuiting. Such tortuous path would create a high pressure drop in each membrane element.
- Connection of multiple membranes. This is currently limited due to the dividers on the draw side of the spiral-wound membranes that restrict the flow and increase pressure drop in each element. The pressure is high enough to limit the in-series operation of the FO membranes to about 3 elements, compared to 7-8 elements for RO. This implies that current FO membranes may be limited in overall water recovery.
- Reverse draw-salt flux. There seems to be a certain amount of draw salt transported from the draw side to the feed side. This is also related to other factors, such as multiple FO membrane connections in series and recirculation rate. With the current level of salt loss, the replenishment of ionic strength in the draw solution can be quite costly and time-consuming for full-scale plants.

- Reduction of recirculation rate for FO and MD membranes. Even though there is no high pressure for FO and the thermal energy for MD can be obtained from low-cost sources, the current rate of recirculation required seems to be too high, and electrical energy consumption is still significantly high.
- For the MD membranes, the most significant improvement needs to be in the heat management along the length of the (membrane) fiber, so that higher water recovery is possible. Compared to other heat-driven desalination systems, MD still needs improvement for the single-pass water recovery rate.

To enable large-scale use and commercialization of the FO-MD technology, it is essential to work with membrane manufacturers to improve the current performance or develop a new concept for these membranes.

7. ACCOMPLISHMENTS

Significant accomplishments and major conclusions from this project are the following:

Awards

- Best Overall Paper Award at a conference—Winglee, Judy, "Modification of Ceramic Membranes for Membrane Distillation," Paper presented at the 2014 AWWA/AMTA Membrane Technology Conference & Exposition, Las Vegas, NV, March 2014.
  - (AWWA = American Water Works Association; AMTA = American Membrane Technology Association)
- 2017 AWWA Austin F. McCormack Jr. Young Professional Award to Judy Winglee for her membrane distillation R&D work and contributions

Publications, Conference Proceedings, and Presentations

- Cunningham, J. and M. Lesemann, "RTI International: Energy & Environmental Technologies," Presentation at the 88th Petroleum Environmental Research Forum [PERF] Meeting, Richmond, CA, November 2013.
- Winglee, J., "Modification of Ceramic Membranes for Membrane Distillation," Paper presented at the 2014 AWWA/AMTA Membrane Technology Conference & Exposition, Las Vegas, NV, March 2014.
  - (AWWA = American Water Works Association; AMTA = American Membrane Technology Association)
- Toy, L., "Advanced, Energy-Efficient Hybrid Membrane System for Industrial Water Reuse," Presentation at the U.S. DOE Advanced Manufacturing Office Peer Review Meeting, Washington, DC, May 2014.
- Toy, L. and M. Lesemann, "Advanced, Energy-Efficient Hybrid Membrane System for Industrial Water Reuse," Invited talk at the Agenda 2020 Technology Alliance Quarterly Meeting, Raleigh, NC, June 2014.
- Hendren, Z., L. Toy, N. Akunuri, S. Mazzarelli, M. Von Holle, and K. Amato, "Forward Osmosis with Membrane Distillation for Industrial Water Reuse: Model Development To Inform Process Integration," Paper presented at the North American Membrane Society [NAMS] 24th Annual Meeting, Houston, TX, June 2014.
- Hendren, Z., L. Toy, N. Akunuri, M. Von Holle, and S. Mazzarelli, "Integration of Forward Osmosis with Membrane Distillation for Industrial Wastewater Reuse: Model Development and Validation," Poster presented at the North American Membrane Society [NAMS] 24th Annual Meeting, Houston, TX, June 2014.
- Toy, L., "Advanced, Energy-Efficient Hybrid Membrane System for Industrial Water Reuse," Presentation at the U.S. DOE Advanced Manufacturing Office Peer Review Meeting, Washington, DC, May 2015.
- Yong, S., "Forward Osmosis: Challenges & Chances for Commercialization," Presentation at the International Forward Osmosis Association [IFOA], Vancouver, British Columbia, September 2015.

- Carpenter, A.W., S.N. Laughton, and M.R. Wiesner, "Enhanced Biogas Production from Nanoscale Zero Valent Iron-Amended Anaerobic Bioreactors." Environ. Eng. Sci., 32(8), 647-655 (2015).
- Lesemann, M., L. Toy, Y. C. Choi, Z. Hendren, G.D. Kim, D. Bollinger, N. Akunuri, S. Yong, and H. Buisson, "Integrated Forward Osmosis/Membrane Distillation Technology for Industrial Water Treatment and Reuse," Paper presented at the 38th Industrial Energy Technology Conference [IETC], New Orleans, LA, May 2016.
- Winglee, J., N. Bossa, Z. Hendren, L. Toy, and M.R. Wiesner, "Direct-Contact Membrane Distillation (DCMD) for Industrial Water Reuse: Managing the Accumulation of Organic Compounds in DCMD Product Water," Paper presented at the North American Membrane Society [NAMS] 26th Annual Meeting, Bellevue, WA, May 2016.
- Choi, Y.C., "Advanced, Energy-Efficient Hybrid Membrane System for Industrial Water Reuse," Presentation at the U.S. DOE Advanced Manufacturing Office Peer Review Meeting, Washington, DC, June 2016.
- Winglee, J., N. Bossa, and M. Wiesner, "Predicting the Accumulation of Organic Compounds in Direct Contact Membrane Distillation Product Water," Poster presented at the 2017 AWWA/AMTA Membrane Technology Conference & Exposition, Long Beach, CA, February 2017.
  - (AWWA = American Water Works Association; AMTA = American Membrane Technology Association)
- Winglee, J.M.,N.Bossa, D. Rosen, J.T. Vardner, and M. Wiesner, "Modeling the Concentration of Volatile and Semi-Volatile Contaminants in Direct Contact Membrane Distillation (DCMD) Product Water." In submission to Environ. Sci. Technol.
- Kim, G.D., Y.C. Choi, L. Toy, Z. Hendren, M. Lesemann, and H. Buisson, "Integrated Forward Osmosis/Membrane Distillation Process Technology for Industrial Water Treatment and Reuse," Conference paper accepted for presentation at The American Society of Mechanical Engineers [ASME] Power & Energy Conference and Exhibition 2017, Charlotte, NC, To be presented in June 2017.
- Winglee, J.M., Z. Hendren, B. Espinasse, J. Cunningham, and M.R. Wiesner, "Modification and Performance Testing of Commercially Available Ceramic Membranes for Direct Contact Membrane Distillation." Manuscript in preparation.

Inventions, Patent Applications, and/or Licenses

No inventions, patent applications, or licenses were derived from this project.

Doctoral (Ph.D.). dissertation

- Winglee, Judith., "Improving Membrane Distillation Performance by Reducing the Effluent Concentration of Volatile Contaminants," Ph.D. Dissertation, Duke University, March 2017.

Website(s) and/or Other Internet Site(s)

No public websites or internet sites were derived from this project.

8. CONCLUSIONS

A major strength of the proposed FO-MD hybrid membrane approach is that it can be configured to treat a wide range of industrial wastewaters. In this study, it was successfully shown that the produced water with high TDS, which could not be treated with current technologies, can be treated and with 90% water recovery using the FO-MD process. This is a significant demonstration that has no precedence at this scale.

As in other membrane processes, skid-mounted membrane modules allow for treatment of waste streams as low as several hundred gallons per day to large multiple effluent streams of millions of gallons per day, and allow facilities to easily expand to meet capacity demands.

This novel water treatment technology was built with a modular design with individual components able to be tailored for specific feed water conditions and treatment requirements. This system flexibility, in addition to the energy- and environment-specific benefits, will allow the technology to be heavily deployed within several industrial markets.

The following technical conclusions were made from this project:

- Multiple FO membrane/draw solution combinations were identified that can effectively achieve water fluxes >15 LMH and 98+% simple salt rejection.
  - Next-generation, thin-film composite FO membranes do have much higher water fluxes (up to 4 times higher) in combination with much higher water/salt selectivity than first-generation cellulosic FO membranes.
  - Reverse draw-salt fluxes are observed to be much lower for the divalent salts than for the monovalent salts. For the chloride salts investigated, the draw salts ranked in order of increasing salt flux as $MgCl_2 < CaCl_2 << NaCl < KCl$ for all FO membranes studied. That is, as hydrated cation size becomes larger, not only is its permeation in the membrane hindered by the larger physical size but also by the lower diffusivity associated with a larger ion.
- However, in terms of water flux performance, effectiveness of draw salts ranked as $KCl > NaCl$, $CaCl_2 > MgCl_2$. This trend is predominantly attributed to ICP within the membrane because the ICP effect becomes more pronounced as draw-solution diffusivity becomes lower with the size and valency of the draw salt.
- It was demonstrated at laboratory, bench, and pilot scales that FO membrane technology can concentrate wastewater feeds up to very high TDS levels (>200,000 ppm) that are at least 2.5 times higher than the TDS level to which RO can achieve. Such high concentration levels corresponded to feed-volume reduction factors in the 3-5 range and apparent water recoveries in the 70-78% range.
- The FO model developed for water flux prediction appeared to be more sensitive to the membrane support structural parameter S used than to the intrinsic water permeability A.
- Bench and pilot-scale, integrated FO-MD operation with bench and full-size membrane modules demonstrated that the MD process can successfully regenerate the FO draw solution to keep a stable FO osmotic-pressure driving force. Without MD regeneration, operation of the FO process by itself resulted in a continuous decline in FO water flux with time. When the FO and MD processes are properly designed with respect to each other's performance and when minimal

fouling occurs, the bench and pilot testing indicate the possible "self-regulating" behavior of the integrated FO-MD system, highlighting that the hybrid FO-MD process could inherently find a steady state with no "process runaway" potential.

- The MD model developed in this project was successfully validated with experimental water permeation data on the MD hollow-fiber membrane modules (both 2.5 in x 8 in. and 8 in. × 20 in. modules). The manufacturer's membrane parameters and different shell- and bore-side flow conditions were used in the MD model to predict the MD water recovery for this module as well as the exit temperatures for both the heated feed and chilled permeate streams exiting the module. The MD exit temperatures predicted by the MD model were found to be in good agreement with the experimental values measured at a range of operational temperature, flow, and salt concentration conditions. This further validates the model that allows for a large-scale assessment of the energy consumption by the MD process at larger scales.

- FO-MD was shown to successfully concentrate RO brine and achieved >90% recovery of a wastewater that is difficult to treat using current technologies. The project results indicated that FO-MD technology is best suited for applications where the TDS concentration is higher than what can be treated via RO (>50,000 mg/L).

- The thermal energy consumption for MD was measured to be approximately 590 kWh/m^3 at 65 °C. This value is higher than reported for commercial thermal evaporators (128-385 kWh/m^3), but suggest that further improvements to optimize heat utilization are potentially achievable.

- Cost projections for FO-MD technology are estimated to be approximately \$35/m^3 for the treatment of industrial wastewater with a feed TDS of 40,000-50,000 mg/L. These values are based on the prototype system performance data treating real wastewater and suggest much higher costs than those reported (~1-3 \$/m^3) in the literature based either on laboratory-scale systems or computer modeling only. The cost increase was attributed to a reduction in the flux and water recovery that is feasible at larger scales as well as an increased specific heat requirement of MD. On the FO side, the larger-scale performance data showed that the fluxes were lower (~40% reduction) using commercial-scale modules and salt makeup requirements were approximately 15% higher than projected based on laboratory data.

- Although MD studies often cite the need for the development of an MD-specific membrane, results from this effort suggest that existing commercial membranes provide more than adequate fluxes and support the idea that a more important need is the development of larger-scale MD module. Specifically, a module that maximizes flow volume to specific surface area and the fact that the module length (and potential recovery) will be driven by heat content. The second area of need for development in MD is the heat management and recovery. Unless multiple stages are incorporated within the module, the lowest theoretical specific-heat usage of MD that can be obtained with existing modules is approximately 300 kWh/m^3, which is much greater than that used by other thermal processes. Our model suggests that, for MD to be competitive with thermal evaporation on cost basis, the energy consumption must approach 200 kWh/m^3. This number is higher than for an evaporator, but the polymer materials of construction would constitute a capital cost advantage and make MD competitive.

- Validation of the contaminant concentration model supports the hypothesis that the volatile/semi-volatile contaminant transport of a multicomponent feed solution in the DCMD process can be accurately described with a Fickian mass transport model. While the Fickian model does not include the diffusional interactions between the diffusing species, the accuracy of the model shows that the contaminant concentration model adequately predicts the change in contaminant concentration in both the feed and permeate collection streams. Validation of the model enables

the same mass transport mechanisms to be used in predicting the contaminant concentrations in large-scale systems as well.

- Commercially available ceramic membranes can be modified to make successful hydrophobic MD membranes. The coating is very durable and can withstand thermal and chemical stresses. However, the barrier to implementation of the ceramic membrane platform is the need for a membrane/module configuration that increases the membrane packing density to values closer to what can be obtained with polymeric membranes.

- Pilot-scale, integrated FO-MD prototype system was successfully operated for more than 15 weeks without a major stoppage. The RO brine from a produced wastewater treatment facility was treated further with FO-MD pilot, and about 90% recovery was possible while concentrating the TDS from 13,000-15,000 ppm up to 190,500 ppm. The FO-MD prototype could reject most contaminants in the wastewater and produce water with TDS lower than 300 ppm, even when the feed TDS was higher than 150,000 ppm.

- No chemical cleaning was necessary during the test period. Flushing the system with dechlorinated tap water was sufficient to reset the membranes for new test condition. Pilot performance and membrane autopsy showed that, even though the feed was concentrated more than 10 times, there was no sign of membrane fouling or defects on the FO and MD membrane surfaces.

- In the pilot-scale testing, the FO membrane rejected most of the inorganic contaminants in the wastewater, and the removal efficiency was more than 99%, except for sodium and chloride which were comprised the FO draw solution. Some VOCs and SVOCs could pass through the FO membrane; however, the MD membrane was able to reduce the SVOCs levels significantly. Post-treatment to remove VOCs or SVOCs in the FO-MD system permeate seems to be required when the raw wastewater contains high level of VOCs or SVOCs.

- When 3 M $MgCl_2$ was used as the FO draw solution, treated water quality was improved, but the high pH of the RO brine from the oil production site worsened the scaling of divalent precipitates on the FO draw side and the MD feed cartridge filter. This was because the feedwater to the RO was processed with lime softening upstream at the site. The divalent ion scaling decreased the FO and MD flow rates simultaneously and deteriorated the overall FO-MD system performance. Wastewater pH adjustment before the FO-MD system would be required before a divalent ion draw solution can used with the feed water tested in the pilot.

- The technical feasibility of the FO-MD was demonstrated in this project by taking the water that was treated with the highest level of current technologies and concentrating that by a factor of 10, using mostly low cost material. On the other hand, the economical feasibility of the process still needs to be further verified. This is mostly because there are not that many manufacturers of FO and MD membranes and it is expected that broader participation from the industry can reduce the cost of FO-MD process

9. RECOMMENDATIONS

We would like to make recommendations as follows

- Conducting more on-site testing is necessary. Different types of industrial and manufacturing process water should be tested using mobile systems.
- It is also necessary to conduct much longer-term testing to evaluate the longevity of the membranes and other system components. Longer-term testing will also benefit from understanding seasonal variation in the feed water conditions, if present.
- The FO-MD technology is a combination of traditional water treatment, membrane-based, and thermal processes. It is necessary to communicate the results to broader communities to collect ideas and inputs for future testing and evaluations.
- Better membranes for both FO and MD needs to be developed. The most important aspects are the recirculation rate and reverse draw-salt flux. Recirculation rates in the current MD and FO membranes are prohibitively high with current designs. Feedback of the performance and suggestions for improvement can be communicated to membrane companies.
- Heat and electrical energy minimization needs to be integrated into not only the system design, but also into the details of the membrane module construction.

References

1. McCutcheon, J.R., R.L. McGinnis, and M. Elimelech, "A Novel Ammonia-Carbon Dioxide Forward (Direct) Osmosis Desalination Process". *Desalination*, 2005. **174**(1): pp. 1-11.

2. Alklaibi, A.M. and N. Lior, "Membrane-Distillaion Desalination: Status and Potential". *Desalination*, 2005. **171**(2): pp. 111-131.

3. BCS Incorporated, *Waste Heat Recovery: Technology and Opportunities in U.S. Industry*. 2008, U.S. Department of Energy, Industrial Technologies Program.

4. Kenny, J.F., N.L. Barber, S.S. Hutson, K.S. Linsey, J.K. Lovelace, and M.A. Maupin, *Estimated Use of Water in the United States in 2005*. 2009, Reston, VA: U.S. Geological Survey Circular 1344. 52.

5. Energetics Inc. and E3M Inc., *Energy Use, Loss and Opportunities Analysis: U.S. Manufacturing and Mining*. 2004, Report prepared for the U.S. Department of Energy, Office of Energy Efficiency and Renewable Energy, Industrial Technologies Program.

6. Viswanathan, V., R. Davies, and J. Holbery, *Opportunity Analysis for Recovering Energy from Industrial Waste Heat and Emissions*. 2005, Pacific Northwest National Laboratory, U.S. Department of Energy, Industrial Materials of the Future Program Review: Chicago, IL.

7. Global Water Intelligence, *Industrial Desalination & Water Reuse: Ultrapure Water, Challenging Waste Streams and Improved Efficiency*. 2015: Global Water Intelligence. 271.

8. Cath, T.Y., M. Elimelech, J.R. McCutcheon, R.L. McGinnis, A. Achilli, D. Anastasio, A.R. Brady, A.E. Childress, I.V. Farr, N.T. Hancock, J. Lampi, L.D. Nghiem, M. Xie, and N.Y. Yip, "Standard Methodology for Evaluating Membrane Performance ini Osmotically Driven Membrane Processes". *Desalination*, 2013. **312**: pp. 31-38.

9. Phillip, W.A., J.S. Yong, and M. Elimelech, "Reverse Draw Solute Permeation in Forward Osmosis: Modeling and Experiments". *Environ. Sci. Technol.*, 2010. **44**(13): pp. 5170-5176.

10. Hoek, E.M.V., A.S. Kim, and M. Elimelech, "Influence of Crossflow Membrane Filter Geometry and Shear Rate on Colloidal Fouling in Reverse Osmosis and Nanofiltration Separations". *Environ. Eng. Sci.*, 2002. **19**(6): pp. 357-372.

11. Hendren, Z.D., J. Brant, and M.R. Wiesner, "Surface Modification of Nanostructured Ceramic Membranes for Direct Contact Membrane Distillation". *J. Membr. Sci.*, 2009. **331**: pp. 1-10.

12. Krajewski, S., W. Kujawski, M. Bukowska, C. Picard, and A. Larbot, "Application of Fluoroalkylsilanes (FAS) Grafted Ceramic Membranes in Membrane Distillation Process of NaCl Solutions". *J. Membr. Sci.*, 2006. **281**(1-2): pp. 253-259.

13. Chen, X., Y. Liu, H. Lu, H. Yang, X. Zhou, and J.H. Xin, "In-situ Growth of Silica Nanoparticles on Cellulose and Application of Hierarchical Structure in Biomimetic Hydrophobicity". *Cellulose*, 2010. **17**(6): pp. 1103-1113.

14. Zakrzewska-Trznadel, G., M. Harasimowicz, and A.G. Chmielewski, "Concentration of Radioactive Components in Liquid Low-Level Radioactive Waste by Membrane Distillation". *J. Membr. Sci.*, 1999. **163**(2): pp. 257-264.

15. Duhon, H., "Produced Water Treatment: Yesterday, Today, and Tomorrow ". *Oil Gas Facil.*, 2012. **1**(1): pp. 29-31.

16. Veil, J. and C. Clark, "Produced Water Volume Estimates and Management Practices". *SPE Prod. Oper.*, 2011. **26**(3): pp. 234-239.

17. Hanlon, J., *Regulating Natural Gas Drilling in the Marcellus Shale Under the NDPES Program*. 2011, U.S. Environmental Protection Agency: Washington, DC.

18. *Small Entity Compliance Guide: Centralized Waste Treatment Effluent Limitations Guidelines and Pretreatment Standards (40 CFR 437)*. 2001, U.S. Environmental Protection Agency.

19. Wijekoon, K.C., F.I. Hai, J. Kang, W.E. Price, T.Y. Cath, and L.D. Ngheim, "Rejection and Fate of Trace Organic Compounds (TrOCs) during Membrane Distillation". *J. Membr. Sci.*, 2014. **453**: pp. 636-642.

20. Gryta, M., "Effect of Flow-Rate on Ethanol Separation in Membrane Distillation Process". *Chem. Pap.*, 2013. **67**(9): pp. 1201-1209.

21. Gryta, M. and M. Barancewicz, "Separation of Volatile Compounds from Fermentation Broth by Membrane Distillation". *Polish J. Chem. Technol.*, 2011. **13**(3): pp. 56-60.

22. Tomaszewska, M., M. Gryta, and A.W. Morawski, "Study on the Concentration of Acids by Membrane Distillation". *J. Membr. Sci.*, 1995. **102**: pp. 113-122.

23. Tomaszewska, M., M. Gryta, and A.W. Morawski, "Mass Transfer of HCl and H_2O across the Hydrophobic Membrane during Membrane Distillation". *J. Membr. Sci.*, 2000. **166**(2): pp. 149-157.

24. Cussler, E.L., *Diffusion: Mass Transfer in Fluid Systems*. 3rd ed. Cambridge Series in Chemical Engineering. 2009, Cambridge, United Kingdom: Cambridge University Press. 647.

25. Gryta, M., "The Fermentation Process Integrated with Membrane Distillation". *Sep. Purif. Technol.*, 2001. **24**(1-2): pp. 283-296.

26. Schwarzenbach, R.P., P.M. Gschwend, and D.M. Imboden, *Environmental Organic Chemistry*. 2nd ed. 2003, Hoboken, NJ: John WIley & Sons.

27. Yaws, C.L., P. Narasimhan, K., and C. Gabbula, *Yaws' Handbook of Antoine Coefficients for Vapor Pressure*. 2nd electronic ed. 2009: Knovel.

28. Stephenson, R.M., S. Malanowski, and D. Ambrose, *Handbook of the Thermodynamics of Organic Compounds*. 1st ed. 1987, New York: Elsevier. 552.

29. Xie, W.H.S., W. Y. and D. Mackay, "A Review of the Effect of Salts on the Solubility of Organic Compounds in Seawater". *Mar. Environ. Res.*, 1997. **44**(4): pp. 429-444.

30. Yaws, C.L., *Yaws' Handbook of Properties for Aqueous Systems*. 2012: Knovel.

31. McCutcheon, J.R. and M. Elimelech, "Influence of Concentrative and Dilutive Internal Concentration Polarization on Flux Behavior in Forward Osmosis". *J. Membr. Sci.*, 2006. **284**(1-2): pp. 237-247.

32. McCutcheon, J.R. and M. Elimelech, "Modeling Water Flux in Forward Osmosis: Implications for Improved Membrane Design". *AIChE J.*, 2007. **53**(7): pp. 1736-1744.

33. Ibrahim, S.S. and Q.F. Alsalhy, "Modeling and Simulation for Direct Contact Membrane Distillation in Hollow Fiber Modules". *AIChE J.*, 2013. **59**(2): pp. 589-603.

34. Wilbert, M.C., J. Pellegrino, J. Scott, and Q. Zhang, *Water Treatment Estimation Routine (WaTER) User Manual*. 1999, U.S. Bureau of Reclamation: Denver, CO.

35. U.S. Environmental Protection Agency, *Final Development Document for Effluent Limitations Guidelines and Standards for the Petroleum Refining Point Source Category*. 1982, EPA-440/1-82/014, U.S. Environmental Protection Agency.

36. American Petroleum Institute, *Water Reuse Studies*. 1977, API Publication No. 949, American Petroleum Institute: Washington, DC.

37. American Petroleum Institute, *Analysis of Refinery Wastewaters for the EPA Priority Pollutants*. 1978, API Publication No. 4296, American Petroleum Institute: Washington, DC.

38. Coburn, J.B., K.S. Schaffner, K.P. Sroka, J.H. Cunningham, D.D. Randall, C.R. Richardson Fry, and M.K. Icenhour, *Emission Estimation Protocol for Petroleum Refineries* 2011, (Report No. Version 2.1.1), Prepared for Office of Air Quality Planning and Standards, U.S. Environmental Protection Agency.

39. U.S. Environmental Protection Agency, *Guidelines for Water Reuse*. 1980, EPA-600/8-80/036, U.S. Environmental Protection Agency.

40. Ma, M. and R.M. Hill, "Superhydrophobic Surfaces". *Curr. Opinion Colloid Interf. Sci.*, 2006. **11**(4): pp. 193-202.

41. Alklaibi, A.M., "The Potential of Membrane Distillation as a Stand-alone Desalination Process". *Desalination*, 2008. **223**(1-3): pp. 375-385.

42. Carlsson, L., "The New Generation in Sea Water Desalination". *Desalination*, 1983. **45**(2): pp. 221-222.

43. Macedonio, F., A. Ali, T. Poerio, E. El-Sayed, E. Drioli, and M. Abdel-Jawad, "Direct Contact Membrane Distillation for Treatment of Oilfield Produced Water". *Sep. Purif. Technol.*, 2014. **126**: pp. 69-81.

44. U.S. Environmental Protection Agency, *Greenhouse Gas Equivalencies Calculator*. 2011, U.S. Environmental Protection Agency: http://www.epa.gov/cleanenergy/energy-resources/calculator.html.

45. U.S. Environmental Protection Agency, *Inventory of U.S. Greenhouse Gas Emissions and Sinks: 1990-2009*. 2011, EPA 430-R-11-005, U.S. Environmental Protection Agency: Washington, DC.

Appendix

1. FO-MD prototype P&ID (intake) [1 of 4]

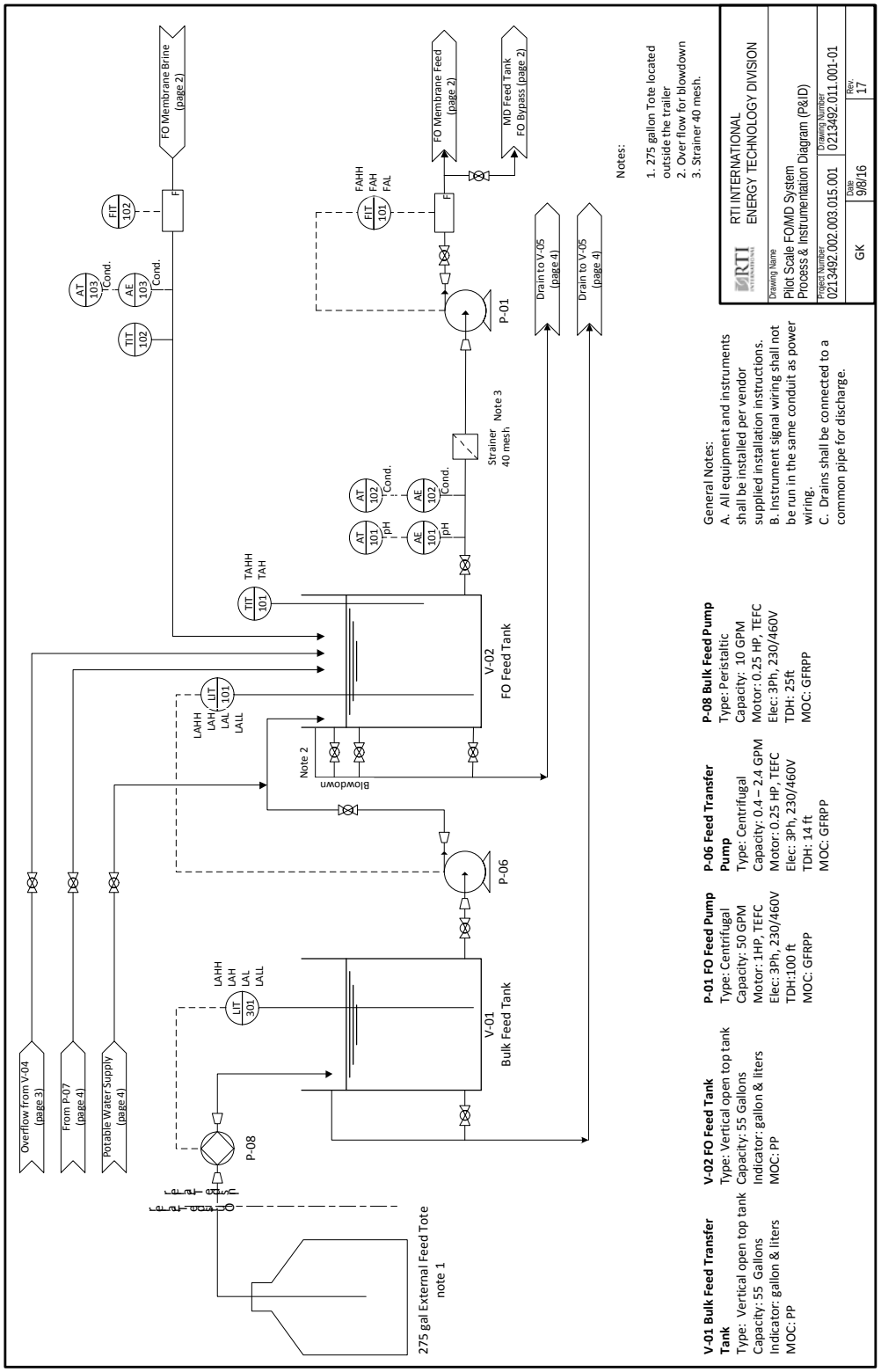

2. FO-MD prototype P&ID (FO system) [2 of 4]

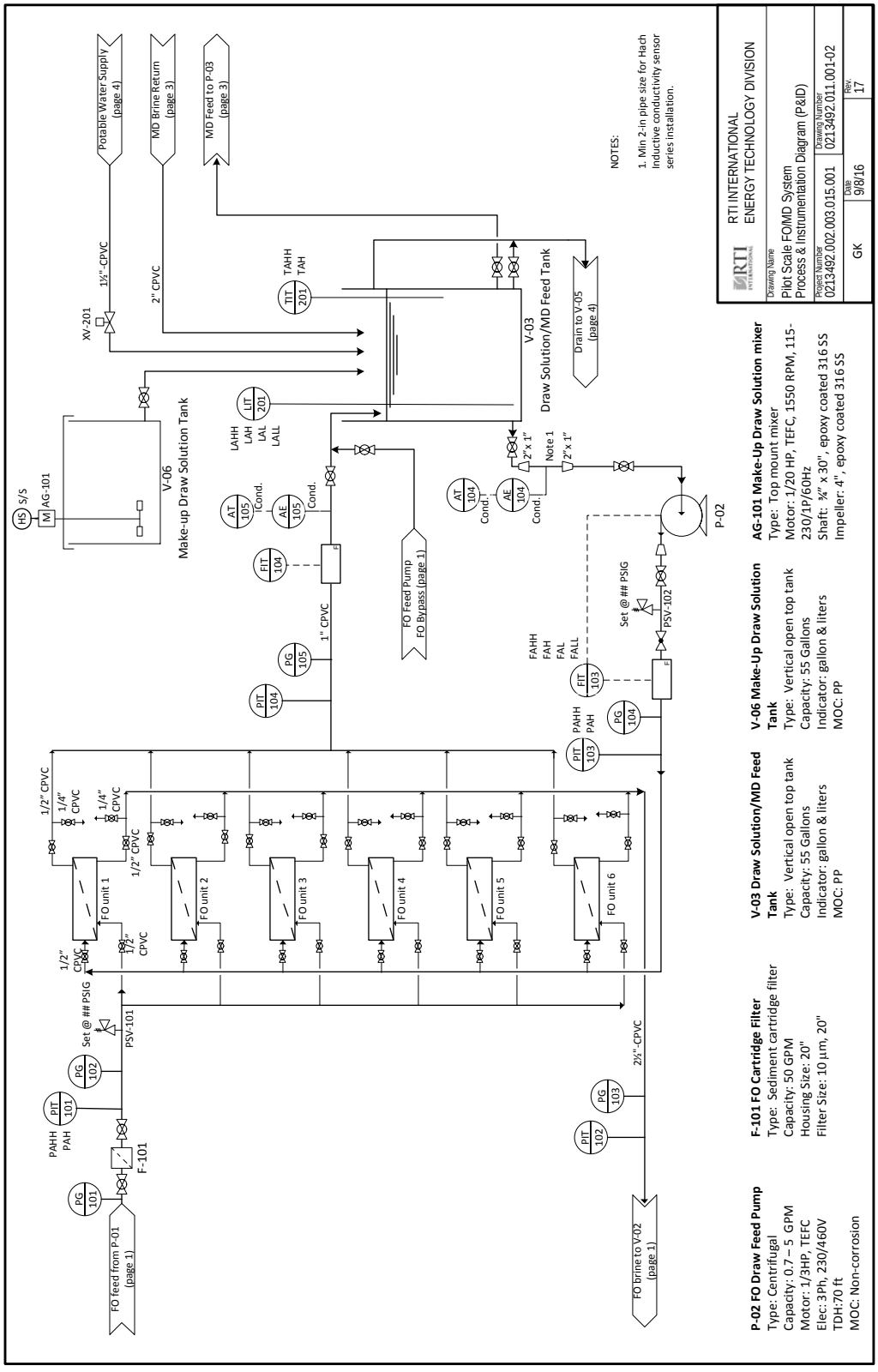

3. FO-MD prototype P&ID (MD system) [3 of 4]

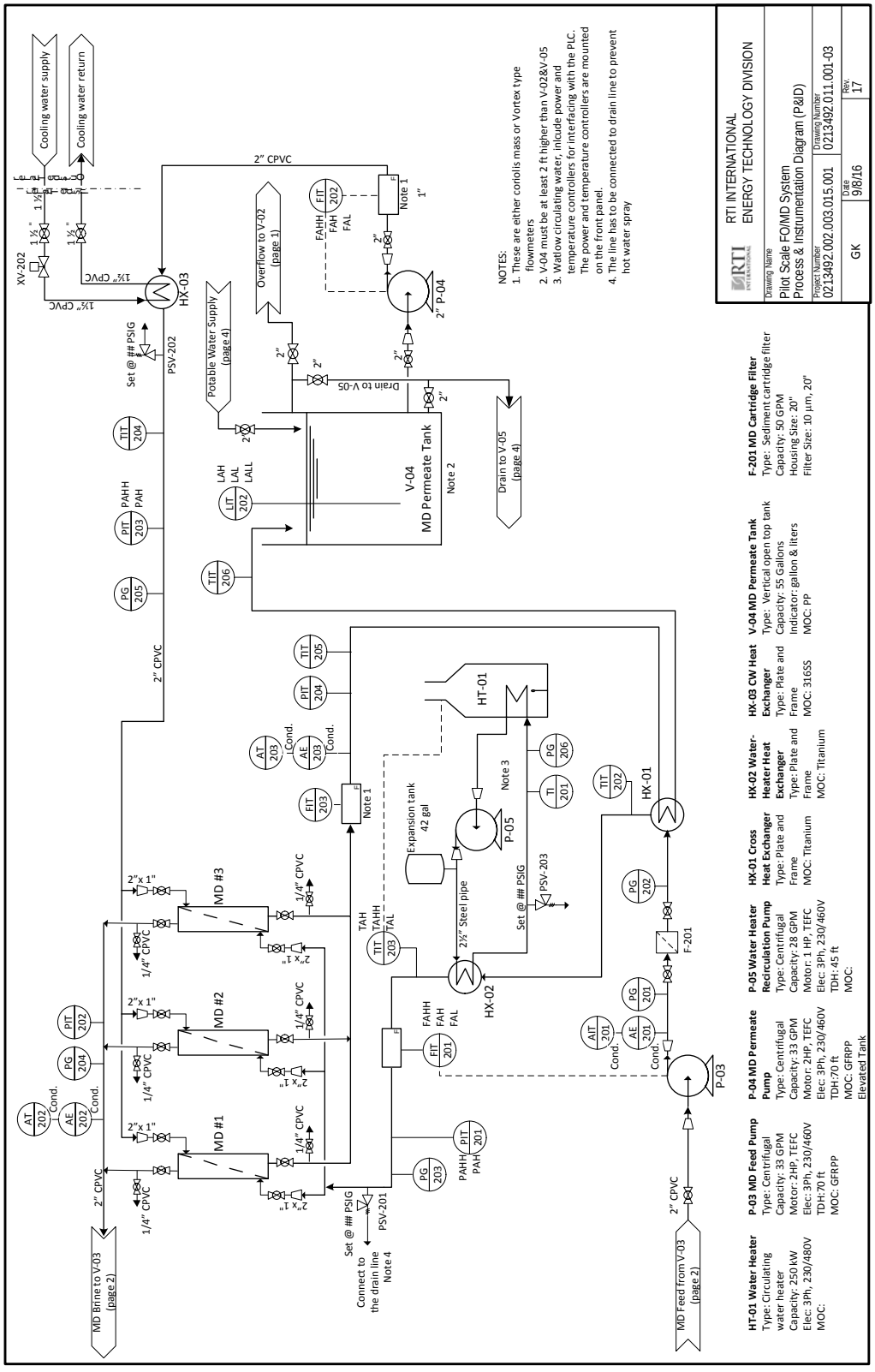

4. FO-MD prototype P&ID (Discharge and drain) [4 of 4]

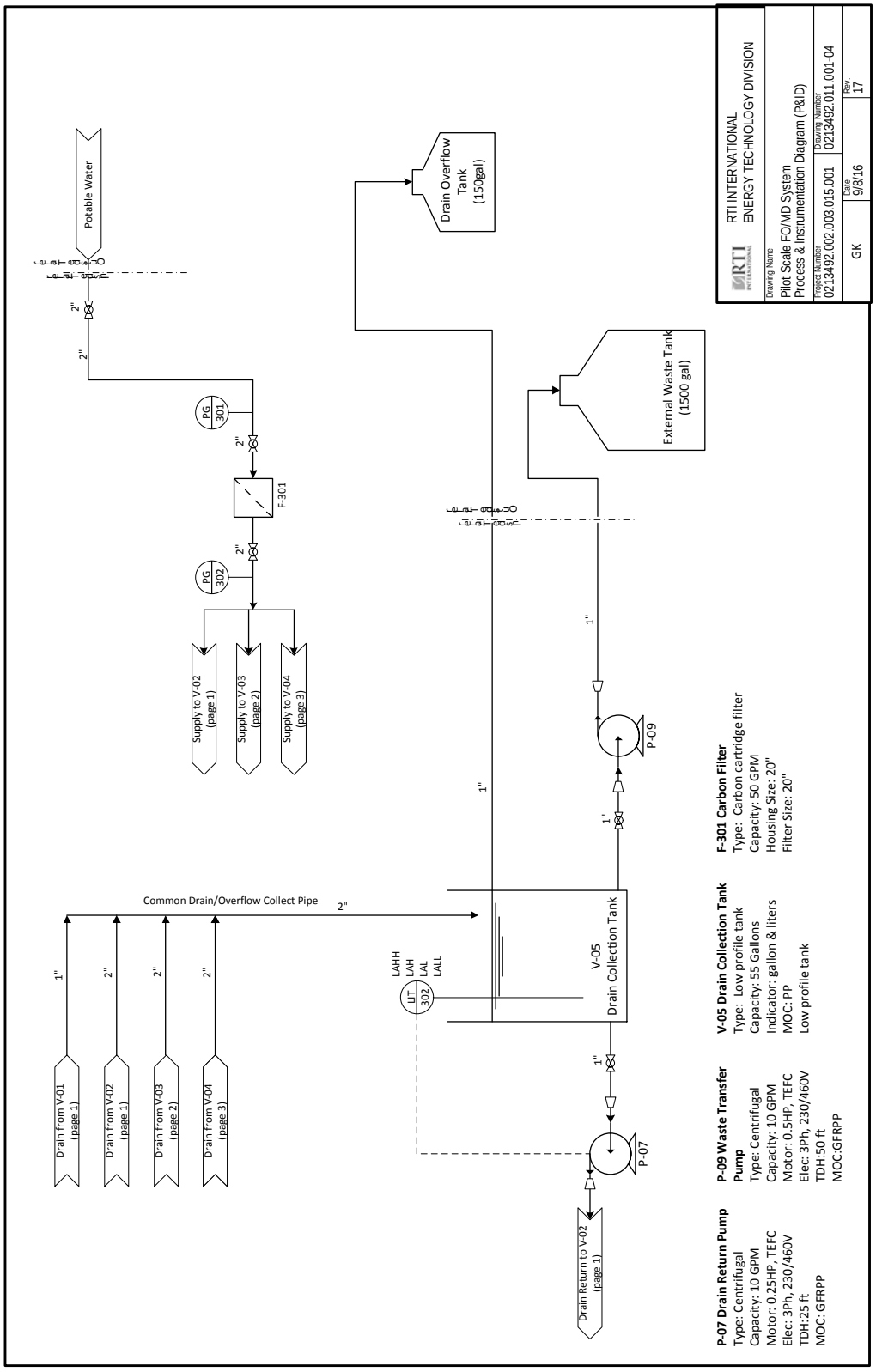

5. Flow chart for FO-MD control logic (FO-MD Recirculation)

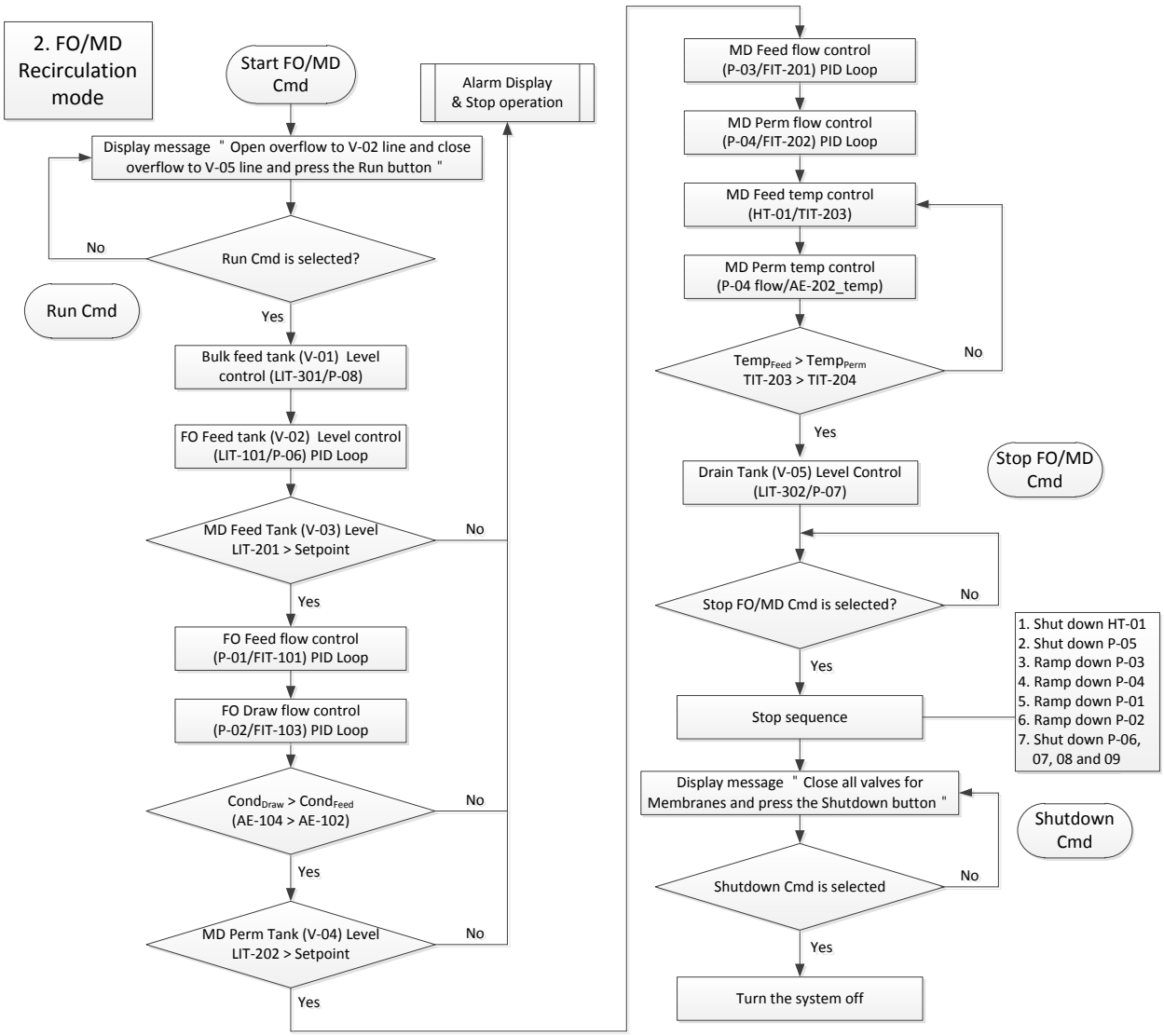

6. Flow chart for FO-MD control logic (Concentration only)

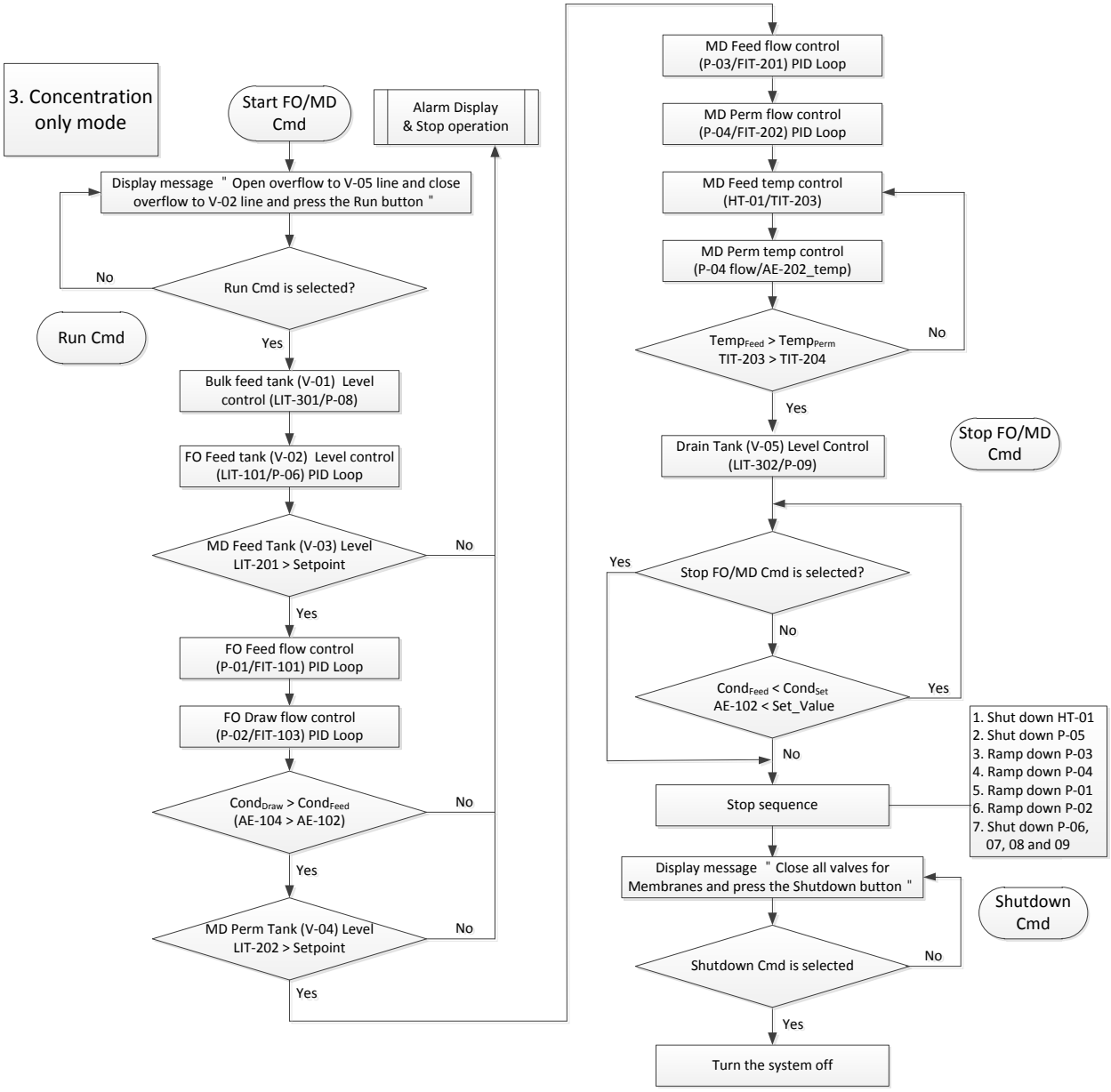

7. Flow chart for FO-MD control logic (MD Once-through mode)

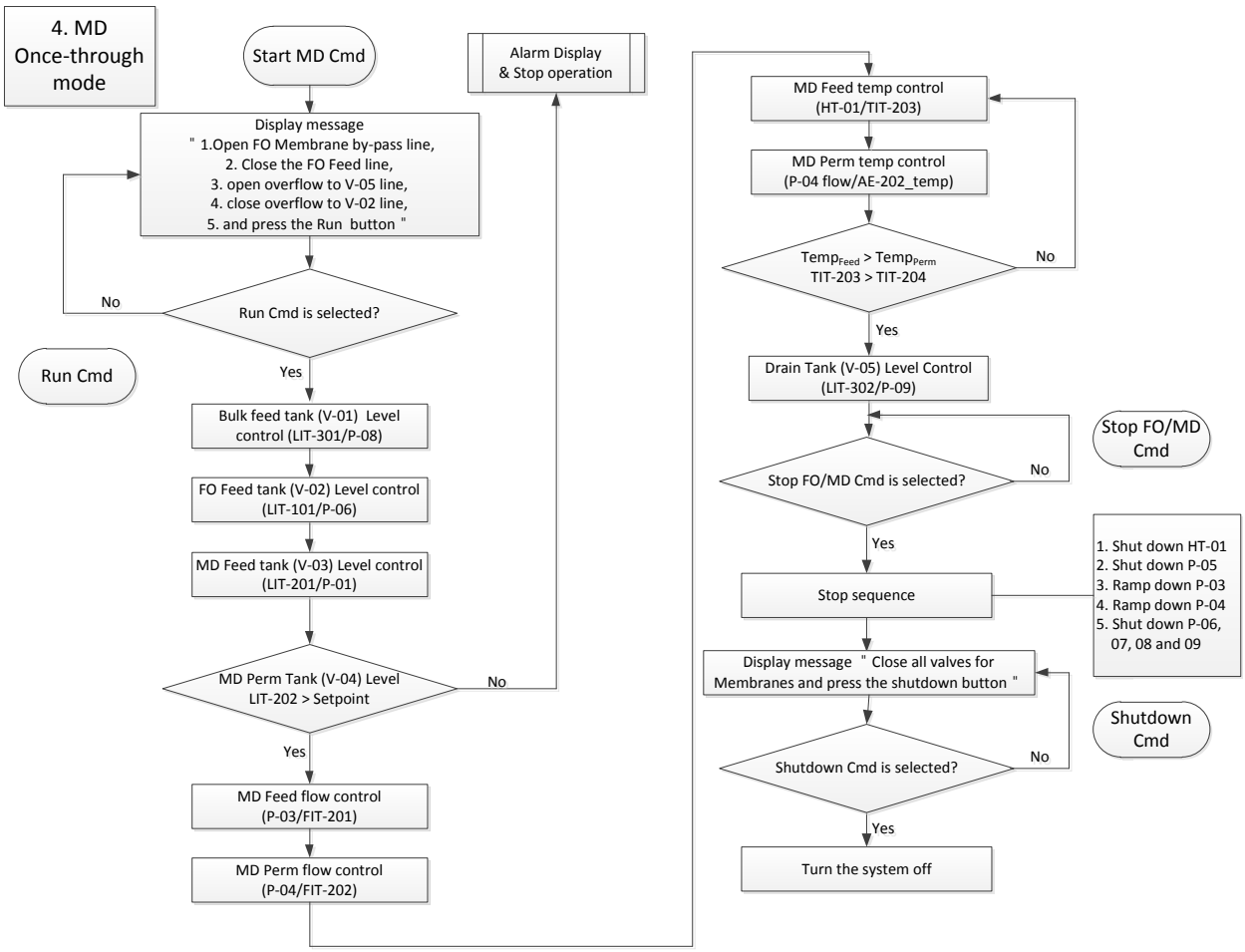

8. Flow chart for FO-MD control logic (MD Recirculation mode)